

PART I: THE KINETICS OF THIOPHENE HYDROGENOLYSIS

PART II: EFFECTIVENESS FACTORS FOR POROUS CATALYSTS:  
LANGMUIR-HINSHELWOOD KINETIC EQUATIONS

BY

GEORGE W. ROBERTS  
B. Ch. E., Cornell University  
(1961)

Submitted in Partial Fulfillment of the  
Requirements for the Degree of  
Doctor of Science in Chemical Engineering  
at the  
Massachusetts Institute of Technology  
July 1965

Signature of Author:

Signature redacted  
Department of Chemical Engineering  
July 1965

Certified by:

Signature redacted  
C. N. Satterfield, Thesis Supervisor

Approved by:

Signature redacted  
Glenn C. Williams, Chairman Dept.  
Committee on Graduate Students

MRL  
OCT 20 1965  
LIBRARY

Thesis  
Chem.  
Eng  
1965  
Sc. D.

GEORGE W. ROBERTS  
E. Ch. E., Cornell University  
(1965)

Submitted in partial fulfillment of the  
requirements for the degree of  
Doctor of Philosophy in Chemical Engineering  
at the  
Massachusetts Institute of Technology  
July 1965

*[Signature]*  
Department of Chemical Engineering  
MIT

*[Signature]*  
Department of Chemical Engineering  
MIT

*[Signature]*  
Department of Chemical Engineering  
MIT



## ABSTRACT

PART I: THE KINETICS OF THIOPHENE HYDROGENOLYSIS  
PART II: EFFECTIVENESS FACTORS FOR POROUS CATALYSTS:  
LANGMUIR-HINSHELWOOD KINETIC EQUATIONS

by

George W. Roberts

Submitted to the Department of Chemical Engineering on July 19, 1965, in partial fulfillment of the requirements for the degree of Doctor of Science.

Part I

The kinetics of the hydrogenolysis of thiophene over a cobalt molybdate catalyst were studied in a differential reactor with recirculation; the total pressure was about 1 atmosphere and the temperature range was 235 to 265°C. The rate of thiophene disappearance went through a maximum as the thiophene partial pressure was increased. A Langmuir-Hinshelwood kinetic equation was used to correlate the data on thiophene disappearance and the constants in this equation suggest that retardation of the reaction by both thiophene and hydrogen sulfide was significant.

The rate of hydrogenation of the butene intermediate was also described with a Langmuir-Hinshelwood rate equation. Butene hydrogenation is inhibited by both butene and hydrogen sulfide.

Part II

Catalyst effectiveness factors were computed for reactions that obeyed Langmuir-Hinshelwood kinetic equations. Strong inhibition of the reaction by a reaction product causes an intraparticle diffusional limitation to set in under much milder conditions than the existing criterion predicts. If a bimolecular reaction is strongly inhibited by one of the reactants, effectiveness factors greater than unity can occur and instability of operation can result.

Thesis Supervisor:  
Title:

Charles N. Satterfield  
Professor of Chemical Engineering



Department of Chemical Engineering  
Massachusetts Institute of Technology  
Cambridge, Massachusetts 02139

July 19, 1965

Professor William Greene  
Secretary of the Faculty  
Massachusetts Institute of Technology  
Cambridge, Massachusetts 02139

Dear Professor Greene:

In accordance with the regulations of the Faculty, I herewith submit a thesis, entitled "Part I: The Kinetics of Thiophene Hydrogenolysis; Part II: Effectiveness Factors for Porous Catalysts: Langmuir-Hinshelwood Kinetic Equations", in partial fulfillment of the requirements for the degree of Doctor of Science in Chemical Engineering at the Massachusetts Institute of Technology.

Respectfully submitted,

**Signature redacted**

George W. Roberts





## Acknowledgements

The subject of this investigation was originally proposed by the author's supervisor, Professor Charles N. Satterfield. The author wishes to thank Professor Satterfield for his very helpful guidance at critical stages of this study.

The author would also like to express his gratitude to the following for their assistance:

The National Science Foundation for financial support in the form of a fellowship;

The MIT Computation Center for the use of their facilities;

The Girdler Catalysts Department of Chemetron Corporation which, through Dr. J. E. Taylor, provided the catalyst used in this study and made the measurements of the physical properties of the catalyst;

The 10.24 group headed by Alfredo Garcia for aid in developing a column for the chromatograph;

Miss Janet Romanowych for determining the areas of the chromatograms;

Gerhard Blasziess, Al Merrill and "Nick" Carter for their help in building the experimental equipment;

Charles Gray and Professor Sam Bodman with whom many pleasant hours were spent during the period of this study;

Miss Jan Vogel for secretarial assistance in the final preparation of this manuscript.

I am deeply indebted to my wife, Mary, for her patience and confidence, and finally, I wish to thank my parents for the understanding and support they have given me throughout the period of my education.





## TABLE OF CONTENTS

	<u>Page</u>
I. Summary	19
A. Introduction and Thesis Objectives	19
B. The Kinetics of Thiophene Hydrogenolysis	21
C. Effectiveness Factors for Porous Catalysts: Langmuir-Hinshelwood Kinetic Equations	29
II. Introduction	37
A. Background	37
B. Thesis Objectives	37
III. The Kinetics of Thiophene Hydrogenolysis	43
A. Literature Review and Criticism	43
1. General Comments	43
2. Reaction Mechanism	44
3. Adsorption of Reaction Components	48
4. Reaction Kinetics	51
5. The Cobalt Molybdate Catalyst	53
6. Langmuir-Hinshelwood Kinetic Equations	56
B. Experimental Apparatus and Procedure	61
1. General Theory of Experiments and Equipment Design	61
2. Apparatus - Details of Construction and Calibration	62
a. Reaction Loop	62
I. Reactor and Catalyst	65
II. Temperature Measurement	67
III. Temperature Control	68
b. Hydrogen Feed System	69
c. Chromatograph	71
d. Thiophene Delivery System	75
e. Hydrogen Sulfide Feed System	77

3. Operation of the Equipment	78
a. Startup	78
b. Approach to Steady-State	79
c. Shutdown	80
4. Data Processing	81
a. Raw Data	81
b. Preliminary Correlation	82
c. Final Correlation	84
C. Results	87
1. Reaction Products	87
2. The Rate of Thiophene Disappearance	87
a. Kinetic Data	87
b. Kinetic Equations--Preliminary Correlations	88
c. Final Kinetic Equation	93
3. The Rate of Butane Formation	94
a. Kinetic Data	94
b. Kinetic Equations--Preliminary Correlations	99
c. Final Kinetic Equation	101
4. The Reliability of the Data	103
a. Material Balances	103
b. Reproducibility	107
5. Unsteady-State Behavior	108
D. Discussion of Results	109
1. Unsteady-State Behavior	109
2. The Reliability of the Data	110
a. Material Balances	110
b. Reproducibility	110
3. The Kinetics of Thiophene Disappearance	111
a. Potential Rate Equations	111
b. Preliminary Correlations	113
c. The Final Rate Equation	115

	I. Accuracy	116
	II. Comments on the Reaction Mechanism	116
	III. The Effect of Thiophene and Hydrogen Sulfide Adsorption	118
	IV. The Activation Energies	118
4.	The Kinetics of Butane Formation	120
	a. Potential Rate Equations	120
	b. Preliminary Correlations	125
	c. The Final Rate Equation	127
	I. Accuracy	127
	II. Comments on the Reaction Mechanism	128
	III. The Effect of Butene and Hydrogen Sulfide Adsorption	129
	IV. The Activation Energies	129
5.	The Effect of Hydrogen Sulfide on the Reaction Selectivity	130
IV.	Effectiveness Factors for Porous Catalysts: Langmuir- Hinshelwood Kinetic Equations	132
A.	Literature Review and Criticism	132
	1. The Effective Diffusivity	132
	2. Effectiveness Factors--Fundamental Results	133
	3. Effectiveness Factors--Langmuir- Hinshelwood Kinetics	138
B.	Mathematical Derivation and Computational Procedure	144
	1. Type I	145
	a. General Derivation	145
	b. Numerical Solution--Calculation of $K_{p_{A, \theta}}$	149
	I. Method	149
	II. Accuracy	150
	2. Type II	152
	a. General Derivation	152



b.	Numerical Solution, $K \neq 0$	154
I.	General Mathematics	154
II.	Calculation of $Kp_{A,0}$	155
III.	Accuracy	158
c.	Analytic Solution, $K = 0$	159
C.	Results	163
1.	Type I	163
2.	Type II	164
D.	Discussion of Results	188
1.	Type I	188
a.	Comparison with Previous Results	188
b.	The Approximate Solution for $\eta$	188
I.	Region of Accuracy	188
II.	Concentration Dependence of $\eta$	189
c.	The $\eta - \Phi$ Relationship	190
I.	Comparison with Integer- Order Rate Equations	190
II.	The Aris Transformation	190
III.	The Effect of Product Adsorption	192
2.	Type II	194
a.	The Approximate Solution for $\eta$	194
I.	Accuracy	194
II.	Concentration Dependence of $\eta$	195
b.	The $\eta - \Phi_{MII}$ Relationship	195
c.	The $\eta - \Phi_L$ Relationship	197
I.	The Effect of Product Adsorption	197
II.	The Effect of Reactant Adsorption	198
d.	The $\eta - E$ Relationship	199
3.	The Diffusional Implications of the Kinetic Equations for Thiophene Hydrogenolysis	200
a.	Effectiveness Factors	200
b.	Selectivity	200



V. Conclusions and Recommendations	202
A. Thiophene Hydrogenolysis	202
1. Conclusions	202
2. Recommendations	203
a. Further Experiments	203
b. Modifications of the Equipment and Procedure	203
B. Effectiveness Factors for Porous Catalysts: Langmuir-Hinshelwood Kinetic Equations	204
1. Conclusions	204
VI. Appendix	205
A. Additional Data on Equipment Performance	205
1. Calibration of Hydrogen Flowmeter	205
2. Calibration of Hydrogen Sulfide Flowmeter	206
3. Performance of Gas Chromatograph	209
a. Separation	209
b. Calibration	210
4. Calibration of Thiophene Pump	213
B. Computer Programs	215
1. Effectiveness Factors for Type I Rate Equations	215
2. Effectiveness Factors for Type II Rate Equations	218
3. Reduction of Experimental Kinetic Data	224
4. Calculation of Constants in Preliminary Rate Equation	228
5. Calculation of Constants in Final Rate Equation	231

C. Data	236
1. Type I	236
2. Type II	238
3. Experimental Data	243
a. Raw Data	243
b. Processed Data	244
D. Illustrative Calculations for Langmuir-Hinshelwood Rate Equations, Using Experimental Data	245
1. Calculation of the Effectiveness Factor	245
2. Examples of the Calculation of $Kp_{A,s}$	250
3. Thiophene Hydrogenolysis	255
E. Calculations on Catalyst Performance	257
1. Calculation of the Maximum Temperature and Concentration Differences between the Catalyst Pellet and the Bulk Stream	257
2. Calculation of the Maximum Temperature Gradient within the Catalyst Pellet	262
3. Calculation of the Effective Diffusivity of Thiophene	263
F. Nomenclature	267
G. Literature Citations	273
H. Biographical Note	279

## LIST OF FIGURES

		<u>Page</u>
III-1	Diagram of Overall Kinetic Apparatus	63
III-2	Diagram of Chromatograph and Auxiliaries	73
III-3	Rate of Thiophene Disappearance versus Thiophene Partial Pressure	23, 89
III-4	Calculated Rate of Thiophene Disappearance versus Experimental Rate of Thiophene Disappearance	95
III-5	Rate of Butane Formation versus Total Butene Partial Pressure	27, 97
III-6	Calculated Rate of Butane Formation versus Experimental Rate of Butane Formation	105
IV-1	$Kp_{A,s}$ versus $Kp_{A,o}$ -- Type II	157
IV-2	The Ratio $p_{A,o}/p_{A,s}$ as a Function of the Modified Thiele Modulus, $\Phi_{MI}$ , for Various Values of $Kp_{A,s}$	165
IV-3	Effectiveness Factor as a Function of the Modified Thiele Modulus, $\Phi_{MI}$ , for Various Values of $Kp_{A,s}$	167
IV-4	Effectiveness Factor as a Function of the Modulus $\Phi_L$ , Type I	33, 169
IV-5	Effectiveness Factor as a Function of the Modified Thiele Modulus, $\Phi_{MII}$ , for Various Values of $Kp_{A,s}$ ; $E = 0$	173
IV-6	Effectiveness Factor as a Function of the Modified Thiele Modulus, $\Phi_{MII}$ , for Various Values of $Kp_{A,s}$ ; $E = 1.0$	175
IV-7	Effectiveness Factor as a Function of the Modified Thiele Modulus, $\Phi_{MII}$ , for Various Values of $Kp_{A,s}$ ; $E = 10.0$	35, 177

		<u>Page</u>
IV-8	Effectiveness Factor as a Function of the Modulus $\Phi_L$ , Type II, $E = 0$	179
IV-9	Effectiveness Factor as a Function of the Modulus $\Phi_L$ , Type II, $E = 1.0$	181
IV-10	Effectiveness Factor as a Function of the Modulus $\Phi_L$ , Type II, $E = 10.0$	183
IV-11	The $\eta$ versus $\Phi_L$ Relationship for Representative Combinations of $Kp_{A,s}$ and $E$ , Type II	185
VI-1	Calibration Curve for Hydrogen Flowmeter	207
VI-2	Calibration Curve for Hydrogen Sulfide Flowmeter	211



## LIST OF TABLES

		<u>Page</u>
III-1	Thermodynamic Properties for Thiophene Hydrogenolysis	44
III-2	Results of Preliminary Kinetic Analysis-- Thiophene Disappearance	92
III-3	Results of Final Kinetic Analysis--Thiophene Disappearance	93
III-4	Final Values of Kinetic Parameters--Thiophene Disappearance	25, 94,
III-5	Results of Preliminary Kinetic Analysis-- Butane Formation	100
III-6	Results of Final Kinetic Analysis--Butane Formation	102
III-7	Final Values of Kinetic Parameters-- Butane Formation	26, 103,
III-8	Results of Reaction Products Closures	104
III-9	Results of Sulfur Balance Closures	104
III-10	Results of Standard Kinetic Runs	107
III-11	Potential Kinetic Equations--Thiophene Disappearance	114
IV-1	Values of $\bar{\Phi}_L$ Corresponding to an Effectiveness Factor of 0.95	191
VI-1	Separation Data for Gas Chromatograph	209
VI-2	Calibration Results for Chromatograph	213
VI-3	Calibration Results for Thiophene Pump	214
VI-4	Pore Size Distribution and Calculation of $D_T$	266





## I. SUMMARY

### A. Introduction and Thesis Objectives

Essentially all of the surface area of most porous, solid catalysts is located in the interior of the catalyst particle. Reactants must diffuse into the catalyst, where they chemisorb and react. The reaction products must then desorb and diffuse back through the porous structure into the bulk stream. If the intrinsic rate of chemical reaction is large compared to the rate at which diffusion can occur, significant concentration gradients will exist within the catalyst particle. These gradients can affect the apparent activity of the catalyst and can also affect the apparent selectivity, if more than one reaction is taking place.

Thiele (69) presented the first mathematical treatment of the effect of intraparticle concentration gradients on the apparent catalytic activity. By solving the differential equation that describes the diffusion and reaction of a reactant within the catalyst, Thiele developed a mathematical relationship for the "effectiveness" of the catalyst particle as a function of a dimensionless modulus, now commonly called the Thiele modulus. The "effectiveness" or "effectiveness factor" is defined by Equation (II-1).

$$\eta = \frac{\text{actual reaction rate per pellet}}{\text{rate if internal gradients were absent}} \quad (\text{II-1})$$

The concept of catalyst "effectiveness" has been adopted and extended by many other investigators (10), (75), (79), (80), (83).

Almost all derivations of the catalyst effectiveness factor contain the assumption that the reaction obeys either a zero, first or second-order rate equation. However, these simple kinetic expressions cannot describe effects such as retardation of the reaction rate by high

concentrations of either reaction products or reactants; such inhibition effects can be very important in heterogeneous catalytic reactions. Under conditions where intraparticle concentration gradients are significant, inhibition effects can affect the behavior of catalysts in a way that is not predictable from models based on integer-order rate equations (4). Langmuir-Hinshelwood rate equations afford the simplest mathematical description of reaction inhibition by reactants and products, but derivations of the catalyst effectiveness factor for Langmuir-Hinshelwood rate equations are very few (14), (58), (59), and are lacking in generality.

Mathematical treatments of the effect of an intraparticle diffusional resistance on the reaction selectivity have also been presented (48), (78), (83). However, all of the work to date has been based on simple, integer-order rate equations. Experimental studies of the effect of pore diffusion on the catalytic activity have been numerous. The results are summarized in a recent book (60). Experimental investigations of the selectivity effect, however, are few (7), (81), and have not provided rigorous tests of the mathematical models.

The fundamental purpose of this study was to lay the basis, both theoretically and experimentally, for predicting and understanding the activity and selectivity effects that can occur when intraparticle concentration gradients exist, and when the kinetics of the reactions are best described by complex rate equations. The specific objective of the thesis was twofold: 1) to mathematically derive catalyst effectiveness factors for a wide range of Langmuir-Hinshelwood rate equations; 2) to experimentally determine the intrinsic kinetics for a reaction of the form

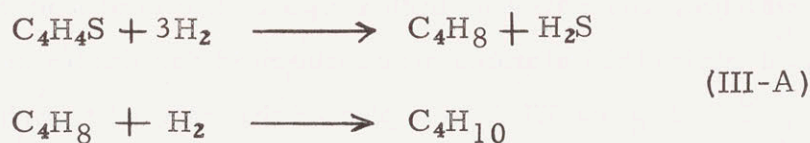




for a system where complex rate equations are required to describe the kinetics of both steps of the reaction. This intrinsic kinetic study is intended as a first step in a program to investigate the effect of a diffusional retardation on the activity and selectivity of the reaction.

### B. The Kinetics of Thiophene Hydrogenolysis

Several studies of the reaction of thiophene and hydrogen, over various catalysts, have been made in the temperature range 200 - 400°C and at a total pressure of one atmosphere (20), (29), (45), (46), (49). The principal reaction products were hydrogen sulfide, n-butane and the three isomers of n-butene. There is general agreement that the reaction proceeds as shown below.



Thus, the hydrogenolysis of thiophene is a reaction of the form shown in (II-A).

Cobalt molybdate, which was the catalyst used in the present work, was employed in two of the above studies. A detailed kinetic study was not made in either case, although Pease and Keighton (49) suggested that the reaction rate was inhibited by a reaction product, and Owens and Amberg (45) stated that hydrogen sulfide exerted an inhibiting effect on the reaction.

The present experimental work was performed at a total pressure of about one atmosphere, and at one of three reactor temperatures, 235°C, 251°C and 265°C. The apparatus used can be classified into five sections; the hydrogen feed system, the hydrogen sulfide

feed system, the thiophene pump, the reaction loop and the chromatograph. The reaction loop contained the reactor, a pump and several thermocouples. The function of the pump was to continuously circulate the gas in the reaction loop through the catalyst bed, at a rate that was much larger than the feed rate. Thus, at steady-state, the composition was essentially uniform at all points in the reaction loop. The feeds were introduced just below the reactor and a purge was taken off at a rate such that the pressure in the loop remained constant. The composition of the purge stream was measured with the chromatograph. Thiophene was fed as a liquid by a calibrated hypodermic pump. The hydrogen and hydrogen sulfide feed systems were very similar, in that both gases were fed from cylinders at measured and controlled rates. Using the values of the feed rates and the purge composition, the rates of both steps of the reaction were calculated, and two material balances were checked for each run.

Figure III-3 is a plot of the rate of thiophene disappearance versus the thiophene partial pressure. At each of the three reactor temperatures, a distinct maximum in the reaction rate occurred as the thiophene partial pressure was raised, for the runs with no hydrogen sulfide in the feed. The data points for runs made with hydrogen sulfide in the feed fall below the points for no hydrogen sulfide at the same reactor temperature. The maximum in the reaction rate and the inhibition by hydrogen sulfide preclude the use of an integer-order rate equation to describe the data. Correlations were attempted only with various Langmuir-Hinshelwood rate equations.

The rate equation given by Equation (III-19) produced the best correlation of the data on thiophene disappearance.

$$r_T = k p_T p_H / (1 + K_T p_T + K_{H_2S} p_{H_2S})^2 \quad (\text{III-19})$$



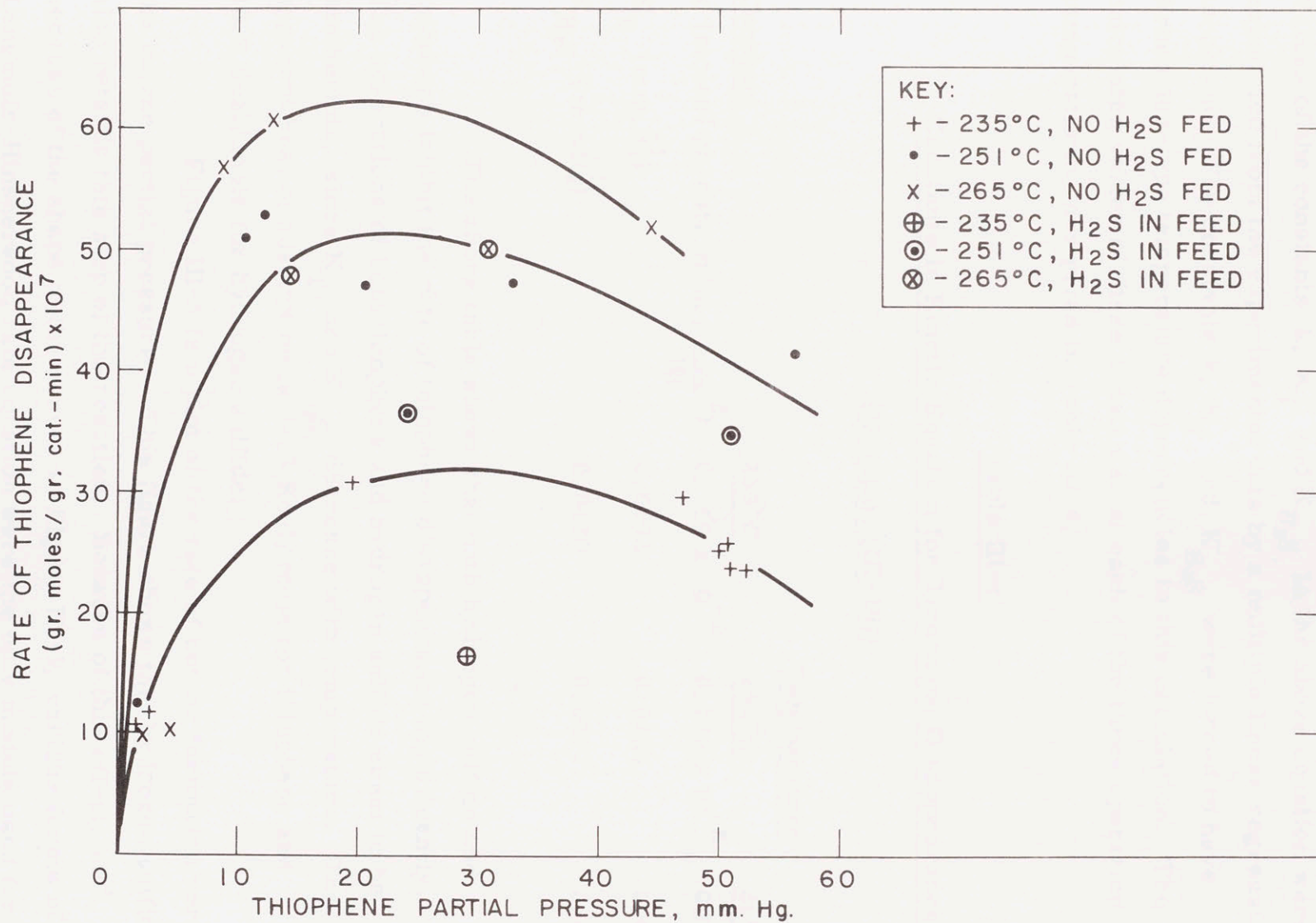


FIGURE III-3 RATE OF THIOPHENE DISAPPEARANCE VERSUS THIOPHENE PARTIAL PRESSURE



Values of the constants  $k$ ,  $K_T$  and  $K_{H_2S}$  in the above equation were calculated from the experimental data by a multiple linear regression technique. The constants  $k$ ,  $K_T$  and  $K_{H_2S}$  were forced to have Arrhenius-type temperature dependencies in this calculation. The calculated values of these constants, at each of the three operating temperatures, are given in Table III-4.

Table III-4

Constants in Kinetic Equation for Thiophene Disappearance

(Equation (III-19))

<u>Constant</u>	<u>Temperature</u>		
	<u>235°C</u>	<u>251°C</u>	<u>265°C</u>
$k$ (moles/ gr. cat., min., $\frac{\text{mm.}^2}{\text{Hg}}$ )	$0.159 \times 10^{-8}$	$0.178 \times 10^{-8}$	$0.195 \times 10^{-8}$
$K_T$ ( $\text{mm. Hg}^{-1}$ )	0.0592	0.0284	0.0155
$K_{H_2S}$ ( $\text{mm. Hg}^{-1}$ )	0.0420	0.0237	0.0148

The above table shows that both hydrogen sulfide and thiophene inhibit the rate of thiophene disappearance significantly. The adsorptions of both thiophene and hydrogen sulfide seem to be exothermic, since  $K_T$  and  $K_{H_2S}$  decrease with temperature. The apparent heat of adsorption is 24.3 Kcal/ mole for thiophene and 18.9 Kcal/ mole for hydrogen sulfide.

Figure III-5 is a plot of the rate of butane formation versus the butene partial pressure. This figure shows that hydrogen sulfide also retards this step of the reaction. Because of this effect, and because of the shape of the curves in Figure III-5, various forms of Langmuir-Hinshelwood rate equation were the only models used for



correlation of the data.

Several attempts were made to fit the data to equations that were based on the assumption that butene hydrogenation took place, to some extent, on the original desulfurization site, without intermediate desorption and re-adsorption of butene. However, the best correlation of the data was given by Equation (III-32) below. This equation is based on the assumption that all butene desorbs and re-adsorbs before it hydrogenates to butane.

$$r_c = \hat{k}p_B / (1 + \hat{K}_B p_B + \hat{K}_{H_2S} p_{H_2S}) \quad (\text{III-32})$$

Values of the constants  $\hat{k}$ ,  $\hat{K}_B$  and  $\hat{K}_{H_2S}$  were calculated from the experimental data by the same technique used for thiophene disappearance, and are given in Table III-7.

Table III-7

Constants in Kinetic Equation for Butane Formation

<u>Constant</u>	<u>(Equation (III-32))</u>		
	<u>Temperature</u>		
	<u>235°C</u>	<u>251°C</u>	<u>265°C</u>
$\hat{k}$ (moles/ gr. cat., min., mm / Hg.)	$0.386 \times 10^{-5}$	$0.269 \times 10^{-5}$	$0.200 \times 10^{-5}$
$\hat{K}_B$ (mm. Hg. <sup>-1</sup> )	2.33	0.463	0.122.
$\hat{K}_{H_2S}$ (mm. Hg. <sup>-1</sup> )	0.234	0.0884	0.0422

The above table shows that both butene and hydrogen sulfide retard the rate of butane formation significantly, with butene exerting the stronger effect. The adsorptions of both butene and hydrogen



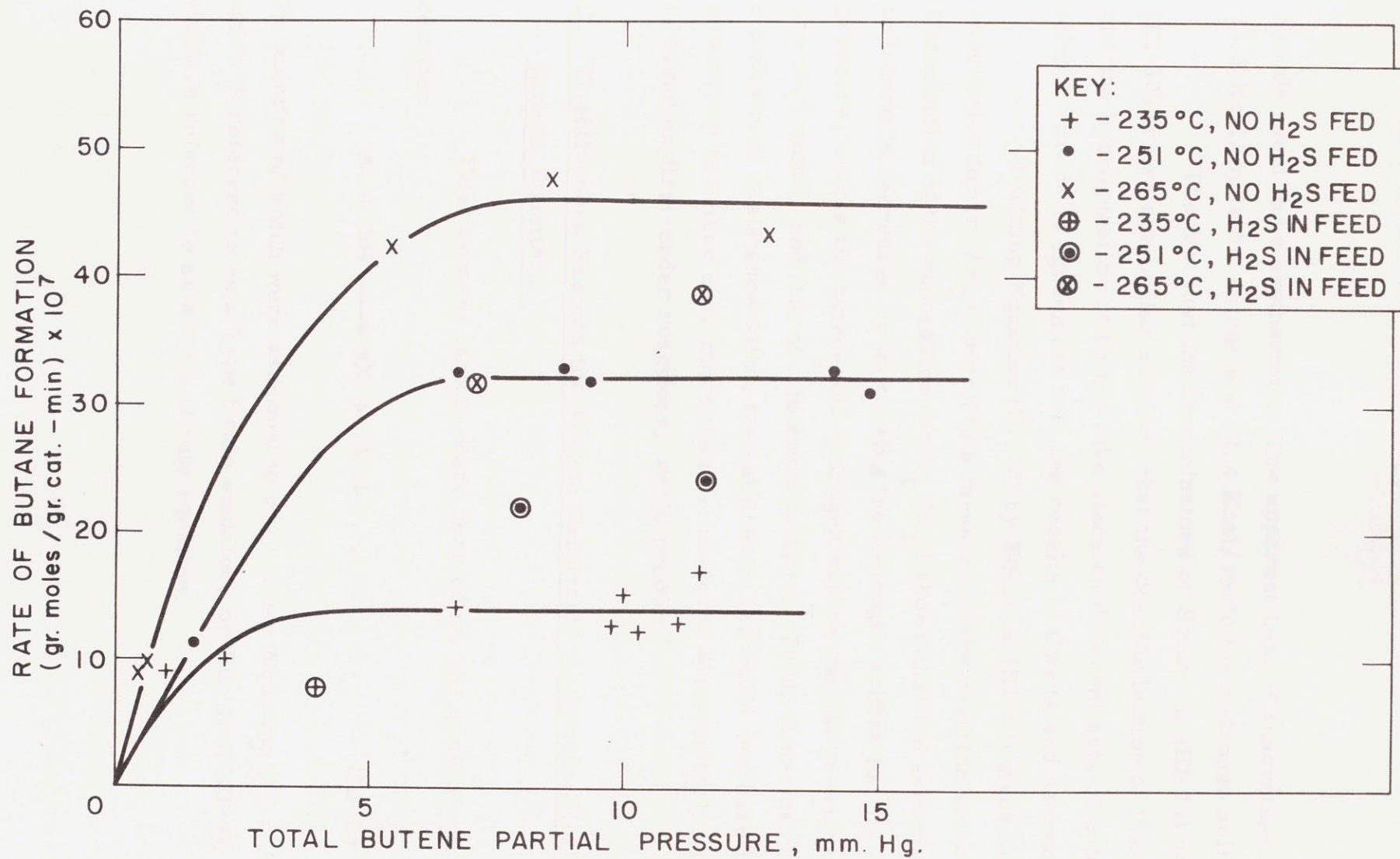


FIGURE III-5 RATE OF BUTANE FORMATION VERSUS TOTAL BUTENE PARTIAL PRESSURE



sulfide seem to be exothermic. The apparent heat of adsorption is 53.8 Kcal/ mole for butene and 32.4 Kcal/ mole for hydrogen sulfide.

The fact that the denominators of Equations (III-19) and (III-32) are so dissimilar suggests that the desulfurization of thiophene and the hydrogenation of butene take place on different sets of catalyst sites. This is in agreement with the results of Owens and Amberg (45).

Dividing Equation (III-32) by Equation (III-19) gives an expression for  $(r_C / r_T)$ , which is a measure of the reaction selectivity. Examination of the expression for  $(r_C / r_T)$  shows that the selectivity to butene is decreased by increasing the hydrogen sulfide partial pressure, unless the butene and hydrogen sulfide partial pressures are very small, and that of thiophene is large. Thus, it seems that a diffusional resistance within the catalyst pellet would decrease the selectivity to butene even more than the model of Wheeler (83), which is based on first-order reactions, would predict.

### C. Effectiveness Factors for Porous Catalysts: Langmuir-Hinshelwood Kinetic Equations

Effectiveness factors were derived for the general catalytic reaction



the kinetics of which were assumed to obey either Equation (III-6), which is referred to as a Type I rate equation, or Equation (III-9), which is referred to as a Type II rate equation.



$$r_A = k_I p_A / (1 + K_A p_A + \sum_i K_i p_i) \quad (\text{III-6})$$

$$r_A = k_{II} p_A p_B / (1 + K_A p_A + \sum_i K_i p_i)^2 \quad (\text{III-9})$$

The effective diffusivities of all species were assumed to be constant, but not necessarily equal. The catalyst was assumed to be a semi-infinite slab of width  $L$ , exposed to the gas stream on one face and sealed on the other.

A relation between  $p_A$  and  $p_i$  was derived. Substitution of this expression into Equations (III-6) and (III-9) reduced these equations to forms containing  $p_A$  as the only variable. The differential equation describing the simultaneous diffusion and reaction of A inside the catalyst particle was then integrated. This integration was performed in two steps: the first step was accomplished analytically, but the second step required a numerical procedure. The result of the last step was the value of the effectiveness factor,  $\eta$ .

For Type I rate equations,  $\eta$  is a function of two dimensionless parameters: a modified Thiele modulus,  $\Phi_{MI}$ , and the quantity  $Kp_{A,s}$ , which is the product of a modified adsorption constant,  $K$ , and the partial pressure of A at the exposed surface of the catalyst,  $p_{A,s}$ . If the reaction is strongly inhibited by reaction products, the value of  $Kp_{A,s}$  approaches -1. If strong reactant inhibition occurs,  $Kp_{A,s}$  is a large, positive number.

A plot of  $\eta$  versus  $\Phi_{MI}$  was prepared for a family of  $Kp_{A,s}$  values ranging from -0.98 to 50. The catalyst effectiveness can be estimated by means of this plot if the intrinsic kinetic equation, the effective diffusivities and the operating conditions are known.



A plot of  $\eta$  versus the dimensionless modulus  $\Phi_L$  was also prepared, for the same values of  $Kp_{A,s}$ . Since  $\Phi_L$  can be computed directly from experimental data without knowing the intrinsic kinetic equation, the probable presence or absence of internal diffusion effects can be checked directly from a measured reaction rate, by means of the  $\eta - \Phi_L$  plot.

The  $\eta - \Phi_L$  plot for Type I reactions is given in Figure IV-4. This figure shows that when the reaction is strongly inhibited by reaction products, the  $\eta - \Phi_L$  curve lies significantly below the  $\eta - \Phi_L$  curve for a second-order reaction. Therefore, the criterion of Weisz and Prater (80) for the absence of diffusion effects is not generally valid, since it is implicitly based on the assumption that the  $\eta - \Phi_L$  curve for a second-order reaction lies lower than the same curve for any other realistic kinetic equation. Several examples of rate equations whose  $\eta - \Phi_L$  curves fall significantly below the second-order curve were found in the literature (18), (38), (77).

For Type II rate equations,  $\eta$  is a function of three dimensionless parameters: a different modified Thiele modulus,  $\Phi_{MII}$ ,  $Kp_{A,s}$ , and a modified stoichiometric excess at the pellet surface,  $E$ . Three plots of  $\eta$  versus  $\Phi_{MII}$  were prepared, for values of  $E$  equal to 0, 1 and 10. Each of these plots covers a range of  $Kp_{A,s}$  values from -0.90 to 100.

Figure IV-7 is the  $\eta - \Phi_{MII}$  plot for  $E = 10$ . This figure shows that, under certain circumstances, effectiveness factors greater than unity can occur under isothermal conditions and that, if  $\eta$  is greater than one, the effectiveness factor may be a triple-valued function of  $\Phi_{MII}$ . The occurrence of these effects is not, however, limited to the values of  $Kp_{A,s}$  and  $E$  on which Figure IV-7 is based. A consequence of the multiplicity in the  $\eta - \Phi_{MII}$  curve

is that operation may be unstable in the region of multiplicity and that the steady-state reaction rate may depend on the direction from which steady-state is approached.

Plots of  $\eta$  versus  $\Phi_L$  were also prepared for the same values of  $E$ , and the same range of  $Kp_{A,s}$  values. These plots confirmed the conclusion, reached earlier, that strong product inhibition causes an internal diffusional retardation to set in under milder conditions than would be predicted by the Weisz and Prater criterion.

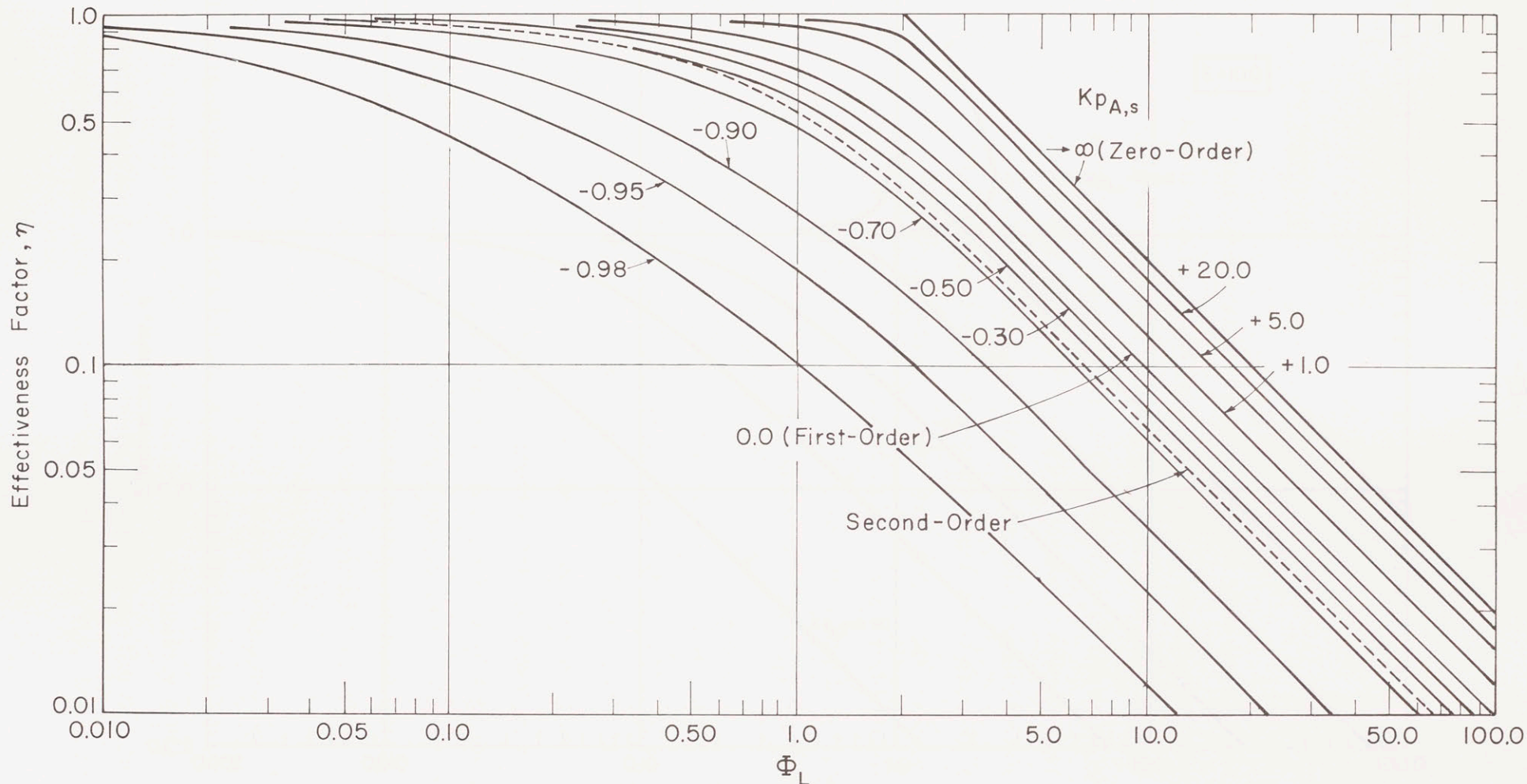


Figure IV-4 Effectiveness Factor,  $\eta$ , as a Function of the Modulus  $\Phi_L$ , Type I





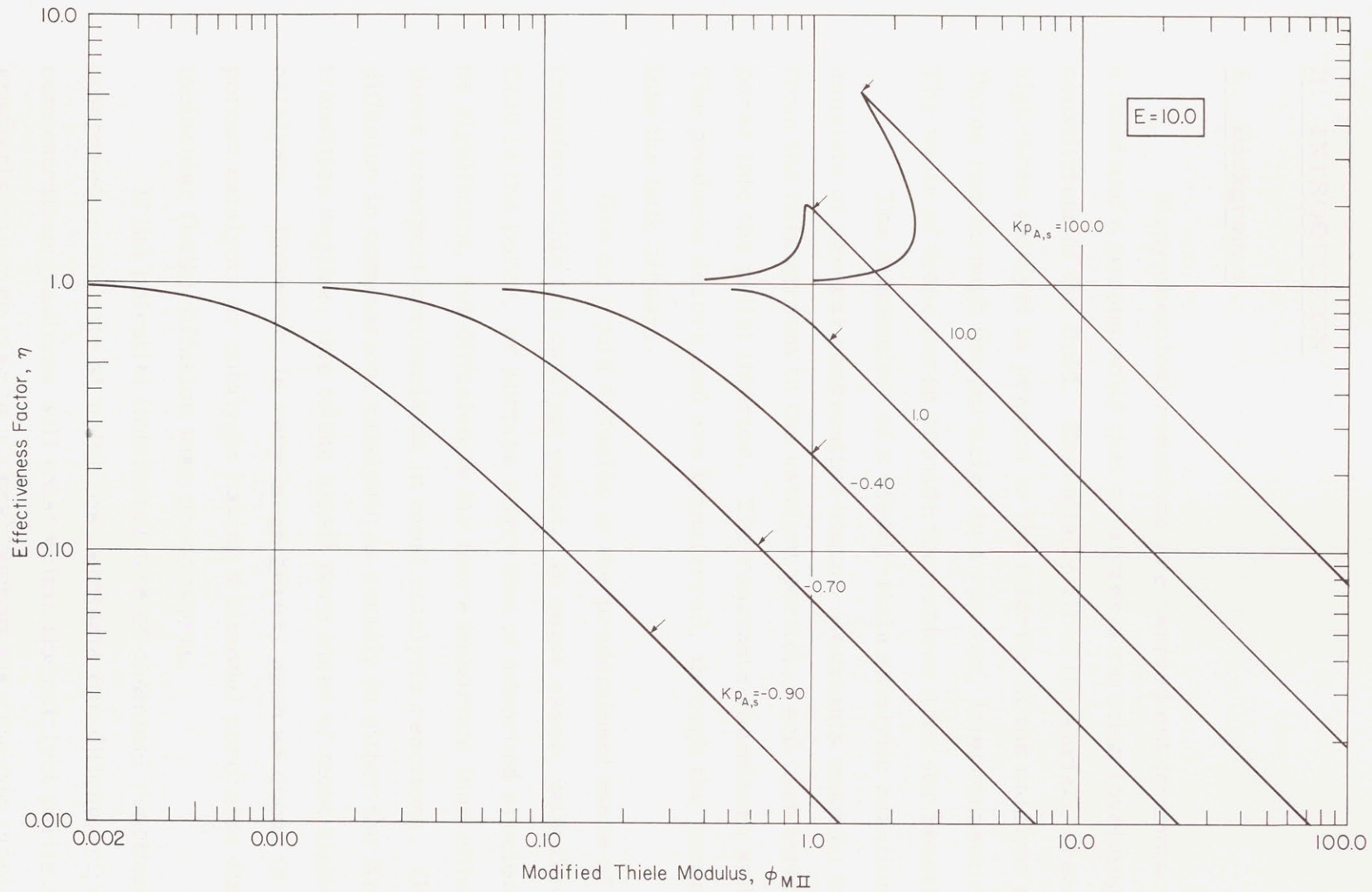


Figure IV-7 Effectiveness Factor as a Function of the Modified Thiele Modulus,  $\phi_{MII}$ , for Various Values of  $K\rho_{A,s}$ ;  $E = 10.0$



## II. INTRODUCTION

### A. Background

Many chemical reactions are carried out by contacting a fluid and a porous solid that catalyzes a reaction involving some constituent of the fluid. Essentially all of the surface area of a high-area catalyst is present in the interior of the catalyst particles. Pores run through the particles in a random, interconnecting fashion. The walls of these pores provide the surface area for reaction.

The mechanism of a steady-state catalytic reaction, then, consists of several consecutive steps. Reactants must be transferred from the bulk stream to the catalyst particle, and then through the pores into the pellet interior. The reactants chemisorb and react. The products desorb and are transferred, through the pores, back into the bulk stream.

Gas or liquid diffusion is the predominant mode of mass transfer within the catalyst pellet. In some cases, bulk flow of fluid in the pores, or surface migration of adsorbed species might be significant, but diffusion is far more important than either of these transport mechanisms in most catalytic reactions. Gaseous diffusion in commercial catalysts is usually in either the Knudsen or transition regime, due to the small pore sizes of most high-area catalysts. However, in very large pores, such as occur in low-area porous catalysts or catalysts having a bimodal pore-size distribution, molecular (bulk) diffusion may predominate.

If the potential (intrinsic) rate of chemical reaction is large compared to the rate at which the reactants can diffuse, significant concentration gradients will exist within the catalyst particle. Such gradients can give rise to several phenomena, the two most important being a change in the apparent catalytic activity, and a change in the



apparent selectivity if more than one reaction is occurring. Temperature gradients within the catalyst can also contribute to these effects.

The influence of an intraparticle diffusional resistance on the apparent activity of catalysts has been experimentally established by many investigators. Studies confirming the effect have been summarized in a recent book (60). The number of experimental demonstrations of the selectivity effect is not as large, but several studies have appeared in the literature (7), (81).

It is important to be able to predict the conditions under which intraparticle concentration gradients will occur, and the effect of these gradients on activity and selectivity. A knowledge of the activity and selectivity, and how they vary with process conditions, is necessary in the design of commercial reactors. Scale-up of experimental data would be dangerous if a method of predicting the effect of an intraparticle diffusional resistance were not available. Moreover, it has been suggested (16) that in certain cases an optimum reactor design would require operation with concentration gradients present in the catalyst particle. A quantitative method for predicting the effects of a diffusional retardation is therefore necessary. Another important use for a quantitative treatment of the phenomena occurs in experimental catalytic studies, where it must be established that the results were not influenced by internal diffusion.

The earliest quantitative treatments of diffusion within catalyst pellets dealt with a single reaction only. Thiele (69), and Zeldowitsch (85) presented the first results and their work was later extended by Wheeler (83) and Weisz and Prater (80) to include a wide range of reaction orders, pellet geometries and degrees of molal change. For all cases, the modification of the apparent activity is best presented by means of the "effectiveness" or "effectiveness factor", which is usually denoted by the symbol  $\eta$ , as defined in



Equation (II-1) below.

$$\eta = \frac{\text{actual rate per pellet}}{\text{rate if internal gradients were absent}} \quad (\text{II-1})$$

In order to determine the effectiveness factor, the differential equations describing the simultaneous diffusion and reaction of the reactant inside the catalyst particle must be solved, subject to the appropriate boundary conditions. The result of such a solution is the concentration profile of the reactant within the pellet. The reaction rate per pellet can be derived from this concentration profile.

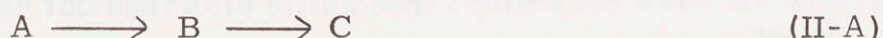
In order to formulate a differential equation, the rate equation and the diffusion equation must be known. Most investigators have assumed that diffusion follows Fick's law with a constant diffusion coefficient, and have further assumed that the reaction rate is proportional to the reactant concentration to either the zero, first or second power.

Kinetic expressions which are proportional to the reactant concentration to an integer power are reasonably accurate over a limited concentration range, but more fundamental and complex forms are usually required to describe heterogeneous catalytic reaction rates over wide ranges of partial pressure. The most frequently used complex form is the Langmuir-Hinshelwood type of rate equation. This type of rate equation permits a simple mathematical description of any inhibition of the reaction rate by either reactants or reaction products; inhibition effects are important in many catalytic reactions. Even though integer-power rate expressions do not adequately describe such effects, only very limited attention has been given to deriving effectiveness factors for more complex kinetic equations.

Besides affecting the apparent catalytic activity, a diffusional resistance within a porous catalyst can also influence the apparent

selectivity, if more than one reaction is taking place. However, the specific effect of a diffusional resistance depends on the relation to each other of the reactions taking place. Wheeler (83) qualitatively described the selectivity modification that would be expected for: 1) branching reactions; 2) successive reactions; and 3) competing reactions. Quantitative treatments of the selectivity for branching reactions have been presented (43), (48), as have quantitative treatments of successive reactions (12), (81), (83), competing reactions (83), and the so-called triangular reactions (78). The method of calculating the reaction selectivity is similar to that for calculating the catalyst effectiveness, except that the number of simultaneous differential equations that must be solved is larger.

The effect of internal diffusion on successive reactions can be important. Thus, considering the model reaction,



if a diffusional retardation is present, the intermediate B becomes "trapped" in the catalyst pores, and the yield of B relative to C is decreased. Depending on whether B or C is the desired material, this situation can be undesirable or advantageous. This qualitative argument however, is implicitly based on the assumption that both reaction steps follow integer-order kinetics. For some other types of kinetic behavior, specifically behavior involving inhibition of the second step of the reaction by products of the first step, it is not clear that the yield of B will be decreased. Inhibition of the second step might possibly be so severe that the yield of B would be increased. Despite the unusual selectivity effects that complex rate equations might create, to date all quantitative treatments of the diffusional retardation of successive reactions have assumed that both reactions are first-order.



## B. Thesis Objectives

The fundamental purpose of the present work was to lay the basis, both theoretically and experimentally, for predicting and understanding the activity and selectivity effects that can occur when pore diffusion is important in a catalyst particle, and when the kinetics of the chemical reactions are best described by complex rate equations. The thesis had two specific objectives.

The first objective was to mathematically derive effectiveness factors for a wide range of Langmuir-Hinshelwood rate equations, in a form such that the catalyst effectiveness could be predicted either from experimental data or from a knowledge of the intrinsic reaction kinetics. The attainment of this objective would, for the first time, allow the effectiveness factor to be predicted to the accuracy with which the effective diffusivity is known.

The second objective was to experimentally determine the intrinsic kinetics for both steps of a successive reaction of the form shown in (II-A), for a reaction where integer-order rate equations were likely to be inadequate kinetic models. The experimental phase of the thesis was designed to facilitate subsequent experimental investigations of the effect of an intraparticle diffusion resistance on the activity and selectivity of the reaction. An experimental study is a logical first step in the investigation of the effect of pore diffusion on selectivity, since a mathematical treatment would be difficult, and its value would be doubtful until an experimental study had been made. However, a knowledge of the intrinsic kinetics of the reaction must be available before the selectivity effect can be studied experimentally in a quantitative manner.

The hydrogenolysis of thiophene, which is frequently used as a prototype for hydrodesulfurization reactions, was selected as

the reaction to be studied. The determination of a kinetic equation for this reaction, besides contributing to a future selectivity study, might lead to a better understanding of the design and operation of commercial hydrodesulfurization reactors.



### III. THE KINETICS OF THIOPHENE HYDROGENOLYSIS

#### A. Literature Review and Criticism

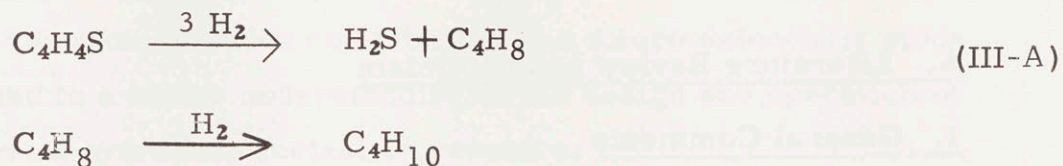
##### 1. General Comments

Thiophene is one of the simplest sulfur-containing cyclic compounds. Consequently, its hydrogenolysis is of industrial interest as a prototype of the reactions taking place in commercial hydrodesulfurization processes such as Hydrofining and Unifining. Because of this, many studies of the reaction have been carried out at conditions similar to those that are used in commercial units (22), (39), (40). Typically, industrial reactors operate at temperatures around 400°C and pressures up to 1000 psig. However, a few studies of the reaction have been made at atmospheric pressure and temperatures between 200 and 400°C (20), (29), (45), (46), (73). The present study was carried out in the latter region.

Thiophene hydrogenolysis has been carried out over a variety of catalysts including chromia-alumina, vanadium pentoxide, nickel sulfide, molybdenum sulfide and the so-called cobalt molybdate catalyst, which, under reaction conditions, is a cobalt-molybdenum sulfide. A cobalt molybdate catalyst on an alumina support is used in most commercial processes and was the catalyst employed in this work. In general, as McKinley (36) has pointed out in an excellent review, any hydrogenation catalyst may be employed for hydrodesulfurization. The catalyst support can be quite important in the reaction, in that it may or may not contribute hydrocracking activity. Alumina carriers have minor hydrocracking activity (36).

In all of the previous atmospheric pressure studies of thiophene hydrogenolysis, substantial amounts of butene have been detected in the reaction products. Investigators agree that butene is an intermediate in the formation of butane, the final product. Thus,

the reaction scheme may be written



and it can be seen that the reaction is of the form discussed earlier, and given in (II-A). In (II-A), the reactant A corresponds to thiophene, the intermediate B to butene, and the final product C corresponds to butane.

The thermodynamics of the reaction are known, and pertinent quantities are given in Table III-1. These quantities correspond to a temperature of 500°K, which is close to that used in the present study.

Table III-1 (19),(36)

Thermodynamic Properties for Thiophene Hydrogenolysis

<u>Reaction</u>	<u>log<sub>10</sub> K<sub>f</sub></u>	<u>ΔH°<sub>R</sub> (Kcal/ mole)</u>
A → B	5.57	-44.21
B → C	6.49	-34.14
A → C	12.06	-78.35

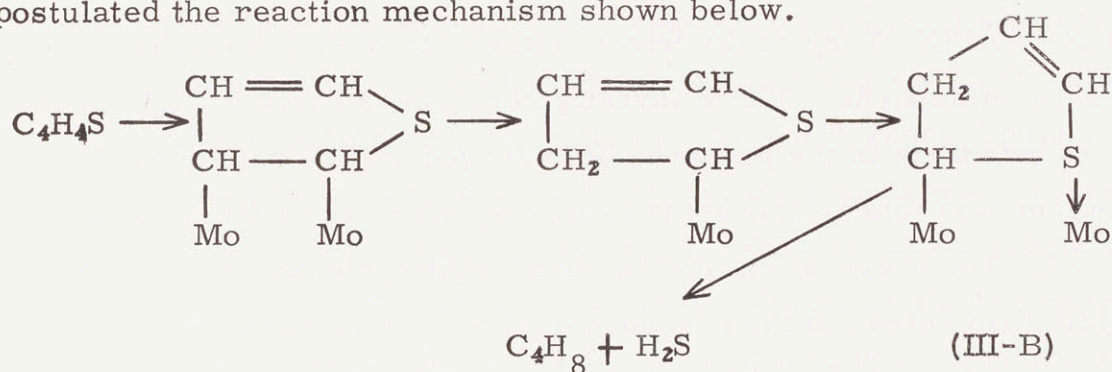
The large values of the equilibrium constants for the individual reaction steps insure that both steps can justifiably be assumed to be irreversible.

## 2. Reaction Mechanism

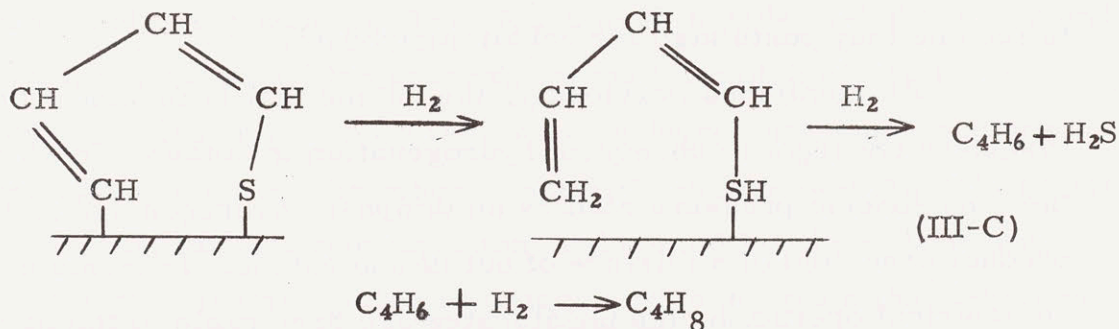
All investigators who have speculated about the probable reaction mechanism agree that the reaction proceeds in a series of consecutive steps, but the nature of the steps involved has been disputed.



Early investigators (13), (40), working at commercial conditions, found that tetrahydrothiophene was a product of thiophene hydrogenolysis, and suggested that this compound was a reaction intermediate. However, Griffith, Marsh, and Newling (20), using nickel and molybdenum sulfide catalysts at atmospheric pressure, in the region 200-500°C, could not detect the presence of tetrahydrothiophene. They suggested that the presence of this compound in the earlier work was the result of a catalyst that was not fully sulfided. Griffith, Marsh and Newling postulated the reaction mechanism shown below.



Komarewsky and Knaggs (29) studied the reaction at 400°C over a vanadium oxide catalyst supported on alumina. They detected butadiene in the reaction products and speculated that mercaptans were also present. On this basis, these investigators proposed a slightly different mechanism.



The above mechanism differs from the previous one in two respects: 1) two-point adsorption on the catalyst surface takes place by a carbon-sulfur linkage in (III-C), rather than by opening the carbon-carbon double bond as in (III-B); 2) the initial step in (III-C) is scission and hydrogenation of the carbon-sulfur bond, as opposed to hydrogenation of the double bond in (III-B).

Owens and Amberg (45) studied thiophene hydrogenolysis over a cobalt molybdate catalyst on an alumina support between 200 and 400°C. They could detect neither butadiene, mercaptan, nor tetrahydrothiophene. These investigators also studied the hydrogenation of butadiene in the presence of hydrogen sulfide and found that butadiene was totally converted to butene, with very little butane formed. The observation that butadiene hydrogenates much more rapidly than butene in the presence of H<sub>2</sub>S has also been made by Kirsch and Shull (27). This difference in relative hydrogenation rates led Owens and Amberg to conclude that butadiene was a reaction intermediate and that the first step in the reaction was C-S bond cleavage, rather than hydrogenation of the ring. In studies of thiophene hydrogenolysis over a chromia catalyst, Owens and Amberg (45),(46) were able to detect butadiene, but no organo-sulfur compounds. They concluded, therefore, that the reaction mechanism was similar to the one they postulated for cobalt molybdate.

As mentioned previously, the butene that is formed from thiophene undergoes subsequent hydrogenation to butane. In all of the atmospheric pressure studies on thiophene hydrogenolysis, the product consisted of a mixture of butene and butane. In terms of commercial operation, the unsaturates are preferable to the saturates, and there has been effort to find a catalyst that will desulfurize without hydrogenating the monoolefins (21). For the atmospheric pressure studies, the chromia catalyst of Owens and Amberg (45)



shows the best selectivity in this respect, with the C<sub>4</sub> product containing only about 9% butane in one run at 415°C. With their cobalt molybdate catalyst, these investigators found a "typical" distribution of 21% butane and 79% butene in the range between 270 and 400°C. They reported that the distribution was not strongly temperature dependent. Unfortunately, since most of the Owens and Amberg work was done in a microreactor, it is impossible to draw conclusions as to the effects of concentration and residence time on the butene-butane distribution. Griffith, Marsh and Newling stated that the hydrocarbon portion of the reaction product was approximately 60% butene and 40% butane, but the effect of temperature and concentration on these percentages was not explored. Komarewsky and Knaggs studied the effect of liquid hourly space velocity on the butene-butane distribution. At an LHSV of 0.02, the hydrocarbon product was about 90% butane; this percentage decreased to about 45% at an LHSV of 0.20. The increase in the conversion of butene to butane as the residence time increases is reasonable.

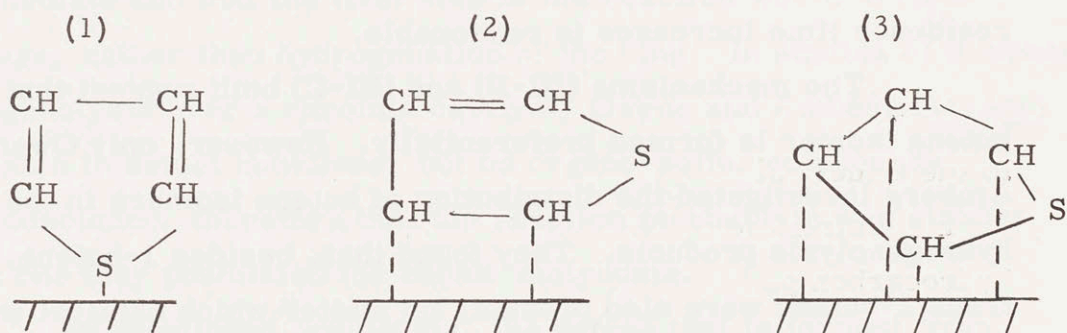
The mechanisms (III-B) and (III-C) both suggest that the 1-butene isomer is formed preferentially. However, only Owens and Amberg investigated the distribution of butene isomers in the thiophene hydrogenolysis products. They found that, besides 1-butene, cis and trans 2-butene were also present, no matter which catalyst was employed. Isobutene, however, was not found, nor was isobutane. Over both catalysts, the concentration of 1-butene was slightly greater than the equilibrium concentration, calculated for the double-bond and cis-trans isomerization reactions. This suggests that 1-butene is the first product in the reaction sequence and then undergoes a fairly rapid isomerization to 2-butene. The presence of the isomerization reaction was confirmed by Owens and Amberg by making a run with pure 1-butene feed; isomerization to 2-butene took place.

In both studies, the ratio of cis to trans 2-butene was higher than equilibrium.

Kirsch and Shull presented similar results in their study of butadiene and butene hydrogenation over sulfided cobalt molybdate catalyst. Again, no skeletal isomerization to isobutene took place; the ratio of 1-butene to 2-butene was higher than equilibrium, and the ratio of cis to trans 2-butene was also higher than equilibrium.

### 3. Adsorption of Reaction Components

In an effort to elucidate the reaction mechanism, several investigators have studied the adsorption of various reaction components on the catalyst. Nicholson (42) used infrared spectrometry to study the adsorption of thiophene on various cobalt molybdate and molybdenum sulfide catalysts. His catalyst samples were presulfided before use and were held at about 400°C during adsorption. The three types of adsorption shown below were identified.



Owens and Amberg (45) studied the adsorption of thiophene, the C<sub>4</sub>'s, H<sub>2</sub> and H<sub>2</sub>S by measuring the delay in the appearance of their peaks when samples of these materials were injected into a carrier gas flowing through a bed of cobalt molybdate catalyst. Thiophene adsorption was studied between 125 and 233°C using hydrogen as a carrier. Some reaction, therefore, took place.



The thiophene peak delay was temperature sensitive, having a coefficient of about 9.5 Kcal/ mole of thiophene, thus suggesting a relatively slow adsorption-desorption process. In fact, the data indicated that a small portion of the thiophene is adsorbed irreversibly. Attempts to use nitrogen as a carrier gas were unsuccessful because thiophene adsorption was very strong, and a significant portion of the adsorption was irreversible in the presence of nitrogen. This observation implies that hydrogen is preferentially adsorbed on certain very active sites, thereby blocking thiophene adsorption. The authors also found that hydrogen sulfide that was adsorbed on the catalyst reduced the thiophene peak delay by 10 to 30 percent, which suggests a competition between thiophene and hydrogen sulfide for catalyst sites.

Owens and Amberg conducted all their butene adsorption studies in the presence of hydrogen sulfide in order to repress hydrogenation to butane. They found that butene adsorption was faster and more reversible than thiophene adsorption. The temperature coefficient was about 8.5 Kcal/ mole. As with thiophene, adsorption was very strong unless a hydrogen carrier gas was used.

Two modes of hydrogen adsorption from an inert carrier could be distinguished. One was a very rapid adsorption, the other being appreciably slower. Subsequent experiments showed that although both types of sorbed hydrogen could react with thiophene, the reaction occurred primarily with the rapidly desorbing hydrogen. It was also experimentally established that thiophene cannot successfully compete with hydrogen for adsorption sites.

Studies of the adsorption of hydrogen sulfide on a fully-sulfided catalyst showed two types of adsorption. The first was an irreversible adsorption, the absolute amount of which was dependent on temperature. The second type exhibited a very rapid adsorption

and a desorption whose rate was approximately proportional to surface coverage. It was also shown that hydrogen could displace hydrogen sulfide from the catalyst surface.

Owens and Amberg (47) used the same technique to study the adsorption of thiophene, butene, hydrogen and hydrogen sulfide on a sulfided chromia catalyst at reaction temperatures. The results were very similar to those for cobalt molybdate in all major respects, except that the retention volumes of thiophene and butene were the same in both hydrogen and helium carrier gases, and the retention volume of butene was not affected appreciably by preadsorbed hydrogen sulfide. Owens and Amberg concluded that the rate of thiophene adsorption or butene desorption was unlikely to be rate-limiting but that the rate of hydrogen adsorption could not be eliminated as a possible controlling step.

Griffith, Marsh, and Newling also speculated that adsorption of hydrogen might be rate-controlling, based on the data of Badger, Griffith, and Newling (5). The latter, in a study of hydrogen and thiophene adsorption on molybdenum oxide-molybdenum sulfide between 0 and 300°C, found that hydrogen underwent a slow, reversible, activated adsorption which did not begin until 150°C.

The results of the adsorption studies described above should be generalized to reaction studies only qualitatively and even then with the greatest caution. In the first place, only a small fraction of adsorption sites contribute to reaction, and, in an adsorption study, the behavior of these sites may be obscured. Secondly, the adsorption studies were not all made under conditions similar to those for reaction. Consequently, the catalyst surface may have been different than during reaction.



#### 4. Reaction Kinetics

No detailed investigation of the kinetics of thiophene hydrogenolysis has been made to date. However, some information is available that may contribute at least qualitatively to an understanding of the reaction kinetics and may help in formulating a rate equation.

Griffith, Marsh and Newling measured the rate of thiophene disappearance over nickel sulfide and molybdenum oxide-molybdenum sulfide catalysts in an integral reactor at temperatures ranging from 200 to 500°C. Initial thiophene concentrations were between 150 and 550 parts per million, the remainder of the feed being hydrogen. On nickel sulfide, the reaction was very nearly first-order in thiophene. On molybdenum oxide-molybdenum sulfide, the order was between 0.20 and 0.60; the order increased as the temperature was raised or the thiophene concentration lowered. On pure molybdenum sulfide, the order with respect to thiophene was very nearly zero. Hydrogen sulfide in the feed was found to retard the reaction to a certain extent, but full activity was recovered when addition of hydrogen sulfide was stopped. Ethylene exhibited a similar effect. However, with cyclopentadiene poisoning was permanent and progressive.

During one series of runs, Owens and Amberg (46) operated their microreactor as a steady-state, integral reactor. The catalyst was sulfided chromia and the feed was hydrogen containing about 7 percent thiophene. Runs were made between 260° and 400°C; in this region the activation energy of the reaction was about 25 Kcal/mole. Reaction rates measured by injecting pulses of thiophene into a hydrogen stream did not check well with the steady-state data. In a subsequent study (47), Owens and Amberg found that preadsorbed hydrogen sulfide had a slight inhibiting effect on both thiophene hydrogenolysis and subsequent butene hydrogenation. This conclusion is

somewhat uncertain, however, since it is based on data obtained by injecting thiophene pulses into the reactor.

Two studies have been made on the kinetics of the reaction over a cobalt molybdate catalyst. Pease and Keighton (49) studied the hydrodesulfurization of thiophene in the presence of benzene and nitrogen, using an integral flow reactor. The temperature was 200°C and the thiophene concentration in the feed was between 0.1 and 0.7 percent. Pease and Keighton found that the reaction rate was independent of the benzene and nitrogen concentrations, and almost independent of the hydrogen concentration. The latter observation suggests that hydrogen adsorption is not rate-limiting on this catalyst. The reaction order with respect to thiophene was less than first; the authors suggested that this might have been due to inhibition by a reaction product.

Owens and Amberg (45), using an integral flow reactor with a feed containing 2 percent thiophene in hydrogen, found the disappearance of thiophene to have an activation energy of 25 Kcal/mole in the temperature region 270 to 400°C. However, as with the results on sulfided chromia, the apparent activation energy declined at high conversions. This decline may be due to one or both of two effects. The calculation of the activation energy was based on a plot of the percent conversion versus the reciprocal of the absolute temperature. Such a plot is theoretically valid only for zero-order reactions. For a reaction greater than zero-order, the plot should show downward curvature at high conversions. The actual downward curvature makes this explanation plausible, but it is also possible that the variation in activation energy reflects a mechanism that is changing, either with temperature or with concentration. Hinshelwood (23) has shown that the activation energy can be affected by changes in the surface coverage of either reactants or products. Once again, reaction rates measured by injecting pulses of thiophene did not check



the steady-state runs. However, using the pulse technique, it was established that preadsorbed hydrogen sulfide lowered thiophene conversion appreciably, and had an even greater effect on butene hydrogenation. The authors interpreted this to mean that desulfurization and hydrogenation took place, at least to some extent, on different sites. This view was supported by the finding that hydrogen sulfide had no effect on either the isomerization of butene or the hydrogenation of butadiene.

In order to test the effect of olefin adsorption on the rate of desulfurization, Owens and Amberg measured the conversion of shots of thiophene in the presence of hexene. When equimolar amounts of hexene and thiophene were injected, the retardation of thiophene hydrogenolysis was insignificant. Conversion was lowered by about 20% when the hexene to thiophene ratio was 3:1. On the basis of this information, it seems unlikely that butene adsorption could seriously retard the desulfurization of thiophene.

It should be emphasized that care must be taken in interpreting the results of unsteady-state kinetic experiments, such as the microreactor runs of Owens and Amberg. The condition of the catalyst surface is undoubtedly not the same as during a steady-state run, because the adsorption and desorption of hydrogen sulfide and hydrogen are not infinitely rapid. Since these species have an important influence on the reaction kinetics, the unsteady-state results described above should be viewed as qualitative.

## 5. The Cobalt Molybdate Catalyst

Despite their widespread use, very little is known about the structure of cobalt molybdate catalysts, especially under reaction conditions. The most comprehensive study of this catalyst to date has been done by Richardson (55), who used magnetic susceptibility



techniques to investigate the nature and composition of the components of a "fresh", i. e., unsulfided, catalyst. Richardson's catalysts were prepared by impregnating  $\gamma$ - $\text{Al}_2\text{O}_3$  with solutions of cobalt acetate and ammonium paramolybdate, followed by air drying and heat treatment. Although this was not the procedure used to manufacture the catalyst used in this study, the Mo: $\text{Al}_2\text{O}_3$  ratio (0.10) is the same for both catalysts and the Co: Mo ratio for the present catalyst (0.35) is within the range studied by Richardson (0.10 to 1.0).

According to Richardson, the "fresh" catalysts are mixtures of  $\text{Al}_2\text{O}_3$  and  $\text{CoAl}_2\text{O}_4$ , both of which are inactive for hydrodesulfurization,  $\text{CoO}$ ,  $\text{MoO}_3$ , and  $\text{CoMoO}_4$ , all of which have moderate activity, and a highly-active "complex Co-Mo oxide".  $\text{CoMoO}_4$  does not exist in catalysts heat treated below  $650^\circ\text{C}$ , and  $\text{CoO}$  does not exist if heat treatment took place above this temperature.

Since  $\text{Co}^{+2}$  ions occur in an octahedral environment of oxygen ions in all of the above cobalt compounds except  $\text{CoAl}_2\text{O}_4$ , where a tetrahedral environment exists, measurements of the magnetic susceptibility of the fresh catalyst allowed the fraction of cobalt existing as  $\text{CoAl}_2\text{O}_4$  to be calculated. By treating the catalyst in  $\text{H}_2$  at  $400^\circ\text{C}$ , all the cobalt in  $\text{CoO}$  or  $\text{CoMoO}_4$  was reduced to the metal and the magnetic susceptibility was again measured. The fraction of cobalt existing as either  $\text{CoO}$  or  $\text{CoMoO}_4$  could then be calculated, since cobalt in  $\text{CoAl}_2\text{O}_4$  and the active complex does not reduce. Thus, with the amount of cobalt in the active complex determined by difference, the Co:Mo ratio in the active oxide was calculated.

For one series of catalysts, Richardson held the initial Co:Mo ratio at unity and varied the temperature of heat treatment, with the following results: at low temperatures,  $\text{CoAl}_2\text{O}_4$  existed and as the

temperature of heat treatment was raised the amount of  $\text{CoAl}_2\text{O}_4$  increased at the expense of  $\text{CoO}$  and the active cobalt complex. At a temperature of  $650^\circ\text{C}$ ,  $\text{CoMoO}_4$  begins to form at the expense of  $\text{CoAl}_2\text{O}_4$ . As the temperature is raised further, the amounts of both  $\text{CoMoO}_4$  and active cobalt complex increase as the amount of  $\text{CoAl}_2\text{O}_4$  declines. In other experiments, Richardson varied the initial Co:Mo ratio and heat-treated all catalyst samples at the same temperature. Even at temperatures less than  $650^\circ\text{C}$ , no  $\text{CoAl}_2\text{O}_4$  formed until the initial Co:Mo ratio exceeded 0.30. For values of this ratio less than 0.30, most Co went to form the active complex, with a small amount going into  $\text{CoO}$ . When the value of the initial Co:Mo ratio exceeds 0.30, the formation of  $\text{CoAl}_2\text{O}_4$  maintained the Co:Mo ratio in the active species at 0.30 when the temperature of heat treatment was  $530^\circ\text{C}$ . At a temperature of  $650^\circ\text{C}$ , the active Co:Mo ratio reached a maximum of 0.30 when the initial ratio was 0.30, but decreased slightly as the initial ratio was increased, as a result of the formation of  $\text{CoAl}_2\text{O}_4$ . Below an initial ratio of 0.30, the temperature of heat treatment had no effect on the Co:Mo ratio in the active species.

In an auxiliary study, Richardson tested the activity of his catalysts, and several commercial catalysts, for the desulfurization of a gas oil fraction. Maximum activity occurred when the Co:Mo ratio in the active species was about 0.18.

When a desulfurization reaction takes place over a cobalt molybdate catalyst, hydrogen sulfide is the main sulfur-containing product. Some of the previously-mentioned components of the "fresh" catalyst exist as sulfides, rather than oxides, when exposed to  $\text{H}_2\text{S}$  at reaction temperatures.  $\text{Al}_2\text{O}_3$  and  $\text{CoAl}_2\text{O}_4$  do not sulfide, but  $\text{CoO}$  sulfides to  $\text{Co}_9\text{S}_8$ ,  $\text{CoMoO}_4$  sulfides to a mixture of  $\text{Co}_9\text{S}_8$  and either  $\text{MoOS}$  or a mixture of  $\text{MoO}_2$  and  $\text{MoS}_2$ .  $\text{MoO}_3$  sulfides



completely to  $\text{MoS}_2$ . Both  $\text{MoO}_2$  and  $\text{MoS}_2$  are mildly active, but Richardson concluded that the true catalyst is  $\text{MoS}_2$  promoted with cobalt. Presumably, this "true catalyst" results from the sulfiding of the complex Co:Mo oxide which was referred to earlier.

Examination of Figures 10 and 12 of Reference (36) reveals that  $\text{Co}_9\text{S}_8$  and  $\text{MoS}_2$  are the stable forms of the cobalt and molybdenum sulfides under the reaction conditions used in this study. Thus, some of Richardson's conclusions may be at least qualitatively valid for the present catalyst.

## 6. Langmuir-Hinshelwood Kinetic Equations

The type of kinetic equation that is commonly termed "Langmuir - Hinshelwood", and will henceforth be abbreviated L-H, is the result of Hinshelwood's application (23) of the adsorption theory of Langmuir (31) to heterogeneous catalytic reactions. It was assumed in Hinshelwood's original derivation that, in the sequence of steps of which the overall reaction consists, the rate-limiting step (RLS) is the surface reaction of an adsorbed specie or species. Hougen and Watson (25) later pointed out that rate expressions similar in form to Hinshelwood's equations could be derived from other assumptions about the RLS, for instance, that the overall rate of reaction is controlled by the rate of adsorption of one reactant, or the rate of desorption of a product. The term "Hougen-Watson" is generally applied to any rate equation in which one step is rate-limiting, be it adsorption, desorption or a surface process. The term Langmuir-Hinshelwood is reserved for expressions which are derived from the assumption that some surface reaction is the RLS. However, it is possible for one particular form of kinetic expression to be derivable from two or more different possible rate-limiting steps. All kinetic expressions developed in this thesis



are based on the "Langmuir-Hinshelwood" model and are so termed, but no specific RLS is implied.

A discussion of L-H rate equations is necessary for two reasons: 1) this type of rate equation has been used to correlate the experimental data on the rates of thiophene hydrogenolysis and butene hydrogenation; 2) the calculation of effectiveness factors, described in Section IV, is based on L-H rate equations.

Langmuir's adsorption theory provides a method for relating the equilibrium surface concentration of an adsorbed species to the partial pressure of that species. The following assumptions are involved: 1) adsorbed molecules are localized at definite sites on the surface; 2) the differential energy of adsorption is independent of surface coverage; 3) the maximum possible adsorption corresponds to a monolayer; 4) the rate of adsorption is proportional to the product of the partial pressure and the number of unoccupied sites; 5) the rate of desorption is proportional to the number of molecules adsorbed.

If these assumptions are made, an expression for the fractional surface coverage of any species, in terms of the partial pressures of all species present, may be derived by equating the rates of adsorption and desorption. The results may be summarized very simply. If no dissociation of any molecule occurs when adsorption takes place

$$\sigma_A = K_A p_A / (1 + K_A p_A + \sum_i K_i p_i) \quad (\text{III-1})$$

In Equation (III-1), the subscript  $i$  refers to any species other than A. Similarly, if a species A dissociates into two parts on adsorption,

$$\sigma_A = \sqrt{K_A p_A} / (1 + \sqrt{K_A p_A} + \sum_i K_i p_i) \quad (\text{III-2})$$

$$\sigma_i = K_i p_i / (1 + \sqrt{K_A p_A} + \sum_i K_i p_i) \quad (\text{III-3})$$

The constants  $K$  are commonly called adsorption constants.

In order to derive kinetic expressions from the above adsorption isotherms, some assumption about the rate-limiting step of the reaction must be made. Thus, consider the general reaction



Suppose that the rate-limiting step is the rearrangement, e.g., the decomposition or isomerization of undissociated, adsorbed A. The reaction rate is then proportional to  $\sigma_A$ , where  $\sigma_A$  is the fraction of the catalyst surface covered with adsorbed A.

$$r_A = k'' \sigma_A \quad (\text{III-4})$$

If the surface reaction is very slow compared to the other processes, adsorption equilibrium should be established for all species and (III-1) can be substituted into (III-4) to give

$$r_A = k'' K_A p_A / (1 + K_A p_A + \sum_i K_i p_i) \quad (\text{III-5})$$

$$r_A = k_I p_A / (1 + K_A p_A + \sum_i K_i p_i) \quad (\text{III-6})$$

Adsorption of a reactant can also be the rate-limiting step. In the reaction



Suppose that adsorption of A is the RLS. Then  $\sigma_A \cong 0$  and the reaction rate is given by

$$r_A = k_I p_A (1 - \sum_i \sigma_i) \quad (\text{III-7})$$

Now, if the rate of adsorption of A is very slow, then the net reaction rate is slow, and it is fair to assume that all other adsorptions are at equilibrium. Equations such as (III-1) are valid for all species except A; substitution of such equations into (III-7) gives

$$r_A = k_I p_A / (1 + \sum_i K_i p_i) \quad \text{(III-8)}$$

Note that Equations (III-6) and (III-8) are of the same form, even though the assumed RLS was different in each derivation.

In a similar manner, it can be shown that if, in (III-E), the RLS is the surface reaction between an adsorbed A and an adsorbed B, and if A and B are both undissociated,

$$\begin{aligned} r_A &= k'' \sigma_A \sigma_B \\ r_A &= k'' K_A p_A K_B p_B / (1 + K_A p_A + \sum_i K_i p_i)^2 \\ r_A &= k_{II} p_A p_B / (1 + K_A p_A + \sum_i K_i p_i)^2 \end{aligned} \quad \text{(III-9)}$$

If, in (III-E), adsorption of A is the RLS, and A dissociates on adsorption

$$\begin{aligned} r_A &= k' p_A (1 - \sum_i \sigma_i)^2 \\ r_A &= k' p_A / (1 + \sum_i K_i p_i)^2 \end{aligned} \quad \text{(III-10)}$$

The above derivations do not cover the whole range of situations that can occur in catalytic reactions. Detailed derivations for a variety of situations have been given by Hinshelwood, Hougen and Watson, and Walas (76).

The criticisms of the L-H approach to catalytic reaction rates have been summarized by Weller (82). It has been shown



experimentally that the assumption of a constant heat of adsorption is invalid, but this objection has been answered by Hinshelwood and by Boudart (8). The simple theory cannot, however, account for the fact that a component will, on occasion, be adsorbed by a solid to a greater extent from a mixture than from its pure vapor.

On practical grounds, the L-H rate equation has the disadvantage of possessing a large number of arbitrary constants, and a form that makes the derivation of an integral rate equation quite difficult. These arguments have validity, but the fact remains that many catalytic reaction rates cannot be described as accurately with simpler models, especially when the reaction is inhibited by the reactants or by reaction products. Some of the data presented by Weller illustrate this point. The use of L-H equations in this study is probably best justified by the great use and success they have enjoyed in the past. This is especially true for the calculations of the effectiveness factor, since these calculations will hopefully find application on both past and future experimental data.

A major objection has been made to the use of L-H kinetic expressions in "proving" the mechanism of a reaction, i. e., concluding that the actual RLS is the one associated with the kinetic equation that best describes the experimental data. For this purpose, the use of L-H equations is invalid. As mentioned above, several different RLSs can sometimes lead to the same rate equation, and frequently several rate equations will fit the kinetic data to within experimental accuracy. A knowledge of the reaction mechanism helps in the formulation of a rate equation, but the converse is not true. The use of L-H equations in the present work should not be taken to imply a particular reaction mechanism.

## B. Experimental Apparatus and Procedure

### 1. General Theory of Experiments and Equipment Design

The object of the experimental program was to determine the intrinsic kinetics of the reaction between thiophene and hydrogen over a cobalt-molybdate catalyst, from measurements of the rates of formation and disappearance, at steady-state, of all species. Because of the complexity of the reaction, and the number of possible products, a differential reactor is preferred to an integral reactor. In order to avoid the necessity of measuring very small concentration differences, the differential reactor was run with a recirculation loop. Briefly, the reaction system consisted of a loop which contained the reactor and a pump. The feed was introduced just below the reactor, at a rate such that the pumping rate was much greater than the feed rate. Therefore, at steady-state, the composition was essentially the same at all points in the loop. A purge was taken off the loop at such a rate that the pressure in the loop did not vary with time. Details of the reaction system are given in Section III-B-2.

Provision was made for feeding not only thiophene and hydrogen, but also hydrogen sulfide. Experiments with a feed containing hydrogen sulfide were made in order to investigate any retarding effect that  $H_2S$  might exhibit on the reaction rate. A definitive test of this effect could be made only by being able to vary the hydrogen sulfide concentration independently.

In order to calculate the rates of reaction, it was necessary to measure the reactant feed rates, and the mole fractions of some of the components in the reaction loop. It was desirable to make enough measurements to check the data by closing material balances. Consequently, all the feed rates were measured, together with the mole fractions of all species in the loop, except hydrogen and thiophene.



Using these measurements, all the reaction rates and the thiophene and hydrogen concentrations could be calculated, and the cleanness of the reaction and the sulfur balance could be checked. The details of these calculations are discussed in Section III-B-4. Gas chromatography was used for both qualitative and quantitative analysis of the components in the reaction loop.

## 2. Apparatus--Details of Construction and Calibration

Figure III-1 is a schematic diagram of the experimental equipment. The apparatus can be divided into five sections: the reaction loop, the hydrogen feed system, the chromatograph, the thiophene pump, and the hydrogen sulfide feed system. Each of these sections is described in detail below.

### a. Reaction Loop

The gas feed stream and the liquid thiophene feed entered the loop just below the reactor and mixed with the hot gases leaving the reaction zone. The mixture then passed into a three foot long section of tubing, coiled to a diameter of about eight inches and immersed in a battery jar of water. Gas left the coil at the temperature of the water, which was slightly above room temperature.

Immediately downstream of the coil was a cross which had a pressure gauge and a 1 psig. Nupro A4C check valve connected to two of its ports. The function of the check valve was to maintain a constant pressure in the reaction loop. Some of the gas leaving the coil passed through the check valve, through the chromatograph sampling valve and to vent. The remainder of the gas stream entered a Model 7062 BantamDyna-Vac diaphragm pump, and was pumped through a preheater and then into the reactor. Cooling of the hot gas leaving the reactor was necessary in order to protect the pump and to



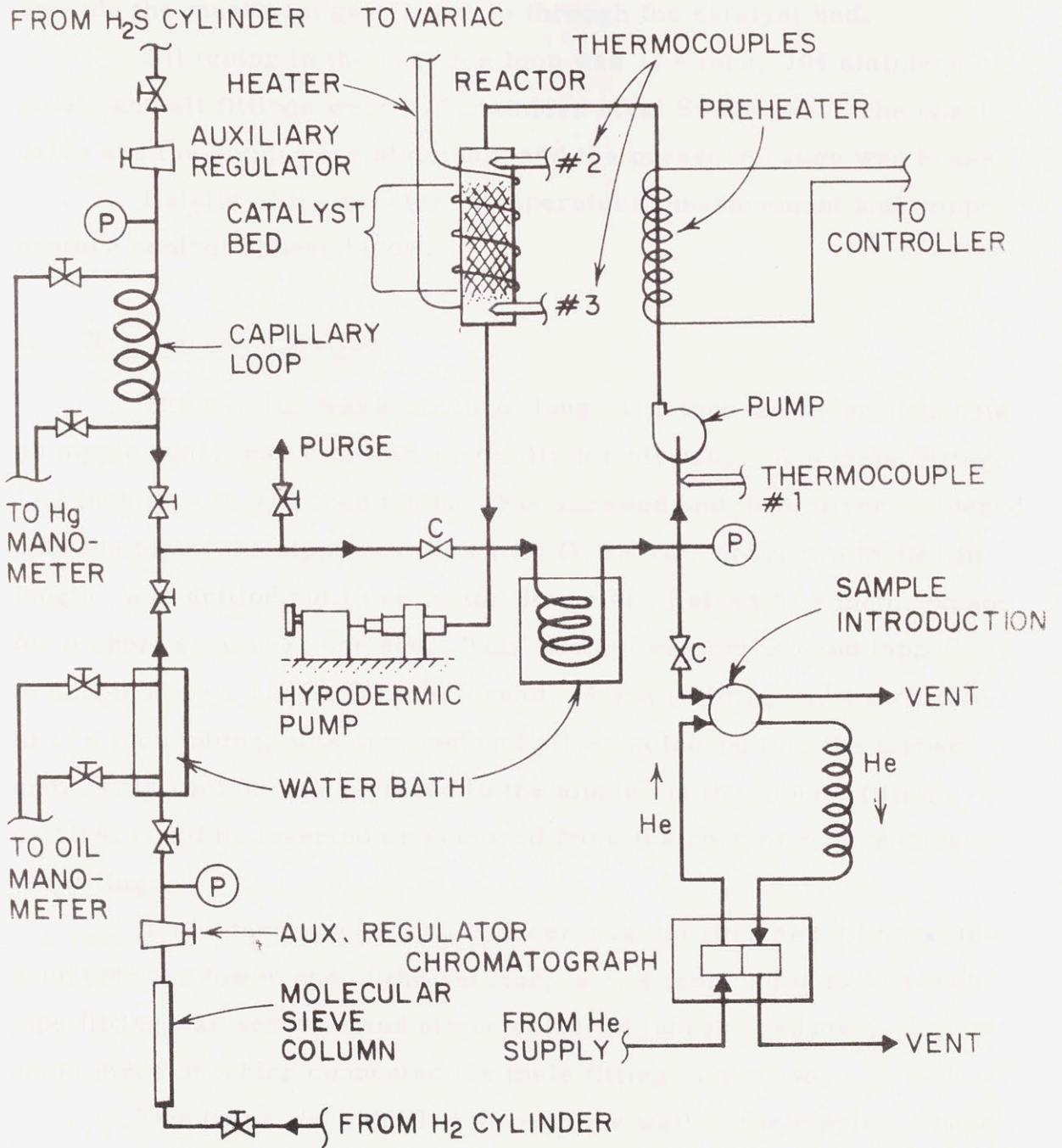


FIGURE III-1 DIAGRAM OF OVERALL KINETIC APPARATUS



provide the maximum gas flow rate through the catalyst bed.

All tubing in the reaction loop was 1/4 inch, 304 stainless steel, and all fittings were 316 stainless steel Swageloks. The check valve and the pump were aluminum and the pressure gauge was brass.

Details of the reactor, temperature measurement and temperature control appear below.

### I. Reactor and Catalyst

The reactor was a six inch long, 1/2 inch diameter, Schedule 40 nipple which was mounted vertically for all runs. A female fitting, 1/2 inch pipe to 3/4 inch tubing, was screwed and then silver-soldered onto the top of the nipple. A 3/4 inch O.D. bar, about two inches in length, was drilled out to an inside diameter of about 5/8 inch, except for a short section at one end. This section was drilled and tapped to accommodate a 1/4 inch male thread. A male fitting, 1/4 inch pipe to 1/4 inch tubing, was screwed and silver-soldered into the tapped end. This section was fastened to the nipple via the female fitting; catalyst could be inserted or removed from the reactor by breaking the fitting.

A 1/2 inch to 1/4 inch reducer was screwed and silver-soldered onto the lower end of the reactor; a 1/4 inch tubing to 1/4 inch pipe fitting was screwed and silver-soldered into the reducer. A short piece of tubing connected the male fitting to a cross.

Two holes were drilled through the wall of the nipple. These holes were tapped and 1/8 pipe to 1/4 inch tubing male fittings were screwed in and silver-soldered in place. These fittings were located about one inch from the ends of the nipple, and provided the means for inserting thermocouples into the reactor.

The catalyst pellets were supported on a fine screen that was silver soldered onto a wire ring whose diameter was about equal



to the inside diameter of the reactor. Wire "legs" were soldered to the ring. The length of the legs was such that the screen, and therefore the catalyst bed, was held just above the lower thermocouple port.

All parts of the reactor were of 304 stainless steel, except for the Swagelok fittings, which were 316 stainless steel.

### Catalyst

For all runs, the catalyst bed consisted of one charge of 8.157 grams of Girdler T-1209 cobalt molybdate catalyst which was never removed from the reactor. The catalyst composition, as received, was reported by the manufacturer to be approximately 3.5 percent cobalt oxide and 10 percent molybdenum oxide on activated alumina. The catalyst was an extrudate with an average outside diameter of 0.109 inches; the pellets used in the reactor were  $1/2 \pm 1/16$  inches in length. The surface area of the catalyst was 343 square meters per gram, as reported by the manufacturer, and the apparent density was measured to be about 1.17 grams per cubic centimeter, by mercury displacement.

Prior to the first kinetic run, the catalyst was activated by passing hydrogen sulfide at a temperature of  $662^{\circ}\text{F}$  and at atmospheric pressure through the reactor containing the catalyst. The gas flow rate was approximately one liter per hour and the treatment was continued for about three hours.

The calculations in Appendix E-1 and E-2 show that: 1) concentration and temperature differences between the bulk stream and the pellet surface were negligible; 2) the pellet may justifiably be considered isothermal throughout. The effective diffusivity of thiophene is calculated in Appendix E-3.

## II. Temperature Measurement

The temperature was measured at three places in the reaction loop. A thermocouple was located at the inlet to the diaphragm pump, and two thermocouples were located in the reactor, above and below the catalyst bed. These reactor thermocouples will be subsequently referred to as the upper and lower thermocouples, respectively. The pump thermocouple is shown as Number 1 on Figure III-1, and the upper and lower thermocouples are shown as Numbers 2 and 3 respectively.

For all three thermocouples, the wires were run through about two inches of two-hole ceramic insulator, and the insulator was cemented into a piece of 1/4 inch O.D. stainless steel tubing. Epoxy was used to cement and seal Thermocouple No. 1, and Sauereisen cement was used on the reactor thermocouples. In addition, the point at which the wires exited from the thermocouple housing was sealed with epoxy on all three thermocouples. The thermocouples were inserted into the gas by Swagelok fittings. The ceramic insulator was positioned in the stainless-steel tubing such that the thermocouple tip was located in the middle of the gas stream. The thermocouples were not shielded, since the walls of the reactor were at essentially the same temperature as the gas.

The pump thermocouple was made of 24 gauge iron-constantan wire, and both reactor thermocouples were of 20 gauge chromel-alumel wire. The reactor thermocouples were connected to reference thermocouples made of 28 gauge chromel-alumel wire. The two reference thermocouples were immersed in an ice bath during operation.

The leads from all three thermocouples were connected to a rotary switch. Copper wire was used to connect the switch to the Rubicon 2732 potentiometer which was used to measure the thermocouple voltages.



A proportional controller was connected in parallel with the taps on the rotary switch for the upper reactor thermocouple. Therefore, since the controller drew current from the thermocouple, the potentiometer reading for the upper thermocouple was low. This error was compensated for by measuring the thermocouple voltage with the controller connected, and then disconnected, at the start of the run, i. e., with the reactor at reaction temperature. The difference in voltages was added to the voltage measured during the run. Since disconnecting the controller tended to upset the temperature stability of the reactor, it was impractical to measure the disconnected voltage after steady-state had been reached.

### III. Temperature Control

The preheater consisted of a one-foot section of 1/4 inch stainless steel tubing, which was wrapped with a 96 watt, heavy-insulated heating tape, and then insulated over its whole length with about a two inch depth of Johns-Manville Cerafelt insulation, Type CRF-800. The heating tape leads were connected to the output of a control system consisting of a Stepless Controls Corporation Model No. PP-14-115 silicon diode rectifier, to which a signal was supplied by a Wheelco Model 407 D proportional controller. The leads from the upper reactor thermocouple were hooked to the proportional controller, on which the desired temperature was set. The upper reactor temperature varied by less than  $\pm 0.50^{\circ}\text{C}$  during the steady-state portion of any run.

A second 96 watt heating tape was wrapped around the reactor, and the unit was insulated as described in the section above. A zero to three ohm variable resistor and a zero to one ampere AC ammeter were connected in series with the heating tape, and the combined load was plugged into a Variac. The Variac, in turn, was connected



to a one ampere Sola constant voltage transformer, which was supplied with 110 volt line voltage. The temperature at the lower reactor thermocouple was controlled by adjusting the Variac and, for fine control, the variable resistor.

In all runs, temperature control was such that the maximum difference between the upper and lower thermocouple readings was  $2.5^{\circ}\text{C}$ , but this difference was typically less than  $1.0^{\circ}\text{C}$ .

#### b. Hydrogen Feed System.

Airco prepurified-grade hydrogen was fed from a cylinder equipped with a two-stage regulator into an Englehard D-10-50 Deoxo Purifier, which converted traces of oxygen to water. The gas then passed through a valve into a four foot section of 1/2 inch copper tubing that was packed with about 0.13 pounds of Linde 13X molecular sieve, in the form of 1/16 inch diameter extrudate, about 1/8 inch in length. The function of the bed was to remove the water from the hydrogen stream. The sieve was activated prior to use by heating to  $500^{\circ}\text{F}$  for about 10 hours, while bleeding hydrogen through at a rate of about 0.1 cubic foot per hour.

Hydrogen leaving the sieve bed was reduced to a pressure of about five pounds by a non-bleeding Conoflow pressure regulator and passed through a 25A Nupro metering valve and then through a one foot long piece of 23 gauge capillary tubing, which was epoxied into a section of 1/4 inch tubing. The capillary tubing, which served as part of a flowmeter, was immersed in a waterbath whose temperature was constant to  $\pm 1^{\circ}\text{F}$ . Swagelok tees at each end of the capillary served as taps for connecting a manometer which was filled with vacuum pump oil. Valves were installed in the manometer leads and the downstream lead also contained a plexiglass trap.

After leaving the capillary, hydrogen passed through an exit

valve and then into a tee where it joined the hydrogen sulfide line. Just downstream of the tee was a second tee, to which was attached a valve leading to vent. The second tee was connected to a 1/3 pound 4CA Nupro check valve which was connected to the Swagelok cross on the lower end of the reactor.

All materials upstream of the exit valve were copper, except for the aluminum regulator, the brass valves and the stainless steel capillary tubing. Except for the aluminum check valve, all materials downstream of the valve were stainless steel. The purge line was polyethylene.

#### Calibration

The capillary flowmeter was calibrated by passing hydrogen through the system and measuring the flow rate, which was adjusted with the needle valve. The waterbath temperature and atmospheric pressure were recorded at the start of each run, and the manometer reading was recorded each time the hydrogen flow rate was measured. The hydrogen flow was measured by passing the gas through a 25 cubic centimeter burette, introducing a soap film into the gas and timing the rise of the film through the burette. The calibration was reproducible to about one-half percent. The calibration curve, and its basis, appear in Appendix A-1,

Prior to calibration, the manometer was drained and the lines were flushed with hydrogen. The manometer was then refilled. This procedure was necessary to insure that the gas in the manometer lines was pure hydrogen. If another gas were present in the leads, it would gradually diffuse out and upset the calibration.



### c. Chromatograph

The chromatograph used in this study was a Chronofrac VP-1, by Precision Scientific Company. The detector in this unit consists of two thermal conductivity cells, each forming an arm in a Wheatstone bridge. One cell is a reference; only pure helium passes through it. The gas emerging from the column passes through the second cell, causing an imbalance in the bridge when a peak appears. The chromatograph column was a 7.5 foot section of 25 percent dibutyl phthalate on 50-60 mesh Chromosorb, plus a 4.5 foot section of Burell standard concentration dimethyl sulfolane packing. The packings were held in 1/4 inch copper tubing and the two sections were joined by a union; the dibutyl phthalate section was upstream. During operation, the whole column was immersed in an ice bath.

A schematic diagram of the chromatograph and its auxiliaries is shown in Figure III-2. The carrier gas, helium, was supplied from a cylinder equipped with a two-stage regulator and was reduced to a pressure of about 15 pounds by a second regulator, which was a non-bleeding Conoflow regulator. The helium then passed through a valve and a six-inch long bed of silica gel. The silica gel removed traces of oil when oil-pumped helium was used. The helium then entered a six-inch long section of 1/2 inch O.D. glass tube containing indicating drierite, which, together with the silica gel, removed traces of water from the helium. The gas next entered a one-foot long section of 21 gauge stainless-steel capillary tubing that served as part of a flowmeter. The capillary tubing was epoxied into a piece of 1/4 inch copper tubing, and was connected across a manometer which contained red gage oil as the indicating fluid. Two valves were installed in the manometer lead lines and a plexiglass trap was located downstream of the flowmeter.

Helium leaving the trap flowed through the reference cell



of the chromatograph and then through a sampling device. Two different methods of introducing the sample into the column were used. During calibration of the chromatograph, the sample was introduced through the serum stopper, which came installed on the chromatograph. Hamilton Gas-Tight syringes, of 1/4 and 1/2 cubic centimeters, equipped with a one-inch long, 27 gauge hypodermic needle, were used to inject the gas sample through the serum stopper. During the kinetic experiments, a Perkin-Elmer Model 154-0068 gas sampling valve was used to introduce samples. A five cubic centimeter sample loop was installed on the sampling valve. The serum stopper was removed when the sampling valve was installed.

Gas leaving the sampling device passed through the column, through the sample cell of the chromatograph, through a valve and out to vent. Unless specifically mentioned, all lines in the helium circuit were 1/4-inch copper tubing. Valves were brass.

Power was supplied to the chromatograph from a six-volt storage battery. An Electro EC-2 battery charger was connected across the battery and was set for a charging current of about two amperes when the chromatograph was in operation. Thus, the charger supplied a current very close to that drawn by the chromatograph, thereby maintaining a constant battery voltage over long periods of time. A series of resistors within the chromatograph was adjusted so that the voltage supplied to the Wheatstone bridge was 2.2 volts. The signal from the chromatograph was recorded with a Microcord 44 recorder, using a chart speed of two inches per minute.

The helium flowmeter was calibrated using the method described in Section III-B-2-b. During chromatograph operation, the manometer reading was always  $37.0 \pm 0.5$  centimeters. This corresponded to a helium flow of about 125 cubic centimeters STP per minute.

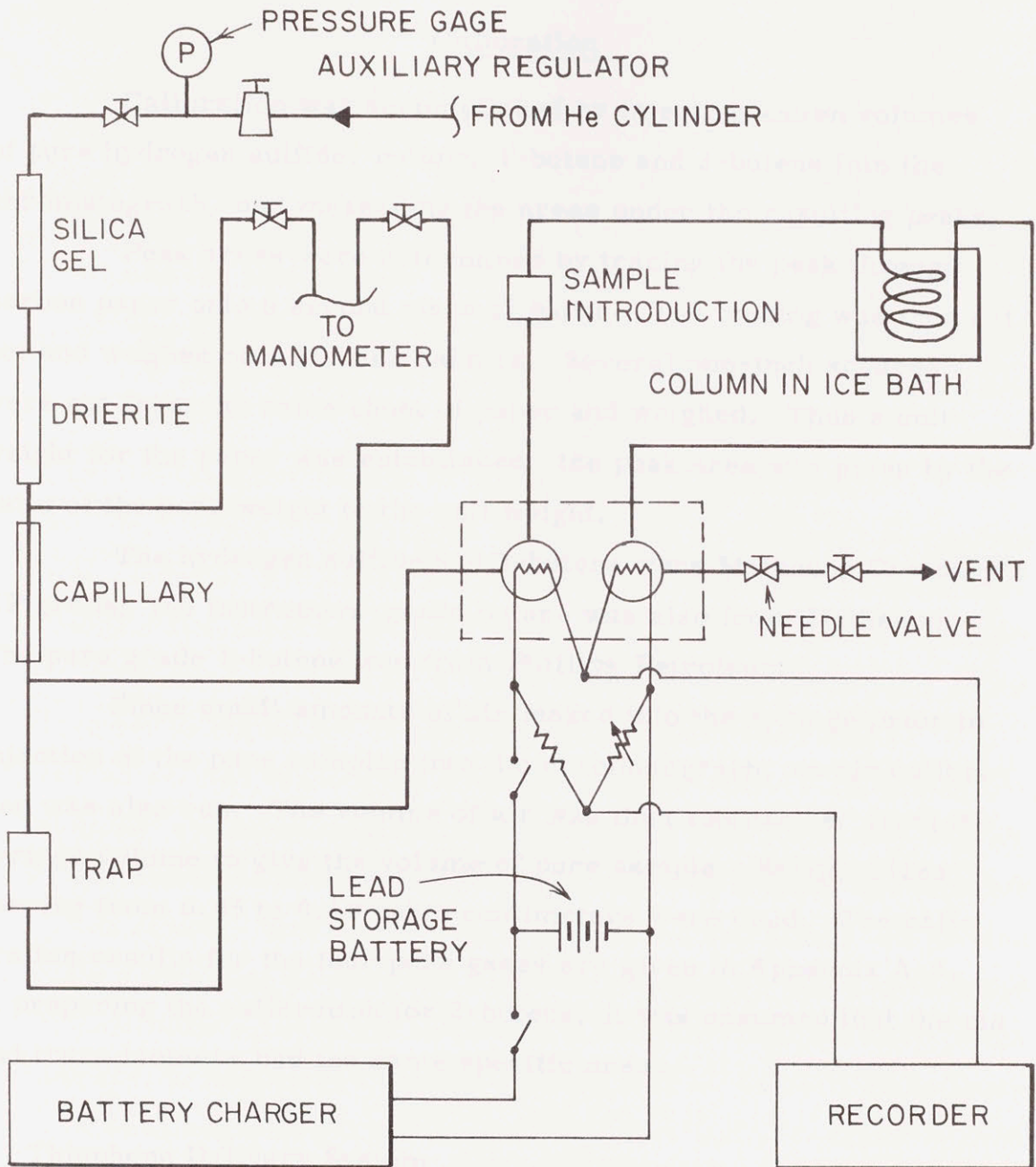


FIGURE III-2 DIAGRAM OF CHROMATOGRAPH AND AUXILIARIES





### Calibration

Calibration was accomplished by injecting known volumes of pure hydrogen sulfide, butane, 1-butene and 2-butene into the chromatograph, and measuring the areas under the resulting peaks.

Peak areas were determined by tracing the peak through carbon paper onto a second piece of paper. The tracing was then cut out and weighed on a Mettler balance. Several one-inch squares were cut from the same sheet of paper and weighed. Thus a unit weight for the paper was established; the peak area was given by the ratio of the peak weight to the unit weight.

The hydrogen sulfide and 2-butene were Matheson Company's CP grade; the instrument-grade butane was also from Matheson. The pure grade 1-butene was from Phillips Petroleum.

Since small amounts of air leaked into the syringe prior to injection of the pure samples into the chromatograph, an air calibration was also run. The volume of air was then subtracted from the syringe volume to give the volume of pure sample. Sample sizes varying from 0.05 to 0.50 cubic centimeters were used. The calibration results for the four pure gases are given in Appendix A-3. In preparing the calibration for 2-butene, it was assumed that the cis and trans isomers had the same specific area.

#### d. Thiophene Delivery System

Thiophene was fed to the reactor by a positive displacement pump, similar to that described by Loftus (33). A synchronous motor, connected through two gears, was used to drive a screw, which had a metal plate attached to the end. The plate butted against the plunger of a hypodermic syringe, the body of which was epoxied into an aluminum block. The block was fastened to the same base plate on which the synchronous motor was mounted. The motion of the traveling

screw pushed the plunger into the barrel of the syringe, thereby displacing thiophene.

The connection between the syringe and the reaction loop was made with a 15 gauge stainless-steel hypodermic needle, one foot in length. The appropriate end of the needle was epoxied onto the barrel of the syringe, and a  $90^{\circ}$  bend was put into the needle near this joint. The other end of the needle was silver-soldered into a short piece of 1/4-inch stainless steel tubing which was connected to the cross just below the reactor.

Reproducible mounting of the aluminum block containing the syringe was insured by two strips of aluminum, 1/2-inch high, that were epoxied onto the base plate, spaced so that the aluminum block fit snugly between them. A threaded hole in the block was aligned with a hole in the base plate and a screw was inserted and tightened.

To prevent binding of the plunger in the barrel of the syringe, and to prevent leakage of liquid between the plunger and the barrel, the plunger was lubricated lightly with silicone grease before filling the syringe with thiophene. Filling of the syringe was accomplished by holding the assembled pump so that the syringe was vertical and pointed upwards. Thiophene was then drawn in by pulling the plunger down. The air that collected at the top of the syringe was then expelled by pushing the plunger in. Several repetitions of this procedure eliminated all air from the syringe and the attached needle.

The hypodermic pump was designed to permit synchronous motors of various rpm to be mounted interchangeably, but only a 1/4-rpm motor was used. One and five cubic centimeter hypodermic syringes were used.

The pump was calibrated by filling the syringe with mercury, catching the expelled mercury in a beaker, and weighing the beaker at various times during the operation of the pump. Calibration data



are given in Appendix A-4.

Thiophene was supplied by Pennsalt Chemicals. The purity was a minimum of 98 percent, and typically around 99 percent. The principal impurities were benzene, carbon disulfide and mercaptans. The thiophene was used as supplied.

#### e. Hydrogen Sulfide Feed System

Hydrogen sulfide was fed from a cylinder equipped with a two-stage regulator, through a valve and then through a non-bleeding, non-relieving Conoflow regulator. Downstream of this regulator was a pressure gauge, and a 10-foot section of 30-gauge needle tubing. The needle tubing served two functions: 1) as part of a capillary flowmeter, 2) to introduce a large pressure drop, which stabilized the flow. The hydrogen sulfide flow rate was adjusted by changing the regulator setting. Swagelok tees at each end of the capillary served as taps for connecting a mercury manometer. Valves were present in both manometer lead lines. Downstream of the capillary was a valve; the hydrogen sulfide line joined the hydrogen line just below this valve.

The cylinder was connected to the upstream valve with 1/4-inch copper tubing. Stainless steel tubing of the same diameter connected the valve to the regulator, and the regulator to the capillary. The capillary tubing was stainless steel, and 1/8-inch, stainless-steel tubing connected the capillary to the downstream valve.

The hydrogen sulfide used was Matheson Company's technical grade, which has a minimum purity of 98.5 percent.

#### Calibration

Calibration of the hydrogen sulfide flowmeter was accomplished in the manner previously described for hydrogen, with two



exceptions. First, since no waterbath was used, the capillary was assumed to be at room temperature. Secondly, the soap bubble was introduced into a 1.0 cc burette. The calibration was reproducible to about one percent. The calibration curve and its basis are given in Appendix A-2.

### 3. Operation of the Equipment

#### a. Startup

Runs were started in one of two ways: 1) by activating the equipment after it had been shut down for a period of time, 2) by changing the temperature and/or the feed rates from those that had been established, without an intervening shutdown. This section describes the procedure for making the first type of run.

The first step was to leak-test the helium circuit in the chromatograph, and to leak-test the hydrogen and hydrogen sulfide circuits. These tests were made by bringing the circuits up to normal operating pressure, and closing the valves at the line exits. A zero manometer reading indicated no appreciable leak. The hydrogen circuit that was tested always included the reactor with the Dyna-Vac pump running, and the hypodermic pump disconnected and the port capped. If the equipment had not been used for several days, the hydrogen and hydrogen sulfide manometers were drained, the lines flushed, and the manometers refilled prior to the leak tests.

After the leak tests, the filled hypodermic pump was connected, the gas feeds were started and the Dyna-Vac pump was turned on. The constant temperature bath was plugged in, and the preheater and the reactor heater were turned on. When the temperature of the lower reactor thermocouple got to about 150°C, the thiophene feed was started. The proportional controller setting was adjusted to give

the desired reactor temperature, and the Variac and the variable resistor were adjusted to make the reactor isothermal. After the constant-temperature bath had reached the desired temperature, the hydrogen flow was adjusted by setting the needle valve in the line. The hydrogen sulfide flow was adjusted by means of the pressure regulator in the line.

Because of the time required to stabilize, the chromatograph was turned on as soon as the helium leak test was complete, and the helium flow had been set at the proper value.

#### b. Approach to Steady-State

Sampling of the purge leaving the reaction loop was started after the desired reactor temperature had been reached, and was continued at 45-minute to one-hour intervals until the composition of the purge stream had reached steady-state. The variation of the peak heights of the components was used to determine when steady-state had been reached. It was considered that steady-state had been achieved when the peak height of every component varied no more than two chart paper units from the average, and when no trend was evident in the variations. After steady-state had been reached, one or two more samples were taken.

At some time during the approach to steady-state, the following data were read and recorded; atmospheric pressure, waterbath temperature, hypodermic pump (syringe volume and motor speed), chromatograph bridge voltage and helium manometer reading. At the time each sample was taken, the following data were recorded: time, room temperature, upper and lower reactor thermocouple readings, pump thermocouple reading, reading of pressure gauge on reaction loop and reading of the hydrogen sulfide and hydrogen manometers. In addition, the recorder setting and the attenuation of



the chromatograph were recorded on the chart paper of the recorder, just preceding the peak to which they corresponded.

The comments in this section apply regardless of whether the run was made by changing previous conditions, or starting from a shutdown condition.

### c. Shutdown

The usual shutdown procedure was as follows: 1) the Variac and the temperature controller were shut off; 2) the waterbath was unplugged; 3) the valves on the hydrogen and helium manometers were closed; 4) the chromatograph was shut off; 5) the ice bath for the chromatograph column was drained; 6) the helium flow was shut off; 7) the thiophene flow was shut off and the hypodermic pump was disconnected. The connection was sealed with a Swagelok plug; 8) the hydrogen flow was shut off at the cylinder. When the pressure in the hydrogen line had fallen to less than 2 psig, the valves at the cylinder and the reactor entrance were closed; 9) the hydrogen sulfide flow was shut off at the cylinder. When the pressure in the lines had fallen to about 1 psig, the valve at the entrance to the reactor was closed; 10) the Dyna-Vac pump was shut off.

The order of the above steps was not important except in three cases: 1) the chromatograph bridge voltage was shut off before the helium flow was stopped, to avoid burning out the detector filaments; 2) in order to avoid desulfiding the catalyst, the thiophene or hydrogen sulfide flow was continued during the period when the reactor was cooling down. The thiophene flow was shut off when the lower reactor thermocouple reached a temperature of about 125°C. In order to avoid possible thiophene cracking, the gas feed was continued until the lower reactor temperature was about 100°C; 3) when both hydrogen and hydrogen sulfide were fed, the hydrogen was shut off first and the



valve at the exit was tightly closed. The hydrogen sulfide was then allowed to flow for about 10 minutes to clear hydrogen out of the lines. After this time, the hydrogen sulfide flow was stopped and the exit valve closed tightly. These precautions were taken to avoid contaminating the manometer leads.

#### 4. Data Processing

##### a. Raw Data

The bulk of the data reduction was performed on the computer, but several preliminary calculations were done by hand in order to provide the input data for the computer. First, it was necessary to decide what chromatograms would be used to calculate the concentrations in the reactor and the reaction rates. Usually, the last three chromatograms for any run were used. Peak areas were determined with a planimeter, and an average area for each peak was calculated by taking the arithmetic mean of the peak areas of each sample.

A mean hydrogen manometer reading was determined by averaging the readings taken during the period corresponding to the chromatograms being analysed. Similarly, average readings were determined for the hydrogen sulfide manometer, the upper and lower reactor thermocouples, room temperature and reactor pressure. The average thermocouple readings were converted from millivolts to degrees Centigrade using the thermocouple reference tables, and the average reactor temperature was taken to be the mean of the upper and lower reactor temperatures. The average manometer readings were used to determine the hydrogen and hydrogen sulfide flow rates from the calibration curves, and the thiophene flow rate was determined from the calibration of the hypodermic pump.

The quantities that formed the input data for the computer

program for data reduction were: run number, average room temperature, average reactor temperature, average reactor pressure, atmospheric pressure and the average areas of the three chromatogram peaks. The computer then calculated the mole fractions and partial pressures of all species, the purge rate, the rates of thiophene disappearance and butane formation,  $\Phi_L$ , and various parameters that had potential use for manual plotting of the data. In addition, the computer checked to see whether thiophene could have condensed in the cooling coils. In order to calculate the composition in the reactor, the program automatically computed the equilibrium amount of 1-butene from the amount of 2-butene present, and subtracted the 1-butene peak area from the total area of the second peak to give the butane peak area.

A print-out of the data analysis program is found in Appendix B-3.

#### b. Preliminary Correlation

For reasons that are discussed in Section III-D, various forms of the Langmuir-Hinshelwood rate equation were the only correlating equations used to fit the experimental data on the rates of thiophene disappearance and butane formation. An approximate analysis of the data on thiophene disappearance indicated that the denominator of any L-H equation would have to contain terms for the adsorption of both thiophene and hydrogen sulfide; no other terms were included in the denominator. The preliminary correlation of the kinetic data on thiophene disappearance, then, required the determination of the best values of the rate constant and adsorption constants in the L-H rate equation

$$r_T = k p_T^{n_T} p_H^{n_H} / (1 + K_T p_T + K_{H_2S} p_{H_2S})^{n_D} \quad (\text{III-11})$$



For specified values of  $n_T$ ,  $n_H$  and  $n_D$ , which were always integers in this study, the best values of  $k$ ,  $K_T$ , and  $K_{H_2S}$  at each of the three experimental temperatures were calculated by the method of multiple linear regression, which is a least-squares technique involving more than one independent variable, as described by Hoel (24). These calculations were performed on the computer; the program is given in Appendix B-4. In order to use the multiple regression technique, the rate equation, Eqn. (III-11), was linearized as shown in Eqn.

(III-12).

$$M = \left\{ \frac{\begin{matrix} p_T^{n_T} & p_H^{n_H} \\ r_T \end{matrix}}{r_T} \right\}^{1/n_D} = \frac{1}{k^{1/n_D}} + \frac{K_T p_T}{k^{1/n_D}} + \frac{K_{H_2S} p_{H_2S}}{k^{1/n_D}} \quad \text{(III-12)}$$

Thus, the deviations in  $M$ , rather than the deviations in  $r_T$ , were minimized when the quantities  $(1/k^{1/n_D})$ ,  $(K_T/k^{1/n_D})$  and  $(K_{H_2S}/k^{1/n_D})$  were calculated. The errors inherent in this procedure have been discussed by Lapidus and Peterson (32) and by Kittrell, Watson, and Hunter (28). However, the added calculational complexity of a non-linear, least-squares technique was not considered justifiable in the present case.

In order to help determine the most effective form of the L-H rate equations for correlation purposes, the best values of  $k$ ,  $K_T$  and  $K_S$  were calculated for a number of combinations of  $n_T$ ,  $n_H$  and  $n_D$ . The difference between the experimental reaction rate and the rate calculated using the best values of the kinetic constants was then determined for each run, together with the sum of the squares of these deviations and the statistical parameter  $F$ . These calculations were incorporated into the computer program shown in Appendix B-4.

This program was also used for preliminary correlation of the data on the second step of the reaction, the hydrogenation of



butene. By reading in the butene partial pressure in place of the thiophene partial pressure, the rate equation was given a numerator consisting of a butene partial pressure and a hydrogen partial pressure, each to an arbitrary power, with a denominator containing terms for the adsorption of both butene and hydrogen sulfide. Further, by reading in the butene partial pressure in place of the hydrogen partial pressure, and setting  $n_T = 0$ , a rate equation of the form

$$r_c = \frac{\hat{k} p_B^{n_B}}{(1 + \hat{K}_T p_T + \hat{K}_{H_2S} p_{H_2S})^{n_D}} \quad \text{(III-13)}$$

was tested.

The results of the preliminary correlation calculations described above were used to choose the best kinetic model, i. e., the best values of  $n_T$ ,  $n_H$  and  $n_D$  for each of the two steps of the overall reaction. The choice of the best model was based on the minimum sum of the squares of all the differences between the calculated and the experimental reaction rates. The rate and adsorption constants in the chosen model were then recalculated, as described in the next section.

### c. Final Correlation

The preliminary program produced a correlation that used nine arbitrary constants, (one rate constant and two adsorption constants at each of three temperatures) to fit the data. As calculated, these constants were not always related by an Arrhenius-type temperature dependence. The object of the final calculation was to fit the experimental data to a kinetic equation of the form

$$r_T = \frac{k^* \cdot e^{E_a/RT} \cdot p_T^{n_T} \cdot p_H^{n_H}}{(1 + K_T^* \cdot e^{E_T/RT} \cdot p_T + K_{H_2S}^* \cdot e^{E_{H_2S}/RT} \cdot p_{H_2S})^{n_D}} \quad (\text{III-14})$$

using the "best" values of  $n_T$ ,  $n_H$  and  $n_D$  as determined previously. Mathematically, the problem was to calculate the least-square values of the six arbitrary constants,  $k^*$ ,  $E_a$ ,  $K_T^*$ ,  $E_T$ ,  $K_{H_2S}^*$  and  $E_{H_2S}$ . Thus, the number of arbitrary constants was reduced by three, all the constants were forced to have Arrhenius-type temperature dependencies, and correction was made for slight temperature differences between the runs at a given temperature.

This calculation was performed using the computer program given in Appendix B-5. Basically, this program performed a linear multiple regression calculation very similar in nature to that in the preliminary program. However, several points about the new program deserve comment. First, the rate equation was again linearized as shown in Equation (III-12). Second, the rate and the adsorption constants were all expressed in terms of the deviations from the value at 524°K, as illustrated below for the constant  $k$ .

$$k = k(524) \cdot e^{\frac{E_a}{R} \left( \frac{524 - T}{524 \cdot T} \right)} \quad (\text{III-15})$$

For the present data, the exponents in the above expressions for all three kinetic constants were always less than one.

The exponential part of the kinetic constants was then expanded in the series

$$e^x = 1 + x + \frac{x^2}{2!} + \frac{x^3}{3!} + \dots \quad (\text{III-16})$$

Substitution of expressions similar to Equations (III-15) and (III-16) into Equation (III-12) yields a form of the rate equation that permits



the values of  $k^*$ ,  $E_a$ ,  $K_T^*$ ,  $E_T$ ,  $K_{H_2S}^*$  and  $E_{H_2S}$  to be calculated by a linear technique. The procedure is iterative, however, in that estimates of the quantities  $E_a$ ,  $E_T$  and  $E_{H_2S}$  must be used to evaluate all but the first two terms of the exponential expansions. Therefore, the program in Appendix B-5 first makes a calculation using initial estimates of  $E_a$ ,  $E_T$  and  $E_{H_2S}$ , which are part of the input data, and are based on the results of the preliminary correlation calculations. The new values of  $E_a$ ,  $E_T$  and  $E_{H_2S}$  are then used as the starting place for a new calculation, and so forth.

In practice, the program was forced to make from twenty to forty iterations for each rate equation. The number of iterations required depended on the accuracy of the initial estimates of  $E_a$ ,  $E_T$  and  $E_{H_2S}$ . However, convergence was always achieved in forty or fewer iterations. The value of the sum of the squares of the deviations of the calculated reaction rates from the experimental reaction rates was calculated for each iteration.

As with the preliminary calculations, the above procedure suffers from the drawback that it minimizes the deviations in  $M$ , rather than  $r_T$ . At the end of several of the early iterations, the sum of the squares of the deviations was slightly lower than the final value of this quantity.

Although the development in this section has been specific to the first step of the overall reaction, i. e., the disappearance of thiophene, the program just described was also used to produce the final correlation for the second reaction step, the formation of butane. Inputting the butene partial pressures in place of the thiophene partial pressures was the only modification necessary.



## C. Results

### 1. Reaction Products

The identity of the reaction products was determined chromatographically, by comparing the "retention volume" (i. e., the volume of carrier gas required to elute a component from the column) of an unknown peak with the retention volumes of various pure samples. Thus it was established that hydrogen sulfide, n-butane, 1-butene and cis and trans 2-butene were the primary reaction products. In addition, trace amounts of three lighter hydrocarbons were also formed. The peaks of these light hydrocarbons were so small and ill-defined that definite identification was not possible. However, it is probable that these three hydrocarbons were methane, ethane, and propane. In all cases, the amounts of the light components that were formed were negligible. Therefore, these components were neglected in the kinetic analysis.

No butadiene, isobutene or isobutane were found in the reaction products, even though these components would have been easily detected and identified. Due to the very large retention volume of tetrahydrothiophene, the presence or absence of this component could not be established definitely, but it was assumed to be absent.

As mentioned in Section III-B-4-a and in Appendix A-3-a, the 1-butene and total 2-butene were in equilibrium to within experimental accuracy. Because of poor separation of the cis and trans 2-butene isomers, the approach to equilibrium of the cis-trans isomerization could not be checked.

### 2. The Rate of Thiophene Disappearance

#### a. Kinetic Data

The raw and partially-processed data are given in Appendix C-3. Runs 1 through 4 are not listed, as they were preliminary in nature; a steady-state was never achieved during any of these runs. Runs 7 through 18 have also been omitted because the reactor was not close to isothermal operation; a temperature drop of about 8°C from inlet to outlet existed during these runs. Runs 21 and 41 were omitted because subsequent reduction of the data indicated that thiophene had condensed in the reaction loop. Run 34 was an exploratory run at 285°C and steady-state was probably never achieved.

Figure III-3 is a plot of the rate of thiophene disappearance versus the thiophene partial pressure, at each of three reactor temperatures, 235°C, 251°C, and 265°C. Different symbols were used to identify the data points corresponding to runs made with and without hydrogen sulfide in the feed to the reactor; identification can be made by referring to the key given on the figure. The three solid lines on Figure III-3 are not meant to describe the best fit of the points, but merely serve to connect the points for which there was no hydrogen sulfide in the feed, at each of the three reactor temperatures.

All of the runs given in Appendix C-3 are included in Figure III-3, except for Run 28. The value of  $\Phi_L$  for this run was about 0.85. Thus, a significant effect of internal diffusion was probably present during this run. For all other runs, the highest value of  $\Phi_L$  was about 0.12, with most values much lower. It is shown in Appendix D-3 that all runs except Run 28 reflect intrinsic kinetic behavior.

#### b. Kinetic Equations--Preliminary Correlations

As mentioned in Section III-B-4-b, all of the rate equations considered for thiophene disappearance were of the form

$$r_T = k p_T^{n_T} p_H^{n_H} / (1 + K_T p_T + K_{H_2S} p_{H_2S})^{n_D} \quad (\text{III-11})$$



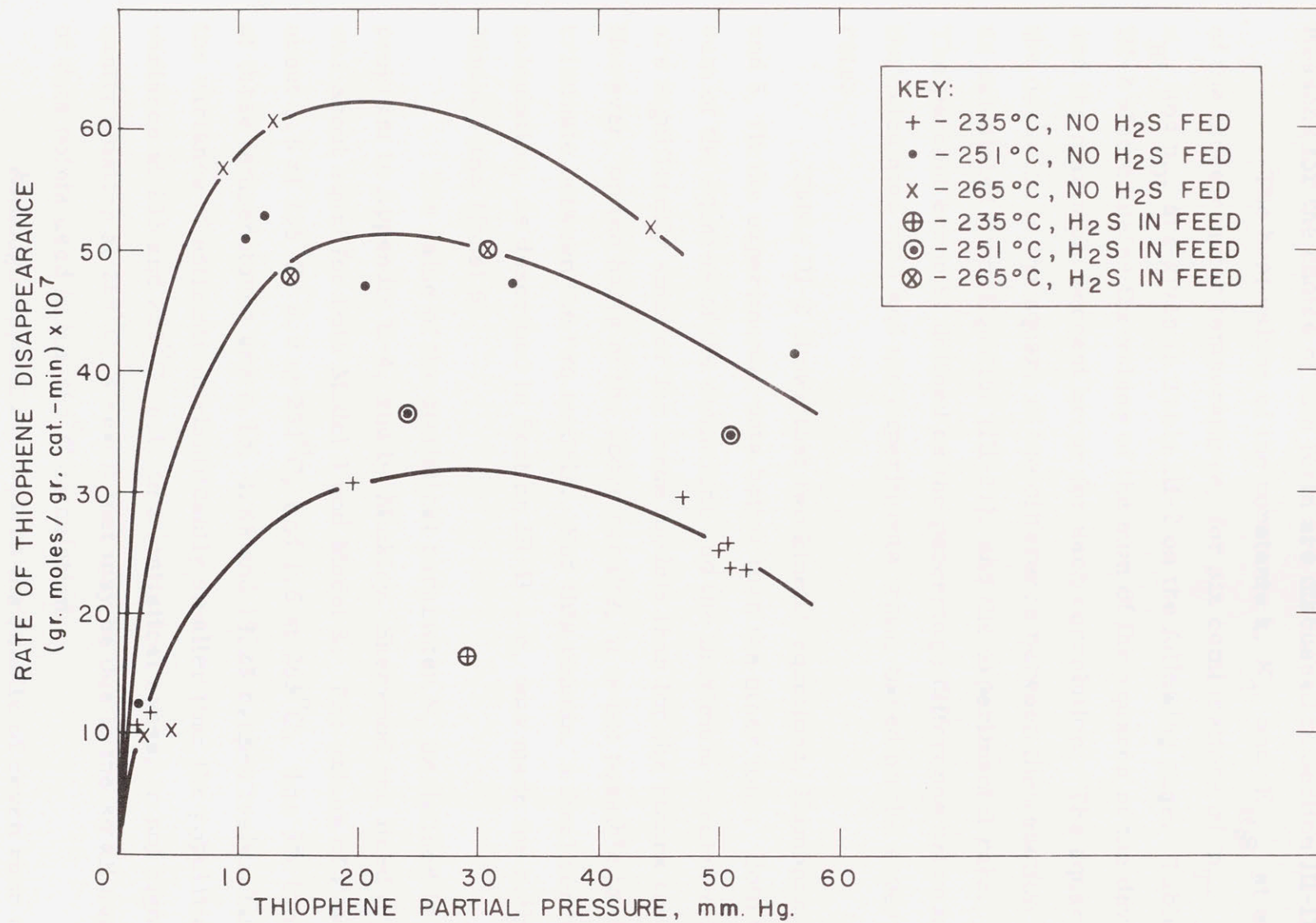


FIGURE III-3 RATE OF THIOPHENE DISAPPEARANCE VERSUS THIOPHENE PARTIAL PRESSURE





Reasons for the choice of this form are discussed in Section III-D-3-a.

The best values of the constants  $k$ ,  $K_T$  and  $K_{H_2S}$  at each of the three reactor temperatures, for six combinations of  $n_T$ ,  $n_H$ , and  $n_D$ , are given in Table III-2 on the following page. Table III-2 also contains the values of the sum of the squares of the deviations and the maximum percent error for each correlation. The square of the deviation is the square of the difference between the reaction rate, as calculated from Equation (III-11), and the experimental rate. The percent error is defined as the percentage difference between the calculated rate and the experimental rate, based on the experimental rate.

Table III-2 shows that two kinetic equations, Numbers 3 and 5, fit the experimental data better than the other four. Both the sum of the squares of the deviations and the maximum percent errors are significantly smaller for these models than for the others tested. However, on the basis of the above results, it is not possible to discriminate between the two models. For this reason, a final correlation calculation, as described in Section III-B-4-c, was made for both Model 3 and Model 5.

The value of the statistical parameter  $F$ , as defined in the program in Appendix B-4, and by Mickley, Sherwood and Reed (37), was about equal for both Model 3 and Model 5. The values of  $F$  were about 5.5 at 235°C, 6.0 at 251°C, and 1.5 at 265°C. The 5% limits at these temperatures are 4.15, 4.88 and 19.25 respectively. Thus, the variance of estimate is significantly smaller than the population variance at 235 and 251°C, but, in a statistical sense, is not significantly smaller at 265°C, a result that may be due to the small number of data points used in the 265°C calculation.

Although Appendix C-3 gives the results of seven runs at 265°C, only 5 runs were used for the calculations that are summarized

TABLE III-2

## Results of Preliminary Kinetic Analysis-Thiophene Disappearance

Model Number	$n_T$	$n_H$	$n_D$	T(°C)	k	$K_T$	$K_{H_2S}$	Sum of Squares of Deviations	Maximum Percent Error
1	1	1	3	235	$0.119 \times 10^{-8}$	0.0234	0.0182	$0.91 \times 10^{-12}$	21.4
				251	0.126	0.0144	0.00763	1.87	24.0
				265	0.153	0.0150	0.00409	0.25	6.9
								$3.03 \times 10^{-12}$	
2	1	2	3	235	$0.152 \times 10^{-11}$	0.0222	0.0176	$1.01 \times 10^{-12}$	24.0
				251	0.157	0.0124	0.00720	2.06	25.8
				265	0.188	0.0112	0.00385	0.21	- 6.3
								$3.28 \times 10^{-12}$	
3	1	0	2	235	$0.125 \times 10^{-5}$	0.0599	0.0436	$0.54 \times 10^{-12}$	-19.6
				251	0.141	0.0385	0.0203	1.12	15.2
				265	0.156	0.0456	0.00781	0.37	8.7
								$2.03 \times 10^{-12}$	
4	1	1	4	235	$0.109 \times 10^{-8}$	0.0146	0.0116	$1.19 \times 10^{-12}$	26.9
				251	0.115	0.00944	0.00473	2.31	27.4
				265	0.144	0.00951	0.00285	0.25	- 7.3
								$3.75 \times 10^{-12}$	
5	1	1	2	235	$0.156 \times 10^{-8}$	0.0558	0.0417	$0.58 \times 10^{-12}$	-18.9
				251	0.164	0.0311	0.0183	1.25	17.6
				265	0.180	0.0328	0.00740	0.28	- 7.0
								$2.11 \times 10^{-12}$	
6	1	1	1	235	$-0.110 \times 10^{-8}$	-0.260	-0.168	$3.42 \times 10^{-12}$	20.8
				251	-0.134	-0.123	-0.0946	1.37	-13.6
				265	-0.125	-122	-13.7	0.60	7.7
								$5.39 \times 10^{-12}$	

K in mm.Hg., k in (moles/gr., min., mm.Hg.  $(n_T + n_H)$ )



in Table III-2. Runs 29 and 30 were not included in the analysis because, during early attempts to correlate the data, it was noticed that these two runs were inconsistent with the remainder of the data. This inconsistency can be noticed on Figure III-3.

c. Final Kinetic Equation

As mentioned in Section III-C-3-b, the least-square values of the constants  $k^*$ ,  $E_a$ ,  $K_T^*$ ,  $E_T$ ,  $K_{H_2S}^*$ , and  $E_{H_2S}$  in the rate equation

$$r_T = \frac{k^* \cdot e^{E_a/RT} \cdot p_T \cdot p_H^{n_H}}{(1 + K_T^* \cdot e^{E_T/RT} \cdot p_T + K_{H_2S}^* \cdot e^{E_{H_2S}/RT} \cdot p_{H_2S})^2} \quad \text{(III-14)}$$

were calculated by the final program, which was described in Section III-B-4-c, for  $n_H = 0$  and 1. The results of the final calculations for Models 3 and 5 are presented Table III-3 below.

Table III-3

Results of Final Kinetic Analysis-Thiophene Disappearance

	Model 3 ( $n_H = 0$ )	Model 5 ( $n_H = 1$ )
$k^*$ (moles/ min., gr. cat., mm. <sup>(1+n<sub>H</sub>) Hg)</sup>	$0.8830 \times 10^{-2}$	$0.6019 \times 10^{-7}$
$E$ (Kcal/ mole)	-9.028	-3.670
$K_T^*$ (mm.Hg <sup>-1</sup> )	$0.1224 \times 10^{-8}$	$0.2112 \times 10^{-11}$
$E_T$ (Kcal/ mole)	17.90	24.29
$K_{H_2S}^*$ (mm.Hg <sup>-1</sup> )	$0.317 \times 10^{-6}$	$0.3085 \times 10^{-9}$
$E_{H_2S}$ (Kcal/ mole)	11.80	18.91
Maximum Error (%)	22.6	18.2
Sum of Squares of Deviations	$0.3995 \times 10^{-11}$	$0.3152 \times 10^{-11}$

Because the sum of the squares of the deviations is smaller for Model 5 than for Model 3, Model 5 is preferred.

Table III-4

Final Values of Kinetic Parameters--Thiophene Disappearance

Model No. 5,  $n_T = 1$ ,  $n_H = 1$ ,  $n_D = 2$

<u>Constant</u>	<u>Temperature</u>		
	<u>235 °C</u>	<u>251 °C</u>	<u>265 °C</u>
$k(\text{moles/ gr.cat., min, mm.}^2_{\text{Hg}})$	$0.1589 \times 10^{-8}$	$0.1775 \times 10^{-8}$	$0.1945 \times 10^{-8}$
$K_T (\text{mm.Hg}^{-1})$	0.05923	0.02842	0.01549
$K_{H_2S} (\text{mm.Hg}^{-1})$	0.04198	0.02370	0.01478

Figure III-4 is a plot of the calculated values of the thiophene disappearance rate versus the experimental values. The final kinetic equation, Model 5, with the constants shown in Table III-3, was used to generate the calculated rates in this figure.

3. The Rate of Butane Formation

a. Kinetic Data

Figure III-5 is a plot of the rate of butane formation versus the total butene partial pressure, at each of the three reactor temperatures. As shown in the key on Figure III-5, different symbols were used to identify the points corresponding to runs made with and without hydrogen sulfide in the feed to the reactor. The three solid lines on this figure are not meant to describe the best fit of the points, but merely serve to connect the points for which there was no hydrogen sulfide in the feed, at each of the three reactor temperatures.

For the reason discussed in Section III-C-2-a, Run 28 is not

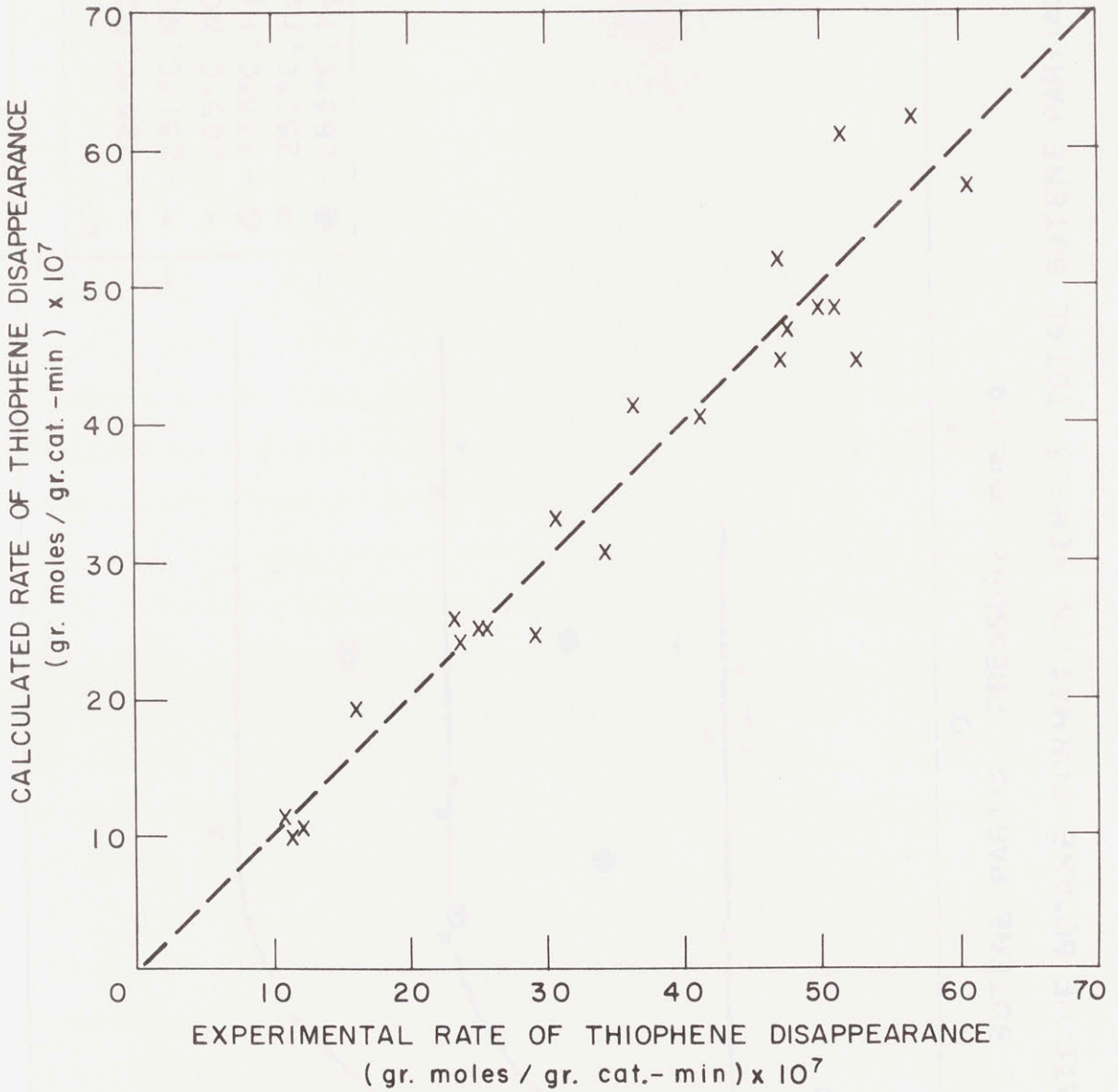


FIGURE III - 4 CALCULATED RATE OF THIOPHENE DISAPPEARANCE (MODEL 5) VERSUS EXPERIMENTAL RATE OF THIOPHENE DISAPPEARANCE





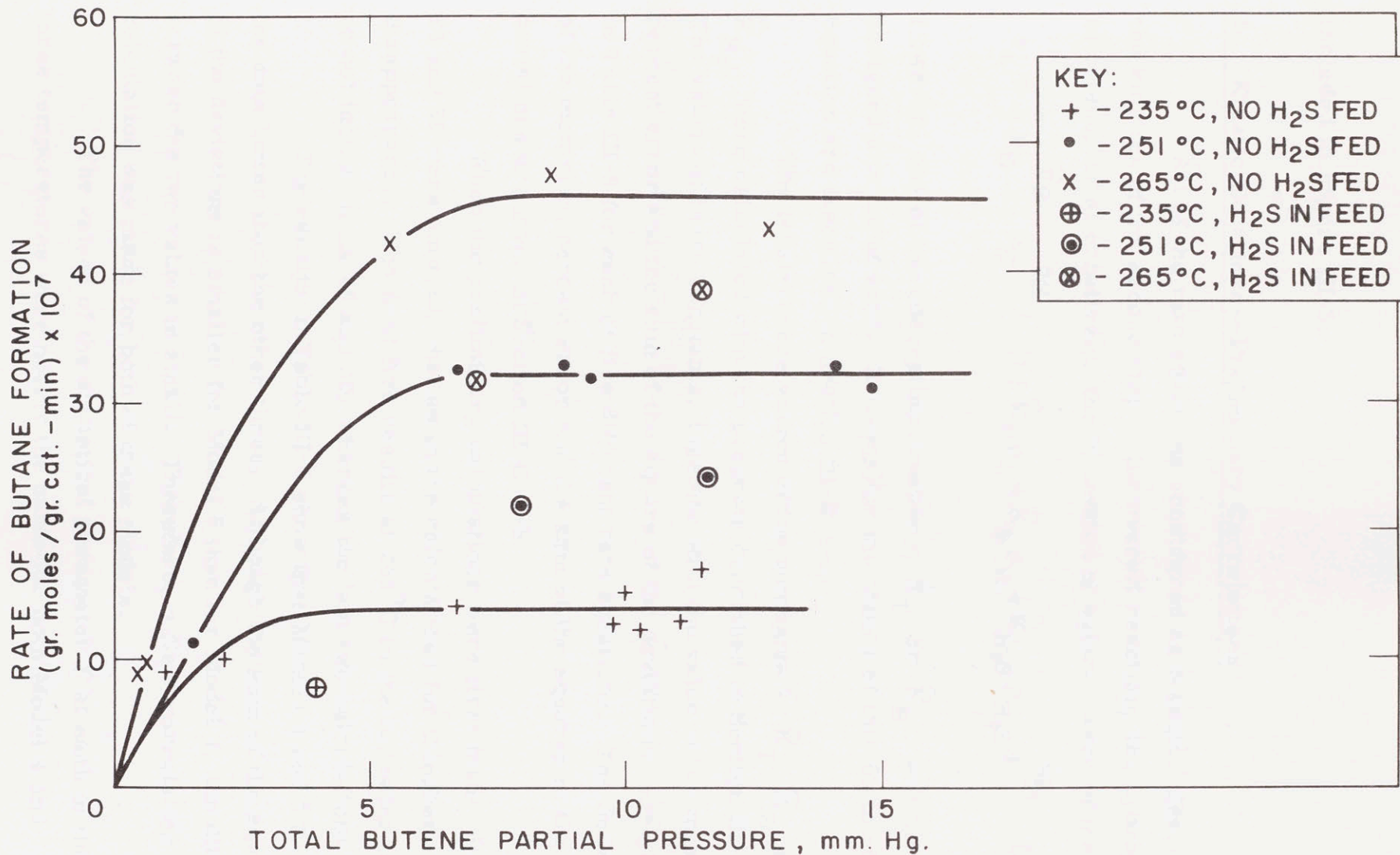


FIGURE III-5 RATE OF BUTANE FORMATION VERSUS TOTAL BUTENE PARTIAL PRESSURE





included in Figure III-5.

b. Kinetic Equations--Preliminary Correlations

All of the rate equations considered as potential descriptions of the kinetics of the second step of the overall reaction, the hydrogenation of butene, or alternatively, the formation of butane, were of the form

$$r_c = \hat{k} p_B^{\hat{n}_B} p_H^{\hat{n}_H} / (1 + \hat{K}_T p_T + \hat{K}_B p_B + \hat{K}_{H_2S} p_{H_2S})^{\hat{n}_D} \quad (III-17)$$

However, one of the adsorption constants,  $\hat{K}_T$  or  $\hat{K}_B$ , was always assigned a value of zero. Reasons for the choice of this form of rate equation are discussed in Section III-D-4-a.

The least-square values of the constants  $\hat{k}$ ,  $\hat{K}_T$ ,  $\hat{K}_B$  and  $\hat{K}_{H_2S}$  were calculated with the program described in Section III-B-4-b. The values of these constants, together with the value of the maximum percent error and the sum of the square of the deviations, are given in Table III-5 for each of five different rate equations. The definitions of the maximum percent error and the sum of the squares of the deviations are given in Section III-C-2-b.

When the preliminary calculations were first made, Runs 29 and 30 were omitted, just as in the calculations for thiophene disappearance. The first five results at 265°C in the following table do not include Runs 29 and 30, whereas the last two calculations do.

The results in Table III-5 show that Models 4 and 5 fit the data better than the other three. Although the sum of the squares of the deviations is smaller for Model 5 than for Model 4, the difference between the two values is small. Therefore, a final correlation calculation was made for both of these models.

The values of the statistical parameter F at each of the three temperatures were nearly the same for both Model 4 and

TABLE III-5

## Results of Preliminary Kinetic Analysis-Butane Formation

Model Number	$\hat{n}_B$	$\hat{n}_H$	$\hat{n}_D$	T(°C)	$\hat{k}$	$\hat{K}_T$	$\hat{K}_{H_2S}$	$\hat{K}_B$	Sum of Squares of Deviations	Maximum Percent Error
1	1	0	1	235	$0.598 \times 10^{-6}$	0.0737	-0.00369	0	$0.29 \times 10^{-12}$	-38.8
				251	0.649	0.0323	0.00776	0	0.69	-25.4
				265	1.18	0.0114	0.0240	0	0.14	- 6.9
								$1.12 \times 10^{-12}$		
2	1	0	2	235	$0.637 \times 10^{-6}$	0.0229	0.00315	0	$0.48 \times 10^{-12}$	-35.9
				251	0.598	0.0114	0.00211	0	0.99	-26.6
				265	1.00	0.00260	0.00728	0	0.25	- 8.3
								$1.72 \times 10^{-12}$		
3	1	1	2	235	$0.148 \times 10^{-8}$	0	0.0176	0.139	$0.29 \times 10^{-12}$	-21.9
				251	0.118	0	0.00562	0.0442	0.29	19.9
				265	0.121	0	0.00629	-0.00294	0.18	- 7.0
								$0.76 \times 10^{-12}$		
4	1	1	1	235	$0.319 \times 10^{-8}$	0	0.123	1.31	$0.19 \times 10^{-12}$	-17.8
				251	0.153	0	0.0261	0.164	0.19	14.9
				265	0.130	0	0.0180	-0.0111	0.11	- 6.1
								$0.49 \times 10^{-12}$		
5	1	0	1	235	$0.350 \times 10^{-5}$	0	0.191	2.03	$0.20 \times 10^{-12}$	-18.7
				251	0.167	0	0.0505	0.267	0.14	11.6
				265	0.150	0	0.0634	0.0634	0.13	6.5
								$0.47 \times 10^{-12}$		
Additional Calculations for 265°C, including Runs 29 and 30										
4	1	1	1	265	$0.250 \times 10^{-8}$	0	0.0222	0.156	$0.44 \times 10^{-12}$	-28.9
									$0.82 \times 10^{-12}$	
5	1	0	1	265	$0.239 \times 10^{-8}$	0	0.0395	0.225	0.28	-25.5
									$0.62 \times 10^{-12}$	

$\hat{K}$  in mm. Hg.,  $\hat{k}$  in (moles/ gr. cat., min., mm. Hg. ( $\hat{n}_B + \hat{n}_H$ ))



Model 5, having a value of about 2.6 at 235°C, 16.0 at 251°C and 5.5 at 265°C, if Runs 29 and 30 are omitted, and 23.2 if Runs 29 and 30 are included. The value of F at 235°C is lower than the 5% limit and the value at 251°C is well above the 5% limit. The value at 265°C is below the 5% limit if Runs 29 and 30 are omitted and well above if Runs 29 and 30 are included. For this reason, Runs 29 and 30 were included in the final correlation calculations.

Finally, a series of calculations was made using the rate equation of Model 5, but using modified values of the reaction rate in the calculations. Instead of feeding the actual reaction rates to the computer, values of the quantity  $(r_c - f \cdot r_T)$  were fed. The meaning of the parameter  $f$  is discussed in Section III-D-4-a. Calculations were performed for values of  $f$  equal to 0.20 and 0.40. In every case, the largest percent error was greater for  $f = 0.20$  than for  $f = 0$  and the value of the statistical parameter  $F$  was significantly smaller for  $f = 0.20$  than for  $f = 0$ . Similarly, the largest percent error was greater for  $f = 0.40$  than for  $f = 0.20$  and the value of  $F$  was significantly smaller for  $f = 0.40$  than for  $f = 0.20$ . The sum of the squares of the deviations was about the same for all values of  $f$ , which is surprising since the value of the rate,  $(r_c - f \cdot r_T)$ , declined as  $f$  was increased.

### c. Final Kinetic Equation

As mentioned in the preceding section, least-square values of the constants  $\hat{k}^*$ ,  $\hat{E}_a$ ,  $\hat{K}_B^*$ ,  $\hat{E}_B$ ,  $\hat{K}_{H_2S}^*$ , and  $\hat{E}_{H_2S}$  in the rate equation

$$r_c = \frac{\hat{k}^* \cdot e^{\hat{E}_a/RT} \cdot p_B \cdot p_H^{\hat{n}_H}}{(1 + \hat{K}_B^* \cdot e^{\hat{E}_B/RT} \cdot p_B + \hat{K}_{H_2S}^* \cdot e^{\hat{E}_{H_2S}/RT} \cdot p_{H_2S})} \quad \text{(III-18)}$$



were calculated by the final program, for values of  $\hat{n}_H = 0$  and 1. The results of the final calculations for Models 4 and 5 are presented in Table III-6.

Table III-6

Results of Final Kinetic Analysis-Butane Formation

	Model 4 ( $\hat{n}_H = 1$ )	Model 5 ( $\hat{n}_H = 0$ )
$\hat{k}^*$ (moles/ min., gr.cat., mm. Hg. $(1 + \hat{n}_H)$ )	$0.4165 \times 10^{-11}$	$0.2917 \times 10^{-10}$
$\hat{E}_a$ (Kcal. / mole)	6.685	11.99
$\hat{K}_B^*$ (mm.Hg $^{-1}$ )	$0.1315 \times 10^{-20}$	$0.2468 \times 10^{-22}$
$\hat{E}_B$ (Kcal. / mole)	49.12	53.77
$\hat{K}_{H_2S}^*$ (mm.Hg $^{-1}$ )	$0.2221 \times 10^{-14}$	$0.3296 \times 10^{-14}$
$\hat{E}_{H_2S}$ (Kcal. / mole)	32.19	32.42
Maximum Error (%)	-26.1	-22.2
Sum of Squares of Deviations	$0.8724 \times 10^{-12}$	$0.5064 \times 10^{-12}$

Because the sum of the squares of the deviations is smaller for Model 5 than for Model 4, Model 5 is preferred and will subsequently be referred to as the final kinetic equation for butane formation. The final values of the kinetic parameters at the three reaction temperatures are given in Table III-7.

Table III-7

Final Values of Kinetic Parameters-Butane Formation

Model No. 5,  $\hat{n}_B = 1$ ,  $\hat{n}_H = 0$ ,  $\hat{n}_D = 1$

<u>Constant</u>	<u>Temperature</u>		
	<u>235 °C</u>	<u>251 °C</u>	<u>265 °C</u>
$\hat{k}$ (moles/ gr. cat., min., , $\frac{\text{mm.}^1}{\text{Hg}}$ )	$0.3859 \times 10^{-5}$	$0.2692 \times 10^{-5}$	$0.1999 \times 10^{-5}$
$\hat{K}_B$ ( $\text{mm.}\cdot\text{Hg}^{-1}$ )	2.330	0.4630	0.1218
$\hat{K}_{H_2S}$ ( $\text{mm.}\cdot\text{Hg}^{-1}$ )	0.2341	0.08837	0.04216

Figure III-6 is a plot of the calculated values of the rate of butane formation versus the experimental values. The final kinetic equation, with the constants shown in Table III-7, was used to generate the calculated rates.

4. The Reliability of the Data

a. Material Balances

As stated in Section III-B-1, two material balances were checked for each run. The results of the reaction products balance, which is defined as the difference between the amount of hydrogen sulfide produced by the reaction and the total amount of C<sub>4</sub>'s thus produced, divided by the sum of these amounts, are summarized in Table III-8 below. The results of the sulfur balance closure, which is defined as the difference between the molar purge rate of total sulfur (thiophene plus hydrogen sulfide) and the molar feed rate of total sulfur, divided by the sum of the thiophene and hydrogen sulfide feed rates, are summarized in Table III-9 below. Tables III-8 and III-9 are based on the runs shown in Appendix C-3; the values of the closures for the

individual runs are given in Appendix C-3.

Table III-8

Results of Reaction Products Closures

	<u>Percent Closure</u>	<u>Run Numbers</u>
Root Mean Square Closure	3.0	----
Range	-5.8 → 5.2	31-5

If Runs 28-33 are omitted, the root mean square reaction products closure is reduced to 2.4 percent and the range becomes -4.0 → 5.2 percent. Further, the reaction products closures for Runs 28-33 are all negative, indicating that the rate of production of C<sub>4</sub>'s was greater than the rate of H<sub>2</sub>S production.

Table III-9

Results of Sulfur Balance Closures

	<u>Percent Closure</u>	<u>Run Numbers</u>
Root Mean Square Closure	5.6	----
Range	-15.3 → 4.1	31 - 5

Omission of Runs 28-33 reduces the RMS closure of the sulfur balance to 2.4 percent and the range to -3.7 → 4.1 percent. Once again, the closures for Runs 28-33 are all negative, indicating that the purge stream was sulfur deficient during these runs.



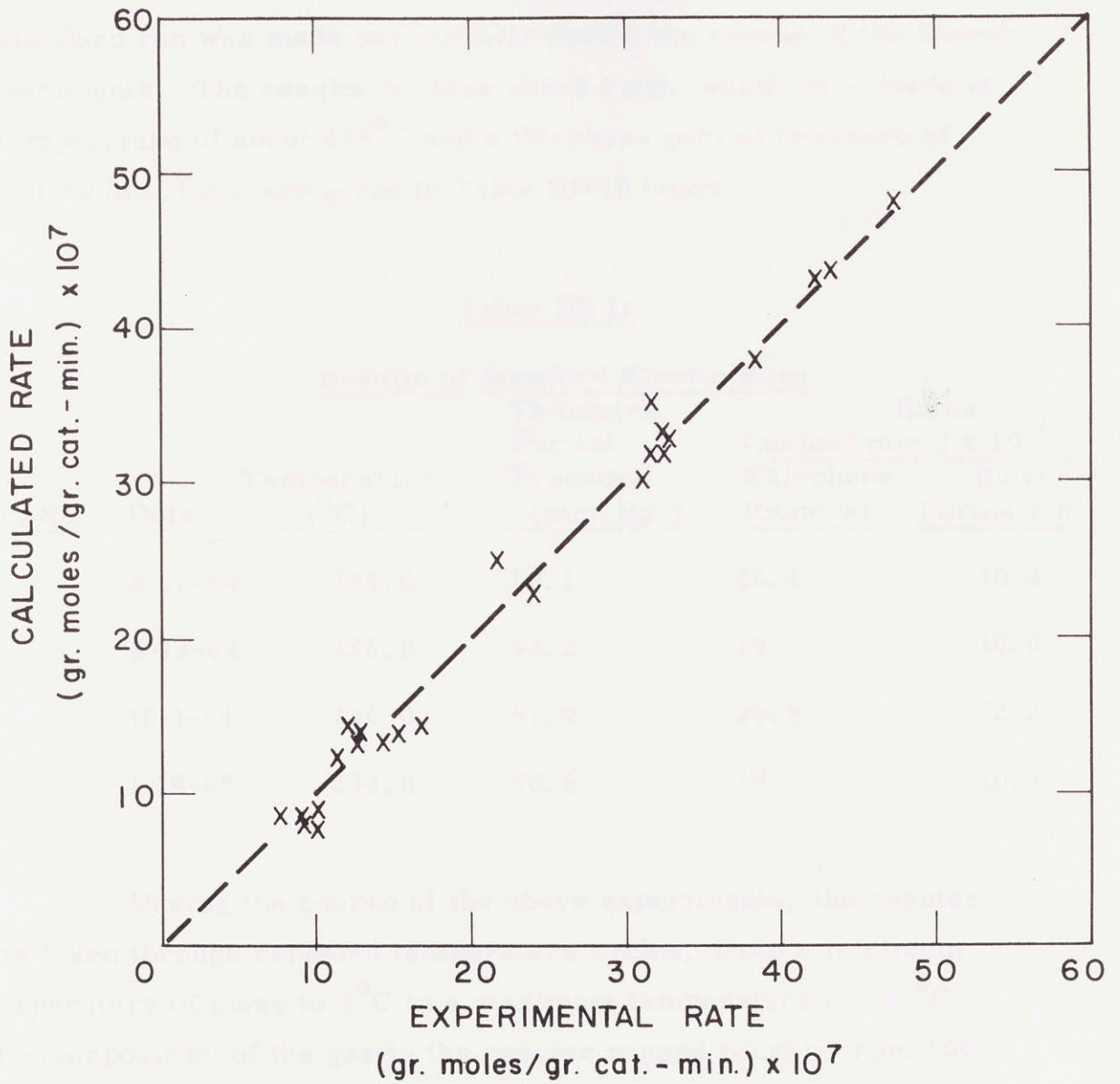


FIGURE III -6 CALCULATED RATE OF BUTANE FORMATION (MODEL 5) VERSUS EXPERIMENTAL RATE OF BUTANE FORMATION



b. Reproducibility

In order to check for possible changes in catalyst activity, a standard run was made periodically during the course of the kinetic experiments. The results of these check runs, which were made at a temperature of about 235°C and a thiophene partial pressure of about 50 mm.Hg., are given in Table III-10 below.

Table III-10

<u>Run No.</u>	<u>Date</u>	<u>Results of Standard Kinetic Runs</u>			
		<u>Temperature (°C)</u>	<u>Thiophene Partial Pressure (mm. Hg.)</u>	<u>Rates (moles/ min.) x 10<sup>-6</sup></u>	
				<u>Thiophene Removal</u>	<u>Butane Formation</u>
5	8-12-64	235.6	50.1	20.4	10.4
6	8-13-64	236.0	52.2	19.1	10.0
19	10-1-64	236.0	51.9	20.8	12.2
44	1-18-65	234.8	50.8	19.2	10.3

During the course of the above experiments, the reactor was taken through repeated temperature cycles, from a minimum temperature of close to 0°C to a maximum temperature of 309°C. The composition of the gas in the reactor ranged roughly from 100 percent hydrogen to 100 percent hydrogen sulfide. Further, although prolonged exposure of the catalyst to air was avoided, especially at high temperatures, some air undoubtedly was introduced into the catalyst bed during the connection and disconnection of the thiophene pump.

If the effects of the small variations in thiophene partial pressure and temperature are discounted, the results of Table III-10



provide a quantitative estimate of the reproducibility. Thus, the maximum difference in the rate of thiophene disappearance was about 9 percent, and the maximum difference in the rate of butane formation was about 22 percent.

### 5. Unsteady-State Behavior

When runs were made, starting from a shut-down condition, the unsteady-state behavior of the reactor followed a typical pattern: 1) no products of the reaction could be detected until several hours after the thiophene feed was started, 2) butane was the first product to appear, followed closely by the butenes and later by  $H_2S$ , 3) butane and the butenes reached a steady-state composition before hydrogen sulfide did.

When runs were made by changing the operating conditions, without an intervening shutdown, the unsteady-state behavior was difficult to characterize, possibly because the changes in temperature or feed rate frequently were small. It appeared, however, that both  $H_2S$  and the  $C_4$ 's approached steady-state at nearly equal rates.

### III. - D. Discussion of Results

#### 1. Unsteady-State Behavior

Quantitative interpretation of the unsteady-state behavior mentioned in Section III-C-5 is difficult because measurements were made infrequently during the unsteady-state period, and because the effects of a changing catalyst surface are hard to separate from the effect of unsteady-state mixing in the reaction loop. It was not possible to determine whether the catalytic activity changed during the unsteady-state period or whether the activity remained constant, but the amount of material adsorbed changed with time.

Qualitatively, the observation that the hydrogen sulfide composition took longer to reach steady-state than did the butene and butane compositions is consistent with a catalyst surface that is sulfur deficient. It appears that some of the hydrogen sulfide formed in the initial stages of the reaction either reacts with unsulfided components of the catalyst and/ or is retained by the catalyst as adsorbed hydrogen sulfide.

The interpretation of the observation that butane is the first reaction product to appear may depend on the mechanism by which the catalyst retains sulfur during the unsteady-state. Thus, if the catalyst is sulfiding during the unsteady-state, it may be that when reaction occurs on unsulfided sites, butene is not desorbed but reacts to butane on the original desulfurization site. Alternatively, it may be that hydrogenation occurs on sites which adsorb hydrogen sulfide strongly, and therefore the formation of butane is repressed as hydrogen sulfide builds up on the catalyst surface.



## 2. The Reliability of the Data

### a. Material Balances

The material balance closures, which were presented in Section III-C-4-a, are generally good. These closures support the conclusion that hydrogen sulfide, butane, 1-butene and cis and trans 2-butene were the only reaction products that needed to be considered. Thus, the reaction scheme shown in (III-A) appears to be an adequate representation of the major reactions that occurred during this study.

Both the reaction products closures and the sulfur balance closures were significantly poorer for Runs 28-33 than for the other runs, and the direction of these closures indicates that the effluent from the reactor was sulfur deficient in all six runs. Runs 28 through 33 were the only experiments carried out with a 1cc. syringe in the hypodermic pump and the thiophene feed rate was about one-sixth of the rate for the other runs. Hydrogen sulfide was not fed during any of Runs 28-33. The retention of sulfur by the catalyst during the unsteady-state portion of a run, as discussed in the preceding section, was probably responsible for these relatively poor material balance closures. Because of the low sulfur feed rate, the steady-state was approached slowly, and it is probable that complete saturation of the catalyst surface with sulfur was not achieved during some of the low feed-rate runs. This explanation is consistent with the direction of the material balance closures.

### b. Reproducibility

Table III-10 shows that the reproducibility of the catalytic activity was excellent, and that no significant drift in activity took place during the period of the kinetic experiments. It is significant that the activity was unaffected by repeated temperature cycles and



even by exposure to air.

### 3. The Kinetics of Thiophene Disappearance

#### a. Potential Kinetic Equations

Several characteristics of the kinetic data, that are pertinent to the choice of potential kinetic models, are evident in Figure III-3. In the first place, as shown by the solid lines on this figure, the reaction rate goes through a maximum with increasing thiophene partial pressure, for the runs with no hydrogen sulfide in the feed. A distinct maximum occurs at each of the three reactor temperatures.

The existence of these maxima precludes the possibility of describing the reaction rate in a meaningful manner with a simple, integer-power rate equation such as a zero, first or second-order rate equation. Therefore, Langmuir-Hinshelwood rate equations were the only kinetic equations with which a correlation of the data was attempted.

The points on Figure III-3 that correspond to the runs made with hydrogen sulfide in the feed all fall significantly below the lines connecting the points with no hydrogen sulfide fed, at the same reactor temperature. Thus, it was necessary to include a term for the adsorption of hydrogen sulfide in the denominator of the L-H equations. The maximum in the reaction rate suggests the existence of a large adsorption constant for thiophene and such a term was also included in the denominator of the rate equation.

An adsorption term for hydrogen was not included. The hydrogen partial pressure was relatively constant for all the runs, ranging from 605 to 782 mm. Hg., a variation of about 30%. Thus, even if the hydrogen adsorption term in the denominator of the rate equation were large, the term would be difficult to evaluate from the present data. Under these circumstances, neglecting the hydrogen

adsorption causes no loss in accuracy. The small variation in the hydrogen partial pressure also makes it difficult to determine whether hydrogen should appear in the numerator of the rate equation and, if so, to what exponent. There is precedent for neglecting the effect of hydrogen on the reaction rate; as discussed in Section III-A-4, Pease and Keighton (49) found almost no effect.

No adsorption terms for butene and butane were included in the denominator of the rate equation. From chemical considerations, it is difficult to conceive that any type of butane adsorption could be strong enough to retard the reaction, i. e., compete effectively with thiophene for available catalyst sites. With butene, a fairly strong adsorption, of magnitude comparable to thiophene, can be visualized. However, as discussed in Section III-A-4, the results of Owens and Amberg (45) indicated that butene could not seriously retard the reaction. Further, since butene and butane were never present in the feed, the partial pressures of these components varied in a regular manner with the thiophene partial pressure and it is doubtful whether meaningful adsorption constants for these components could be calculated from the present data.

Thus, all the rate equations for which preliminary correlation calculations were made were of the form shown in Equation (III-11).

$$r_T = k p_T^{n_T} p_H^{n_H} / (1 + K_T p_T + K_{H_2S} p_{H_2S})^{n_D} \quad (\text{III-11})$$

No calculations were made for the case  $n_T = 0$ , because Equation (III-11) does not go through a maximum as  $p_T$  increases when  $n_T = 0$ . Therefore, this case cannot meaningfully describe the data. As discussed in Section III-A-6, the case  $n_T = 0$  corresponds mechanistically to the assumption that the adsorption of hydrogen on a uniform catalyst surface is the rate-limiting step. Thus, although several



investigators (20),(47) have suggested that hydrogen adsorption could control the reaction rate, the present data are not consistent with that assumption.

The ten rate equations shown in Table III-11 were chosen as the best potential models of the kinetic process. Table III-11 also lists the assumptions from which each equation is derivable. Although the equations for which  $n_D = 1$  would seem not to possess a maximum in  $p_T$ , they were considered because the partial pressure of hydrogen sulfide generally was large when  $p_T$  was large, and vice versa. Thus, it seemed conceivable that the decrease in rate at high thiophene partial pressures might be the result of increased retardation by hydrogen sulfide.

A preliminary correlation was calculated for each of the first six models in Table III-11 and the results are presented in Table III-2 in Section III-C-2-b. No calculation was made for Model 7 because, in view of the constancy of the hydrogen partial pressure from run to run, this model is a special case of Model 6. No preliminary calculations were done for Models 8 and 9, because the constancy of the hydrogen partial pressure makes them indistinguishable from Models 5 and 1, respectively. Similarly, other kinetic equations not shown in Table III-11 can be postulated, but in almost all cases they differ from one of those shown only by a factor of  $p_H$  to some small power, and would therefore be indistinguishable from one of the equations considered.

No separate calculation was made for Model 10 because this model is a special case of Model 3.

#### b. Preliminary Correlations

The results of preliminary correlation calculations for Models 1 through 6 were presented in Section III-C-2-b. These results



Table III-11

## Potential Kinetic Equations - Thiophene Disappearance

Model Number	Equation	Surface	RLS	H <sub>2</sub> Adsorption	C <sub>4</sub> H <sub>4</sub> S Adsorption
1	$k p_{T} p_{H} / (1 + K_{T} p_{T} + K_{H_2 S} p_{H_2 S})^3$	homogeneous	surface reaction	atomic	two point
2	$k p_{T} p_{H}^2 / (1 + K_{T} p_{T} + K_{H_2 S} p_{H_2 S})^3$	homogeneous	surface reaction	molecular	two point
3	$k p_{T} / (1 + K_{T} p_{T} + K_{H_2 S} p_{H_2 S})^2$	two types of site; C <sub>4</sub> H <sub>4</sub> S+H <sub>2</sub> S on one, the other essentially sat'd with H	surface reaction	either	two point
4	$k p_{T} p_{H} / (1 + K_{T} p_{T} + K_{H_2 S} p_{H_2 S})^4$	homogeneous	surface reaction	atomic	two point
5	$k p_{T} p_{H} / (1 + K_{T} p_{T} + K_{H_2 S} p_{H_2 S})^2$	homogeneous	surface reaction	molecular	one point
		two types of site; C <sub>4</sub> H <sub>4</sub> S+H <sub>2</sub> S on one, H on the other (low coverage)	surface reaction	either	two point
6	$k p_{T} p_{H} / (1 + K_{T} p_{T} + K_{H_2 S} p_{H_2 S})$	"	surface reaction	either	one point
7	$k p_{T} / (1 + K_{H_2 S} p_{H_2 S})$	-----	adsorption of thiophene	---	one point
8	$k p_{T} \sqrt{p_{H}} / (1 + K_{T} p_{T} + K_{H_2 S} p_{H_2 S})^2$	homogeneous	surface reaction	atomic	one point
		two types, C <sub>4</sub> H <sub>4</sub> S+H <sub>2</sub> S on one, H on the other	surface reaction	atomic	two point
9	$k p_{T} \sqrt{p_{H}} / (1 + K_{T} p_{T} + K_{H_2 S} p_{H_2 S})^3$	homogeneous	surface reaction	atomic	two point
10	$k p_{T} / (1 + K_{H_2 S} p_{H_2 S})^2$	-----	adsorption of thiophene	---	two point

show that Models 3 and 5 are superior to the others tested. Although the sum of the squares of the deviations is slightly smaller for Model 3 than for Model 5, the difference between the two is insignificant. Final correlations were calculated for both Model 3 and Model 5. The fact that these two models produce correlations that are virtually indistinguishable is not surprising since the models differ by only a factor of  $p_H$  in the numerator of the rate equation. The partial pressure of hydrogen,  $p_H$ , varies very little from run to run. A more detailed discussion of Models 3 and 5 appears in the next section.

The poor performance of Model 6 relative to Models 3 and 5 is of interest. Not only are the sum of the squares of the deviations and the maximum percent error relatively high for Model 6, but also the constants  $k$ ,  $K_T$ , and  $K_{H_2S}$  are all negative, a situation that has no meaning from a physical standpoint. Model 6 is a generalization of the rate equation that results from the assumption that the RLS is the one-point adsorption of thiophene. Thus, the kinetic data are not consistent with this mechanism.

Using the values of  $K_T$  for Model 3, as given in Table III-2, the value of  $K_T p_T$  was calculated to be, roughly, unity. The  $K_T p_T$  term in the denominator of the rate equation is not negligible, as it should be if Model 10 provided a good description of the data. Thus, again, the kinetic data is not consistent with the assumption that thiophene adsorption is the rate-limiting step. This is in agreement with the work of Owens and Amberg (45),(47) who concluded, on the basis of measurements of the rate of adsorption, that thiophene adsorption was unlikely to be rate-controlling.

### c. The Final Rate Equation

As shown in Section III-C-2-c, Model 5 provided the best fit of the experimental data. Therefore, the form of the final rate



equation for thiophene disappearance is

$$r_T = k p_T p_H / (1 + K_T p_T + K_{H_2S} p_{H_2S})^2 \quad (\text{III-19})$$

Values of  $k$ ,  $K_T$ , and  $K_{H_2S}$  are given in Table III-4, and these constants are expressed in terms of activation energies and pre-exponential factors in Table III-3.

The form of the final rate equation is interesting in that, at constant hydrogen sulfide partial pressure, the reaction rate goes through a maximum as  $p_T$  is increased. This property was suggested in Figure III-3. Such a maximum has important implications in the area of internal diffusion effects, as will be discussed in Section IV.

### I. Accuracy

Table III-3 shows that the maximum error in the correlation for all the data points is +18.2 percent. The arithmetic average of the absolute magnitude of the percent errors is 8.7 percent and the best estimate of the standard deviation for the correlation is  $3.87 \times 10^{-7}$  gr. moles/ gr. cat., min.

A visual representation of how well the final rate equation fits the experimental data is given in Figure III-4 of Section III-C-2-c. This figure, together with the above statistical values, shows that the final correlating equation describes the kinetic data very well.

### II. Comments on the Reaction Mechanism

As stated in Table III-11, the final form of the rate equation is consistent with at least two models of the kinetic process. The first involves a homogeneous surface on which hydrogen adsorbs as a molecule, and on which thiophene attaches to a single site. The rate-limiting step is the combination of adsorbed thiophene and adsorbed



hydrogen molecules. The main objection to this picture is the assumption that thiophene is adsorbed at only one site. All the reaction mechanisms that have been postulated to date involve two-point adsorption of thiophene, either by opening of a C-C double bond or by rupture of a C-S bond. Although Nicholson (42) did detect a one-point adsorption of thiophene, with the sulfur atom attached to the catalyst surface, it is difficult to imagine how this complex could be reactive towards hydrogen.

The second mechanism that is consistent with the final rate equation involves a catalyst surface that has two types of sites. Thiophene and hydrogen sulfide can adsorb on one type, but only hydrogen adsorbs on the second. Thiophene undergoes a two-point adsorption, hydrogen sulfide occupies a single site. The RLS is the combination of adsorbed thiophene with adsorbed hydrogen.

The fact that the numerator of the rate equation contains  $p_H$  to the first power suggests that hydrogen is adsorbed as molecules, with the surface coverage relatively low. However, since the hydrogen partial pressure was almost constant from run to run, it is probable that  $\sqrt{p_H}$  in the numerator would also correlate the data well. A numerator containing  $\sqrt{p_H}$  would imply atomic adsorption at low coverages.

The second mechanism is more in agreement with reality than the first. As mentioned earlier, a two-point thiophene adsorption is generally regarded as necessary. Further, the picture of a heterogeneous surface has a physical rationale. Thiophene, once it covers the surface in moderate amounts, presents a steric hinderance to the adsorption of large molecules, even if the sites are available. However, since hydrogen is a small molecule, it might have access to sites that larger molecules cannot reach. Thus, even a homogeneous surface might appear heterogeneous, in a reaction sense, because of steric effects.

It should be emphasized that the resulting form of the rate equation does not prove that one of the above mechanisms is the correct one. The preceding discussion is meant only to show that the rate equation is consistent with a reasonable physical picture of the kinetic process.

### III. The Effect of Thiophene and Hydrogen Sulfide Adsorption

Using the data in Appendix C-3 and Table III-4, the values of  $K_T p_T$  and  $K_{H_2S} p_{H_2S}$  can be calculated for each experimental run. The maximum value of  $K_T p_T$  for any run was 3.09 and the maximum value of  $K_{H_2S} p_{H_2S}$  was 1.98. Since both of these values are large relative to unity, inhibition of the reaction by both thiophene and hydrogen sulfide was significant, with thiophene having the stronger effect, at least for the present study.

### IV. The Activation Energies

If  $K_T$  and  $K_{H_2S}$  are the actual adsorption-equilibrium constants for thiophene and hydrogen sulfide respectively, then the quantities  $-E_T$  and  $-E_{H_2S}$  are the energies of chemisorption of these two species. In reality,  $K_T$  and  $K_{H_2S}$  must be regarded as empirical constants rather than true equilibrium constants. Nevertheless, it is interesting to speculate on the temperature dependencies of  $K_T$  and  $K_{H_2S}$ . For the sake of simplicity,  $-E_T$  and  $-E_{H_2S}$  will be referred to as heats of chemisorption in the following discussion.

Table III-3 shows that the values of  $E_T$  and  $E_{H_2S}$  are +24.29 Kcal/ mole and +18.91 Kcal/ mole, respectively. These values were calculated from data that covered a very narrow temperature range of about 30°C, and consequently may not be as accurate as values derived from data taken over a wider range of temperature.



Nevertheless, based on these values of  $E_T$  and  $E_{H_2S}$ , the values of the heats of chemisorption of thiophene and hydrogen sulfide, respectively, are -24.29 Kcal/ mole and -18.91 Kcal/ mole. Since endothermic chemisorptions are quite rare, it is gratifying that the adsorptions of thiophene and hydrogen sulfide appear to be exothermic. The present value of the heat of adsorption for thiophene does not agree well with the value of -9.5 Kcal/ mole measured chromatographically by Owens and Amberg (45), but checks better with the value of -17 Kcal/ mole derived from rate measurements on sulfided chromia by van Looy and Limido (72).

The value of the quantity  $E_a$  is shown in Table III-3 to be 3.670 Kcal/ mole. Once again, this value may not be accurate due to the narrow temperature range of the experiments. Note that the negative of  $E_a$  is the activation energy that would be calculated from an Arrhenius plot of data obtained under conditions where the denominator of Eqn.(III-19) was unity.

The value of  $-E_a$  compares very poorly with the value of 25 Kcal/ mole, which Owens and Amberg (45),(46) reported as the activation energy of the reaction, on both cobalt molybdate and sulfided chromia catalysts. However, the activation energies in the present study and in the Owens and Amberg studies do not have the same basis. As discussed in Section III-A-4, the value of Owens and Amberg was derived from the slope of a semi-log plot of the conversion in an integral reactor versus the reciprocal of the absolute temperature, a procedure that is strictly valid only for a zero-order reaction. Note that in the case of complex reaction kinetics, the slope of such a plot reflects not only the temperature dependence of the rate constant  $k$ , but also of the adsorption constants  $K_i$ . Some rough calculations on the present rate equation will illustrate this point.

Table III-4 shows that  $K_T$  and  $K_{H_2S}$  are nearly equal;



therefore assume  $K_{H_2S}$  equals  $K_T$ . Further, at any point in an integral, plug-flow reactor, the sum of  $p_T$  and  $p_{H_2S}$  is very nearly equal to the partial pressure of thiophene in the feed,  $p_{T,f}$ . Thus, Equation (III-19) becomes

$$r_T = k p_T p_H / (1 + K_T p_{T,f})^2 \quad \text{(III-20)}$$

Since  $p_H$  was large in the Owens and Amberg experiments, the reaction rate might appear to be first-order in thiophene.

If  $K_T p_{T,f} \ll 1$ ,  $r_T \cong k p_T p_H$  and the slope of a conversion versus  $(1/T)$  plot is equal to  $E_a/R$ , if the conversion is low. However, if  $K_T p_{T,f} \gg 1$ ,  $r_T \cong (k/K_T^2 p_{T,f}^2) p_T p_H$ . Under these circumstances, the slope of the plot is equal to  $(E_a - 2E_T)/R$ . For intermediate values of  $K_T p_{T,f}$ , the slope will be somewhere between the two extremes above. If the values of  $K_T$ ,  $E_a$  and  $E_T$  determined here can be applied to the Owens and Amberg study,  $K_T p_{T,f} \cong 1$ , so that the slope should lie between  $(3.67/R)$  and  $(3.67 + 2 \times 24.27)/R = 52.25/R$ . The value of  $(25/R)$  measured by Owens and Amberg lies between these extremes so the value of Owens and Amberg is not inconsistent with the present results.

A consequence of the above analysis is that the slope of the conversion versus  $(1/T)$  plot should get smaller as  $T$  is raised, because  $K_T$  declines. The plot of Owens and Amberg exhibits this behavior; but, as discussed in Section III-A-4, this may be a consequence of an improper method of plotting the data.

#### 4. The Kinetics of Butane Formation

##### a. Potential Kinetic Equations

Owens and Amberg (46) concluded that, with a sulfided chromia catalyst, between 25 and 50% of the butane formed in the reaction

resulted from hydrogenation of butene at the original desulfurization site, i. e., without intermediate desorption. No such conclusion was drawn for sulfided cobalt molybdate. Owens and Amberg (45) concluded that, for cobalt molybdate, desulfurization and hydrogenation took place at different sites to a large extent, and this conclusion seems to preclude the possibility that much butene can hydrogenate without first desorbing and subsequently readsorbing.

From the standpoint of investigating the effect of an intraparticle diffusional resistance, it is important to know whether appreciable butene hydrogenation takes place at the original desulfurization site, for if so, the effect of an intraparticle diffusional resistance on the selectivity of the reaction will be slight. If butene hydrogenation occurs to some extent without the desorption-adsorption step, the reaction scheme of (II-A) must be modified as shown in (III-F)



The selectivity behavior for (III-F) can be quite different from that of (II-A), depending on the relative importance of the direct reaction from A to C.

The ability to extract information regarding the importance of the direct reaction, i. e., butene hydrogenation without intermediate desorption, from the present data depends on the complexity of the rate equation for the step  $\text{B} \rightarrow \text{C}$ . Let  $r_c$  denote the total rate of butane formation. Therefore

$$r_c = r_{\text{A} \rightarrow \text{C}} + r_{\text{B} \rightarrow \text{C}}
 \tag{III-21}$$

Let  $\sigma_B$  be the fraction of the original desulfurization sites covered with butene that has never desorbed. Thus,  $\sigma_B$  is not a function



of  $p_B$ . The rate of desorption should be proportional only to  $\sigma_B$  and, since  $p_H$  is essentially constant, the rate of hydrogenation on these sites should be proportional only to  $\sigma_B$ . Therefore, a constant fraction,  $f$ , of the butene molecules being formed will hydrogenate on the original desulfurization site. The rate,  $r_{A \rightarrow C}$ , is

$$r_{A \rightarrow C} = f r_T \quad (\text{III-22})$$

Equation(III-22) shows that  $r_{A \rightarrow C}$  is a function only of the thiophene disappearance rate,  $r_T$ , and is independent of all partial pressures, except as they affect  $r_T$ . Substituting (III-22) into (III-21) gives

$$r_c = f \cdot r_T + r_{B \rightarrow C}$$

$$(r_c / r_T) = f + (r_{B \rightarrow C} / r_T) \quad (\text{III-23})$$

If the kinetic equation for  $r_{B \rightarrow C}$  is simple enough, it may be possible to extract an estimate of  $f$  from the data. Several simple mechanisms were considered as an aid in postulating a rate equation for  $B \rightarrow C$ ; the data shows that  $(r_c / r_T)$  is not a constant at a given temperature, so that  $r_{B \rightarrow C}$  is not zero. To start, it was assumed that desulfurization and hydrogenation took place on the same sites, and that the rate of hydrogenation was proportional to the product  $p_B p_H$ . If these assumptions hold

$$(r_{B \rightarrow C} / r_T) = s(p_B / p_T)(1 + K_T p_T + K_{H_2S} p_{H_2S})^a \quad (\text{III-24})$$

In Eqn. (III-24),  $a$  is an integer and  $s$  is a constant equal to the ratio of the rate constants for the two reactions. Since both rate constants must be positive, so must  $s$ . The adsorption constants,  $K_T$  and



$K_{H_2S}$  have the values previously computed for thiophene disappearance, and given in Table III-4. Combining Eqns. (III-23) and (III-24) gives

$$(r_c / r_T) = f + s(p_B / p_T)(1 + K_T p_T + K_{H_2S} p_{H_2S})^a \quad (III-25)$$

Equation (III-25) suggests that an arithmetic plot of  $(r_c / r_T)$  versus  $(p_B / p_T)(1 + K_T p_T + K_{H_2S} p_{H_2S})^a$  should yield a straight line with a slope  $s$  and an intercept  $f$ . Such plots were made for values of  $a = -1, 0$  and  $1$ . All three plots correlated the data very poorly. Scatter was pronounced and no clear trend in the data was evident. A plot of  $(1 / p_T)(1 + K_T p_T + K_{H_2S} p_{H_2S})$ , which is based on the assumption of a homogeneous surface, with adsorption of molecular hydrogen as the RLS in the second reaction, also failed to correlate the data.

The next plots tried were based on the assumption that butene hydrogenation took place on a second set of sites which were weak enough so that competition for sites was not important. Two different assumptions were made about the rate,  $r_{B \rightarrow C}$ ; the first was that it was proportional only to  $p_B$  and the second was that it was proportional only to  $p_H$ . Thus, for the first assumption

$$(r_c / r_T) = f + s(p_B / r_T) \quad (III-26)$$

and for the second assumption

$$(r_c / r_T) = f + s(p_H / r_T) \quad (III-27)$$

The plots based on the two equations above also failed to correlate the data.

It was felt that any attempt to correlate the data with a rate equation that included several adsorption terms in the denominator

of a L-H rate equation, and also included the constant  $f$ , would not produce a meaningful correlation because of the large number of arbitrary constants to be calculated. Therefore,  $f$  was assumed to equal zero, i. e., all the butene was assumed to desorb before it hydrogenated. With this assumption, the rate of the reaction  $B \rightarrow C$  is equal to the rate of butane formation, and kinetic equations such as those used for thiophene disappearance can be applied to produce a correlation between the rate of butane formation and the various partial pressures. The rate of thiophene disappearance,  $r_T$ , no longer exerts a primary influence on  $r_C$ .

Once again, the general trends of the kinetic data guided the choice of potential rate equations. As shown by the solid lines in Figure III-5, which lines apply only to the data with no hydrogen sulfide in the feed, the reaction rate is low at low butene partial pressures and reaches a flat plateau as the partial pressure of butene is increased. Further, the points on Figure III-5 that correspond to runs made with hydrogen sulfide in the feed fall significantly below the lines connecting the points with no hydrogen sulfide in the feed, at the same reactor temperature. The plateau effect and the effect of hydrogen sulfide in the feed preclude describing the reaction rate in a meaningful manner with a simple, integer-power rate equation. Various forms of L-H rate equation, with a term for hydrogen sulfide adsorption and a term for either butene or thiophene adsorption in the denominator, were the only rate equations tested. In order to minimize the number of arbitrary constants in the rate equation, denominators containing both thiophene and butene were not tested, although there is some possibility that both species could have an inhibiting effect.

Once again, for reasons similar to those mentioned in Section III-D-3-a, it was not necessary to test L-H rate equations



with a numerator consisting only of  $p_H$ , i. e., equations derived from the assumption that hydrogen chemisorption is the rate-limiting step. Also, because of the plateau in the rate versus butene partial pressure curve, it was unnecessary to test rate equations with a power greater than two on the denominator. In fact, it seems unnecessary to test the value of two, but such a test was made for completeness.

The five rate equations given by Eqns. (III-28) through (III-32) below were the only ones for which a preliminary correlation was calculated.

$$\text{Model 1: } r_c = \hat{k} p_B / (1 + \hat{K}_T p_T + \hat{K}_{H_2S} p_{H_2S}) \quad (\text{III-28})$$

$$\text{Model 2: } r_c = \hat{k} p_B / (1 + \hat{K}_T p_T + \hat{K}_{H_2S} p_{H_2S})^2 \quad (\text{III-29})$$

$$\text{Model 3: } r_c = \hat{k} p_B p_H / (1 + \hat{K}_B p_B + \hat{K}_{H_2S} p_{H_2S})^2 \quad (\text{III-30})$$

$$\text{Model 4: } r_c = \hat{k} p_B p_H / (1 + \hat{K}_B p_B + \hat{K}_{H_2S} p_{H_2S}) \quad (\text{III-31})$$

$$\text{Model 5: } r_c = \hat{k} p_B / (1 + \hat{K}_B p_B + \hat{K}_{H_2S} p_{H_2S}) \quad (\text{III-32})$$

These rate equations are similar to some of those considered for thiophene disappearance. The assumptions from which each of the above equations is derivable can be found by consulting the analogous equation for thiophene disappearance in Table III-11.

Other rate equations not listed above can be postulated, but in most cases they differ from Eqns. (III-28) through (III-32) only by a factor of  $p_H$  to some small power and are therefore indistinguishable from Models 1 through 5.

#### b. Preliminary Correlations

The results of the preliminary correlation calculations for



Models 1 through 5, Eqns.(III-28)through(III-32), are given in Section III-C-3-b. These results show that Models 4 and 5 are superior to the others tested. Although the sum of the squares of the deviations is slightly smaller for Model 5 than for Model 4, the difference between the two is probably not significant. The fact that these two models produce correlations that are virtually indistinguishable is not surprising since the rate equations differ by only a factor of  $p_H$  in the numerator. Final correlations were calculated for both models; a more detailed discussion of Models 4 and 5 appears in the next section.

The poor performance of Models 1 and 2 relative to 3, 4 and 5 is of interest, because Models 1 and 2 had a term for thiophene adsorption in the denominator, but no butene term. The opposite situation existed for Models 3, 4 and 5. The poor correlation for Models 1 and 2 is inconsistent with the assumption that both desulfurization of thiophene and hydrogenation of butene take place on the same sites. In this sense, the failure of Models 1 and 2 corroborates the failure of Eqn.(III-25)to correlate the data. The results of the preliminary analysis suggest that different types of sites are involved in the two reactions. Hydrogen sulfide competes for both sites, but butene does not compete for desulfurization sites and thiophene does not compete strongly for hydrogenation sites. Owens and Amberg (45) and Kirsch and Shull (27) have suggested the existence of different types of sites on cobalt molybdate catalysts.

The results of Section III-C-3-b show that the correlations produced when calculations were done with the rate equation of Model 5, and with values of  $f$  equal to 0.20 and 0.40, are significantly poorer than the correlation calculated for  $f$  equal to zero. This result, together with the failure of Eqns. (III-25),(III-26)and(III-27) to correlate the data, suggests that the best value of  $f$  for the present

data is zero. Mechanistically, a value of  $f = 0$  means that no hydrogenation of butene takes place at the original desulfurization site; all the butene desorbs and readsorbs before hydrogenating. This behavior is consistent with the assumption that the two reactions take place at separate sites. Thus, if the original desulfurization sites were active for hydrogenation, a better correspondence between the denominators of the two rate equations would be expected.

The previous two paragraphs have discussed the reaction mechanism in terms of the kinetic data. The purpose of this discussion has been to demonstrate that the data are consistent with a reasonable picture of the mechanism, not to prove or disprove the validity of any mechanism.

### c. The Final Rate Equation

The results of Section III-C-3-c show that Model 5 provides the best fit of the experimental data. Therefore, the form of the rate equation for butane formation is

$$r_c = \hat{k} p_B / (1 + \hat{K}_B p_B + \hat{K}_{H_2S} p_{H_2S}) \quad \text{(III-32)}$$

Values of  $\hat{k}$ ,  $\hat{K}_B$  and  $\hat{K}_{H_2S}$  are given in Table III-7, and these constants are expressed in terms of activation energies and pre-exponential factors in Table III-6.

### I. Accuracy

Table III-6 shows that the maximum error in the correlation for all the data points is -22.2 percent. This value occurred for Run 30, which had such a low value of  $p_B$  that the accuracy of the chromatographic analysis was undoubtedly poor. The next largest error is -16.4 percent. The arithmetic average of the



absolute magnitude of the percent errors is 7.3 percent and the best estimate of the standard deviation for the correlation is  $1.49 \times 10^{-7}$  gr. moles/ gr. cat., min.

Figure III-6 in Section III-C-3-c is a visual representation of how well the final equation fits the experimental data. This figure, together with the above statistical values, shows that the final correlating equation describes the kinetic data very well.

## II. Comments on the Reaction Mechanism

The kinetic equation given by Eqn. (III-32) is consistent with the assumption that the rate-limiting step in butene hydrogenation is a surface reaction involving some type of rearrangement of adsorbed butene. The fact that the denominator of the rate equation has an exponent of unity suggests that butene is non-disassociatively adsorbed on a single catalyst site. If butene were adsorbed as a carbonium ion, the adsorbed complex would occupy only one site, but this adsorption is, of course, disassociative. However, if the adsorptions of butene and hydrogen are assumed to be at equilibrium, a Langmuir expression for the fractional surface coverage of the carbonium ion can be derived. The denominator of this expression has an exponent of unity. Thus, the final kinetic equation is consistent with the assumption that some surface process involving the carbonium ion of butene is the RLS. As discussed by Taylor (68), the carbonium ion has been suggested to be an intermediate in the hydrogenation of olefins. Furthermore, there is strong evidence that the carbonium ion does exist on the present catalyst, since it is generally accepted to be an intermediate in double-bond shift isomerization reactions (15). Double-bond shift isomerization probably occurred in this study, as 1-butene was almost certainly



the first butene isomer to be formed.

The final kinetic equation is not consistent with the assumption that one-point adsorption of butene controls the reaction rate. If adsorption of butene were the RLS, the  $\hat{K}_B p_B$  term should be negligible. However, in this case, the  $\hat{K}_B p_B$  term achieves values as large as 26.

Once again, it must be emphasized that the discussion of mechanisms in light of rate data is not intended as a proof, or disproof, of any given mechanism.

### III. The Effect of Butene and Hydrogen Sulfide Adsorption

Using the data in Appendix C-3 and Table III-7, the values of  $\hat{K}_B p_B$  and  $\hat{K}_{H_2S} p_{H_2S}$  can be calculated for each experimental run. The maximum value of  $\hat{K}_B p_B$  was 26.8 and the maximum value of  $\hat{K}_{H_2S} p_{H_2S}$  was 9.5. Both butene and hydrogen sulfide inhibit the reaction significantly, with butene exhibiting the stronger effect.

### IV. Activation Energies

Very little can be said about the activation energies for the constants  $\hat{k}$ ,  $\hat{K}_B$  and  $\hat{K}_{H_2S}$  because the literature contains very few values for comparison. Further, the accuracy of these values must be questioned because of the small range of temperature covered by the data.

With this reservation, and subject to the theoretical reservations expressed in Section III-D-3-c-IV, the heats of chemisorption for butene and hydrogen sulfide were -53.77 Kcal/ mole and -32.42 Kcal/ mole respectively. Both adsorptions appear to be strongly exothermic. The value of -53.77 Kcal/ mole for butene

adsorption is in extremely poor agreement with the value of -8.5 Kcal/ mole measured chromatographically by Owens and Amberg (45). The value of -32.42 Kcal/ mole for hydrogen sulfide does not check well with the value of -18.91 Kcal/ mole which was derived from the data on thiophene disappearance, although there is no theoretical reason that these two values should check, if desulfurization and hydrogenation occur on different sites.

Finally, because butene was never included in the feed to the reactor, the butene partial pressure was always related to the partial pressures of the other components through stoichiometry. Consequently, the final kinetic equation for butane formation must be regarded with caution. Only by varying the butene partial pressure independently can a rate equation be confidently formulated.

### 5. The Effect of H<sub>2</sub>S on Reaction Selectivity

By means of pulse experiments in a microreactor, Owens and Amberg (45) found that an excess of hydrogen sulfide reduced the rate of butene hydrogenation much more than it reduced the rate of thiophene disappearance. The present data is not amenable to a plot that would show the effect of H<sub>2</sub>S on the reaction selectivity. However, by using the rate equations for each step of the reaction, some information about selectivity can be gained. Eqn. (III-33) results from dividing Eqn. (III-32) by Eqn. (III-19).

$$\frac{r_c}{r_T} = \frac{\hat{k}}{k} \left( \frac{p_B}{p_T p_H} \right) \frac{(1 + K_T p_T + K_{H_2S} p_{H_2S})^2}{(1 + \hat{K}_B p_B + \hat{K}_{H_2S} p_{H_2S})} \quad \text{(III-33)}$$

Eqn. (III-33) applies in a differential reactor, or at any point in an integral reactor.

If  $p_T$ ,  $p_B$  and  $p_H$  are constant and  $p_{H_2S}$  is very large, (III-33) reduces to



$$\frac{r_c}{r_T} = \frac{\hat{k}}{k} \left( \frac{p_B}{\hat{p}_T \hat{p}_H} \right) \left( \frac{K_{H_2S}^2 p_{H_2S}}{\hat{K}_{H_2S}} \right) \quad (\text{III-34})$$

This equation shows that increasing the partial pressure of hydrogen sulfide should increase  $(r_c / r_T)$ , i. e., decrease reaction selectivity to butene.

By differentiating Eqn. (III-33) at constant  $p_B$ ,  $p_T$ , and  $p_H$ , it can be shown that  $(r_c / r_T)$  will have a minimum value when

$$p_{H_2S} = \frac{(1 + K_T p_T)}{K_{H_2S}} - 2 \frac{(1 + \hat{K}_B p_B)}{\hat{K}_{H_2S}} \quad (\text{III-35})$$

If the right-hand side of Eqn. (III-35) has a positive value, increasing the hydrogen sulfide partial pressure from zero to this value should increase the reaction selectivity to butene.

The condition under which  $p_{H_2S}$  in Eqn. (III-35) will be greater than zero is

$$p_T > \frac{2K_{H_2S}}{K_T \hat{K}_{H_2S}} (1 + \hat{K}_B p_B) - \frac{1}{K_T} \quad (\text{III-36})$$

Substitution of the values of  $K_T$ ,  $K_{H_2S}$ ,  $\hat{K}_B$  and  $\hat{K}_{H_2S}$  at 251°C, as given in Table III-4 and III-7, reduces Eqn. (III-36) to

$$p_T > 18.9 (1 + 0.463 p_B) - 42.2$$

Using a typical value of  $p_B = 10$  mm. Hg.,  $p_T$  is calculated to be 64 mm. Hg. Thus, the reaction selectivity to butene can be increased by increasing the partial pressure of  $H_2S$  only when the partial pressures of butene and  $H_2S$  are low and the partial pressure of thiophene is high. These conditions may have existed in the microreactor of Owens and Amberg, but it is doubtful that they could exist during the operation of a commercial desulfurization reactor.

It is also possible that the result of Owens and Amberg was the effect of a catalyst surface that was not at steady-state with respect to hydrogen sulfide.

#### IV. Effectiveness Factors for Porous Catalysts: Langmuir-Hinshelwood Kinetic Equations

##### A. Literature Review and Criticism

##### 1. The Effective Diffusivity

Considering a cross-sectional area inside a catalyst pellet, it is obvious that gaseous diffusion can occur only through that part of the area that consists of voids. Furthermore, since the pores within the pellet are not all perpendicular to a given cross-section, the net flux through an area is greater than the flux normal to that area. However, in the mathematical treatment of gaseous diffusion in porous media, it is convenient to define the diffusion coefficient in terms of the total cross-sectional area, rather than just the void area, and in terms of the normal, rather than the total, flux. This diffusion coefficient, which is called the "effective" diffusivity ( $D_{\text{eff}}$ ) is related to the diffusion coefficient in a straight, round pore ( $D'$ ) by

$$D_{\text{eff}} = \frac{D' \theta}{\tau} \quad (\text{IV-1})$$

In Equation (IV-1),  $\tau$  is a quantity called the "tortuosity" which, theoretically, corrects for the fact that not all pores run in the direction of diffusion. In practice, many other non-idealities are lumped into  $\tau$ . For instance, since not all pores have the same radius,  $D'$  is usually based on the "average" pore radius. Any errors involved in determining this average are thus lumped into  $\tau$ , together with errors caused by variation in the radius of a single pore along its length. For many catalyst materials,  $\tau$  lies between 2 and 6, providing that the pore-size distribution is reasonably narrow.



When the pore-size distribution is broad, as with catalyst particles whose distribution is bi-modal, the computation of  $D'$  cannot be done with accuracy. Smith and coworkers (34)(74) have considered the problem of bimodal pore-size distributions in some detail. Their results show that it is impractical to try to predict  $\tau$  for such catalysts and they have proposed a more fundamental and complex method of predicting  $D_{\text{eff}}$ . The result of interest, however, is that even in very complex catalysts, Fick's Law is applicable, as is the concept of an "effective" diffusion coefficient,  $D_{\text{eff}}$ .

In the work that follows, the subscript eff. will be omitted. All use of the symbol  $D$  will refer to the effective diffusivity.

## 2. Effectiveness Factors--Fundamental Results

As mentioned previously, the differential equation describing the simultaneous diffusion and reaction of the reactant must be solved in order to compute the effectiveness factor. For an irreversible reaction of order  $n$ , and for a constant effective diffusivity, the appropriate differential equation is

$$D_A \nabla^2 C_A = k_n C_A^n \quad (\text{IV-2})$$

and the boundary conditions are

$$\begin{aligned} C_A &= C_{A,s} && \text{- at the surface of the pellet} \\ \nabla C_A &= 0 && \text{- at the center of the pellet} \end{aligned} \quad (\text{IV-3})$$

A great many studies of gaseous diffusion in porous media have been made, especially in recent years. The results show that the assumption of a constant effective diffusivity is justified in three cases: 1) when diffusion is completely within the Knudsen

regime; 2) when binary, equimolar counterdiffusion is taking place; 3) when one component of a mixture is in great excess, no matter what the diffusion regime. Unless at least one of these three conditions is satisfied, the diffusivity in Fick's Law will be dependent on concentration. However, if the structure of the porous material varies in the direction of diffusion, even though the above conditions are fulfilled, the diffusivity will depend on position. Although almost all investigators have considered the pore structure of catalysts to be completely random, Saraf (61) has shown that pellets formed by compaction of powders tend to have rather severe density gradients through the pellet.

Several computations of the effectiveness factor have been done using concentration-dependent effective diffusivities. Scott (64) derived a closed-form expression for  $\eta$ , assuming a first-order reaction and using a diffusion coefficient whose concentration dependence was

$$D_{\text{eff}} \propto \frac{1}{1 - a y} \quad (\text{IV-4})$$

Scott's derivation assumes that the reactant concentration is zero in the pellet interior and consequently is valid only at low effectiveness factors. The expression for the diffusion coefficient that was used by Scott was theoretically derived by Scott and Dullien (65) and Rothfeld (57), and experimentally verified by Rothfeld. The general expression is valid in any regime as long as the total pressure is constant. An extension of this diffusion theory to multicomponent systems has been made by Silveston (66).

Wakao and Smith (74) incorporated the diffusivity expression of Equation (IV-4) into a model for diffusion in catalysts that were prepared by pelletizing a micro-porous powder. Wakao and Smith (75)



then used their model to compute effectiveness factors for a reversible, first-order reaction. Carberry (10) simplified the results of Wakao and Smith by assuming that access to primary particles was only through macropores, and that the effective diffusivity in the macropores was constant. Finally, Butt (9) presented a method of computing effectiveness factors in variable-diffusivity systems that is based on the assumption that the diffusivity is a linear function of length.

The use of a constant diffusion coefficient, however, has certain practical justifications. First, it is likely that the error involved in the estimation of an effective diffusivity is larger than any error than might be introduced through concentration or position dependence. Secondly, the use of a constant diffusivity simplifies the mathematics quite considerably. If rigorous diffusion equations were always employed, it would be impractical to investigate anything but the simplest rate equations. Thirdly, as mentioned previously, the use of a constant effective diffusivity is theoretically valid in many real situations.

Equation (IV-2) has been solved, for various pellet geometries, for zero, first and second-order reactions. A summary of the available solutions is given by Satterfield and Sherwood (60). For spheres, the effectiveness factor is a function only of the dimensionless modulus

$$\phi_s = R_s \sqrt{\frac{k_n C_{A,s}^{n-1}}{D_A}} \quad (\text{IV-5})$$

As  $\phi_s$  increases,  $\eta$  decreases. The  $\eta$  versus  $\phi_s$  curve lies highest for a zero-order reaction and lowest for a second-order reaction, with the first-order curve intermediate. If the catalyst pellet is considered to be a semi-infinite slab of half-width L, the

same general results hold, except that the dimensionless modulus is usually written

$$\Phi_L = L \sqrt{\frac{k_n C_{A,s}^{n-1}}{D_A}} \quad (\text{IV-6})$$

The quantity  $\Phi$  is commonly called the Thiele modulus.

Although the results above have been derived for irreversible reactions, Smith and Amundsen (67) have shown that the  $\eta - \Phi_L$  relationship for a reversible, first-order reaction is the same as for an irreversible reaction, if the modulus  $\Phi_L$  is defined as

$$\Phi_L = L \left( \frac{k_F}{D_F} + \frac{k_r}{D_r} \right)^{1/2} \quad (\text{IV-7})$$

Aris (2) attempted to eliminate the effect of pellet geometry on the  $\eta - \Phi$  relationship by basing  $\Phi$  on a dimension  $L'$ , which is given by Equation (IV-8)

$$\begin{aligned} L' &= \frac{\text{pellet volume}}{\text{geometrical surface area of pellet}} \\ &= \text{characteristic dimension} \end{aligned} \quad (\text{IV-8})$$

$$\Phi_{L'} = L' \left( \frac{k_n C_{A,s}^{n-1}}{D_A} \right)^{1/2} \quad (\text{IV-9})$$

Aris' results show that the curves of  $\eta$  versus  $\Phi_{L'}$ , for spheres, slabs, and cylinders lie very close together for irreversible, first-order reactions. However, Roberts and Satterfield (56) have shown that agreement is not nearly as good for other reaction orders.

The differential equation (IV-2) is based on the assumption that the catalyst pellet is isothermal. In order to investigate the



effect of internal temperature gradients, the simultaneous differential equations for heat generation and heat conduction, and reaction and diffusion must be solved. This has been accomplished by Carberry (11), Tinkler and Metzner (71) and Weisz and Hicks (79). for first and second-order irreversible reactions in spheres and slabs. When temperature gradients are considered,  $\eta$  is no longer a function only of  $\phi$ . Two additional parameters, called  $\beta$  and  $\gamma$  by Weisz and Hicks, are needed to specify the catalyst effectiveness. If intraparticle temperature gradients are severe,  $\eta$  can be greater than unity and can, in some cases, be a double or triple-valued function of  $\phi$ , at constant  $\beta$  and  $\gamma$ .

In order to calculate  $\phi$ , the value of  $k_n$  must be known. Therefore, a trial-and-error procedure is necessary to calculate  $\eta$  from experimental data. Weisz and Prater (80) eliminated the trial-and-error by the use of a new modulus,  $\bar{\Phi}_s$ , which is defined in Equation (IV-10).

$$\bar{\Phi}_s \equiv \frac{R_s^2}{D_A C_{A,s}} \left( \frac{\text{observed reaction rate}}{\text{gross catalyst volume}} \right) = \frac{R_s^2}{D_A C_{A,s}} \left( \frac{-1}{V_c} \frac{dN_A}{dt} \right) \quad (\text{IV-10})$$

For integer-power rate equations,  $\bar{\Phi}_s$  and  $\phi_s$  are related by

$$\bar{\Phi}_s = \eta \phi_s^2 \quad (\text{IV-11})$$

A similar modulus, based on slab geometry, can be defined.

$$\bar{\Phi}_L \equiv \frac{L^2}{D_A C_{A,s}} \left( \frac{\text{observed reaction rate}}{\text{gross catalyst volume}} \right) = \frac{L^2}{D_A C_{A,s}} \left( \frac{-1}{V_c} \frac{dN_A}{dt} \right) \quad (\text{IV-12})$$

The quantity  $\bar{\Phi}$  can be computed directly from experimental data; no assumption about the order of the reaction need be made, even if the reaction rate expression is more complex than those considered so far. However, in order to estimate  $\eta$  from directly-observable quantities, a plot of  $\eta$  versus  $\bar{\Phi}$  is needed, and a specific rate equation must be assumed to prepare such a plot.

Weisz and Prater stated that if  $\bar{\Phi}_s$  is less than 0.30, internal diffusion effects will definitely be absent. This rule-of-thumb is based on the fact that  $\eta$  is approximately equal to 0.95 for a second-order reaction when  $\bar{\Phi}_s = 0.30$ . This criterion therefore contains the implicit assumption that the  $\eta$  versus  $\bar{\Phi}_s$  curve for a second-order reaction lies as low or lower than similar curves for other kinetic expressions. This is true if only zero, first and second-order reactions are considered.

Weisz and Prater also stated that if  $\bar{\Phi}_s$  is greater than 6, diffusion effects will definitely be present. This statement is based on the result that  $\eta = 0.95$  for a zero-order reaction when  $\bar{\Phi}_s = 6$ . Again, an implicit assumption is involved, this time that the  $\eta - \bar{\Phi}_s$  curve for a zero-order reaction lies as high or higher than that for any other kinetic expression.

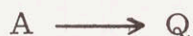
### 3. Effectiveness Factors for Langmuir-Hinshelwood and other Complex Kinetic Equations

Over narrow regions of concentration, Langmuir-Hinshelwood kinetic equations are well approximated by integer-power kinetic equations. On the other hand, if the intraparticle diffusional resistance is high, viz., the effectiveness factor is low, the reactant partial pressure may vary from its value at the pellet surface down to a value approaching zero in the interior of the catalyst. If such is the case, the range of partial pressure will not, in general, be small,



and it is necessary to consider the effect of the more complex rate equation on the effectiveness factor.

The procedure for determining the effectiveness factor when Langmuir-Hinshelwood intrinsic rate equations are involved is basically the same as for integer-power expressions, in that the differential equations for simultaneous diffusion and reaction inside the pellet must be solved. The mathematics, however, are much more complex. Chu and Hougen (14) used a numerical technique to calculate values of  $\eta$  for the reaction



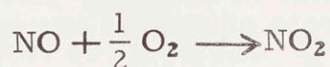
with a kinetic equation of the form

$$r = k_I p_A / (1 + K_A p_A + K_Q p_Q)$$

The results were derived for a slab catalyst and were presented as plots of  $\eta$  versus a dimensionless parameter  $M$ , for various values of the reactant mole fraction at the pellet surface, and for various values of  $K_A p_A$ . All of the solutions are for  $K_Q = 0$ , that is, for no adsorption of reaction products. In addition, constant total pressure throughout the pellet was assumed. If diffusion occurred in the Knudsen or transition region, the total pressure would vary through the pellet to a degree which may be significant in some real cases, as has been illustrated in a recent article by Otani, Wakao and Smith (44). Furthermore, Chu and Hougen used three parameters to specify  $\eta$ . It will be shown later that, by a judicious choice of variables, two parameters suffice, even if product adsorption is considered. Despite the restrictive assumptions and the lack of generality of the Chu and Hougen study, its mathematics is sound and has been utilized to some extent in part of the

present work.

Chu and Hougen also used a numerical technique to determine  $\eta$  for the reaction



which was taken to obey the rate equation

$$r = \frac{p_{\text{NO}}^2 p_{\text{O}_2}}{(a + b p_{\text{NO}}^2 + c p_{\text{NO}_2} + w p_{\text{H}_2\text{O}})}$$

Specific values of the constants  $a, b, c,$  and  $w$  were incorporated in the mathematics, as were values for  $D$  and particle size. Spherical geometry was assumed, and it is not clear that Chu and Hougen's modification of the above kinetic equation is valid inside the catalyst particle.

Prater and Lago (52) also used a numerical technique to derive effectiveness factors for the cracking of cumene to benzene and propylene. They found that the intrinsic rate equation was of the form

$$r = k p_A / (p_A + G K_B p_B + G K_I p_I + G)$$

where the subscript  $A$  refers to cumene,  $B$  to benzene, and  $I$  to any reaction inhibitor that is present, but does not participate in the reaction. The authors presented plots of  $\eta$  versus the modulus  $R_s (k/D)^{1/2}$ , for various values of  $GK_B$ , but the development seems to be specific to their system.

Atroshchenko, Zhidkov, and Zazorin (3) studied the reaction





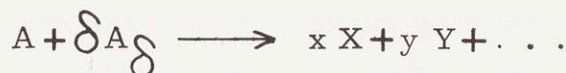
and found the rate equation to be

$$r = k \frac{(CO)}{\sqrt{(CO_2)}} \left( 1 - \frac{K_c (CO_2)(H_2)}{(CO)(H_2O)} \right)$$

Some of their kinetic data shows a variation of catalytic activity with particle size. The authors attempted to calculate the effective diffusivity by a process which involved the integration of the above equation. However, the magnitude and the temperature variation of the calculated diffusivities make the calculation suspect.

Several investigators have obtained closed-form solutions for the effectiveness factors of L-H kinetic expressions by making various assumptions to simplify the mathematical treatment. Akehata, Namkoong, Shindo, and Kubota (1) suggested expanding the kinetic equation in a Taylor series around the outside concentration, neglecting all but the first two terms. No comparison of this method with the more accurate numerical technique is available, nor has a comparison ever been made for the linearization technique of Schilson and Amundson (62)(63) when applied to L-H rate equations.

The most complete works involving approximate techniques have been presented by Rozovskii and coworkers. Rozovskii and Shchekin (58) considered the reaction



which was assumed to obey the rate equation

$$r = k p_A / (1 + K_A p_A + K_\delta p_\delta + K_x p_x + \dots)$$

Here  $A_\delta$  is a diluent that does not react. The authors showed that the rate equation could be transformed to the form

$$r = k' y_A / (1 + B y_A) \tag{IV-13}$$

However, the method used to relate  $B$  and  $k'$  to the adsorption constants appears to be based on a misconception of the method of mass transport in the catalyst interior. Rozovskii and Shchekin assumed that the catalyst is planar, that the mole fraction at the interior of the pellet is zero, i. e., the reactant does not penetrate the pellet completely, and that the reaction rate in the pellet can be described by substituting half the outside mole fraction into Equation (IV-13). In a later paper, Rozovskii (59) eliminated the latter restriction. The resulting formula for the effectiveness factor might be expected to be valid for low values of  $\eta$ , but certainly breaks down at higher values. This is especially true if  $B$  is negative. As will be shown later, the effectiveness factor must be very low before the assumption of a zero partial pressure at the catalyst interior becomes justified, if the reaction is inhibited by reaction products.

Finally, Bischoff (6) has defined a new modulus, which he designates as  $m$ , that has the property that the asymptotic portion of the  $\eta$ - $m$  curve is the same for all kinetic equations. The asymptotic portion of the  $\eta$ - $m$  curve is that portion which can be accurately computed by assuming that the concentration of the reactant is zero at the center of the pellet. Bischoff suggested that by using the modulus  $m$ , the effectiveness factor for any reaction could be estimated from existing curves, even if the reaction obeyed a complex kinetic expression. This procedure will probably give a reasonable estimate of the effectiveness factor in many cases, but will break down when the reaction is strongly inhibited by reaction products, as is discussed in Section IV-D-1-a. Furthermore, as is pointed out in Section IV-D-2-b, some types of Langmuir-Hinshelwood kinetic equations give rise, under certain circumstances,



to effectiveness factors that are greater than unity and are multiple-valued functions of a modified Thiele modulus. The existence of such effects cannot be predicted by applying Bischoff's modulus to existing curves, and effectiveness factors cannot be estimated by Bischoff's method under these circumstances.

Bischoff's modulus can also be applied to reactions where the effective diffusivity is concentration dependent, for the purpose of bringing the large  $m$  portions of all  $\eta$ - $m$  curves together.

## B. Mathematical Derivation and Computational Procedure

Several steps may be taken before it is necessary to introduce a specific rate equation. Let  $r_A$  be a general kinetic expression, expressing the rate of disappearance of reactant A, as shown in Equation (IV-14)

$$r_A = - \left( \frac{1}{V_c} \right) \left( \frac{dN_A}{dt} \right) \quad (\text{IV-14})$$

It will be assumed that: 1) the catalyst pellet is a semi-infinite slab of thickness  $L$ , that is exposed to the gas stream on one face and sealed on the other; 2) diffusion obeys Fick's Law and the effective diffusivities of all chemical species are constant but not necessarily equal; 3) the pellet is isothermal, and; 4) the ideal gas laws are applicable.

A material balance on reactant A, over a differential thickness within the catalyst, gives

$$D_A \frac{d^2 C_A}{dx^2} = D_A \left( \frac{1}{RT} \right) \left( \frac{d^2 p_A}{dx^2} \right) = r_A \quad (\text{IV-15})$$

A similar balance on any other component, either reactant or product, yields

$$D_i \left( \frac{1}{RT} \right) \left( \frac{d^2 p_i}{dx^2} \right) = \nu_i r_A \quad (\text{IV-16})$$

In Equation (IV-16) and throughout the rest of the thesis, the stoichiometric coefficient,  $\nu$ , of a reactant is taken to be negative. The index  $i$  denotes any species other than A.



Combining (IV-15) and (IV-16) gives

$$\frac{-D_i}{\nu_i} \left( \frac{d^2 p_i}{dx^2} \right) = D_A \left( \frac{d^2 p_A}{dx^2} \right) \quad (\text{IV-17})$$

which is subject to the boundary conditions

$$p_A = p_{A,s} ; p_i = p_{i,s} \quad \text{at } x = 0 \text{ (exposed surface)} \quad (\text{IV-18})$$

$$(dp_A/dx) = (dp_i/dx) = 0 \quad \text{at } x = L \text{ (sealed surface)}$$

Integration of (IV-17) and application of (IV-18) gives

$$p_i = -(\nu_i D_A / D_i) p_A + [(\nu_i D_A / D_i) p_{A,s} + p_{i,s}] \quad (\text{IV-19})$$

In some cases, a species that does not participate in the reaction might adsorb on the catalyst and retard the reaction. Such an effect can be accounted for using (IV-19), if an infinite diffusivity is ascribed to the non-reacting component. Thus  $p_i = p_{i,s}$ , which is the correct relationship for a species that does not react.

At this point it is necessary to consider a specific rate expression. Two forms of L-H kinetic equation are considered below.

## I. Type I

### a. General Derivation

The case to be developed in this section is the particular rate equation given in Equation (III-6) below. As indicated previously, this expression includes reactions in which A decomposes or isomerizes by a first-order surface process, or reactions of A with B in which the concentration of B does not appear in the numerator, but may

appear in the denominator. For the reaction of A and B, such an expression might result if adsorption of A on the catalyst is the rate-controlling process.

The general chemical equation describing the reactions under consideration is given by (III-E)



and the rate equation is taken to be

$$r_A = k_I p_A / (1 + K_A p_A + \sum_i K_i p_i) \quad (\text{III-6})$$

Substitution of (IV-19) into (III-6) gives

$$r_A = k_I p_A / (1 + K_A p_A + \sum_i \left[ -(\nu_i D_A / D_i) p_A + \left( (\nu_i D_A / D_i) p_{A,s} + p_{i,s} \right) K_i \right]) \quad (\text{IV-20})$$

$$\text{Let: } \omega = 1 + \sum_i K_i \left[ p_{i,s} + (p_{A,s} \nu_i D_A / D_i) \right] \quad (\text{IV-21})$$

Note that  $\omega$  will usually be positive, but can be negative if a reactant other than A is very strongly adsorbed and has a very small partial pressure. The following derivation is not valid for negative values of  $\omega$ . However, the same general procedure would be followed in a derivation for negative values of  $\omega$ .

$$\text{Let: } k'_I = k_I / \omega \quad (\text{IV-22})$$

$$K = \left[ K_A - D_A \sum_i (K_i \nu_i / D_i) \right] / \omega \quad (\text{IV-23})$$

Using these definitions, Equation (IV-20) reduces to

$$r_A = k'_I p_A / (1 + K p_A) \quad (\text{IV-24})$$



Since  $\omega$  is dimensionless,  $K$  has the dimensions of an adsorption constant and  $k'_I$  has the dimensions of a rate constant. As  $K$  approaches zero, the reaction approaches simple first-order, and as  $K$  approaches infinity the reaction approaches zero-order. A negative value of  $K$  indicates that the sum of the groups  $(K \mathcal{V} D_A / D)$  for the products is greater than the magnitude of the same sum for the reactants. Qualitatively, a negative value of  $K$  means that the reaction is inhibited more strongly by the reaction products than by the reactants, and vice versa.

Using Equation (IV-24), Equation (IV-15) can be rewritten

$$\frac{D_A}{RT} \left( \frac{d^2 p_A}{dx^2} \right) = \frac{D_A}{RT} \left[ \frac{d}{dp_A} \left( \frac{dp_A}{dx} \right) \right] \frac{dp_A}{dx} = \frac{k'_I p_A}{1 + K p_A}$$

(IV-25)

Integrating (IV-25)

$$\frac{1}{2} \left( \frac{dp_A}{dx} \right)^2 \Big|_{x=L}^{x=0} = \left( \frac{k'_I RT}{D_A} \right) \int_{p_{A,0}}^{p_A} \frac{p_A dp_A}{1 + K p_A} \quad (IV-26)$$

In (IV-26),  $p_{A,0}$  is the partial pressure of A at the sealed face;  $p_{A,0}$  is not known experimentally. Evaluation of the integral in (IV-26) yields

$$\frac{dp_A}{dx} = \left( \frac{\sqrt{2}}{K} \right) \left( \frac{k'_I RT}{D_A} \right)^{1/2} \left[ K(p_A - p_{A,0}) - \ln \left| \frac{1 + K p_A}{1 + K p_{A,0}} \right| \right]^{1/2} \quad (IV-27)$$

Let a modified Thiele modulus  $\Phi_{MI}$  be defined as

$$\Phi_{MI} = L \left( \frac{k'_I RT}{D_A} \right)^{1/2} \quad (IV-28)$$

Then

$$\frac{d(Kp_A)}{d(x/L)} = \sqrt{2} \phi_{MI} \left[ K(p_A - p_{A,o}) - \ln \left| \frac{1 + Kp_A}{1 + Kp_{A,o}} \right| \right]^{1/2} \quad (IV-29)$$

The effectiveness factor of the catalyst pellet, which was defined in Equation (II-1), is given by

$$\eta = \left( \frac{-D_A}{RT} \right) \left( \frac{dp_A}{dx} \right)_{x=0} / (L k'_I p_{A,s} / (1 + Kp_{A,s})) \quad (IV-30)$$

Combining (IV-29) and (IV-30)

$$\eta = \left| \frac{\sqrt{2}}{\phi_{MI}} \left( \frac{1 + Kp_{A,s}}{Kp_{A,s}} \right) \left[ K(p_{A,s} - p_{A,o}) - \ln \left| \frac{1 + Kp_{A,s}}{1 + Kp_{A,o}} \right| \right]^{1/2} \right| \quad (IV-31)$$

The modulus  $\bar{\Phi}_L$  is given in terms of the present nomenclature by Equation (IV-32) below. The defining equation for  $\bar{\Phi}_L$ , Equation (IV-12), is still valid, and  $\bar{\Phi}_L$  can still be calculated from experimental data.

$$\bar{\Phi}_L = \eta \phi_{MI}^2 / (1 + Kp_{A,s}) \quad (IV-32)$$

Equation (IV-31) is not useful in itself, since  $p_{A,o}$  is not known. However, when the effectiveness factor is low, the reactant partial pressure at the sealed face,  $p_{A,o}$ , approaches zero. If this assumption is made

$$\tilde{\eta} = \left| \frac{\sqrt{2}}{\phi_{MI}} \left( \frac{1 + Kp_{A,s}}{Kp_{A,s}} \right) \left[ Kp_{A,s} - \ln |1 + Kp_{A,s}| \right]^{1/2} \right| \quad (IV-33)$$



The validity of this equation depends on the actual value of  $K p_{A, o}$ .

However, the equation shows that the effectiveness factor,  $\eta$ , is proportional to  $(1/\Phi_{MI})$  at large values of  $\Phi_{MI}$ .

b. Numerical Solution--Calculation of  $K p_{A, o}$

I. Method

Actual values of  $K p_{A, o}$  were calculated by numerical integration of Equation (IV-29), subject to the boundary conditions

$$\begin{aligned} K p_A &= K p_{A, s} && \text{at } (x/L) = 0 \\ d(K p_A)/d(x/L) &= 0 && \text{at } (x/L) = 1 \end{aligned} \tag{IV-34}$$

The numerical integration was performed on an IBM 7094 computer. For each run, values of  $K p_{A, o}$  and  $\Phi_{MI}$  were specified, and a marching integration was performed starting at the sealed face,  $(x/L) = 1$ , and proceeding out to  $(x/L) = 0$ . The result of the integration was a value of  $K p_{A, s}$  which in general was not equal to the desired value of  $K p_{A, s}$ . Despite this, the value of the ratio  $(p_{A, o}/p_{A, s})$  was formed,  $\eta$  was calculated from Equation (IV-31) and  $\tilde{\eta}$  was calculated from Equation (IV-33).

For a given value of  $\Phi_{MI}$ , two values of  $K p_{A, o}$  were selected by trial-and-error such that they yielded values of  $K p_{A, s}$  that bracketed the desired value very closely. The value of  $\eta$  corresponding to the desired  $K p_{A, s}$  was then calculated by linear interpolation, either of  $\eta$  or of  $(\tilde{\eta} - \eta)$ , whichever varied more gradually with  $K p_{A, s}$ . In no case was the difference in the interpolated quantity greater than 0.015. Final values of the pressure ratio,  $(p_{A, o}/p_{A, s})$ , were also calculated by linear interpolation. The

maximum difference in the pressure ratios that bracketed the interpolated value was always less than 0.010.

As mentioned above, Equation (IV-33) is accurate when  $\eta$  and  $Kp_{A,o}$  are small. Once an exact calculation had established the region of validity of Equation (IV-33), this equation was used to calculate  $\eta$ . Values of the pressure ratio were not calculated in this region.

A print-out of the Fortran program that was used to calculate  $Kp_{A,s}$  appears in Appendix B-1. Basically, the mathematical procedure was as follows. The solution was begun at the sealed face,  $(x/L) = 1,0$ . An approximate value of  $Kp_A$  at the adjacent point was obtained by using the finite-difference approximation to the second derivative, given by Equation (IV-35) below. In Equation (IV-35),  $h$  is the size of the grid.

$$Kp_A = Kp_{A,o} \left[ 1 + (\Phi_{MI}^2 h^2 / 2 (1 + Kp_{A,o})) \right] \quad (IV-35)$$

The value of  $Kp_A$  thus computed was used to calculate  $d(Kp_A)/d(x/L)$  from (IV-29). A final value of  $Kp_A$  was calculated by three iterations with the formula

$$Kp_A = Kp_{A,o} \left[ 1 + (h^2 \Phi_{MI}^2 / 4 (1 + Kp_{A,o})) \right] + (h/4) d((Kp_A)/d(x/L)) \quad (IV-36)$$

which is a form of that given by Kunze (30). The remainder of the solution was performed by using the Kutta-Simpson 3/8 rule at each slice of the grid. A one-hundred slice grid was used for all calculations.

## II. Accuracy

An accuracy test was made by calculating  $Kp_{A,s}$  for 26 values of  $Kp_{A,o}$ , using both fifty and one-hundred slice grids for each  $Kp_{A,o}$  value. The modulus  $\Phi_{MI}$  was equal to 3.0 and  $Kp_{A,s}$



ranged from +24.29 to -0.86. The maximum difference in  $(p_{A,o}/p_{A,s})$  for the two grid sizes was 0.02%, and the maximum difference in  $\eta$  was 0.09%. Both maximum differences occurred at the lowest value of  $Kp_{A,s}$ , i.e., when the partial pressure gradients inside the catalyst were the steepest. Most differences were much smaller than these maxima.

Two other points were run, using both fifty and one-hundred size grids, for the specific purpose of checking the accuracy of the  $Kp_{A,s} = -0.98$  line. For the first point,  $\Phi_{MI} = 0.008$  and  $Kp_{A,o} = -0.9785$ ; for the second point,  $\Phi_{MI} = 0.50$  and  $Kp_{A,o} = -0.6580$ . The maximum difference in  $(p_{A,o}/p_{A,s})$  for the two grid sizes was 0.00415%, and the maximum difference in  $\eta$  was 0.17%. Both maxima occurred for the latter point where the gradients were steepest. A higher value of  $\Phi_{MI}$  was not tested because Equation (IV-33) is very accurate for  $\Phi_{MI} > 0.50$ ,  $Kp_{A,s} = -0.98$ .

Since a value of  $K$  equal to zero corresponds to a simple first-order reaction, a second accuracy test was made by numerically calculating the values of  $\eta$  and  $(p_{A,o}/p_{A,s})$  for  $\Phi_{MI} = 3.0$  and  $Kp_{A,s}$  approaching zero, and comparing the results with the values of  $\eta$  and  $(p_{A,o}/p_{A,s})$  for a first-order reaction with a Thiele modulus,  $\Phi_L$ , equal to 3.0. The Thiele modulus,  $\Phi_L$ , was defined in Equation (IV-6).

When  $Kp_{A,s} = 1.0 \times 10^{-3}$ , the pressure ratio was 0.05% greater than the first-order value, and  $\eta$  was 0.07% greater. When  $Kp_{A,s} = -1.01 \times 10^{-3}$ ,  $(p_{A,o}/p_{A,s})$  was 0.073% less than the first-order value, and  $\eta$  was 0.13% less than its asymptotic value.

It was necessary to program the computer to carry sixteen significant figures in order to insure the accuracy of the numerical

calculations. This was accomplished by using the double precision routine that is available for the IBM 7094.

## 2. Type II

### a. General Derivation

This section describes the calculation of effectiveness factors for reactions obeying the rate equation given in Equation (III-9) below. The general chemical equation describing the reactions under consideration is given in (III-E). The rate equation is taken to be

$$r_A = k_{II} p_A p_B / (1 + K_A p_A + \sum_i K_i p_i)^2 \quad (III-9)$$

which was shown previously to apply to reactions where the RLS is the second-order combination of adsorbed, undisassociated A and B.

Substitution of (IV-19) into (III-9) yields

$$r = \frac{k_{II} p_A \left[ p_{B,s} + (\nu_B D_A p_{A,s} / D_B) - (\nu_B D_A p_A / D_B) \right]}{\left[ 1 + K_A p_A + \sum_i K_i \left( p_{i,s} + (\nu_i D_A p_{A,s} / D_i) \right) - \sum_i K_i \nu_i D_A p_A / D_i \right]^2} \quad (IV-37)$$

Let the parameters  $\chi$  and  $k'_{II}$  be defined by Equation (IV-38) and (IV-39)

$$\chi = -(D_B p_{B,s} / \nu_B D_A) - p_{A,s} \quad (IV-38)$$

$$k'_{II} = -k_{II} \nu_B D_A / \omega^2 D_B \quad (IV-39)$$



Using the above definitions, Equation (IV-37) can be rewritten

$$r = k'_{II} p_A (p_A + \chi) / (1 + K p_A)^2 \quad (IV-40)$$

The quantity  $\chi$  has the dimensions of pressure and  $k'_{II}$  has the dimensions of a second-order rate constant. As discussed previously, a negative value of  $K$  indicates a net inhibition by reaction products.

The defining equation for  $\omega$ , Equation (IV-21), is unchanged for Type II reaction rate expressions. As with Type I, the Type II derivation implicitly assumes a positive value of  $\omega$ . For any Type II reaction, a positive  $\omega$  will result if the reactant with the smallest value of  $(Dp_s / \nu)$  is chosen to be component A. If this rule is followed,  $\chi$  will always be zero or positive.

When  $\chi = 0$ , the rate equation shown in (IV-40) approaches zero-order as  $Kp_A$  becomes very large relative to 1, and approaches second-order as  $Kp_A$  approaches zero. If  $\chi$  is finite, the reaction approaches first-order as  $p_A$  approaches zero and approaches zero-order behavior as  $p_A$  becomes very large. It should be noted that Type II rate equations include the case of a single reactant that disappears by a bimolecular surface process. In this case,  $\chi$  always equals zero.

Substituting (IV-40) into (IV-15) and rearranging gives

$$\left( \frac{dp_A}{dx} \right) d \left( \frac{dp_A}{dx} \right) = \left( \frac{k'_{II} RT}{D_A} \right) \frac{p_A (p_A + \chi)}{(1 + Kp_A)^2} dp_A \quad (IV-41)$$

b. Numerical Solution,  $K \neq 0$

I. General Mathematics

If  $K$  is non-zero, Equation (IV-41) can be integrated to give

$$\frac{d(Kp_A)}{d(x/L)} = \sqrt{2} \phi_{MII} \left[ (Kp_A - Kp_{A,o}) \left[ \alpha + \frac{(\alpha - |K|\chi)}{(1+Kp_{A,o})(1+Kp_A)} \right] - (2\alpha - |K|\chi) \ln \left( \frac{1+Kp_A}{1+Kp_{A,o}} \right) \right]^{1/2} \quad (IV-42)$$

In Equation (IV-42)

$$\phi_{MII} = L \left( \frac{k'_{II} RT}{|K| D_A} \right)^{1/2} \quad (IV-43)$$

$$\alpha = \frac{|K|}{K} \quad (IV-44)$$

The effectiveness factor of the catalyst pellet is given by

$$\eta = \frac{-D_A}{RT} \left( \frac{dp_A}{dx} \right)_{x=0} \bigg/ \frac{(L k'_{II} p_{A,s} (p_{A,s} + \chi))}{(1 + Kp_{A,s})^2} \quad (IV-45)$$

Substitution of (IV-42) into (IV-45) gives

$$\eta = \left| \frac{\sqrt{2} (1+Kp_{A,s})^2}{\phi_{MII} Kp_{A,s} (\alpha Kp_{A,s} + |K|\chi)} \right| \left[ \frac{(Kp_{A,s} - Kp_{A,o})}{(1+Kp_{A,o})(1+Kp_{A,s})} \right]$$



$$\left[ \alpha(1+Kp_{A,o})(1+Kp_{A,s}) + \alpha - |K|\chi \right] - (2\alpha - |K|\chi) \ln \left( \frac{1+Kp_{A,s}}{1+Kp_{A,o}} \right) \Bigg]^{1/2} \quad (IV-46)$$

The modulus  $\Phi_L$ , defined by Equation (IV-12), is given by

$$\Phi_L = \eta \phi_{MII}^2 (\alpha Kp_{A,s} + |K|\chi) / (1+Kp_{A,s})^2 \quad (IV-47)$$

If the assumption that  $Kp_{A,o}$  equals zero is made, an approximation to the effectiveness factor is

$$\tilde{\eta} = \left| \frac{\sqrt{2} (1+Kp_{A,s})^2}{\phi_{MII} Kp_{A,s} (\alpha Kp_{A,s} + |K|\chi)} \left[ \frac{Kp_{A,s}}{(1+Kp_{A,s})} \left[ \alpha(1+Kp_{A,s}) + \alpha - |K|\chi \right] - (2\alpha - |K|\chi) \ln(1+Kp_{A,s}) \right] \right|^{1/2} \quad (IV-48)$$

Equation (IV-48) shows that the effectiveness factor is proportional to  $(1/\phi_{MII})$  at large values of  $\phi_{MII}$ , i.e., as  $Kp_{A,o}$  approaches zero.

In order to determine the exact value of the effectiveness factor, the value of  $Kp_{A,o}$  must be computed.

## II. Calculation of $Kp_{A,o}$

Actual values of  $Kp_{A,o}$  were calculated by numerical integration of Equation (IV-42), subject to the boundary conditions

given in Equation (IV-34). The calculational procedure was very similar to that used for Type I problems.

A preliminary program was written for the 7094 that performed a marching integration of Equation (IV-42) starting at the sealed face,  $(x/L) = 1$ , and proceeding to the exposed face,  $(x/L) = 0$ . Input to the program were the values of  $\Phi_{MII}$ ,  $Kp_{A,o}$  and  $|K|\chi$ ; the result of the calculation was a value of  $Kp_{A,s}$  and the corresponding value of  $\eta$ , calculated from (IV-46).

By trial-and-error, using this program, two values of  $Kp_{A,o}$  were determined such that their corresponding values of  $Kp_{A,s}$  bracketed the desired value of this parameter. A second program was then used to calculate the values of  $Kp_{A,o}$ ,  $\eta$ ,  $\tilde{\eta}$  and  $\Phi_L$  corresponding to the desired value of  $Kp_{A,s}$ , for specified values of  $|K|\chi$  and  $\Phi_{MII}$ . The two values of  $Kp_{A,o}$ , together with the desired value of  $Kp_{A,s}$  and the values of  $\Phi_{MII}$  and  $|K|\chi$  were input to the computer. Values of  $Kp_{A,s}$  corresponding to the input values of  $Kp_{A,o}$  were calculated, as were the corresponding values of  $\eta$ . A test was then made to see if the values of  $\eta$  differed by more than one percent. A similar test was made for  $(p_{A,o}/p_{A,s})$ . If either difference was greater than one percent, a modified Regula-Falsi technique was used to calculate two new values of  $Kp_{A,o}$  which bracketed the true value more closely. The above procedure was then repeated. When two values of  $Kp_{A,o}$  had been determined such that the difference in their  $(p_{A,o}/p_{A,s})$  values was less than one percent, and the difference in the corresponding values of  $\eta$  was also less than one percent, final values of  $Kp_{A,o}$  and the effectiveness factor were calculated by linear interpolation, using  $Kp_{A,s}$  as the independent variable. Values of  $\Phi_L$  and  $\tilde{\eta}$  were then calculated. The program output consisted of the values of  $\eta$ ,  $(p_{A,o}/p_{A,s})$ ,



$\Phi_L$  and  $((\tilde{\eta} - \eta) / \eta) \times 100$ .

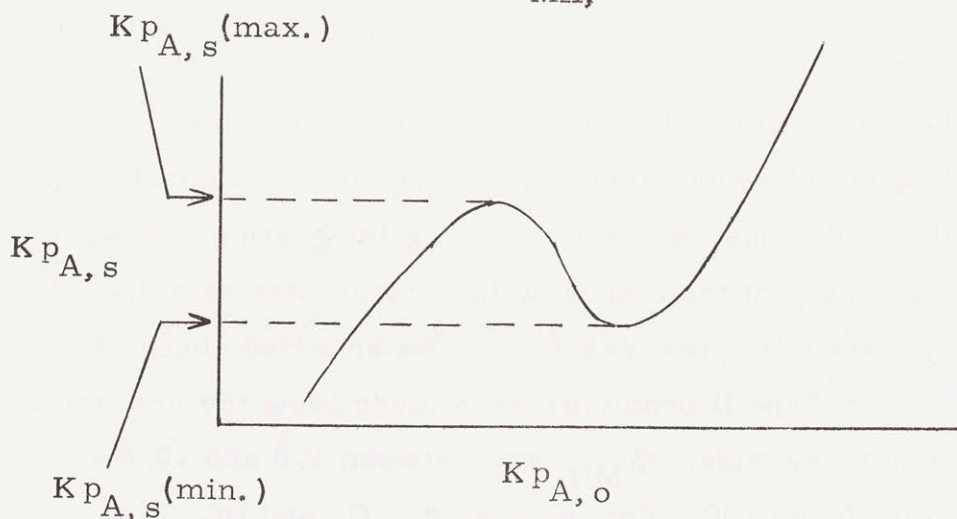
A print-out of the program described above appears in Appendix B-2. A print-out of the preliminary program is not shown since it was incorporated as a function in the larger program. In all runs, a one-hundred slice grid was used.

In certain regions of  $|K|\chi$  and  $\Phi_{MII}$ ,  $Kp_{A,o}$ , and therefore  $\eta$ , are multiple-valued functions of  $Kp_{A,s}$ . It was considered important to accurately determine the bounds of the multiple-valued region. Figure IV-1 is a typical plot of  $Kp_{A,s}$  versus  $Kp_{A,o}$  in the region of multiplicity. The dashed lines on Figure IV-1 delineate the multiple-solution regime.  $Kp_{A,s}(\text{max.})$  is the maximum value of  $Kp_{A,s}$  that occurs in the indeterminate region. For any value of  $Kp_{A,s}$  above  $Kp_{A,s}(\text{max.})$ , only a single value of  $Kp_{A,o}$  can result for a given value of  $Kp_{A,s}$ . Similarly,  $Kp_{A,s}(\text{min.})$  is the smallest value of  $Kp_{A,s}$  in the indeterminate region.

Figure IV-1

$Kp_{A,s}$  versus  $Kp_{A,o}$  -- Type II Reaction

$\Phi_{MII}, |K|\chi = \text{constant}$



Curves such as that shown above were generated using the preliminary program. The locations of  $Kp_{A,s}(\text{max.})$  and  $Kp_{A,s}(\text{min.})$  were very accurately determined by running a large number of closely-spaced values of  $Kp_{A,o}$  in the vicinity of the extremes. In order to determine the values of  $\Phi_{MII}$  and  $Kp_{A,o}$  for which either  $Kp_{A,s}(\text{max.})$  or  $Kp_{A,s}(\text{min.})$  were equal to some specified value, curves similar to Figure IV-1 were generated for a number of values of  $\Phi_{MII}$ , at a constant values of  $|K|\chi$ . The values of  $Kp_{A,s}(\text{max.})$  and  $Kp_{A,s}(\text{min.})$  were determined for each value of  $\Phi_{MII}$ . The values of  $\Phi_{MII}$  for which curves were generated were chosen such that the corresponding values of  $Kp_{A,s}(\text{max.})$ , for instance, bracketed the desired value of  $Kp_{A,s}(\text{max.})$ .

The values of  $\Phi_{MII}$ , for which  $Kp_{A,s}(\text{max.})$  were determined, were spaced closely enough so that a three-point interpolation was accurate to within the accuracy of  $Kp_{A,s}(\text{max.})$ . Values of  $\Phi_{MII}$  and  $Kp_{A,o}$ , corresponding to a given value of  $Kp_{A,s}(\text{max.})$  or  $Kp_{A,s}(\text{min.})$ , were then determined by inverse interpolation. Values of  $\eta$  for these points were then calculated using Equation (IV-46).

### III. Accuracy

The only potential source of error in the numerical technique for calculating effectiveness factors, that could not be checked by simple hand calculations, was the marching integration. However, the general accuracy of the marching integration was established by the accuracy tests for Type I reactions. As an added check, five accuracy tests on Type II problems were made using the preliminary program. For these runs,  $\Phi_{MII}$  was between 1.0 and 10.0 and  $Kp_{A,s}$  was between 0.10 and 100. For each point,  $\eta$  and  $(p_{A,o}/p_{A,s})$



were calculated using fifty and one-hundred slice grids. The differences in these parameters between the two grid sizes were roughly equal for all five points, with the maximum error in  $\eta$  being about 0.006 percent and in  $(p_{A,o}/p_{A,s})$  being about 0.009 percent.

c. Analytic Solution,  $K = 0$

When  $K = 0$ , inhibition effects by reacting species are nil, and the reaction obeys a standard second-order kinetic equation. However, Thiele's derivation of the effectiveness factor for a second-order reaction (69) is valid only when the reactants are present in stoichiometric proportions. The following derivation applies to a second-order reaction, with the reactants in any ratio, including stoichiometric.

For the case  $K = 0$ , Equation (IV-41) becomes:

$$\left(\frac{d p_A}{dx}\right) d \left(\frac{d p_A}{dx}\right) = \left(\frac{k'_{II} RT}{D_A}\right) p_A (p_A + \chi) \quad (IV-49)$$

Integration of the above equation, employing the boundary conditions in Equation (IV-18), yields

$$\frac{d p_A}{dx} = \sqrt{\frac{2 k'_{II} RT}{D_A}} \left[ \frac{(p_A^3 - p_{A,o}^3)}{3} + \frac{(p_A^2 - p_{A,o}^2)}{2} \chi \right]^{1/2} \quad (IV-50)$$

Let:

$$E \equiv (\chi / p_{A,s}) = \left[ (D_B p_{B,s} / b D_A) - p_{A,s} \right] / p_{A,s} \quad (IV-51)$$

$$z \equiv p_A / p_{A,s} ; z_o = p_{A,o} / p_{A,s} \quad (IV-52)$$

Substitution of the above definitions into Equation (IV-50) gives

$$\frac{dz}{dx} = \sqrt{\frac{2}{3}} \left( \frac{\Phi_L}{L} \right) \left[ (z^3 - z_0^3) + \frac{3E}{2} (z^2 - z_0^2) \right]^{1/2} \quad (IV-53)$$

The quantity  $\Phi_L$  is the standard Thiele modulus, defined in Equation (IV-6).

The effectiveness factor is given by

$$\eta = \frac{\sqrt{\frac{2}{3} \left[ (1 - z_0^3) + \frac{3E}{2} (1 - z_0^2) \right]^{1/2}}}{\Phi_L (1+E)} \quad (IV-54)$$

and the approximation to  $\eta$  by

$$\tilde{\eta} = \frac{\sqrt{\frac{2}{3} \left( 1 + \frac{3E}{2} \right)}}{\Phi_L (1+E)} \quad (IV-55)$$

Equation (IV-55) shows that  $\eta$  is proportional to  $(1/\Phi_L)$  at large values of  $\Phi_L$ , since  $z_0$  approaches zero as  $\Phi_L$  increases.

The relationship between  $\Phi_L$  and  $z_0$  is found from the integration of Equation (IV-53)

$$\Phi_L = \sqrt{\frac{3}{2}} \int_{z_0}^1 \frac{dz}{\left[ (z^3 - z_0^3) + \frac{3E}{2} (z^2 - z_0^2) \right]^{1/2}} \quad (IV-56)$$

As shown by Franklin (17), the above integral may be transformed to an elliptic integral, values of which are tabulated in standard references. The result of the integration is



a)  $z_0 > (E/2)$  and  $z_0 > \frac{1}{4} \left[ \sqrt{(9E^2 + 12E + 12)} - 2 - 3E \right]$

---

$$\phi_L = \frac{(\sqrt{3/2}) F'(\alpha', \phi')}{\sqrt[4]{3z_0(z_0 + E)}}$$

$$\alpha' = \text{Sin}^{-1} \left[ \left( \frac{1}{2} - \frac{3(2z_0 + E)}{8\sqrt{3z_0(z_0 + E)}} \right)^{1/2} \right] \quad (\text{IV-57})$$

$$\phi' = \text{Sin}^{-1} \left[ \frac{2(1 - z_0)^{1/2} \sqrt[4]{3z_0(z_0 + E)}}{(1 - z_0) + \sqrt{3z_0(z_0 + E)}} \right]$$

b)  $z_0 > (E/2)$  and  $z_0 < \frac{1}{4} \left[ \sqrt{(9E^2 + 12E + 12)} - 2 - 3E \right]$

---

$$\phi_L = \frac{\sqrt{(3/2)} \left( 2F'(\alpha', \frac{\pi}{2}) - F(\alpha', \phi') \right)}{\sqrt[4]{3z_0(z_0 + E)}} \quad (\text{IV-58})$$

where  $\alpha'$  and  $\phi'$  are as defined in (IV-57)

c)  $z_0 < (E/2)$

---

$$\phi_L = \frac{(\sqrt{3}) 2 \left( F'(\alpha', \frac{\pi}{2}) - F(\alpha', \phi') \right)}{\left[ 3z_0 + 1.5E + (2.25E^2 - 3Ez_0 - 3z_0^2)^{1/2} \right]^{1/2}}$$

$$\alpha' = \text{Sin}^{-1} \left( \left[ \frac{2(2.25E^2 - 3Ez_0 - 3z_0^2)^{1/2}}{3z_0 + 1.5E + (2.25E^2 - 3Ez_0 - 3z_0^2)^{1/2}} \right]^{1/2} \right)$$

(IV-59)

$$\phi' = \text{Sin}^{-1} \left[ \left( \frac{3z_o + 1.5E + (2.25E^2 - 3Ez_o - 3z_o^2)^{1/2}}{2 + z_o + 1.5E + (2.25E^2 - 3Ez_o - 3z_o^2)^{1/2}} \right)^{1/2} \right]$$

In the above equations,  $F'(\alpha', \phi')$  is the elliptic integral of the first kind. It should be noted that substitution of  $E = 0$  into Equations (IV-57) and (IV-58) does not reduce these equations to the equations for a second-order reaction given in Thiele's article, although calculations using Equations (IV-57) and (IV-58) reproduce Thiele's second-order curve. The equations appearing in the original article are in error; this has been confirmed by Thiele in a private communication (70).

For second-order reactions, the modulus  $\Phi_L$  is given by

$$\Phi_L = \eta \phi_L^2 (1 + E) \quad \text{(IV-60)}$$

The  $\eta - \Phi_L$  curve was generated, for a given value of  $E$ , in the following manner. A value of  $z_o$  was assumed and a check was made to determine whether Equation (IV-57), (IV-58) or (IV-59) was applicable. Values of  $\alpha'$  and  $\phi'$  were then calculated and their values were used to calculate the modulus  $\phi_L$ . The effectiveness factor was then calculated from Equation (IV-54), and  $\Phi_L$  was calculated from Equation (IV-60). The  $\eta - \Phi_L$  curves were generated for  $E = 0, 1$  and  $10$ .



## C. Results

### I. Type I

Using the technique described in Section IV-B-1, the effectiveness factor,  $\eta$ , the pressure ratio,  $z_o = (p_{A,o}/p_{A,s})$ , and the modulus  $\Phi_L$  were calculated for various values of  $Kp_{A,s}$  and  $\Phi_{MI}$ . The results are tabulated in Appendix C-1.

Figure IV-2 is a plot, on logarithmic coordinates, of  $(p_{A,o}/p_{A,s})$  versus  $\Phi_{MI}$  for a number of values of  $Kp_{A,s}$  ranging from -0.90 to 50.0, and for a first-order reaction, for which  $Kp_{A,s} = 0$ . Calculations for  $Kp_{A,s} = -0.10$  and  $+0.10$  show that these lines are essentially coincident with the first-order line. Similarly, lines for  $Kp_{A,s} = -0.95$  and  $-0.98$  are essentially coincident with  $Kp_{A,s} = -0.90$ . Lines of constant  $Kp_{A,s}$  are drawn of finite length on Figure IV-2. The left-hand terminus of a line occurs at a value of  $\Phi_{MI}$  corresponding to  $\eta$  greater than 0.95. The right-hand terminus occurs at a value of  $\Phi_{MI}$  for which  $(\tilde{\eta} - \eta)$  is less than 0.005. Thus, for values of  $\Phi_{MI}$  exceeding the right-hand terminus, Equation (IV-33) is very accurate. The ends of the  $Kp_{A,s} = -0.95$  line occur at  $\Phi_{MI}$  values of 0.02 and 1.0; those of the  $Kp_{A,s} = -0.98$  line occur at  $\Phi_{MI}$  values of 0.008 and 1.0.

Figure IV-3 is a log-log plot of  $\eta$  versus  $\Phi_{MI}$  for the same range of  $Kp_{A,s}$  values covered in Figure IV-2. For values of  $Kp_{A,s}$  greater than 50, Equation (IV-33) is accurate to within 5%, except for values of  $\eta$  greater than 0.95. Equation (IV-33) is accurate to better than 0.005 for the region to the right of the dashed line on Figure IV-3.

Figure IV-3 can be used to calculate the effectiveness

factor for a Type I reaction, if the intrinsic kinetics of the reaction, its stoichiometry, the surface partial pressures of all components and the effective diffusivities are known or can be estimated. Interpolation on Figure IV-3 may be facilitated by applying Equation (IV-33) to fix the linear portion of the  $\eta - \Phi_{MI}$  curve for the desired value of  $Kp_{A,s}$ . Alternatively, a value of  $(p_{A,o}/p_{A,s})$  could be interpolated from Figure IV-2, thus permitting  $\eta$  to be calculated from Equation (IV-31). The relative accuracy of these two procedures has not been checked, however.

Figure IV-4 is a plot of  $\eta$  versus the modulus  $\Phi_L$  for the same range of  $Kp_{A,s}$  shown in Figure IV-3, and for zero, first and second-order reactions. The curves for zero and first-order reactions may be regarded as specific members of the Type I family, as was implied in the discussion of Equation (IV-24). The second-order curve, however, cuts across the family of curves. Unless  $|Kp_{A,s}|$  is greater than 0.10, the  $\eta$  versus  $\Phi_L$  curve is essentially coincident with the first-order line. Moreover, if  $Kp_{A,s}$  is greater than 50, the  $\eta - \Phi_L$  curve is essentially coincident with the zero-order line.

The effectiveness factor can be estimated directly from experimental data by employing Figure IV-4, if the reaction order or the value of  $Kp_{A,s}$  is known or is assumed.

## 2. Type II

Using the techniques described in Section IV-B-2, the effectiveness factor,  $\eta$ , the modulus  $\Phi_L$  and the pressure ratio,  $(p_{A,o}/p_{A,s})$ , were calculated for various values of  $\Phi_{MII}$ ,  $Kp_{A,s}$ , and either  $|K|\chi$  or  $E$ . The results are tabulated in Appendix C-2.



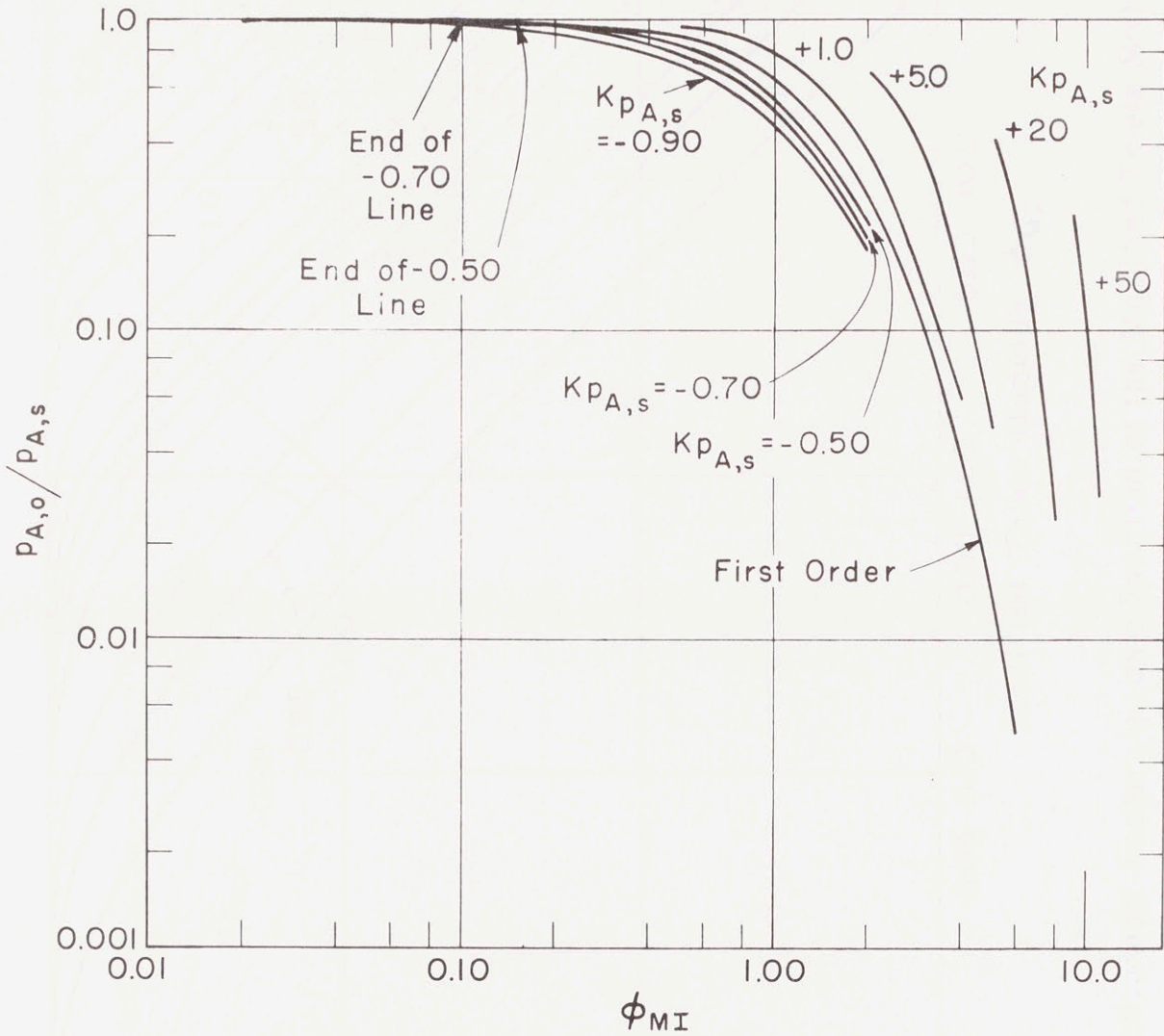


Figure IV-2 The Ratio  $p_{A,o}/p_{A,s}$  as a Function of the Modified Thiele Modulus,  $\phi_{MI}$ , for Various Values of  $K p_{A,s}$





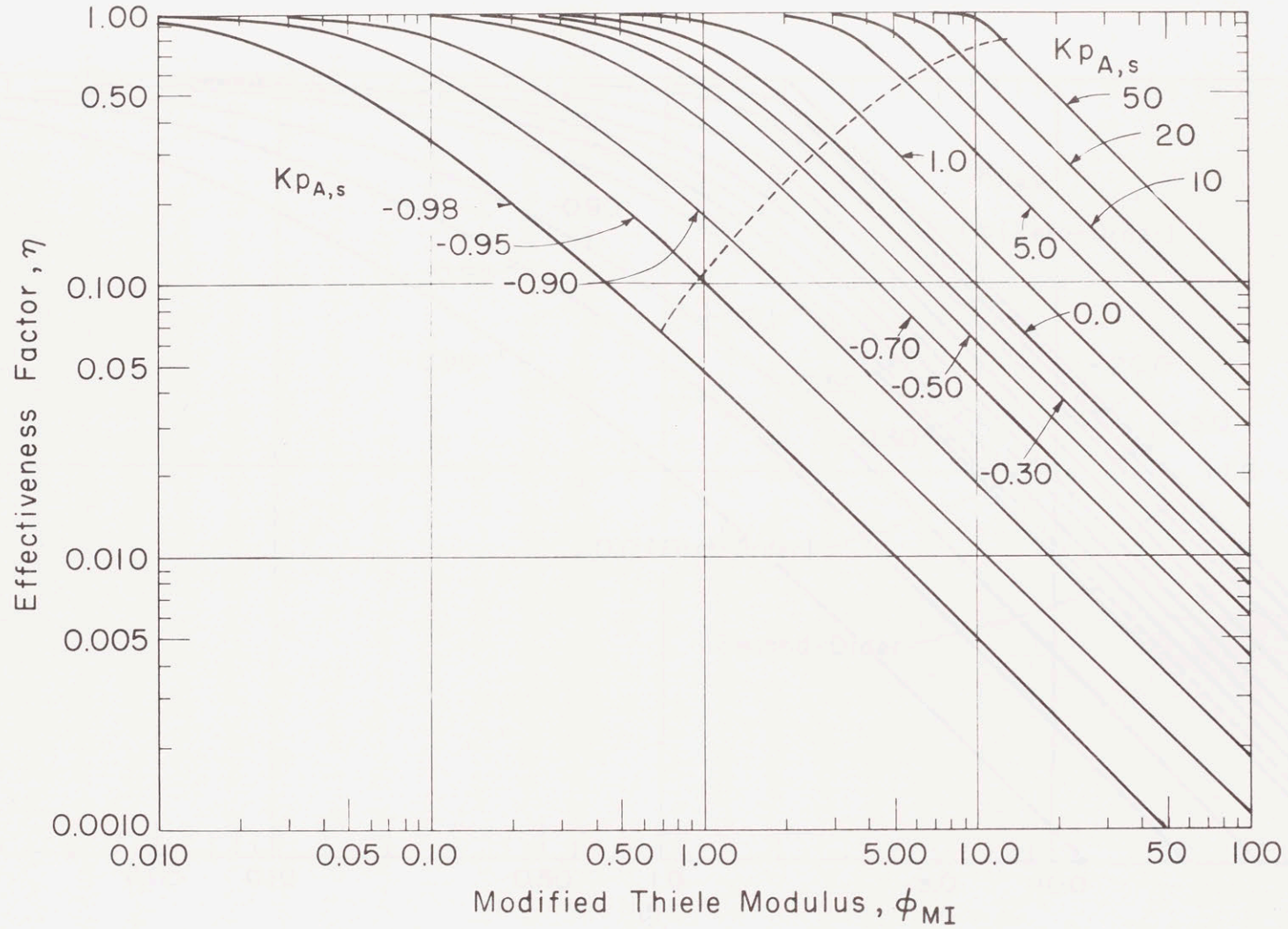


Figure IV-3 Effectiveness Factor,  $\eta$ , as a Function of the Modified Thiele Modulus,  $\phi_{MI}$ , for Various Values of  $Kp_{A,s}$





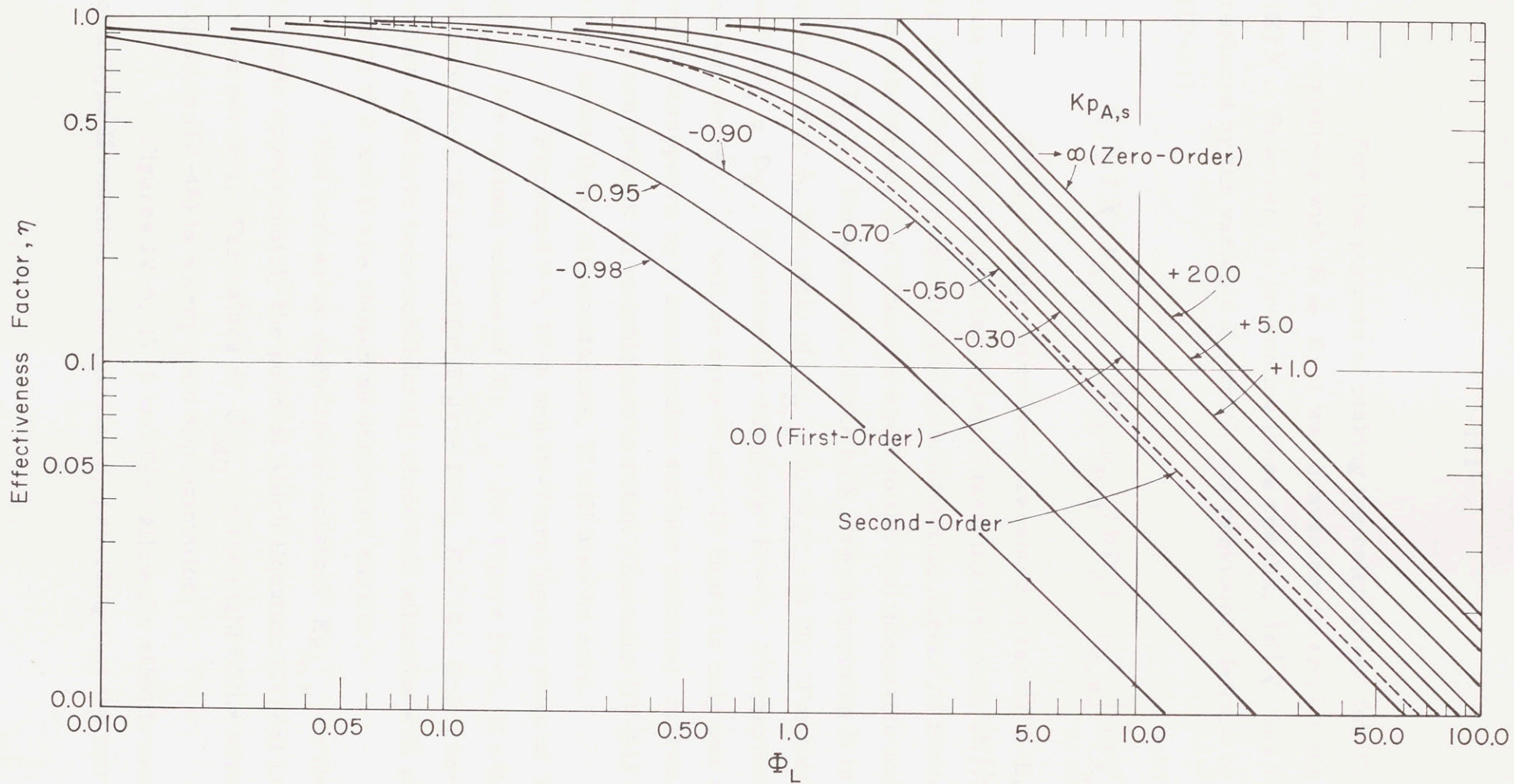


Figure IV-4 Effectiveness Factor,  $\eta$ , as a Function of the Modulus  $\Phi_L$ , Type I



For the purpose of making the calculations for Type II rate equations with  $K \neq 0$ , it was convenient to employ the parameter  $|K|\chi$ . However, in presenting these results,  $|K|\chi$  has been replaced by the variable  $E$ , which was previously defined by Equation (IV-51).

$$E \equiv (\chi / p_{A,s}) = \left[ (D_B p_{B,s} / b D_A) - p_{A,s} \right] / p_{A,s} \quad (\text{IV-51})$$

All the results have been presented in terms of  $E$ , because this variable has a greater physical meaning than does  $|K|\chi$ .  $E$  is very closely related to the stoichiometric excess of B over A in the bulk stream and indeed is equal to the stoichiometric excess if  $D_B = D_A$ . For example, if the bulk stream contains B in 100% excess over A, the ratio of  $p_{B,s}$  to  $p_{A,s}$  is 2b. For this situation, with  $D_B = D_A$ , Equation (IV-51) gives  $E = 1$ . Furthermore, as was shown earlier,  $\chi$  will be zero when: 1) there is only one reactant which disappears by a bimolecular surface process; 2) two reactants are present in stoichiometric ratio. Equation (IV-51) shows that, under these circumstances,  $E$  will also be zero.

Figures IV-5, IV-6 and IV-7 are log-log plots of  $\eta$  versus  $\Phi_{\text{MII}}$  for various values of  $Kp_{A,s}$ ; for Figure IV-5,  $E = 0$ , for Figure IV-6,  $E = 1$  and for Figure IV-7,  $E = 10$ . Only non-negative values of  $E$  have been considered, since this situation will always result if A and B are chosen as described earlier.

The arrows on each line of constant  $Kp_{A,s}$  on these figures indicate approximately the point at which Equation (IV-48) is accurate to one percent. For values of  $\Phi_{\text{MII}}$  to the right of the arrow, Equation (IV-48) is a very good approximation.

Figures IV-5, IV-6 and IV-7 allow the effectiveness factor of a Type II reaction to be calculated, providing that the intrinsic



kinetics, the reaction stoichiometry, the surface partial pressures and the effective diffusivities are known or can be estimated. If the actual value of  $E$  corresponds to one of those considered here, interpolation between lines of constant  $Kp_{A,s}$  can be facilitated by using Equation (IV-48) to fix the linear portion of the  $\eta - \Phi_{\text{MII}}$  curve. Interpolation between values of  $E$ , for one of the  $Kp_{A,s}$  values that was considered, requires a cross-plot together with the application of Equation (IV-48).

Figures IV-8, IV-9 and IV-10 are logarithmic plots of  $\eta$  versus the modulus  $\Phi_L$ , for the same values of  $Kp_{A,s}$  as shown in the previous figures, and for  $Kp_{A,s} = 0$ . The plots are for  $E = 0$ ,  $E = 1$ , and  $E = 10$ , respectively. For orientation, the zero-order curve is shown on all three figures, and the second-order ( $E = 0$ ) curve is shown on Figures IV-8 and IV-9. The second-order curve would be essentially coincident with the  $Kp_{A,s} = -0.40$  curve on Figure IV-10. The curve for a first-order reaction is not shown on any of the figures. However, on Figure IV-8, the first-order curve would lie slightly above the  $Kp_{A,s} = +1.0$  line; on Figure IV-9, it would fall about halfway between  $Kp_{A,s} = 0$  and  $Kp_{A,s} = +1.0$  and on Figure IV-10 it would be essentially coincident with the  $Kp_{A,s} = 0$  curve. The  $\eta - \Phi_L$  curve for a Type I kinetic equation, with  $Kp_{A,s} = -0.90$ , is shown on Figure IV-8.

As implied in the discussion of the rate expression, Equation (IV-40), the second and zero-order curves may be regarded as specific members of the Type II family when  $E = 0$ , i. e., in Figure IV-8. However, the Type I curve in this figure is not a member of the family, as it intersects other Type II curves. When  $E$  is not zero, none of the integer-power curves are specific members of the Type II family.

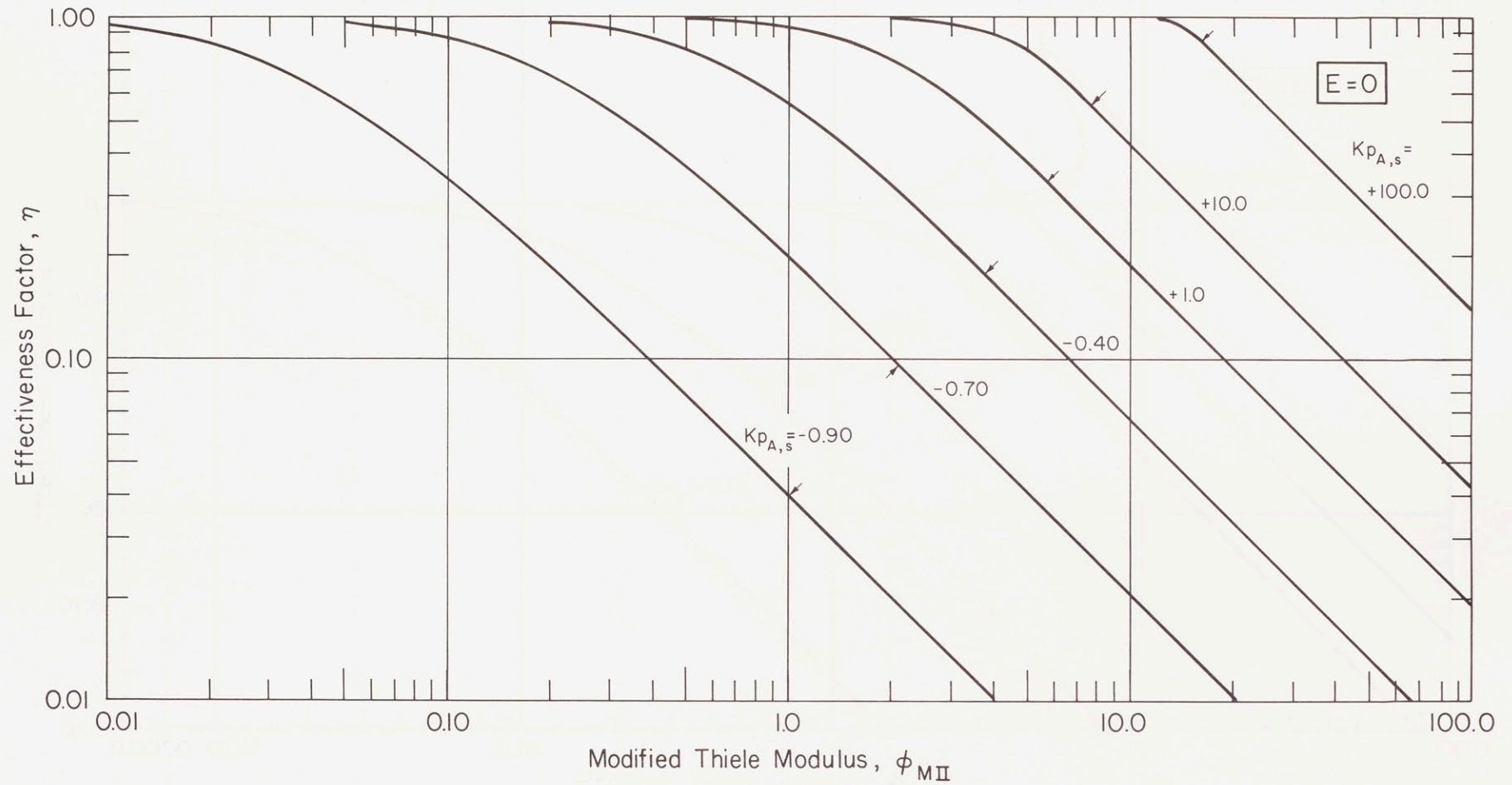


Figure IV-5 Effectiveness Factor as a Function of the Modified Thiele Modulus,  $\phi_{MII}$ , for Various Values of  $Kp_{A,s}$ ;  $E=0$





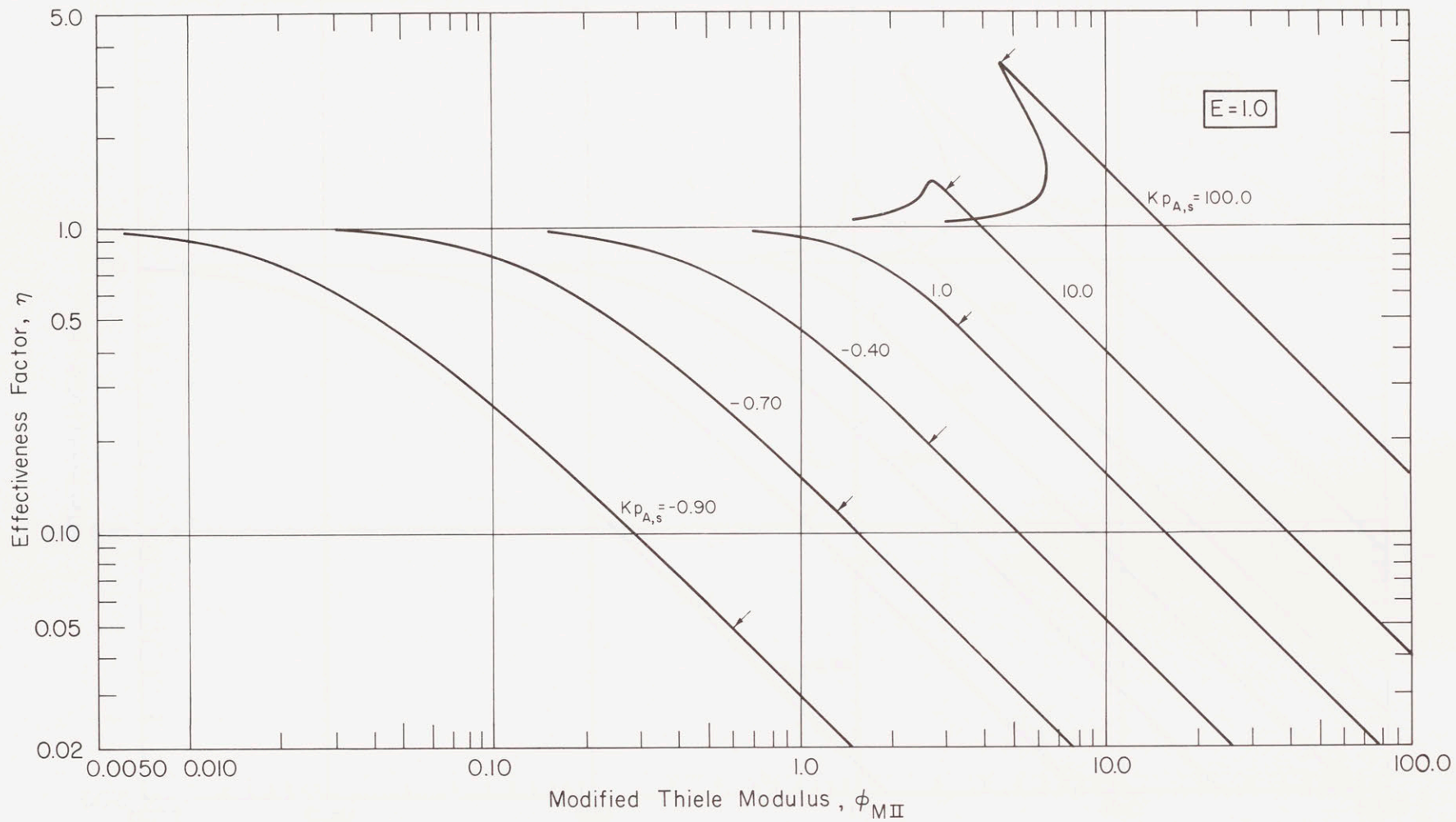


Figure IV-6 Effectiveness Factor as a Function of the Modified Thiele Modulus,  $\phi_{MII}$ , For Various Values of  $Kp_{A,s}$ ;  $E = 1.0$



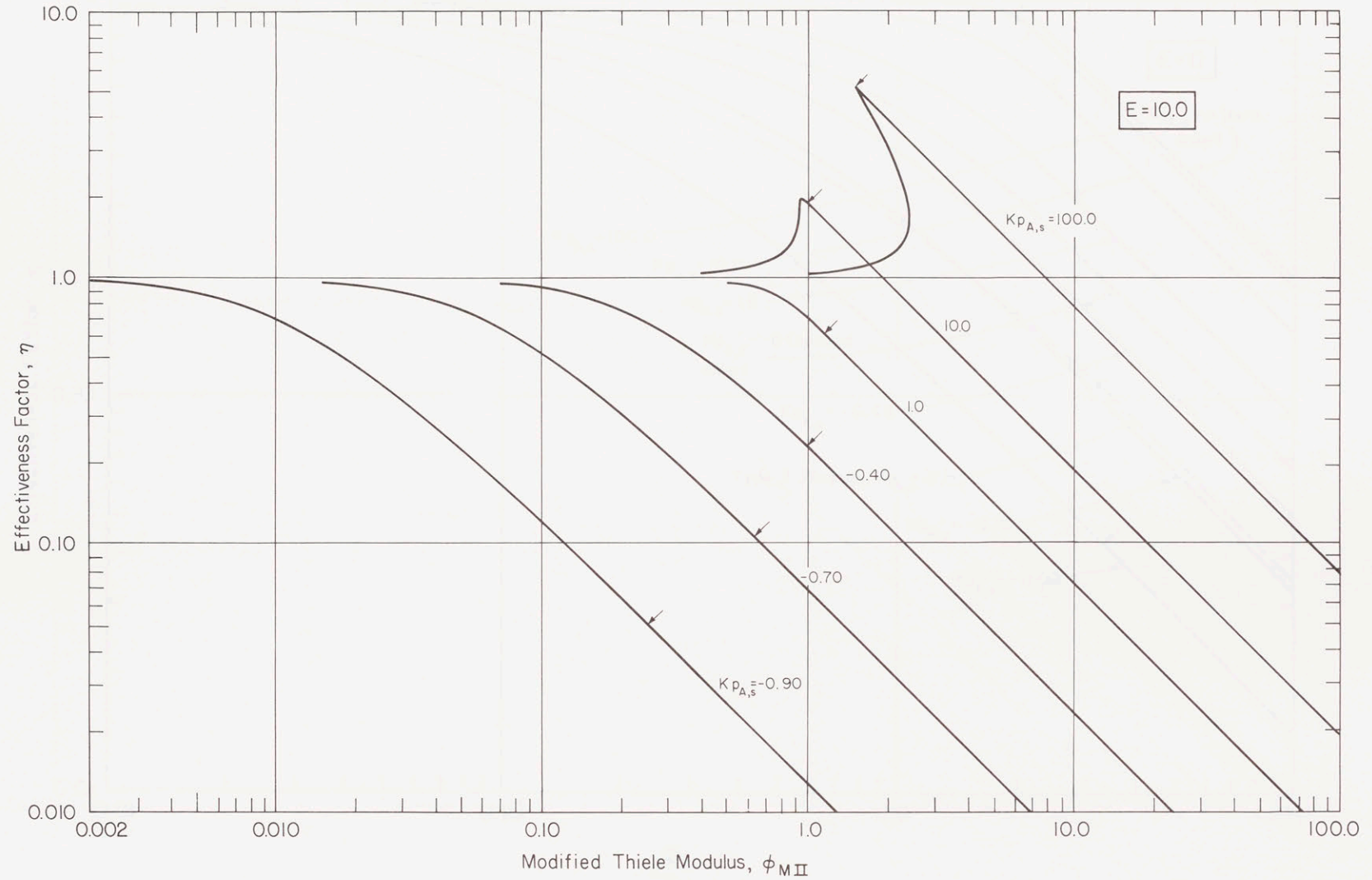


Figure IV-7 Effectiveness Factor as a Function of the Modified Thiele Modulus,  $\phi_{MII}$ , for Various Values of  $K_{p_{A,s}}$ ;  $E = 10.0$





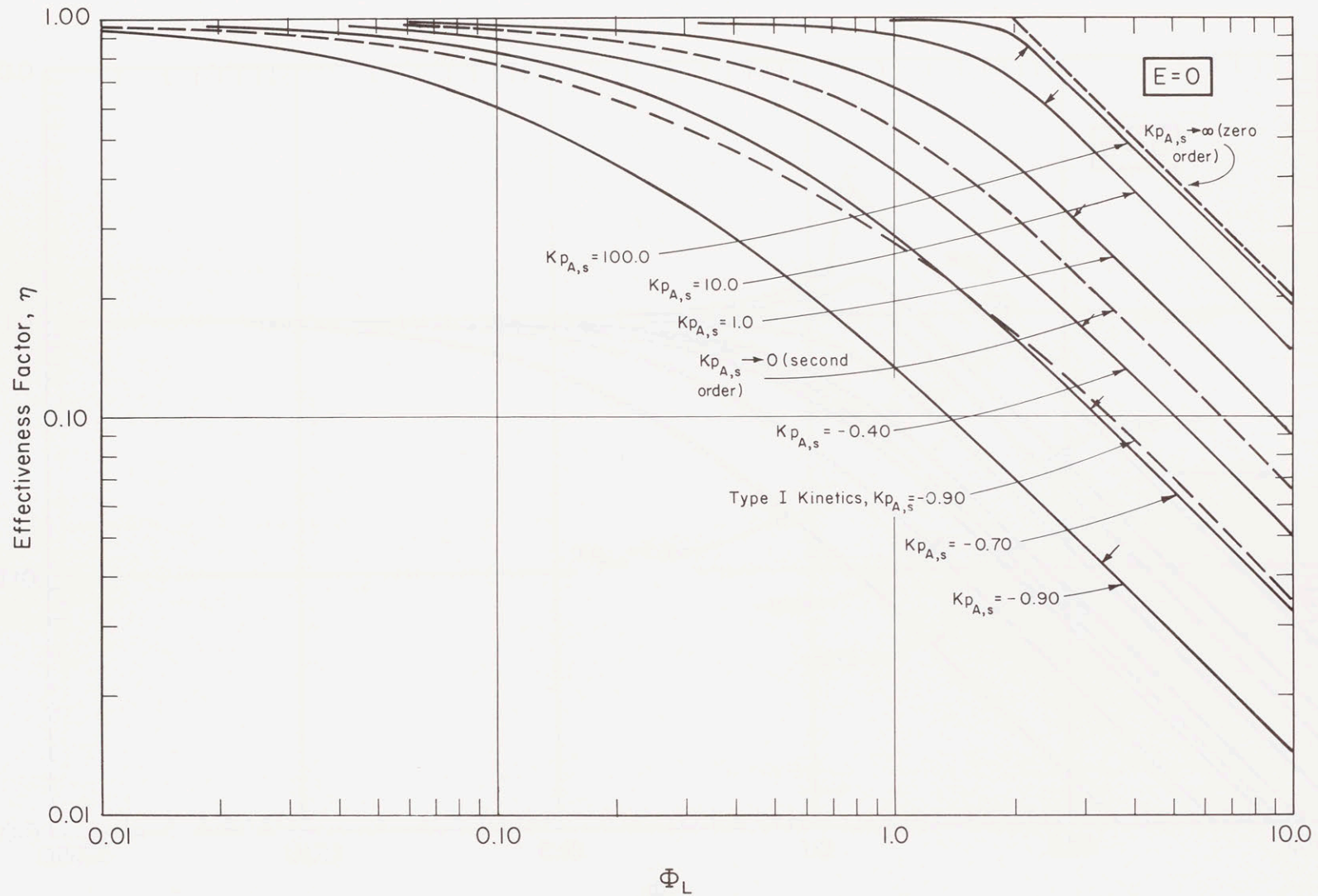


Figure IV-8 Effectiveness Factor as a Function of the Modulus  $\Phi_L$ , Type II,  $E=0$





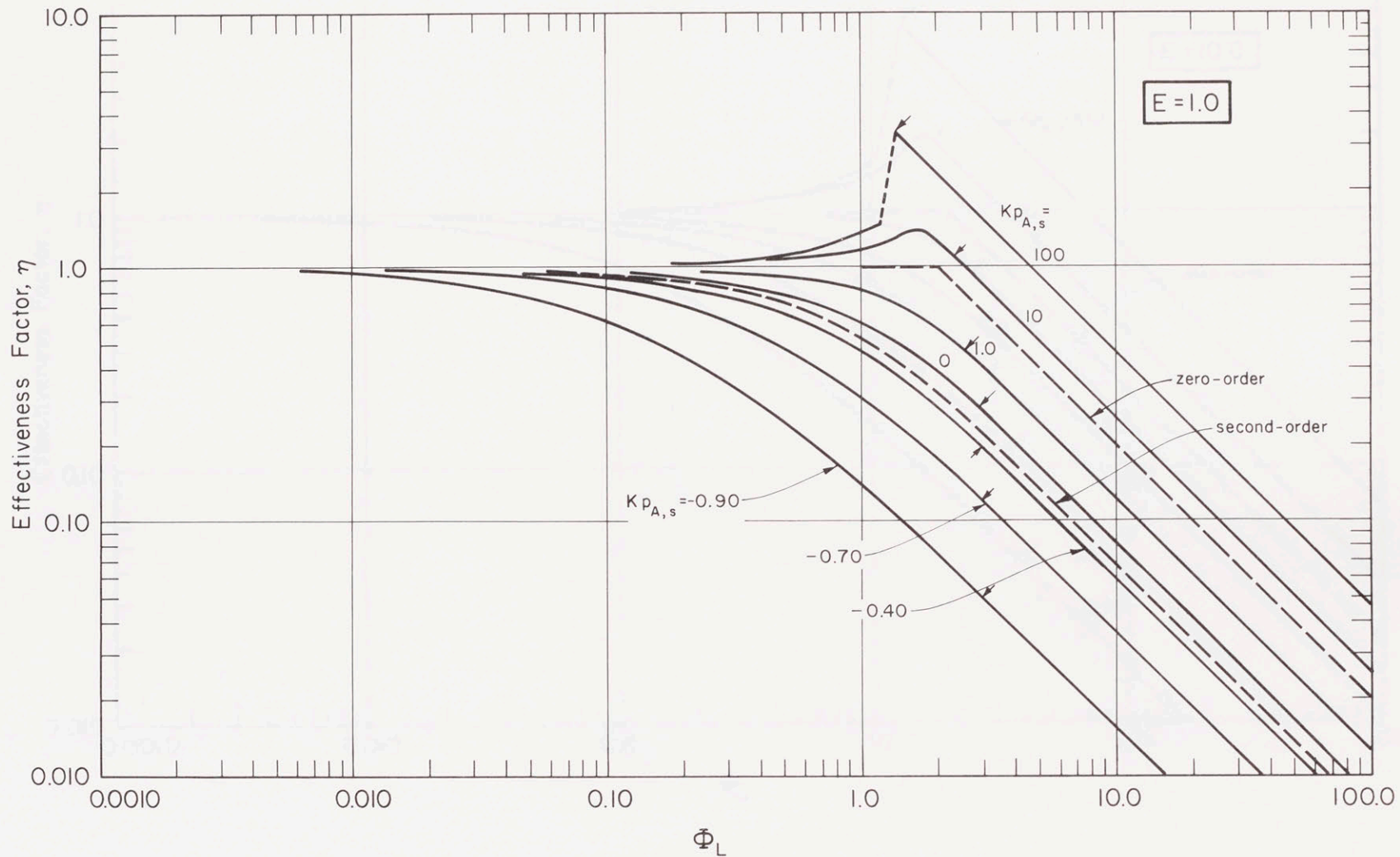


Figure IV-9 Effectiveness Factor as a Function of the Modulus  $\Phi_L$ ,  
Type II,  $E = 1.0$



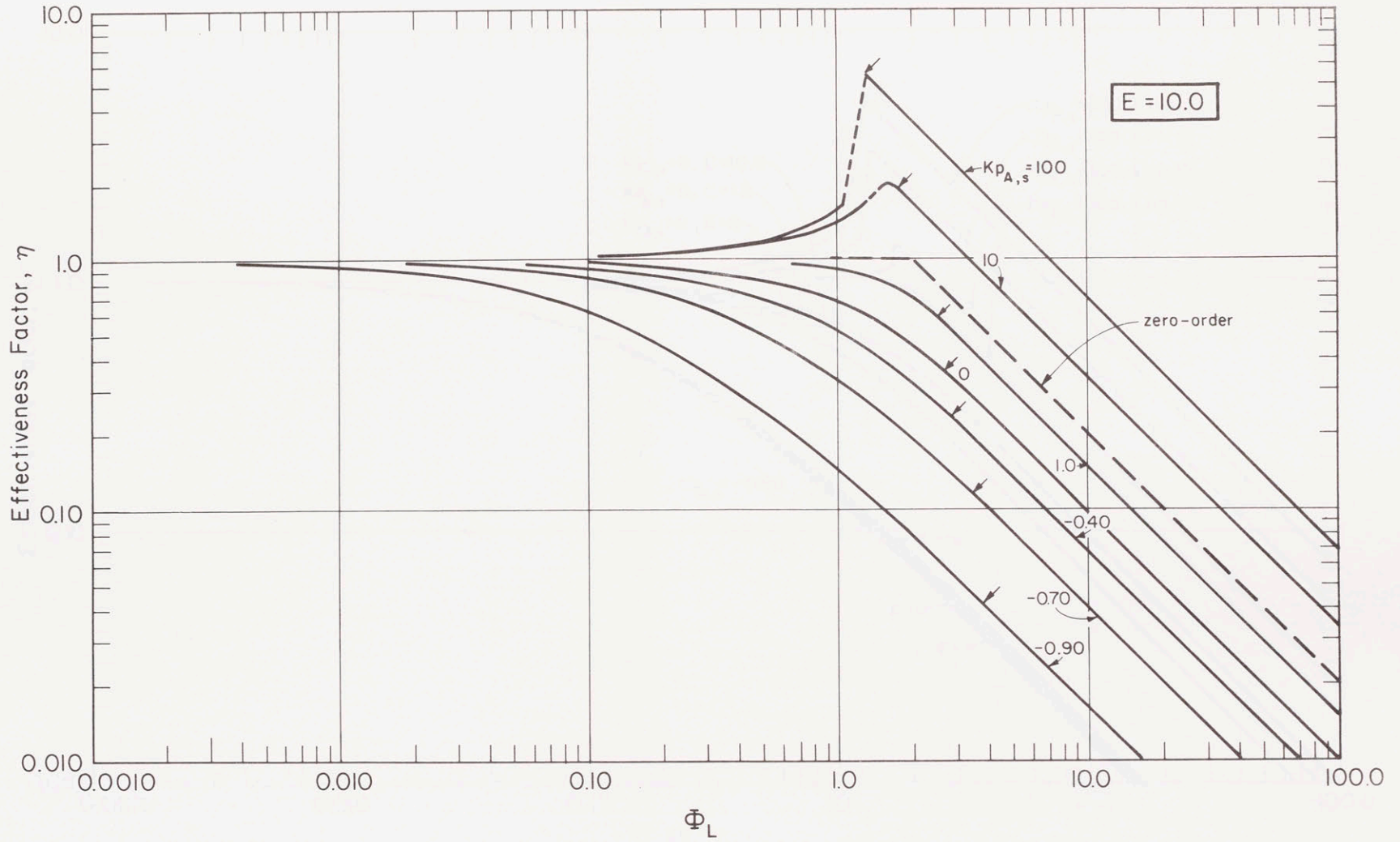


Figure IV-10 Effectiveness Factor as a Function of the Modulus  $\Phi_L$ ,  
Type II,  $E = 10.0$





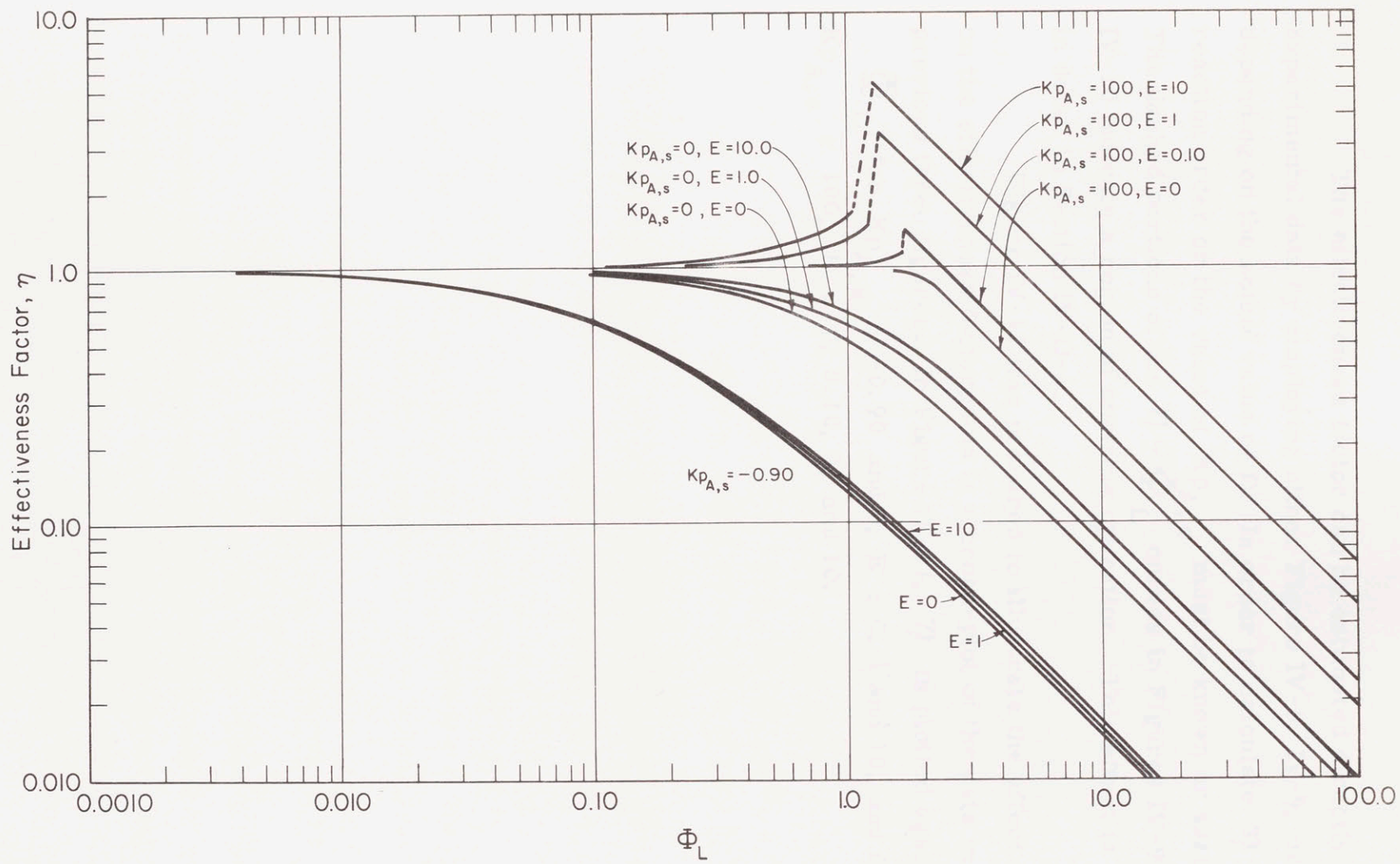


Figure IV-11 The  $\eta$  versus  $\Phi_L$  Relationship for Representative Combinations of  $Kp_{A,s}$  and  $E$ , Type II





The effectiveness factor can be estimated directly from experimental data by employing either Figure IV-8, IV-9, or IV-10, depending on the actual value of  $E$ . In order to calculate  $\eta$ , the reaction order or the value of  $Kp_{A,s}$  must be known or assumed. The dashed portions of the  $\eta - \Phi_L$  curves in Figures IV-9 and IV-10 indicate a region of unstable operation. This effect is discussed in detail in Section IV-D-2.

Figure IV-11 was prepared to illustrate the effect of  $E$  on the effectiveness factor, and is a cross-plot of the data in the previous three figures. In Figure IV-11,  $\eta$  is plotted against  $\Phi_L$ , for  $Kp_{A,s} = -0.90$  and  $0$ ,  $E = 0, 1$  and  $10$ , and for  $Kp_{A,s} = 100$ ,  $E = 0, 0.10, 1$ , and  $10$ .

## D. Discussion of Results

### I. Type I

#### a. Comparison with Previous Results

The effectiveness factor calculations for a Type I L-H rate equation that were presented in Section IV-C-1 do not involve the assumption of constant total pressure throughout the pellet. Furthermore, the present derivation allows the inhibition of the reaction by both reactants and products to be treated, without introducing any more parameters than were used in previous analyses of the problem. In this study, the effectiveness factor is determined by specifying two quantities,  $\Phi_{MI}$  (or  $\Phi_L$ ) and  $Kp_{A,s}$ . Chu and Hougen (14), who considered only reactant adsorption, overspecified their system by using three variables to define the effectiveness factor. The results presented by Chu and Hougen appear to be internally consistent, however, and when comparison is possible, seem to agree with the results of this study.

In the following section, comment is made on the merits of a machine computation, as opposed to the calculation of the effectiveness factor by an approximate technique.

#### b. The Approximate Solution for $\eta$

##### I. Region of Accuracy

Equation (IV-33) is a very accurate approximation to the effectiveness factor in the region to the right of the dashed line in Figure IV-3. Thus, for large positive values of  $Kp_{A,s}$ , the assumption that  $Kp_{A,o} \cong 0$  is valid, for the purpose of calculating  $\eta$ , up

to values of  $\eta$  that are very close to unity. As the value of  $Kp_{A,s}$  declines, the maximum value of  $\eta$  for which (IV-33) can be accurately applied drops to less than 0.10 when  $Kp_{A,s} = -0.98$ .

These results are consistent with the form of the rate equation. In (IV-24), if  $Kp_A$  is large,  $r_A$  is relatively insensitive to the value of  $Kp_A$ . Therefore,  $p_A$  must have a large drop through the pellet in order to affect the catalyst activity. However, for values of  $Kp_A$  approaching -1,  $r_A$  is very sensitive to  $Kp_A$ . A small decline in  $p_A$  through the catalyst particle is sufficient to produce a significant drop in the reaction rate. This reasoning is supported by the results shown in Figure IV-2, which shows that  $\eta$  is less than 0.95 for values of  $(p_{A,o}/p_{A,s})$  that are very close to unity, providing that  $Kp_{A,s}$  is negative. For large, positive values of  $Kp_{A,s}$ ,  $(p_{A,o}/p_{A,s})$  must be much lower before  $\eta$  deviates measurably from unity.

Since the assumption that  $p_{A,o}$  is nearly zero is valid only at very low values of  $\eta$  when strong adsorption of reaction products is involved, the approximate solution of Rozovskii and Shchekin (58) has only limited utility. Machine computation of the effectiveness factors was therefore justified.

## II. Concentration Dependence of $\eta$

Equation (IV-33) shows that, at constant  $\Phi_{MI}$ ,  $\eta$  varies with  $Kp_{A,s}$ , unless  $Kp_{A,s}$  approaches zero. In either an experimental or a commercial reactor,  $\Phi_{MI}$  will be nearly constant through the bed, providing that: 1) the reactor is isothermal, and; 2)  $D_A$  is concentration independent. Since  $Kp_{A,s}$  varies through the bed of an integral reactor, the effectiveness factor will depend on the



position in the bed, or more fundamentally, on conversion. Furthermore, because of the concentration dependence of  $\eta$ , the reaction order will be falsified if an intraparticle diffusional resistance exists.

### c. The $\eta - \Phi$ Relationship

#### I. Comparison with Integer-Order Rate Equations

Figure IV-4 permits visual comparison of the effectiveness factors for various kinetic equations. As mentioned in Section IV-C-1, the  $\eta - \Phi_L$  curve does not deviate significantly from the first-order curve unless  $|Kp_{A,s}|$  is greater than 0.10. For values of  $Kp_{A,s}$  greater than 50, the  $\eta - \Phi_L$  relationship is indistinguishable from that of a zero-order reaction.

Figure IV-4 shows that all curves for positive values of  $Kp_{A,s}$  are bracketed by the first and zero-order lines. Therefore, under conditions where inhibition by reaction products is negligible, limits can easily be put on the effectiveness factor by using the first and zero-order lines, providing that the reaction obeys the intrinsic rate law of Type I reactions (Equation IV-24).

When  $Kp_{A,s} < 0$ , the  $\eta - \Phi_L$  curves always fall below the first-order curve. In fact, for values of  $Kp_{A,s}$  less than about -0.50, the  $\eta - \Phi_L$  curve may fall below that of a second-order reaction. The implications of this result are discussed in Section III below.

#### II. The Aris' Transformation

The actual values of  $\Phi_L$  at which  $\eta$  is approximately equal to 0.95 are given in Table IV-1 for second, first and zero-order

reactions. An approximation to these values was obtained by applying the Aris transformation, which was discussed in Section IV-A-2, to the values of  $\bar{\Phi}_s$  at which  $\eta$  equals 0.95, as calculated by Weisz. For a sphere, the characteristic dimension,  $L'$ , is

$$L' = \frac{\text{pellet volume}}{\text{geometrical surface area}} = R_s/3 \quad (\text{IV-8})$$

For the slab catalyst considered in this analysis,  $L' = L$ .

Application of the Aris transformation to the defining equation for  $\bar{\Phi}_s$  (Equation IV-10) suggests that the values of  $(\bar{\Phi}_s/9)$  and  $\bar{\Phi}_L$  should be directly comparable. Thus, if the effect of pellet geometry on  $\eta$  could be essentially removed by using the characteristic dimension of Aris, the values of  $\bar{\Phi}_L$  and  $(\bar{\Phi}_s/9)$  should be very nearly equal. This comparison is also shown in Table IV-1.

Table IV-1

Values of  $\bar{\Phi}_L$  Corresponding to an Effectiveness Factor of 0.95

<u>Reaction Order</u>	<u><math>\bar{\Phi}_L</math> for Slab</u>	<u><math>\bar{\Phi}_L</math> for Sphere = <math>(\bar{\Phi}_s/9)</math></u>
0	2.1	0.66
1	0.15	0.11
2	0.075	0.033

The difference between the numbers in the second and third columns in the above table is a measure of the effect of catalyst particle geometry on the  $\eta - \bar{\Phi}_L$  relationship. Table IV-1 shows that good agreement between spherical and slab geometry results only



for a first-order reaction, which was the only order considered by Aris. Substantial deviations occur for zero and second-order reactions and the same is probably true for other rate expressions. For a given value of  $\Phi_L$ , the true effectiveness factor in a sphere will be less than that calculated for slab geometry, but the amount of the difference is known only for the simple cases above.

It should be noted that Table IV-1 illustrates only that the Aris transformation lacks generality in the region of  $\eta = 0.95$ . Aris himself pointed out that for first-order reactions, the maximum deviation occurred in this region. The transformation is probably more accurate at lower values of  $\eta$ , where the reactant does not penetrate into the pellet to a large degree, thereby minimizing the importance of a varying cross-sectional area.

### III. The Effect of Product Adsorption

Table IV-1 also gives the slab-geometry analogies to Weisz's criteria for the presence and absence of diffusion effects. These criteria have been discussed in Section IV-A-2. Application of Weisz's reasoning to the present results for slab geometry leads to the conclusion that a diffusional retardation will definitely exist if

$$\Phi_L \geq 2.1 \quad (\text{IV-61})$$

and that diffusional effects will be essentially absent if

$$\Phi_L \leq 0.075 \quad (\text{IV-62})$$

As stated previously, the latter criterion results from the assumption that no important rate equation possesses an  $\eta - \Phi_L$  curve that lies lower than that of a second-order reaction.



Examination of Figure IV-4, however, reveals that when strong product inhibition occurs, i. e.,  $Kp_{A,s}$  has a large negative value, the  $\eta$  versus  $\Phi_L$  curves fall quite low relative to that for a second-order reaction. This is true for values of  $Kp_{A,s}$  less than or equal to -0.50. Values of  $Kp_{A,s}$  less than -0.50 are not uncommon for reactions showing product inhibition. Values in this range have been calculated by the author from Gilliland's data on carbon monoxide oxidation (18), Miller and Kirk's data on the dehydration of alcohols (38), and the data of Walker, et al on the reaction of carbon dioxide with carbon (77). These examples are not inclusive, but are mentioned only to support the contention that many important reactions exhibit a behavior such that a calculation based on second-order rate equation will yield a value of  $\eta$  that is higher than the true value. The error that can arise from application of the criterion based on a second-order reaction to a reaction where product adsorption is important is illustrated by the calculations in Appendix D-1, where the data of Walker, et al is analyzed. Calculations of  $Kp_{A,s}$  from the data of Miller and Kirk and the data of Gilliland appear in Appendix D-2.

Equation (IV-62), therefore, does not constitute a reliable criterion for predicting the absence of diffusional effects in slab catalysts, and it is almost certain that the equivalent criterion for spherical pellets has similar disadvantages. In order to include the case of strong inhibition of the reaction by its products, the criterion for the absence of diffusional effects must be extended to considerably lower values of  $\Phi_L$ . Thus, for  $Kp_{A,s} = -0.98$ , the effectiveness factor,  $\eta$ , is about equal to 0.95 when

$$\Phi_L \leq 0.0031 \quad (\text{IV-63})$$

Since no examples of reactions having  $Kp_{A,s}$  less than -0.98 have been found by the author, Equation (IV-63) is proposed to replace (IV-62) as the criterion for the absence of diffusional effects.

Qualitatively, the situation may be summarized as follows. If strong product adsorption occurs, and if a diffusional resistance is present within the catalyst particle, the reaction rate declines through the pellet because of two factors; the first is a decline in the reactant concentration, the second is an increase in the product concentration. The combination of these two effects causes the  $\eta - \Phi$  curve to be displaced downward from integer-order curves, and causes diffusional limitations to become evident under milder conditions, i. e., lower rates of reaction, than for integer-order reactions.

## 2. Type II

### a. The Approximate Solution for $\eta$

#### I. Accuracy

Equation (IV-48) is a very accurate approximation to  $\eta$  in the region to the right of the arrows in Figure IV-5, IV-6 and IV-7. As with Type I reactions, the assumption that  $Kp_{A,o} \cong 0$  is valid only at very low values of  $\eta$ , when  $Kp_{A,s}$  is negative. At large, positive values of  $Kp_{A,s}$ , Equation (IV-48) is accurate up to much higher values of the effectiveness factor. In fact, in situations where  $\eta$  exceeds unity, Equation (IV-48) is valid almost to, or in some cases at, the maximum value of  $\eta$ . An explanation for this observation has been presented in Section IV-D-1.



## II. Concentration Dependence of $\eta$

Equation (IV-48) shows that, in general, the effectiveness factor varies with  $Kp_{A,s}$  at constant values of  $\Phi_{MII}$  and  $E$ , and that  $\eta$  varies with  $E$  at constant  $\Phi_{MII}$  and  $Kp_{A,s}$ . In an integral reactor,  $\Phi_{MII}$ ,  $E$  and  $Kp_{A,s}$  will vary through the bed and the effectiveness factor will therefore vary through the bed. Falsification of the reaction order will occur if  $\eta$  is less than unity.

### b. The $\eta - \Phi_{MII}$ Relationship

The curves in Figure IV-5 exhibit the general characteristics of the effectiveness factor versus Thiele modulus (or modified Thiele modulus) plots for integer-order or Type I L-H kinetic equations, in isothermal catalyst pellets. Specifically,  $\eta$  approaches unity at low values of  $\Phi$  and declines monotonically as  $\Phi$  increases.

Some of the curves on Figures IV-6 and IV-7 also show this behavior, but several curves do not. In the first place, on Figures IV-6 and IV-7, when  $Kp_{A,s}$  is 10 or 100, effectiveness factors greater than unity result over a certain range of  $\Phi_{MII}$  values. This is a consequence of the fact that the rate equation, Equation (IV-40), possesses a maximum under certain conditions. Thus, by differentiation of (IV-40), it can be shown that effectiveness factors greater than unity will result, over some range of  $\Phi_{MII}$ , when  $Kp_{A,s}$  is greater than  $((E + 2)/E)$ , providing that  $E$  is always positive. This conclusion is in agreement with Figures IV-5 through IV-7, which show that  $\eta$  is always less than unity for any  $Kp_{A,s}$  if  $E$  is zero, and is always less than unity for any value of  $E$  if  $Kp_{A,s}$  is 1.0 or less.



In terms of the Langmuir-Hinshelwood model, the maximum in the rate equation, and consequently effectiveness factors greater than unity, results from a competition between the two reactants for sites on the catalyst surface. If A is strongly adsorbed relative to B, an increase in  $p_A$  will displace B from the catalyst surface when the partial pressure of A is high, i. e., when the catalyst surface is nearly saturated. This displacement of B tends to decrease the reaction rate by decreasing the quantity  $\sigma_A \sigma_B$ . At low surface coverages, i. e., low partial pressures of A, displacement does not occur and the rate of reaction increases with  $p_A$ .

A second unusual characteristic of the  $\eta - \Phi_{MII}$  relationship occurs for  $E = 10$ ,  $Kp_{A,s} = 10$  and  $100$  (Figure IV-7) and for  $E = 1$ ,  $Kp_{A,s} = 100$  (Figure IV-6). For these three curves, a range of  $\Phi_{MII}$  exists over which  $\eta$  is a double or triple-valued function of  $\Phi_{MII}$ . Now,  $E$ ,  $\Phi_{MII}$  and  $Kp_{A,s}$  are uniquely determined by specifying the conditions, e. g., temperature and partial pressures of all components, existing at any point in a reactor. Therefore, the existence of a multiple-valued region of  $\eta$  means that the effectiveness, and therefore the reaction rate, may not be uniquely determined by specifying the conditions in the reactor. The direction from which steady-state is approached may determine which effectiveness factor, and reaction rate, is finally realized. For instance, in any triple-valued region, the highest  $\eta$  is always associated with the lowest value of  $(p_{A,o} / p_{A,s})$ . Thus, if a reactor were at reaction temperature, but no A were present, the initial value of  $p_{A,o}$  would be zero. If A were suddenly admitted at partial pressure  $p_{A,s}$ ,  $p_{A,o}$  would increase. It seems logical to assume that this increase would continue until a value of  $(p_{A,o} / p_{A,s})$  corresponding to a steady-state solution was reached. In the present example,

the lowest value of  $(p_{A,o} / p_{A,s})$  would be encountered first, and operation most likely would take place at the highest value of the effectiveness factor. By a similar process of reasoning, it is likely that the lowest value of  $\eta$  would be realized if  $p_{A,o}$  were initially equal to  $p_{A,s}$ .

The intermediate value of  $\eta$  in the triple-valued region is probably metastable, and not attainable in steady-state operation. Operation of a reactor in this region would therefore be unstable.

The above remarks are based on the assumption that the actual steady-state solution depends only on the direction from which steady-state is approached. In practice, as pointed out by Weisz and Hicks (79), stabilization may result from second-order phenomena such as concentration and temperature dependencies of such parameters as  $D_i$ ,  $K_i$ ,  $D_A$ ,  $K_A$  and  $k_{II}$ .

Effectiveness factors greater than unity have not been previously reported for isothermal catalyst pellets, nor has the existence of a region of multiplicity, or any of its corollaries, ever been suggested for isothermal pellets. However, as discussed in Section IV-A-2, several investigators have reported that both of these effects can occur in non-isothermal pellets.

### c. The $\eta - \Phi_L$ Relationship

#### I. The Effect of Product Adsorption

Figures IV-8, IV-9, and IV-10 show that when  $Kp_{A,s}$  is negative, the  $\eta - \Phi_L$  curves can lie considerably below even the curve for a second-order reaction. Therefore, as with Type I reactions, strong inhibition of the reaction by its products causes diffusional limitations to set in under milder conditions than would



be predicted by the criterion given in Equation (IV-62), which is based on a second-order reaction.

On Figure IV-8, the  $\eta - \bar{\Phi}_L$  line for  $Kp_{A,s} = -0.90$  lies below the  $Kp_{A,s} = -0.90$  line for a Type I rate equation. If the value of  $Kp_{A,s}$  is negative, the curve for a Type II kinetic equation will always fall below that for a Type I equation with the same value of  $Kp_{A,s}$ . It would be interesting to examine the newly-proposed criterion for the absence of internal diffusion effects, Equation (IV-63), in this light. However, very few experimental studies, where product inhibition of the reaction was important and where a Type II kinetic equation was used to correlate the rate data, have appeared. Exceptions are the formation of phosgene from carbon monoxide and chlorine (51) which is inhibited by the phosgene, the hydrogenation of codimer (26) which is inhibited by the saturated product, and the present reaction, the hydrogenolysis of thiophene, which is inhibited by  $H_2S$ . However, in these studies, reactant inhibition was also significant; as shown in Appendices D-2 and D-3, the values of  $Kp_{A,s}$  for these three reactions are either positive or only slightly negative. In no case did the  $\eta - \bar{\Phi}_L$  curve for any Type II reaction lie lower than the  $Kp_{A,s} = -0.98$  line for a Type I reaction. Therefore, Equation (IV-63) is probably a valid general criterion for the absence of diffusion effects.

## II. The Effect of Reactant Adsorption

When  $Kp_{A,s}$  is greater than  $((E + 2)/E)$ , the  $\eta - \bar{\Phi}_L$  curve lies higher than that for a zero-order reaction, as shown in Figures IV-9 and IV-10. In spite of this, it appears that Equation (IV-61) still is a valid criterion for the definite presence of diffusional effects. This is so for the cases studied here, providing that a diffusional



effect is considered to exist unless: 1)  $0.95 \leq \eta \leq 1.05$ , and; 2)  $\eta$  approaches unity as  $\Phi_L$  is indefinitely decreased. Thus, for cases where effectiveness factors greater than unity exist,  $\eta$  will in general be greater than 1.05 until  $\Phi_L < 2.1$ .

The dashed portions of the curves in Figures IV-9 and IV-10 show the region where operation is likely to be unstable, i. e., the region corresponding to the intermediate value of the effectiveness factor when this quantity is triple-valued. The dashed lines are used only to join the stable portions of each curve, and do not define the  $\eta - \Phi_L$  relationship in the unstable region. In some portions of the unstable region,  $\eta$  is a multiple-valued function of  $\Phi_L$ . However, the effectiveness factor is always a unique function of  $\Phi_L$  in the stable portion of the curve.

#### d. The $\eta - E$ Relationship

The effect of  $E$  on the  $\eta - \Phi_L$  relationship is shown in Figure IV-11. For  $Kp_{A,S} = -0.90$ , the  $E = 0$  curve lies lowest on the plot. The  $E = 10$  curve is highest, with the  $E = 1$  line between the two. However, these three curves are so close together that they are almost indistinguishable. For  $Kp_{A,S} = 0$ , the spread between the curves for the same three values of  $E$  is somewhat greater, but still rather small. The curves again fall in the order  $E = 0 < E = 1 < E = 10$ . For  $Kp_{A,S} = 100$ , the  $\eta - \Phi_L$  curves fall in the order  $E = 0 < E = 0.10 < E = 1 < E = 10$ .

The fact that the curves for high values of  $E$  lie above those for low values, at constant  $Kp_{A,S}$ , is consistent with the interpretation of  $E$  as a stoichiometric excess. When  $E$  is large,  $B$  is in excess throughout the catalyst pellet and the product  $p_A p_B$  declines more

slowly than it would if B were present in stoichiometric amounts.

### 3. The Diffusional Implications of the Rate Equations for Thiophene Hydrogenolysis

#### a. Effectiveness Factors

The rate of thiophene disappearance is given by Equation (III-19), which has the form of a Type II rate equation. Therefore, the effectiveness factor of a catalyst particle could potentially be greater than unity for this reaction, and operation of the reactor could potentially be unstable. Values of  $Kp_{A,s} = 0.51$  and  $E = 30$  are calculated for Run 44 in Appendix D-3. For the other runs,  $E$  is about 30 or greater, but 0.51 is about the maximum value that  $Kp_{A,s}$  attained.

With these values of  $E$  and  $Kp_{A,s}$ , the reaction would not have an effectiveness factor greater than unity, nor would unstable operation be possible, since a value of  $Kp_{A,s}$  greater than one is necessary to achieve these effects. The value of  $Kp_{A,s}$  could probably be increased to greater than unity by operating at a higher thiophene partial pressure, or by operating at a lower reactor temperature, thus increasing the value of  $K$ . In order to attain the region of unstable operation,  $Kp_{A,s}$  must be substantially greater than unity, and it is questionable whether unstable operation is possible with the thiophene hydrogenolysis reaction at atmospheric pressure.

#### b. Selectivity

The question of whether selectivity to butene can be increased by operating with an intraparticle diffusion resistance present has not been answered. The discussion of Section III-D-5 seems to indicate



that build-up of  $H_2S$  will not increase the selectivity, unless the partial pressures of butene and  $H_2S$  are low and that of thiophene is high. Since just the opposite situation would exist at the center of a catalyst pellet where diffusional retardation was strong, it does not seem that the selectivity of thiophene hydrogenolysis to butene can be increased. In fact, it seems that the selectivity should be decreased to an even greater extent than the model of Wheeler (83) would predict. However, only by conducting experiments or by solving the appropriate differential equations can a definitive answer be produced.

Operation of the reaction with an internal diffusional resistance present within the catalyst pellet would seem to be a good method of studying the extent to which butene hydrogenation takes place on the original desulfurization sites. If appreciable reaction of butene occurs without intermediate desorption-adsorption, an internal diffusion resistance cannot influence the selectivity to a great extent. However, if all the butene desorbs and re-adsorbs before hydrogenating, the reaction selectivity can be strongly influenced by the presence or absence of a diffusional resistance. With regard to this type of experiment, it would be of interest to contrast the behavior of a sulfided chromia catalyst and the cobalt molybdate catalyst.



## V. Conclusions and Recommendations

### A. Thiophene Hydrogenolysis

#### 1. Conclusions

a. Over the range of conditions covered by the experiments, the kinetics of thiophene disappearance are best described by

$$r_T = k p_T p_H / (1 + K_T p_T + K_{H_2S} p_{H_2S})^2 \quad (\text{III-19})$$

This equation shows that the reaction rate can go through a maximum as the thiophene partial pressure is increased at constant hydrogen sulfide partial pressure. This maximum is evident in the experimental data. Inhibition of the reaction rate by both thiophene and hydrogen sulfide is significant.

b. Over the range of conditions covered by the experiments, the kinetics of butene hydrogenation are best described by

$$r_c = \hat{k} p_B / (1 + \hat{K}_B p_B + \hat{K}_{H_2S} p_{H_2S}) \quad (\text{III-32})$$

Inhibition of the reaction rate by both butene and hydrogen sulfide is significant. The best correlation of the experimental data resulted from the assumption that no butene was hydrogenated on the original desulfurization sites.

c. The data is consistent with the assumption that desulfurization and hydrogenation occur on separate catalyst sites.

d. The selectivity of the overall reaction to butene should be increased by increasing the partial pressure of hydrogen sulfide only when the partial pressures of butene and  $H_2S$  are low and the partial pressure of thiophene is high. Under other conditions, the addition of hydrogen sulfide should lower the selectivity.

## 2. Recommendations

### a. Further Experiments

I. Kinetic experiments that cover a wider range of temperature should be made.

II. Runs with butene included in the feed to the reactor should be made.

III. Runs should be made under conditions where the diffusional resistance within the catalyst pellet is significant, in order to investigate the extent to which butene is hydrogenated on the original desulfurization site. Computer solutions to the equations for the simultaneous diffusion and reaction of thiophene and butene would be useful in conjunction with these experiments and would also indicate whether the build-up of hydrogen sulfide inside the catalyst can give rise to unusual selectivity effects.

### b. Modifications of the Equipment and Procedure

I. A chromatograph column should be developed that will allow thiophene to be measured, in addition to butane, the butenes and hydrogen sulfide.

II. A larger gas sample should be analysed when the feed rate

of the thiophene is low, in order to allow a more accurate measurement of the butene concentration.

III. In order to bring the catalyst surface to steady-state rapidly, hydrogen sulfide should be fed during the start-up of runs made with a low thiophene feed rate.

## B. Effectiveness Factors for Porous Catalysts: Langmuir-Hinshelwood Kinetic Expressions

### 1. Conclusions

a. The effectiveness factor for a porous catalyst, on which a reaction whose kinetics obey either a Type I or a Type II rate equation is taking place, can be computed from the charts presented. The calculation of the effectiveness factor may be based either on a knowledge of the intrinsic kinetics or on experimental rate data.

b. For either Type I or Type II rate equations, if a product inhibits the reaction rate, a diffusional retardation can set in under much milder conditions than would be predicted by the existing criterion.

c. If the reaction kinetics follow a Type II rate equation, effectiveness factors greater than unity can result in an isothermal pellet.

d. For a Type II rate equation, a region of conditions may exist where the effectiveness factor is not uniquely determined by specifying the conditions outside the catalyst particle. In this range of conditions, unstable operation can result.



VI. Appendix

A. Additional Data on Equipment Performance

1. Calibration of the Hydrogen Flowmeter

Since the pressure drop in the capillary tubing was very small, and flow was laminar, the Poiseuille equation may be applied

$$\Delta P = \frac{32 \mu \bar{v} l}{g_c d_c^2} \quad (\text{VI-1})$$

Now, the average velocity  $\bar{v}$  is related to the volumetric flow at STP by

$$\bar{v} = \frac{F_{\text{STP}} \cdot T}{\pi d_c^2 \cdot 273 \cdot P} \quad (\text{VI-2})$$

The pressure drop across the capillary is also given by

$$\Delta P = m \rho_M \quad (\text{VI-3})$$

Combining Equations (VI-1), (VI-2) and (VI-3) and rearranging

$$F_{\text{STP}} = \left( \frac{273 \pi \rho_M g_c d_c^4}{32 l} \right) \left( \frac{m P}{\mu_T} \right) \quad (\text{VI-4})$$

$$F_{\text{STP}} = a \left( \frac{m P}{\mu_T} \right) \quad (\text{VI-5})$$

where a contains only constants or quantities that were fixed once the

manometer and capillary were fixed.

As suggested by Equation (VI-5), the calibration curve for the hydrogen flowmeter was established by plotting  $F_{STP}$  versus  $\frac{m \bar{P}}{\mu T}$ , where P and T are the pressure and temperature in the capillary. The calibration curve for the hydrogen flowmeter is shown as Figure VI-1.

## 2. Calibration of the Hydrogen Sulfide Flowmeter

The pressure drop in the capillary was appreciable in this manometer. The equation governing the pressure drop is given by (VI-6), and contains the assumption of a perfect gas.

$$-dP = 32 \mu \bar{v} dl / g_c d_c^2 \quad (VI-6)$$

Substituting (VI-2) into (VI-6)

$$-dP = \frac{32 \mu}{g_c d_c^2} \left( \frac{F_{STP} \cdot T}{273 P \pi d_c^2} \right) dl \quad (VI-7)$$

Equation (VI-7) can be integrated to give

$$-P^2/2 = (F_{STP} \mu T 32/g_c \pi d_c^4 / 273) l \quad (VI-8)$$

Substituting (VI-3) into (VI-8), using the definition of a and rearranging

$$F_{STP} = a \left( \frac{m \bar{P}}{\mu T} \right) \quad (VI-9)$$

Equation (VI-9) suggests that  $F_{STP}$  should be plotted against  $(m \bar{P} / \mu T)$  for the purpose of calibration. However, since  $\mu$  is not known accurately as a function of temperature for hydrogen sulfide,





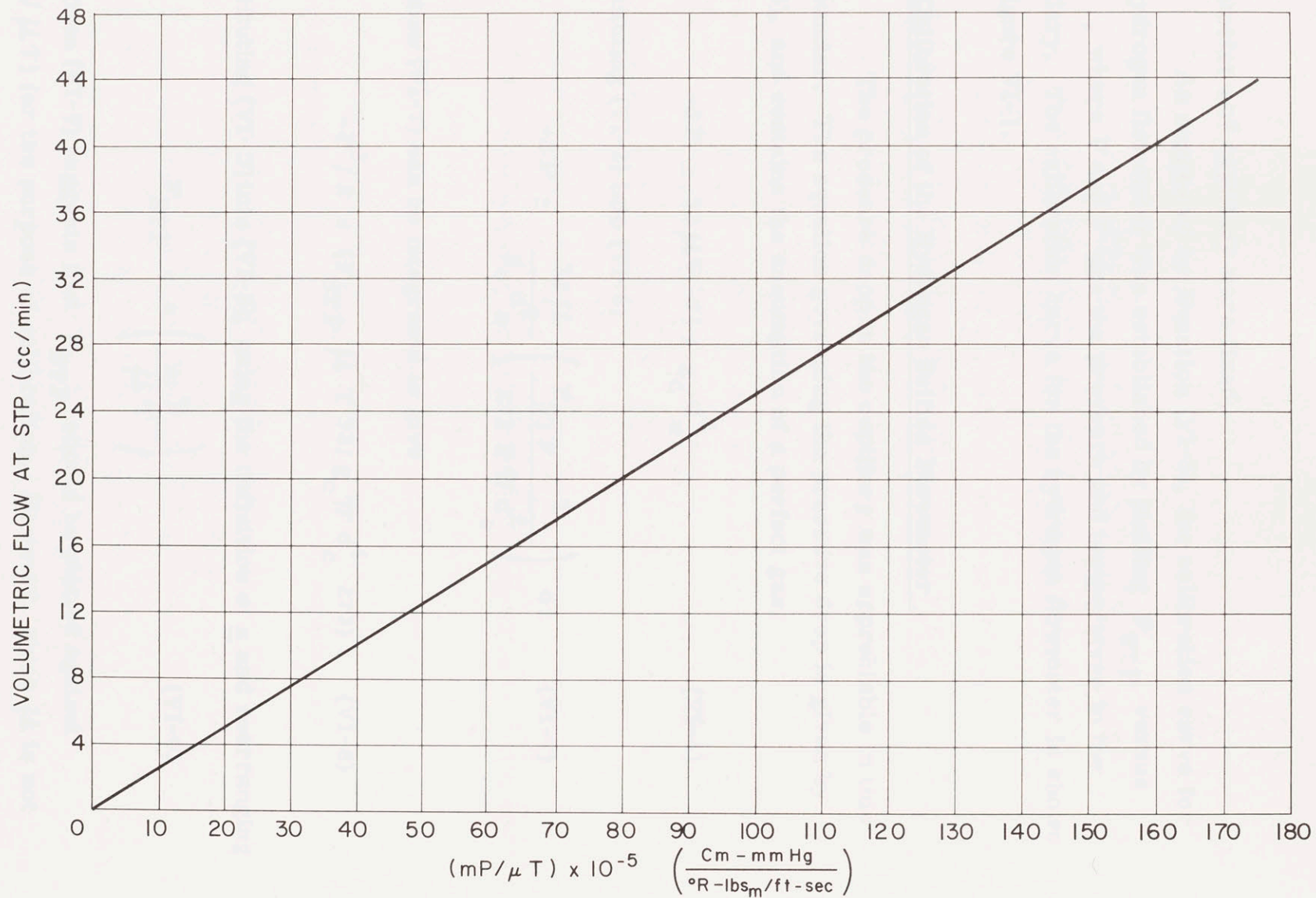


FIGURE VI -1 CALIBRATION CURVE FOR HYDROGEN FLOWMETER

$\mu$  was considered to be constant and the calibration was established by plotting  $F_{STP}$  against  $(m\bar{P}/T)$ . The calibration curve for the hydrogen sulfide flowmeter is shown as Figure VI-2.

### 3. Performance of the Gas Chromatograph

#### a. Separation

Table VI-1 gives the approximate values of the total retention volume and the total retention time for each reaction component. The retention volumes are at STP and the retention times correspond to the operating conditions given in Section III-B-2-c.

Table VI-1

#### Separation Data for Gas Chromatograph

<u>Component</u>	<u>STP Retention Volume</u>	<u>Retention Time</u>
H <sub>2</sub> S	613 cc.	4.90 min.
C <sub>4</sub> H <sub>10</sub>	894	7.15
1-C <sub>4</sub> H <sub>8</sub>	1080	8.60
2-C <sub>4</sub> H <sub>8</sub> (trans)	1430	11.45
2-C <sub>4</sub> H <sub>8</sub> (cis)	1660	13.25

With approximately equal amounts of each component, the separation of the mixture was almost quantitative. However, the purge gas from the reactor contained very small amounts of 1-butene, relative to the amount of butane. Under these conditions, separation

of the 1-butene from the butane was not complete, although two distinct peaks did appear in most cases. The amount of 1-butene was determined for several experimental runs by sketching in by hand the 1-butene and butane peaks from the compound peak. In all cases, the amount of 1-butene determined in this manner was equal to the equilibrium amount to within experimental error. The equilibrium amount of 1-butene was computed by assuming that 1-butene, cis 2-butene and trans 2-butene were all in equilibrium at the reaction temperature. With this assumption, the total amount of 1-butene was related to the total amount of 2-butene, using thermodynamic data taken from Perry (50). The amount of 2-butene was determined from the chromatogram. For the present purposes, this method is probably sufficiently accurate for computing the amounts of butane and butene in the reactor, since the 1-butene area was a small fraction of both the butane and 2-butene areas.

Complete separation of cis and trans 2-butene was not achieved. However, the specific responses of these two isomers are almost identical, so that the lack of complete separation introduced no error into the calculation of the total amount of 2-butene.

#### b. Calibration

Calibration was accomplished in the manner described in Section III-B-2-c. The results for all four components were accurately described by straight lines through the origin of a plot of scaled peak area versus STP volume. The term "scaled peak area" refers to the peak area that would have resulted for a 1X setting on the chromatograph and a 0.50 mv. setting on the recorder. Thus, if during operation the response from the thermal conductivity cell was attenuated, using either the recorder or the chromatograph controls, the actual peak area was



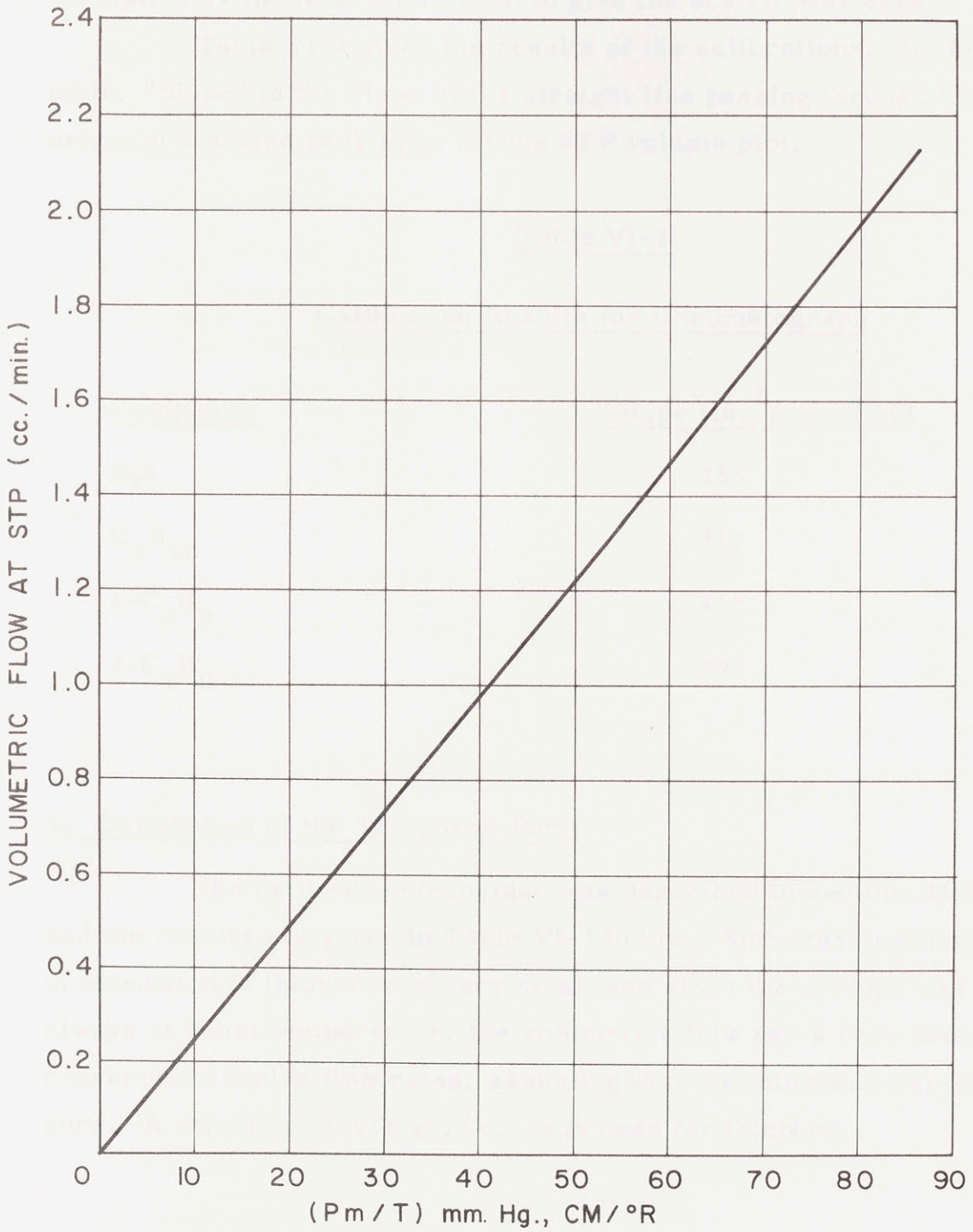


FIGURE VI - 2 CALIBRATION CURVE FOR HYDROGEN SULFIDE FLOWMETER



multiplied by the total attenuation to give the scaled peak area.

Table VI-2 gives the results of the calibrations. In this table, "Slope" is the slope of the straight line passing through the origin of a scaled peak area versus STP volume plot.

Table VI-2

Calibration Results for Chromatograph

<u>Component</u>	<u>Slope (in. <sup>2</sup>/ cc. STP)</u>
H <sub>2</sub> S	255
C <sub>4</sub> H <sub>10</sub>	397
1-C <sub>4</sub> H <sub>8</sub>	413
2-C <sub>4</sub> H <sub>8</sub>	395

4. Calibration of the Thiophene Pump

The calibration technique was described in Section III-B-2-d, and the results are given in Table VI-3 below. Since the coefficient of expansion of thiophene is very small and since the syringe was always at room temperature, the volumetric flow rates have been converted to molar flow rates, assuming that the thiophene was 100% pure. A density of 1.058 gr./cc. was used for thiophene.



Table VI-3

Calibration Results for Thiophene Pump

<u>Syringe (cc.)</u>	<u>Motor (rpm)</u>	<u>Molar Flow (gr. moles/ min.)</u>
1.0	0.25	$0.1092 \times 10^{-4}$
	0.50	0.2184
	1.0	0.4368
	2.0	0.8735
	4.0	1.747
2.0	0.25	0.3641
	0.50	0.7282
	1.0	1.456
	2.0	2.913
	4.0	5.825
5.0	0.25	0.6532
	0.50	1.306
	1.0	2.612
	2.0	5.224
	4.0	10.45

B. COMPUTER PROGRAMS

1. EFFECTIVENESS FACTORS FOR TYPE I RATE EQUATIONS

EXPLANATION OF INPUT DATA (DATA IS READ IN MAIN PROGRAM)

NSLICE=NUMBER OF GRID DIVISIONS

R=PHI SUR M1

C2APAI=KPA,O

```

C      DERIVATIVE FUNCTION FOR TYPE 1
      FUNCTION DER(P,C2APAI,T)
 1     FORMAT(4F18.8)
      IF((P+1.0)/100,100,10)
D10    A=P-C2APAI
D      V=A/(1.0+C2APAI)
      IF((ABS(V)-0.0001)/20,30,30)
D20    R=-V*(1.0-(V/2.0)+((V*V)/3.0)-(((V*V)*V)/4.0))
      GO TO 40
D30    R=-LOGF((1.0+V))
D40    APB=A+B
      IF(APR)200,50,50
 50    IF(P)60,300,70
D60    DER=-(T)*SQRTF(APB)
      GO TO 80
D70    DER=(T)*SQRTF(APR)
D80    RETURN
 100   PRINT 105
 105   FORMAT(1H0,4X16H CP LESS THAN -1)
      GO TO 500
 200   PRINT 205
 205   FORMAT(1H0,4X22H SQUARE ROOT IMAGINARY)
      GO TO 500
 300   PRINT 305
 305   FORMAT(1H0,4X14H CP EQUAL ZERO)
 500   R=T/SQRTF(2.0)
      PRINT 505
 505   FORMAT(10X2H R,14X7H C2APAI,13X2H P)
      PRINT 1,R,C2APAI,P
      PRINT 600
 600   FORMAT(4X19H PROGRAM TERMINATED)
      CALL EXIT
      FND(1,0,0,0,0,0,0,0,0,0,0,0,0,0,0,0,0)

```

```
C      MAIN PROGRAM
1      FORMAT(2E18.8,I14)
2      FORMAT(4E18.8)
3      FORMAT(4I18)
D      DIMENSION R(1),C2APAI(1)
10     READ 3,NSLICE
      IF(NSLICE)999,15,15
15     PRINT 16
16     FORMAT(1H1,21H START OF NEW PROBLEM)
      READ 2,R,C2APAI
      R(2)=0.00
      C2APAI(2)=0.00
      PRINT 17
17     FORMAT(10X2H R,14X7H C2APAI)
      PRINT 2,R,C2APAI
D      DEL=1.0/FLOAT(NSLICE)
D      H2=(R*R*DEL*DEL)/(1.0+C2APAI)
D      T=R*SQRT(2.0)
      PRINT 20
20     FORMAT(19H START OF ITERATION)
      PRINT 25
25     FORMAT(9X3H CP)
D      CPA=C2APAI*(1.0+(0.50)*H2)
      PRINT 2,CPA
30     DO 35 J=1,3
D      CP=C2APAI*(1.0+(0.25)*H2)+(0.25)*DEL*DER(CPA,C2APAI,T)
      PRINT 2,CP
D      CPA=CP
35     CONTINUE
40     PRINT 41
41     FORMAT(21H START OF RUNGE-KUTTA)
      PRINT 42
42     FORMAT(9X3H CP)
      DO 45 I=2,NSLICE
D      D1P=(DER(CP,C2APAI,T))*(DEL)
D      CP1=CP+(D1P/3.0)
D      D2P=(DER(CP1,C2APAI,T))*DEL
D      CP2=CP+D2P-(D1P/3.0)
D      D3P=(DER(CP2,C2APAI,T))*DEL
D      CP3=CP+D3P-D2P+D1P
D      D4P=(DER(CP3,C2APAI,T))*DEL
D      D=(0.125)*(D1P+3.0*D2P+3.0*D3P+D4P)
D      CP=CP+D
      PRINT 2,CP
45     CONTINUE
D      C2APAO=CP
      PR=C2APAI/C2APAO
D      ETA=(DER(C2APAO,C2APAI,T))*(1.0+C2APAO)/(R*R*C2APAO)
      CAPPHI=ETA*R*R/(1.0+C2APAO)
      PHI1=R/SQRT((1.0+C2APAO))
      ETA1=TANH(PHI1)/PHI1
      PRINT 50
```



```
50  FORMAT(1H1,33H FINAL SOLUTION TO TYPE 1 PROBLEM)
    PRINT 55
55  FORMAT(1H0,5H DATA)
    PRINT 60
60  FORMAT(12X2H R,11X7H K2APAI,16X2H N)
    PRINT 1,R,C2APAI,NSLICE
    PRINT 65
65  FORMAT(1H0,8H ANSWERS)
    PRINT 70
70  FORMAT(7X7H K2APAO,10X8H PAI/PAO,14X4H ETA,
210X8H CAP PHI)
    PRINT 2,C2APAO,PR,ETA,CAPPHI
    ETAAP=(DEF(C2APAO,0.00,T))*(1.0+C2APAO)/(R*R*C2APAO)
    PRINT 75
75  FORMAT(9X5H PHI1,13X5H ETA1,11X7H ETA AP)
    PRINT 2,PHI1,ETA1,ETAAP
    GO TO 10
999  CALL EXIT
     END(1,0,0,0,0,0,0,0,0,0,0,0,0,0,0,0)
```

## 2. EFFECTIVENESS FACTORS FOR TYPE II RATE EQUATIONS

EXPLANATION OF INPUT DATA (DATA IS READ IN MAIN PROGRAM)  
NSLICE=NUMBER OF GRID DIVISIONS  
M - IF M IS +, D,DER2,ALPHA AND KP WILL BE PRINTED OUT  
EACH TIME THEY ARE CALCULATED IN DER2 AND PRESS  
R2=PHI SUB M2  
CX=IKI\*CHI  
CPS=DESIRED VALUE OF KPA,S  
CPO1,CPO2=VALUES OF KPA,O THAT BRACKET THE ACTUAL  
VALUE - THE INPUT ORDER IS IMMATERIAL

```
C   DERIVATIVE FUNCTION FOR TYPE 2
      FUNCTION DER2(CP,CPO,CX,R,M)
1   FORMAT(18X,4E18.8)
2   FORMAT(18X,3E18.8)
3   FORMAT(4E18.8)
      IF(M)60,60,10
10  PRINT 15
15  FORMAT(17X16H DERIVATIVE DATA)
      PRINT 25
25  FORMAT(29X3H KP,14X4H KPO,15X3H KX,15X3H R2)
      PRINT 1,CP,CPO,CX,R
D   60  T=SQRTF(2.00)*R
D       ALPHA=(ABSF(CP))/CP
D       A=1.00+CPO
D       B=1.00+CP
D       C=ALPHA-CX
D       F=(ALPHA+(C/(A*B)))*(CP-CPO)
D       V=(CP-CPO)/A
      IF((ABSF(V)-0.010))61,65,65
D   61  G=- (ALPHA+C)*V*(1.00-(V/2.00)+((V*V)/3.00)-(((V*V)*V)/
      24.00)+(V*V)*(V*V)*((1.00/5.00)-(V/6.00))+ (V*V)*(V*V)*
      3(V*V)*((1.00/7.00)-(V/8.00)))
      GO TO 70
D   65  G=- (ALPHA+C)*LOGF((1.00+V))
D   70  D=F+G
      IF(D)600,75,75
      75  IF(CP)80,700,90
D   80  DER2=-T*SQRTF(D)
      GO TO 100
D   90  DER2=T*SQRTF(D)
100  IF(M)150,110,110
110  PRINT 115
115  FORMAT(17X18H DERIVATIVE VALUES/30X2H D,13X5H DER2,
      212X6H ALPHA)
      PRINT 2,D,DER2,ALPHA
D   150 RETURN
600  PRINT 605
605  FORMAT(1H0,22H SQUARE ROOT IMAGINARY)
      GO TO 900
700  PRINT 705
705  FORMAT(1H0,14H KP EQUAL ZERO)
      GO TO 900
900  PRINT 905
```

```
C      FUNCTION FOR CALCULATING KPA,S
      FUNCTION PRESS(CPO,CX,R,N,M)
      1  FORMAT(36X,E18.8)
      2  FORMAT(4E18.8)
      PRINT 1,CPO
D      DEL=1.00/FLOATF(N)
D      ALPHA=(ABSF(CPO))/CPO
D      H=DEL*DEL*R*R*(ALPHA*CPO+CX)/((1.00+CPO)*(1.00+CPO))
D      CPA=CPO*(1.00+(H/2.00))
      IF(M)100,100,10
      10 PRINT 15
      15 FORMAT(10X4H DEL,16X2H H,12X6H ALPHA)
      PRINT 2,DEL,H,ALPHA
      PRINT 20
      20 FORMAT(1H ,10H ITERATION)
      PRINT 25
      25 FORMAT(11X3H KP)
      PRINT 2,CPA
      100 DO 150 I=1,3
D      CP=CPO*(1.00+(H/4.00))+(DEL/4.00)*DER2(CPA,CPO,CX,R,M)
      IF((CP+1.00))500,500,101
      101 IF(M)120,120,105
      105 PRINT 2,CP
D      120 CPA=CP
      150 CONTINUE
      IF(M)170,170,151
      151 PRINT 155
      155 FORMAT(1H ,12H RUNGE-KUTTA/10X3H KP)
      170 DO 200 J=2,N
D      D1P=DEL*DER2(CP,CPO,CX,R,M)
D      CP1=CP+(D1P/3.00)
      IF((CP1+1.00))500,500,171
D      171 D2P=DEL*DER2(CP1,CPO,CX,R,M)
D      CP2=CP+D2P-(D1P/3.00)
      IF((CP2+1.00))500,500,172
D      172 D3P=DEL*DER2(CP2,CPO,CX,R,M)
D      CP3=CP+D3P-D2P+D1P
      IF((CP3+1.00))500,500,173
D      173 D4P=DEL*DER2(CP3,CPO,CX,R,M)
D      D=(0.1250)*(D1P+3.00*(D2P+D3P)+D4P)
D      CP=CP+D
      IF((CP+1.00))500,500,175
      175 IF(M)200,200,180
      180 PRINT 2,CP
      200 CONTINUE
D      PRESS=CP
      GO TO 600
D      500 PRESS=0.0000
D      600 RETURN
      END
```



```
905 FORMAT(19H PROGRAM TERMINATED/16H DERIVATIVE DATA/  
211X3H KP,14X4H KPO,15X3H KX,15X3H R2)  
PRINT 3,CP,CPO,CX,P  
CALL EXIT  
END
```

```
C     MAIN PROGRAM - INTERPOLATION ROUTINE
C     INTERPOLATION PROBLEM
1     FORMAT(4I18)
2     FORMAT(4E18.8)
D     DIMENSION R2(1),CX(1),CPO1(1),CPO2(1),CPS(1)
10    PRINT 11
11    FORMAT(1H1,21H START OF NEW PROBLEM)
     READ 1,NSLICE,M
     IF(NSLICE)900,900,20
20    READ 2,R2,CX,CPS
     READ 2,CPO1,CPO2
     R2(2)=0.000
     CX(2)=0.000
     CPO1(2)=0.000
     CPO2(2)=0.000
     CPS(2)=0.0000
     PRINT 30
30    FORMAT(16X2H N,16X2H M)
     PRINT 1,NSLICE,M
     PRINT 35
35    FORMAT(11X3H R2,15X3H KX,14X4H KPS)
     PRINT 2,R2,CX,CPS
     PRINT 40
40    FORMAT(1H0,27H INSIDE PRESSURE ITERATIONS/8X6H ABOVE,
21X6H BELOW,11X7H TRIALS)
C     CALCULATION OF CONSTANTS
D     ALPHA=(ARSF(CPS)/CPS)
D     G=((1.00+CPS)**2.00)/((R2**2.00)*CPS*(ALPHA*CPS+CX))
D     P=((ALPHA*CPS+CX)*R2*R2)/((1.00+CPS)*(1.00+CPS))
D     A=PRESS(CPO1,CX,R2,NSLICE,M)
D     B=PRESS(CPO2,CX,R2,NSLICE,M)
     IF((ARSF(A-0.0001)))500,500,45
45    IF((ARSF(B-0.0001)))500,500,50
C     START OF ITERATION
50    IF((A-CPS))70,580,55
D     T=(A-CPS)
D     55 ABOVE=CPO1
     IF((CPS-B))800,585,60
D     60 BELOW=CPO2
D     S=(B-CPS)
     GO TO 90
D     70 BELOW=CPO1
D     S=(A-CPS)
     IF((CPS-B))80,585,800
D     80 ABOVE=CPO2
D     T=(B-CPS)
     GO TO 90
90    PRINT 2,ABOVE,BELOW
C     START OF REGULA-FALSI
D 100 CP=BELOW+(((ABOVE-BELOW)*S)/(S-T))
D     C=PRESS(CP,CX,R2,NSLICE,M)
     IF((ARSF(C-0.0001)))500,500,105
```

```

105 IF((CPS-C))200,590,110
D 110 BELOW=CP
D     S=(C-CPS)
D     CPS2=C
D     T1=(0.750)*T
D 120 CP=BELOW+(((ABOVE-BELOW)*S)/(S-T1))
D     C=PRESS(CP,CX,R2,NSLICE,M)
D     IF((ABS(C-0.0001)))500,500,125
125 IF((C-CPS))130,590,140
D 130 T1=(T1/2.00)
D     GO TO 120
D 140 ABOVE=CP
D     T=(C-CPS)
D     CPS1=C
D     GO TO 295
D 200 ABOVE=CP
D     T=(C-CPS)
D     S1=(0.750)*S
D     CPS1=C
D 210 CP=BELOW+(((ABOVE-BELOW)*S1)/(S1-T))
D     C=PRESS(CP,CX,R2,NSLICE,M)
D     IF((ABS(C-0.0001)))500,500,215
215 IF((C-CPS))230,590,220
D 220 S1=(S1/2.00)
D     GO TO 210
D 230 BELOW=CP
D     S=(C-CPS)
D     CPS2=C
D     GO TO 295
295 PRINT 2,ABOVE,BELOW
C     CALCULATE PARAMETERS
D     F2=DER2(CPS2,BELOW,CX,R2,M)
D     F1=DER2(CPS1,ABOVE,CX,R2,M)
D     ETA1=F1*(1.00+CPS1)*(1.00+CPS1)/(R2*R2*CPS1*(ALPHA*
2     CPS1+CX))
D     ETA2=F2*(1.00+CPS2)*(1.00+CPS2)/(R2*R2*CPS2*(ALPHA*
2     CPS2+CX))
D     Q=(((ABS(ETA1-ETA2)))*2.00)/(ETA1+ETA2)
D     IF((Q-0.01))320,320,300
D 300 T=(CPS1-CPS)
D     S=(CPS2-CPS)
D     GO TO 100
D 320 PR1=BELOW/CPS2
D     PR2=ABOVE/CPS1
D     W=(((ABS(PR1-PR2)))*(2.00))/(PR1+PR2)
D     IF((W-0.01))330,330,100
C     FINAL SOLUTION
D 330 ETA=ETA2+(((ETA1-ETA2)*(CPS-CPS2))/(CPS1-CPS2))
D     PR=PR2+(((PR1-PR2)*(CPS-CPS2))/(CPS1-CPS2))
D 335 PHI=ETA*P
D     ETAAP=(DER2(CPS,0.000,CX,R2,M))*G
D     PCT=(ETAAP-ETA)*100.0/ETA
D     PRINT 340

```



```
340 FORMAT(1H1,33H FINAL SOLUTION TO TYPE 2 PROBLEM)
    PRINT 345
345 FORMAT(1H ,5H DATA/11X3H R2,15X3H KX,14X4H KPS)
    PRINT 2,R2,CX,CPS
    PRINT 350
350 FORMAT(1H0,19H CALCULATED RESULTS/10X4H ETA,15X3H PR,
210X8H CAP PHI,6X12H PCT DEL ETA)
    PRINT 2,ETA,PR,PHI,PCT
    GO TO 10
500 PRINT 505
505 FORMAT(1H0,37H KP LESS THAN -1,PROBLEM DISCONTINUED)
    GO TO 10
D 580 CPO=CP01
    GO TO 600
D 585 CPO=CP02
    GO TO 600
D 590 CPO=CP
600 PRINT 605
605 FORMAT(1H0,20H KPS HIT ON THE NOSE)
D     ETA=G*DER2(CPS,CPO,CX,R2,M)
D     PR=CPO/CPS
    GO TO 335
800 PRINT 805
805 FORMAT(1H0,38HKPS NOT BRACKETED-PROBLEM DISCONTINUED)
    GO TO 10
900 PRINT 905
905 FORMAT(1H0,28H N NEGATIVE - RUN TERMINATED)
    CALL EXIT
    END
```

### 3. REDUCTION OF EXPERIMENTAL KINETIC DATA

#### EXPLANATION OF INPUT DATA

N=RUN NUMBER  
M=DIAMETER OF CATALYST IN 1/8THS OF AN INCH  
IP=REACTOR PRESSURE, MM.HG.  
IPA=ATMOSPHERIC PRESSURE, MM.HG.  
T=PEACTOR TEMPERATURE, DEG.C.  
FT=THIOPHENE FEED RATE, GR.MOLES/MIN.  
FH=HYDROGEN FEED RATE, GR.MOLES/MIN.  
RT=ROOM TEMPERATURE, DEG.F.  
FS=HYDROGEN SULFIDE FEED RATE, GR.MOLES/MIN.  
F1BF=1-BUTENE FEED RATE, GR.MOLES/MIN.  
A1=SCALED AREA OF HYDROGEN SULFIDE PEAK, SQ.IN.  
A2=SCALED AREA OF BUTANE + 1-BUTENE PEAK, SQ.IN.  
A3=SCALED AREA OF 2-BUTENE PEAK, SQ.IN.

C PROGRAM FOR DATA REDUCTION  
1 FORMAT(1H1,29HDATA ANALYSIS FOR RUN NUMBER I3/  
24X22H ATMOSPHERIC PRESSURE=I3,5X18H ROOM TEMPERATURE=  
3F4.1//18H PROCESS VARIABLES)  
3 FORMAT(1H ,5X20HAVERAGE TEMPERATURE=F5.1,10H DEGREES C/  
25X18H REACTOR PRESSURE=I3,7H MM.HG./  
35X13H PELLET SIZE=F5.3,8H IN.DIA.)  
6 FORMAT(1H ,5X15HTHIOPHENE FLOW=E10.4,11H MOLES/MIN./  
25X15H HYDROGEN FLOW=E11.5,11H MOLES/MIN./  
35X23H HYDROGEN SULFIDE FLOW=E10.4,11H MOLES/MIN./  
45X15H 1-BUTENE FLOW=E10.4,11H MOLES/MIN.)  
7 FORMAT(1H ,5X11HTOTAL FLOW=F11.5,11H MOLES/MIN./  
25X20H HYDROGEN/THIOPHENE=F5.1)  
10 FORMAT(1H0,24HPRODUCT COMPOSITION DATA/  
25X18H SCALED PEAK AREAS/20X10H COMPONENT,  
34X21H SCALED AREA (SQ.IN.))  
13 FORMAT(1H ,13X16HHYDROGEN SULFIDE,8XF7.3/  
214X16H BUTANE+1-BUTENE,8XF7.3/  
321X9H 2-BUTENE,8XF7.3)  
16 FORMAT(1H0,12HCALCULATIONS//23H RATES AND COMPOSITIONS)  
18 FORMAT(1H ,5X27H REACTION PRODUCTS CLOSURE=F5.1,4H PCT/  
26X24H SULFUR BALANCE CLOSURE=F5.1,4H PCT/  
36X12H PURGE RATE=E18.8,11H MOLES/MIN.)  
19 FORMAT(1H ,5X34H THIOPHENE VAPOR PRESSURE EXCEEDED/  
210X16H VAPOR PRESSURE=F5.1,7H MM.HG.)  
20 FORMAT(1H0,5X33H AVERAGE PARTIAL PRESSURES,MM.HG./  
26X6H C4H4S,9X3H H2,8X4H H2S,5X7H 1-C4H8,  
35X7H 2-C4H8,7X5H C4H8,6X6H C4H10)  
22 FORMAT(1H0,5X23H AVERAGE MOLE FRACTIONS/  
26X6H C4H4S,9X3H H2,8X4H H2S,5X7H 1-C4H8,  
35X7H 2-C4H8,6X6H C4H10)  
23 FORMAT(1H0,16H PCT. CONVERSION,10X8H RATE(A),  
210X8H RATE(C),2X16H RATE(A)/GR.CAT.,  
32X16H RATE(C)/GR.CAT.)  
24 FORMAT(1H0,20H PLOTTING PARAMETERS//8X10H RATE(B/A),  
28X10H RATE(C/A),13X5H FT/P,12X6H PB/PA)  
26 FORMAT(1H0,12X6H PB/PC,10X8H PT/R(A),8X10H PTPH/R(A),  
27X11H SQRT(TH/R),4X14H SQRT(BH/R(C)))

```
27 FORMAT(1H ,5X27H AREA(1-C4H8)/AREA(2-C4H8)=F5.3)
28 FORMAT(1H0,10H CAP. PHI=F8.5)
30 FORMAT(4I18)
31 FORMAT(5E18.8)
32 FORMAT(7F12.4)
33 FORMAT(6F12.6)
40 READ 30,N,M,IP,IPA
   IF(N)900,900,45
45 DIA=FLOATE(M)/(8.00)
   READ 31,T,FT,FH,RT
   READ 31,FS,F1BE
   READ 31,A1,A2,A3
   FTOT=FT+FH+FS+F1BE
   RATIO=FH/FT
   PRINT 1,N,IPA,RT
   PRINT 3,T,IP,DIA
   PRINT 6,FT,FH,FS,F1BE
   PRINT 7,FTOT,RATIO
   PRINT 10
   PRINT 13,A1,A2,A3
   PA=FLOATE(IPA)
   VSSTP=(5.00)*(492.0/(RT+460.0))*(PA/760.0)
C   COMPUTE EQUILIBRIUM
   TK=273.2+T
   EQ125=EXPF(684.0/(1.987*298.0))
   EQ225=EXPF(-1210.0/(1.987*298.0))
   EQ1T=EQ125*EXPF((-1043.0/1.987)*((1.00/298.0)
2-(1.00/TK)))
   EQ2T=EQ225*EXPF((1642.0/1.987)*((1.00/298.0)-
2(1.00/TK)))
   R12=EQ2T/(1.00+EQ1T)
   AR12=R12*(413.0/395.0)
   A1B=A3*AR12
   AB=A2-A1B
C   CALCULATE RATES AND COMPOSITIONS
   YH2S=(A1/(255.0))/VSSTP
   YB=(AB/(397.0))/VSSTP
   Y1B=(A1B/(413.0))/VSSTP
   Y2B=(A3/(395.0))/VSSTP
   YBE=Y1B+Y2B
   P=(FTOT+2.00*F1BE)/(1.00+2.00*YBE+3.00*YB)
   DELMB=((P*YH2S-FS)-(P*(YB+YBE)-F1BE))*100.0/
2((P*YH2S-FS)+(P*(YB+YBE)-F1BE))
   RATEC=P*(YB+YBE)-F1BE
   RATEFS=P*YH2S-FS
   RATEFA=(0.500)*(RATEC+RATEFS)
   YAH2S=(RATEFA+FS)/P
   RF=(RATEFA+F1BE)/(RATEC+F1BE)
   YAB=YB*RF
   YA1B=Y1B*RF
   YA2B=Y2B*RF
   YABE=YA1B+YA2B
   PR=FLOATE(IP)
```



```
PH2S=PR*YAH2S
PR=PR*YAB
P1B=PR*YA1B
P2B=PR*YA2B
PBE=PR*YABF
SY=YAH2S+YAB+YA1B+YA2B
YH1=((FH+3.00*F1BE)/P)-3.00*YABE-4.00*YAB
YT1=1.00-YH1-SY
SBC=((P*(YT1+YAH2S)-FT-FS)*100.0)/(FT+FS)
YTA=(FT-RATEA)/P
YHA=1.0000-YTA-SY
PH=PR*YHA
PT=PR*YTA
PCTCON=RATEA*(100.00)/FT
RATC=P*YAB
RATEAG=RATEA/8.1567
RATECG=RATC/8.1567
C PRINT OUT RATES AND COMPOSITIONS
PRINT 16
PRINT 18,DELMB,SBC,P
PRINT 27,AR12
PRINT 20
PRINT 32,PT,PH,PH2S,P1B,P2B,PBE,PB
PRINT 22
PRINT 33,YTA,YHA,YAH2S,YA1B,YA2B,YAB
PRINT 23
PRINT 31,PCTCON,RATEA,RATC,RATEAG,RATECG
C CALCULATE PLOTTING PARAMETERS
RATBA=(P*YABE-F1BE)/RATEA
RATCA=RATC/RATEA
FTP=FT/P
PBPA=PBE/PT
PBPC=PBE/PB
PTRAT=PT/RATEA
THR=PTRAT*PH
SRTHR=SQRTF(THR)
SRBHC=SQRTF(PBE*PH/RATC)
ELSQ=0.004791
DE=0.0181
CAS=(PT/760.0)/(82.06*TK)
ORR=RATEA/(6.97*60.0)
CAPPHI=(ELSQ*ORR)/(DE*CAS)
C PRINT OUT PLOTTING PARAMETERS
PRINT 24
PRINT 31,RATBA,RATCA,FTP,PBPA
PRINT 26
PRINT 31,PBPC,PTRAT,THR,SRTHR,SRBHC
PRINT 28,CAPPHI
PRINT 100
100 FORMAT(1H0,35H THEORETICAL THIOPHENE RATE USED TO ,
232H CALCULATE RATES AND COMPOSITIONS/14H D(EFF)=0.0181/
326H INFINITE CYLINDER ASSUMED/
424H ARIS APPROXIMATION USED/22H GRAMS CATALYST=8.1567)
```

```
C      CHECK THIOPHENE VAPOR PRESSURE
      VPT=(10.00)*EXPF(4314.834*(0.003832886-(1.00/(273.2+
      2*((RT-32.0)/1.80))))))
      IF((PT-VPT))40,300,300
300 PRINT 19,VPT
      GO TO 40
900 PRINT 905
905 FORMAT(1H1,37H RUN NUMBER NEGATIVE,RUN DISCONTINUED)
      CALL EXIT
      END
```

4. CALCULATION OF CONSTANTS IN PRELIMINARY RATE EQUATION

EXPLANATION OF INPUT DATA

NORS=NUMBER OF DATA POINTS  
TEMP=REACTOR TEMPERATURE  
PT=THIOPHENE PARTIAL PRESSURE, MM.HG.  
PH=HYDROGEN PARTIAL PRESSURE, MM.HG.  
PS=HYDROGEN SULFIDE PARTIAL PRESSURE, MM.HG.  
R=REACTION RATE, GR.MOLES/GR.CAT.,MIN.  
NRUN=RUN NUMBER  
NPOWT=EXPONENT ON PT IN NUMERATOR OF RATE EQUATION  
NPOWH=EXPONENT ON PH IN NUMERATOR OF RATE EQUATION  
NPOWD=EXPONENT ON DENOMINATOR OF RATE EQUATION

C MULTIPLE LINEAR REGRESSION FOR THREE CONSTANTS

```
1 FORMAT(I5,F10.1)
2 FORMAT(6F12.2)
3 FORMAT(1H1,25H START OF NEW CALCULATION//
  25X21H REACTOR TEMPERATURE=F5.1,7H DEG.C./
  35X32H RATE EQUATION TESTED- R=K*(PT**I1,
  47H)*(PH**I1,21H)/(1.0+KT*PT+KS*PS)**I1)
4 FORMAT(1H0,4X38H INPUT DATA AND CALCULATED VALUES OF M
  2//8X2H I,1X4H RUN,5X3H PT,6X3H PH,8X3H PS,8X5H RATE,
  39X2H M/(I10,I5,3F10.3,2E12.4))
5 FORMAT(1H0,4X15H AVERAGE VALUES//6X3H PT,7X3H PS,
  24X6H PT**2,4X6H PS**2,4X6H PT*PS,7X2H M,9X5H M*PT,
  37X5H M*PS,10X2H R/5F10.3,4E12.4)
6 FORMAT(1H0,4X30H LINEAR LEAST-SQUARE ESTIMATES//
  27X3H A=F10.4,3X3H B=E10.4,3X3H C=E10.4/7X3H K=E10.4,
  329H GR.MOLES/GR.CAT.,-MIN.,-ATM.**I1/
  47X4H KT=E10.4,7H MM.HG./7X4H KS=E10.4,7H MM.HG.)
7 FORMAT(6F12.4)
8 FORMAT(1H0,4X39HRATES,DEVIATIONS,STATISTICAL PARAMETERS
  2//8X2H I,1X4H RUN,8X12H RATE(CALC.),9X11H RATE(EXP.),
  311X9H PCT.FRR./(I10,I5,2E20.4,F20.4))
9 FORMAT(1H0,4X35H SUM OF SQUARES OF RATE DEVIATIONS=E10.4/
  25X39H ESTIMATE OF POPULATION VARIANCE=SP**2=E10.4/
  35X28H VARIANCE OF ESTIMATE=SE**2=E10.4/5X3H F=F10.4/
  410X43H DEGREES OF FREEDOM FOR LESSER MEAN SQUARE=I2/
  510X44H DEGREES OF FREEDOM FOR GREATER MEAN SQUARE=I2)
10 FORMAT(7I10)
    DIMENSION R(10),PT(10),PS(10),PH(10),V(10),RC(10),
    2D(10),FRR(10),NRUN(10)
    TOLD=0.00
    NOLD=0
15 READ 1,NORS,TEMP
    IF(NORS)900,900,20
20 IF((NORS-NOLD))30,25,30
25 IF((ABSF(TEMP-TOLD)-0.0001))40,30,30
30 READ 2,(PH(I),I=1,NORS)
    READ 2,(PT(I),I=1,NORS)
    READ 2,(PS(I),I=1,NORS)
    READ 7,(R(I),I=1,NORS)
    READ 10,(NRUN(I),I=1,NORS)
40 READ 10,NPOWT,NPOWH,NPOWD
```



```
DO 50 I=1,NOBS
  V(I)=(((PT(I)**NPOWT)*(PH(I)**NPOWH))/R(I))**
2(1.0/FLOAT(NPOWD))
50 CONTINUE
C CALCULATE AVERAGE VALUES
  FN=1.0/FLOAT(NOBS)
  VAVG=0.00
  PSAVG=0.00
  VPSAVG=0.00
  PTAVG=0.00
  PTPSAV=0.00
  VPTAVG=0.00
  PS2AVG=0.00
  PT2AVG=0.00
  RAVG=0.00
  DO 100 I=1,NOBS
    PSAVG=PSAVG+(PS(I)*FN)
    PTAVG=PTAVG+(PT(I)*FN)
    VAVG=VAVG+(V(I)*FN)
    PS2AVG=PS2AVG+(PS(I)*PS(I)*FN)
    PT2AVG=PT2AVG+(PT(I)*PT(I)*FN)
    RAVG=RAVG+(R(I)*FN)
    VPTAVG=VPTAVG+(V(I)*PT(I)*FN)
    VPSAVG=VPSAVG+(V(I)*PS(I)*FN)
    PTPSAV=PTPSAV+(PT(I)*PS(I)*FN)
100 CONTINUE
C CALCULATE LINEAR LEAST-SQUARE PARAMETERS
  T1=(VAVG*PSAVG-VPSAVG)/(PTAVG*PSAVG-PTPSAV)
  T2=(VAVG*PTAVG-VPTAVG)/(PTAVG*PTAVG-PT2AVG)
  T3=(PSAVG*PSAVG-PS2AVG)/(PTAVG*PSAVG-PTPSAV)
  T4=(PTAVG*PSAVG-PTPSAV)/(PTAVG*PTAVG-PT2AVG)
  C=(T1-T2)/(T3-T4)
  R=T2-C*T4
  A=VAVG-C*PSAVG-R*PTAVG
C CHECK PARAMETERS
  F1=VPTAVG-A*PTAVG-R*PT2AVG-C*PTPSAV
150  IF((ABS(F1/VPTAVG))-0.0001)150,500,500
  F2=VPSAVG-A*PSAVG-R*PTPSAV-C*PS2AVG
  IF((ABS(F2/VPSAVG))-0.0001)200,500,500
C CALCULATE KINETIC CONSTANTS
200  CT=R/A
     CS=C/A
     CRATE=(1.0/A)**NPOWD
     J=NPOWT+NPOWH
C OUTPUT ORIGINAL DATA, AVERAGES, LEAST-SQUARE ESTIMATES
  PRINT 3,TEMP,NPOWT,NPOWH,NPOWD
  PRINT 4,(I,NRUN(I),PT(I),PH(I),PS(I),R(I),V(I),I=1,NOBS)
  PRINT 5,PTAVG,PSAVG,PT2AVG,PS2AVG,PTPSAV,VAVG,VPTAVG,
2  VPSAVG,RAVG
  PRINT 6,A,B,C,CRATE,J,CT,CS
C CALCULATE RATES, DEVIATIONS AND STATISTICAL PARAMETERS
  SSQ=0.00
  SP2=0.00
```

```
DO 250 I=1,NOBS
  RC(I)=(CRATF*(PT(I)**NPOWT)*(PH(I)**NPOWH))/((1.00+
2CT*PT(I)+CS*PS(I))**NPOWD)
  D(I)=RC(I)-R(I)
  SSQ=SSQ+D(I)*D(I)
  FRR(I)=(D(I)*100.0)/R(I)
  SP2=SP2+(((R(I)-RAVG)**2.0)/FLOATF(NOBS-1))
250 CONTINUE
  SF2=SSQ/FLOATF(NOBS-3)
  F=SP2/SF2
  LFREE1=NOBS-3
  LFREE2=NOBS-1
C   OUTPUT RATES, DEVIATIONS AND STATISTICAL PARAMETERS
  PRINT 8,(I,NRUN(I),RC(I),R(I),FRR(I),I=1,NOBS)
  PRINT 9,SSQ,SP2,SE2,F,LFREE1,LFREE2
  NOLD=NOBS
  TOLD=TEMP
  GO TO 15
500 PRINT 510
510 FORMAT(1H0,33H ORIGINAL EQUATIONS NOT SATISFIED/
219H PROGRAM TERMINATED)
  PRINT 7,A,B,C
  GO TO 1000
900 PRINT 910
910 FORMAT(1H1,31H N NEGATIVE, PROGRAM TERMINATED)
1000 CALL EXIT
      END
```

### 5. CALCULATION OF CONSTANTS IN FINAL RATE EQUATION

#### EXPLANATION OF INPUT DATA

NORS=NUMBER OF DATA POINTS  
NRUN=RUN NUMBER  
T=REACTOR TEMPERATURE, DEG.K.  
PT=THIOPHENE PARTIAL PRESSURE, MM.HG.  
PH=HYDROGEN PARTIAL PRESSURE, MM.HG.  
PS=HYDROGEN SULFIDE PARTIAL PRESSURE, MM.HG.  
RATE=REACTION RATE, GR.MOLES/GR.CAT.,MIN.  
NPOWT=EXPONENT ON PT IN NUMERATOR OF RATE EQUATION  
NPOWH=EXPONENT ON PH IN NUMERATOR OF RATE EQUATION  
NPOWD=EXPONENT ON DENOMINATOR OF RATE EQUATION  
NITER=NUMBER OF ITERATIONS TO BE MADE  
E=INITIAL ESTIMATE OF E \*  
ET=INITIAL ESTIMATE OF ET \*  
ES=INITIAL ESTIMATE OF ES \*  
AK=INITIAL ESTIMATE OF AK \*  
AT=INITIAL ESTIMATE OF AT \*  
AS=INITIAL ESTIMATE OF AS \*

\* FOR FURTHER EXPLANATION, SEE STATEMENT 1 BELOW

```
C ITERATIVE MULTIPLE LINEAR REGRESSION FOR SIX CONSTANTS
1  FORMAT(1H1,36H START OF CALCULATIONS FOR NEW MODEL//
22X42H RATE EQUATION TESTED-  $R=AK*EXP(E/T)*(PT**I1,$ 
37H) $*(PH**I1,41H)/(1.0+AT*EXP(ET/T)*PT+AS*EXP(ES/T)*PS)$ 
4**I1)
2  FORMAT(1H0,11H INPUT DATA/8X2H I,1X4H RUN,5X3H PT,
26X3H PH,8X3H PS,6X5H TFMP,7X5H RATE/
3(I10,I5,4F10.3,E12.4))
3  FORMAT(1H0,37H ESTIMATES OF KINETIC CONSTANTS AFTER,
218H ITERATION NUMBER I2/5X3H AK=E12.4,5X3H E=F10.3/
34X4H AT=E12.4,4X4H ET=F10.3/4X4H AS=E12.4,4X4H ES=F10.3)
4  FORMAT(1H0,21H RATES AND DEVIATIONS/8X2H I,1X4H RUN,
28X12H RATE(CALC.),9X11H RATE(EXP.),11X9H PCT.ERR./
3(I10,I5,2E20.4,F20.4))
5  FORMAT(1H0,30H SUM OF SQUARES OF DEVIATIONS=E12.4)
6  FORMAT(1H0,21H ITERATIONS COMPLETED/
21X39H VALUES ABOVE REPRESENT FINAL ESTIMATES)
7  FORMAT(1H1,27H START OF ITERATION NUMBER I2)
8  FORMAT(1H0,5X8H K(251)=E12.4,5X9H KT(251)=E12.4,
25X9H KS(251)=F12.4)
10  FORMAT(7I10)
11  FORMAT(7F10.3)
12  FORMAT(6F12.4)
    T0=524.2
    DIMENSION NRUN(25),T(25),PT(25),PH(25),PS(25),
2RATE(25),V(25),RC(25),PCT(25)
    READ 10,NORS
    READ 10,(NRUN(I),I=1,NORS)
    READ 11,(T(I),I=1,NORS)
    READ 11,(PT(I),I=1,NORS)
    READ 11,(PH(I),I=1,NORS)
    READ 11,(PS(I),I=1,NORS)
```



```
READ 12,(RATE(I),I=1,NOBS)
50 READ 10,NPOWT,NPOWH,NPOWD,NITER
   IF(NPOWT)9000,60,60
60 D=(1.00/FLOAT(NPOWD))
   NI=0
   DO 100 I=1,NOBS
100 V(I)=(((PT(I)**NPOWT)*(PH(I)**NPOWH))/RATE(I))**D
   CONTINUE
   READ 12,F,FT,FS,AK,AT,AS
   PRINT 1,NPOWT,NPOWH,NPOWD
C   PRINT OUT INPUT DATA
   PRINT 2,(I,NRUN(I),PT(I),PH(I),PS(I),T(I),RATE(I),
2 I=1,NOBS)
400 GO TO 2000
   PRINT 7,NI
   XBAR=0.00
   YBAR=0.00
   ZBAR=0.00
   WBAR=0.00
   UBAR=0.00
   VBAR=0.00
   XZBAR=0.00
   YZBAR=0.00
   ZZBAR=0.00
   WZBAR=0.00
   UZBAR=0.00
   VXBAR=0.00
   VYBAR=0.00
   VZBAR=0.00
   VWBAR=0.00
   VUBAR=0.00
   XYBAR=0.00
   XZBAR=0.00
   XWBAR=0.00
   XUBAR=0.00
   YZBAR=0.00
   YWBAR=0.00
   YURAR=0.00
   ZWBAR=0.00
   ZURAR=0.00
   WURAR=0.00
   EN=FLOAT(NOBS)
   DO 450 I=1,NOBS
   DFL=T0-T(I)
   TSQ=T(I)*T0
   R=DFL/TSQ
   X1=-D*F*R
   X2=(FT-D*F)*R
   X3=(FS-F*D)*R
   RPAK1=1.00+(X1/2.00)+(X1**2/6.00)+(X1**3/24.00)+
2 (X1**4/120.00)+(X1**5/720.00)
   RPAK2=1.00+(X2/2.00)+(X2**2/6.00)+(X2**3/24.00)+
2 (X2**4/120.00)+(X2**5/720.00)
```

BRAK3=1.00+(X3/2.00)+(X3\*\*2/6.00)+(X3\*\*3/24.00)+  
2(X3\*\*4/120.00)+(X3\*\*5/720.00)

X=R\*BRAK1  
Y=PT(I)  
Z=PT(I)\*R\*BRAK2  
W=PS(I)  
U=PS(I)\*R\*BRAK3  
XRAR=XBAR+X/FN  
YBAR=YBAR+Y/FN  
ZBAR=ZBAR+Z/FN  
WBAR=WBAR+W/FN  
URAR=URAR+U/FN  
VRAR=VRAR+V(I)/FN  
X2BAR=X2BAR+X\*X/FN  
Y2BAR=Y2BAR+Y\*Y/FN  
Z2BAR=Z2BAR+Z\*Z/FN  
W2BAR=W2BAR+W\*W/FN  
U2BAR=U2BAR+U\*U/FN  
XYBAR=XYBAR+X\*Y/FN  
XZBAR=XZBAR+X\*Z/FN  
XWBAR=XWBAR+X\*W/FN  
XUBAR=XUBAR+X\*U/FN  
YZBAR=YZBAR+Y\*Z/FN  
YWBAR=YWBAR+Y\*W/FN  
YUBAR=YUBAR+Y\*U/FN  
ZWBAR=ZWBAR+Z\*W/FN  
ZURAR=ZURAR+Z\*U/FN  
WUBAR=WUBAR+W\*U/FN  
VXRAR=VXRAR+V(I)\*X/FN  
VYBAR=VYBAR+V(I)\*Y/FN  
VZBAR=VZBAR+V(I)\*Z/FN  
VWRAR=VWRAR+V(I)\*W/FN  
VURAR=VURAR+V(I)\*U/FN

450 CONTINUE

XX1=X2BAR-XBAR\*XBAR  
VX1=VXRAR-VBAR\*XBAR  
XY1=XYBAR-XBAR\*YBAR  
XZ1=XZBAR-XBAR\*ZBAR  
XW1=XWBAR-XBAR\*WBAR  
XU1=XUBAR-XBAR\*UBAR  
YY1=Y2BAR-YBAR\*YBAR  
YZ1=YZBAR-YBAR\*ZBAR  
YW1=YWBAR-YBAR\*WBAR  
YU1=YUBAR-YBAR\*UBAR  
VY1=VYBAR-VBAR\*YBAR  
ZZ1=Z2BAR-ZBAR\*ZBAR  
ZW1=ZWBAR-ZBAR\*WBAR  
ZU1=ZURAR-ZBAR\*UBAR  
VZ1=VZBAR-VBAR\*ZBAR  
WW1=W2BAR-WBAR\*WBAR  
WU1=WUBAR-WBAR\*UBAR  
VW1=VWBAR-VBAR\*WBAR  
UU1=U2BAR-UBAR\*UBAR

VU1=VUBAR-VRAR\*UBAR  
YY2=YY1-(XY1/XX1)\*XY1  
YZ2=YZ1-(XY1/XX1)\*XZ1  
YW2=YW1-(XY1/XX1)\*XW1  
YU2=YU1-(XY1/XX1)\*XU1  
VY2=VY1-(VX1/XX1)\*XY1  
ZZ2=ZZ1-(XZ1/XX1)\*XZ1  
ZW2=ZW1-(XZ1/XX1)\*XW1  
ZU2=ZU1-(XZ1/XX1)\*XU1  
WW2=WW1-(XW1/XX1)\*XW1  
WU2=WU1-(XW1/XX1)\*XU1  
VZ2=VZ1-(VX1/XX1)\*XZ1  
VW2=VW1-(VX1/XX1)\*XW1  
UU2=UU1-(XU1/XX1)\*XU1  
VU2=VU1-(VX1/XX1)\*XU1  
ZZ3=ZZ2-(YZ2/YY2)\*YZ2  
ZW3=ZW2-(YZ2/YY2)\*YW2  
ZU3=ZU2-(YZ2/YY2)\*YU2  
VZ3=VZ2-(VY2/YY2)\*YZ2  
WW3=WW2-(YW2/YY2)\*YW2  
WU3=WU2-(YW2/YY2)\*YU2  
VW3=VW2-(VY2/YY2)\*YW2  
UU3=UU2-(YU2/YY2)\*YU2  
VU3=VU2-(VY2/YY2)\*YU2  
WW4=WW3-(ZW3/ZZ3)\*ZW3  
WU4=WU3-(ZW3/ZZ3)\*ZU3  
VW4=VW3-(VZ3/ZZ3)\*ZW3  
UU4=UU3-(ZU3/ZZ3)\*ZU3  
VU4=VU3-(VZ3/ZZ3)\*ZU3  
UU5=UU4-(WU4/WW4)\*WU4  
VU5=VU4-(VW4/WW4)\*WU4  
FF=VU5/UU5  
T1=((XZ1/XX1)\*XBAR-ZBAR)-((XY1/XX1)\*XBAR-YBAR)\*  
2(YZ2/YY2)  
T2=((XW1/XX1)\*XBAR-WBAR)-((XY1/XX1)\*XBAR-YBAR)\*  
2(YW2/YY2)  
T3=((XU1/XX1)\*XBAR-UBAR)-((XY1/XX1)\*XBAR-YBAR)\*  
2(YU2/YY2)  
T4=((XY1/XX1)\*(YW2/YY2)-(XW1/XX1))-((XY1/XX1)\*(YZ2/  
2YY2)-(XZ1/XX1))\*(ZW3/ZZ3)  
T5=((XY1/XX1)\*(YU2/YY2)-(XU1/XX1))-((XY1/XX1)\*(YZ2/  
2YY2)-(XZ1/XX1))\*(ZU3/ZZ3)  
T6=((YZ2/YY2)\*(ZU3/ZZ3)-(YU2/YY2))-((YZ2/YY2)\*(ZW3/  
2ZZ3)-(YW2/YY2))\*(WU4/WW4)  
FE=(VW4/WW4)-(WU4/WW4)\*FF  
DD=(VZ3/ZZ3)-(ZW3/ZZ3)\*(VW4/WW4)+FF\*((ZW3/ZZ3)\*  
2(WU4/WW4)-(ZU3/ZZ3))  
CC=(VY2/YY2)-(YZ2/YY2)\*(VZ3/ZZ3)+((YZ2/YY2)\*(ZW3/ZZ3)  
2-(YW2/YY2))\*(VW4/WW4)+T6\*FF  
RR=(VX1/XX1)-(XY1/XX1)\*(VY2/YY2)+((XY1/XX1)\*(YZ2/YY2)-  
2(XZ1/XX1))\*(VZ3/ZZ3)+T4\*(VW4/WW4)+FF\*(T5-T4\*(WU4/WW4))  
AA=VRAR-XBAR\*(VX1/XX1)+((XY1/XX1)\*XBAR-YBAR)\*(VY2/YY2)  
2+T1\*(VZ3/ZZ3)+(T2-T1\*(ZW3/ZZ3))\*(VW4/WW4)+FF\*((T3-



```
2T1*(ZU3/ZZ3))- (T2-T1*(ZW3/ZZ3))*(WU4/WW4))
DTE=VYBAR-AA*YBAR-PP*XYBAR-CC*Y2BAR-DD*YZBAR-EE*YWBAR
2-EE*YHBAR
TE((ARSE((DTE/VYBAR))-0.0001))500,8000,8000
500 CO=(1.00/AA)**NPOWD
E=- (PP/AA)/D
CTO=CC/AA
FT=(DD/CC)+D*E
CSO=FF/AA
FS=(FF/FE)+D*E
AK=CO/EXPE((E/T0))
AT=CTO/EXPE((FT/T0))
AS=CSO/EXPE((FS/TC))
2000 PRINT 3,NI,AK,E,AT,FT,AS,ES
PRINT 8,CO,CTO,CSO
SUMD=0.00
3000 DO 3100 I=1,NOBS
RC(I)=AK*EXPE((E/T(I)))*(PT(I)**NPOWT)*(PH(I)**NPOWH)/
2(1.0+AT*EXPE((FT/T(I)))*PT(I)+AS*EXPE((FS/T(I)))*
3PS(I))**NPOWD
DEV=RC(I)-RATE(I)
SUMD=SUMD+DEV*DEV
PCT(I)=DEV*100.0/RATE(I)
3100 CONTINUE
C PRINT RATES AND DEVIATIONS
PRINT 4,(I,MRUN(I),RC(I),RATE(I),PCT(I),I=1,NOBS)
PRINT 5,SUMD
NI=NI+1
IF((NI-NITER))400,400,5000
5000 PRINT 6
GO TO 50
9000 PRINT 9050
9050 FORMAT(1H0,33H ORIGINAL EQUATIONS NOT SATISFIED/
219H PROGRAM TERMINATED)
GO TO 9100
9000 PRINT 9050
9050 FORMAT(1H1,26H N NEGATIVE,RUN TERMINATED)
9100 CALL EXIT
END
```

C. Data

1. Computer Calculations - Type I

$K_{P_{A,s}}$	$\phi_{MI}$	$(P_{A,o}/P_{A,s})$	$\eta$	$\Phi_L$
50.0	9.0	0.2373	0.9717	1.445
	10.0	0.1015	0.9437	1.850
	11.0	0.02891	0.8848	2.099
20.0	5.0	0.4311	0.9668	1.151
	6.0	0.2246	0.9315	1.597
	7.0	0.07823	0.8587	2.004
	8.0	0.02415	0.7634	2.327
10.0	3.0	0.6087	0.9663	0.7906
	4.0	0.3500	0.9206	1.340
	5.0	0.1374	0.8279	1.881
	6.0	0.04486	0.7108	2.326
5.0	2.0	0.6857	0.9555	0.6370
	3.0	0.3739	0.8750	1.312
	4.0	0.1420	0.7390	1.971
	5.0	0.04850	0.6055	2.523
1.0	0.50	0.9389	0.9789	0.1224
	1.0	0.7759	0.9174	0.4587
	2.0	0.3710	0.7092	1.418
	3.0	0.1388	0.5147	2.316
	4.0	0.05026	0.3917*	3.134
-0.30	0.25	0.9576	0.9600	0.08571
	0.50	0.8515	0.8644	0.3087
	1.0	0.5912	0.6500	0.9286
	2.0	0.2366	0.3836	2.192
	3.0	0.08887	0.2619*	3.368
-0.50	0.15	0.9783	0.9715	0.04372
	0.25	0.9431	0.9271	0.1159
	0.50	0.8164	0.7836	0.3918
	1.0	0.5488	0.5416	1.083
	2.0	0.2177	0.3052	2.442
-0.70	0.10	0.9840	0.9655	0.03218
	0.15	0.9658	0.9282	0.06962
	0.25	0.9165	0.8379	0.1766
	0.50	0.7678	0.6302	0.5252
	1.0	0.5034	0.3989	1.330
	2.0	0.1991	0.2178*	2.903

\* -  $\eta$  was computed from Equation (IV-33)

$K_{P_{A,s}}$	$\phi_{MI}$	$(P_{A,o}/P_{A,s})$	$\eta$	$\Phi_L$
-0.90	0.030	0.9956	0.9718	0.008746
	0.050	0.9886	0.9294	0.02324
	0.10	0.9622	0.7993	0.07993
	0.15	0.9301	0.6829	0.1537
	0.25	0.8625	0.5190	0.3244
	0.50	0.7030	0.3195	0.7988
	1.0	0.4552	0.1782	1.782
	2.0	0.1803	0.09305*	3.722
-0.95	0.020	0.9962	0.9524	0.007619
	0.030	0.9920	0.9046	0.01628
	0.050	0.9810	0.8011	0.04006
	0.10	0.9474	0.5966	0.1193
	0.15	0.9118	0.4711	0.2120
	0.25	0.8418	0.3313	0.4141
	0.50	0.6838	0.1911	0.9555
	1.0	0.4424	0.1032	2.064
-0.98	0.0080	0.9985	0.9525	0.003048
	0.010	0.9977	0.9296	0.004648
	0.020	0.9924	0.8026	0.01605
	0.030	0.9859	0.6891	0.03101
	0.050	0.9715	0.5313	0.06641
	0.10	0.9343	0.3384	0.1692
	0.15	0.8947	0.2503	0.2816
	0.25	0.8274	0.1664	0.5200
	0.50	0.6714	0.09156	1.145
	1.0	0.4342	0.04832	2.416

\* -  $\eta$  was computed from Equation (IV-33)



2. Computer Calculations - Type II

<u>E</u>	<u>K<sub>pA,s</sub></u>	<u>φ<sub>MI</sub></u>	<u>(p<sub>A,o</sub>/p<sub>A,s</sub>)</u>	<u>η</u>	<u>Φ<sub>L</sub></u>
0.0	100.0	12.0	0.3149	0.9786	1.381
		15.0	0.05139	0.9094	2.006
		16.0	0.02321	0.8608	2.160
10.0	10.0	2.0	0.8393	0.9780	0.3233
		3.0	0.6547	0.9444	0.7024
		4.0	0.4388	0.8849	1.170
		5.0	0.2529	0.7947	1.642
		6.0	0.1392	0.6918	2.058
		7.0	0.08133	0.6008	2.433
1.0	1.0	0.50	0.9696	0.9795	0.06122
		1.0	0.8871	0.9227	0.2307
		2.0	0.6558	0.7506	0.7506
		3.0	0.4547	0.5843	1.315
		4.0	0.3197	0.4616	1.846
		5.0	0.2329	0.3763	2.352
-0.40	-0.40	6.0	0.1758	0.3160	2.844
		0.20	0.9790	0.9545	0.04242
		0.30	0.9558	0.9063	0.09063
		0.50	0.8963	0.7935	0.2204
		0.70	0.8318	0.6858	0.3734
		1.0	0.7401	0.5559	0.6715
		1.5	0.6134	0.4100	1.025
		2.0	0.5162	0.3217	1.430
		3.0	0.3814	0.2212	2.212
		4.0	0.2943	0.1676	2.980
-0.70	-0.70	0.050	0.9908	0.9600	0.01867
		0.070	0.9827	0.9268	0.03532
		0.10	0.9674	0.8681	0.06752
		0.15	0.9374	0.7663	0.1341
		0.20	0.9054	0.6746	0.2099
		0.30	0.8437	0.5326	0.3728
		0.50	0.7378	0.3652	0.7101
		0.70	0.6535	0.2746	1.047
		1.0	0.5555	0.1987	1.545
		1.5	0.4399	0.1351	2.364
-0.90	-0.90	2.0	0.3596	0.1021	3.173
		0.0090	0.9965	0.9556	0.006966
		0.010	0.9958	0.9461	0.008515
		0.015	0.9912	0.8928	0.01808
		0.020	0.9857	0.8326	0.02997
		0.030	0.9731	0.7219	0.05847
		0.040	0.9600	0.6276	0.09037
0.050	0.9471	0.5529	0.1244		

$E$	$K_{p_{A,s}}$	$\phi_{MIT}$	$(p_{A,o}/p_{A,s})$	$\eta$	$\Phi_L$	
0.0	-0.90	0.10	0.8884	0.3370	0.3033	
		0.20	0.7976	0.1865	0.6714	
		0.30	0.7280	0.1285	1.041	
		0.50	0.6235	0.07886	1.774	
		1.0	0.4594	0.03997	3.597	
0.10	100.0	8.0	0.6444	1.024	0.7061	
		10.0	0.4236	1.052	1.134	
		**10.6064	0.008741	1.392	1.687	
		11.0	0.2664	1.089	1.421	
		11.0	0.03700	1.301	1.697	
		**11.4201	0.1263	1.165	1.637	
1.0	100.0	3.0	0.9082	1.032	0.1820	
		4.0	0.8290	1.062	0.3332	
		** 4.5301	0.004315	1.357	3.372	
		5.0	0.7186	1.115	0.5467	
		5.0	0.03487	2.815	1.380	
		6.0	0.5378	1.232	0.8694	
		6.0	0.1396	1.968	1.389	
		** 6.4392	0.3201	1.484	1.207	
	10.0		1.50	0.8025	1.048	0.3896
			2.0	0.6251	1.104	0.7299
			2.30	0.4649	1.171	1.024
			2.40	0.3912	1.208	1.150
			2.50	0.3025	1.262	1.304
			2.60	0.1766	1.351	1.509
			2.70	0.07719	1.402	1.689
2.75	0.05650	1.395	1.744			
1.0		0.70	0.8838	0.9592	0.2350	
		1.0	0.7766	0.9175	0.4587	
		1.5	0.5661	0.8214	0.9241	
		2.0	0.3710	0.7091	1.418	
		2.5	0.2295	0.6029	1.884	
		3.0	0.1388	0.5147	2.316	
-0.40		0.15	0.9764	0.9563	0.04782	
		0.20	0.9597	0.9266	0.08237	
		0.30	0.9178	0.8564	0.1713	
		0.40	0.8697	0.7824	0.2782	
		0.50	0.8200	0.7121	0.3956	
		0.60	0.7701	0.6485	0.5188	
		0.80	0.6770	0.5431	0.7724	
		1.0	0.5943	0.4625	1.028	

\*\* - Boundary of multiple-valued region; see Section IV-B-2 for calculational procedure



<u>E</u>	<u>K<sub>P<sub>A,S</sub></sub></u>	<u>φ<sub>MII</sub></u>	<u>(P<sub>A,0</sub>/P<sub>A,S</sub>)</u>	<u>η</u>	<u>Φ<sub>L</sub></u>	
1.0	-0.40	1.5	0.4312	0.3312	1.656	
		2.0	0.3142	0.2550	2.267	
		3.0	0.1693	0.1729	3.457	
	-0.70	0.030	0.030	0.9932	0.9727	0.01362
			0.050	0.9822	0.9305	0.03619
			0.070	0.9678	0.8732	0.06695
			0.10	0.9417	0.7953	0.1237
			0.15	0.8947	0.6698	0.2344
			0.20	0.8479	0.5701	0.3548
			0.30	0.7625	0.4323	0.6053
			0.40	0.6874	0.3451	0.8590
			0.50	0.6231	0.2860	1.112
			0.70	0.5154	0.2119	1.615
			1.0	0.3945	0.1517	2.359
			1.5	0.2587	0.1024	3.584
	-0.90	0.0060	0.0060	0.9969	0.9611	0.006228
			0.0080	0.9947	0.9348	0.01077
			0.010	0.9921	0.9047	0.01628
			0.015	0.9842	0.8233	0.03334
			0.020	0.9752	0.7444	0.05360
			0.030	0.9563	0.6131	0.09933
			0.040	0.9379	0.5160	0.1486
			0.050	0.9201	0.4437	0.1997
			0.080	0.8715	0.3102	0.3573
			0.10	0.8425	0.2578	0.4641
			0.15	0.7795	0.1809	0.7326
			0.20	0.7259	0.1391	1.002
			0.30	0.6374	0.09503	1.539
			0.40	0.5657	0.07207	2.076
			0.50	0.5056	0.05802	2.611
0.70	0.4093	0.04170	3.678			
10.0	100.0	1.0	0.9437	1.035	0.1116	
		1.5	0.8645	1.089	0.2643	
		**1.5070	0.003971	5.270	1.291	
		1.75	0.8063	1.134	0.3746	
		1.75	0.04604	3.975	1.313	
		2.0	0.7267	1.204	0.5193	
		2.0	0.1051	3.063	1.321	
		2.25	0.6080	1.333	0.7278	
		2.25	0.2056	2.320	1.267	
		**2.4082	0.4008	1.673	1.046	

\*\* - Boundary of multiple-valued region; see Section IV-B-2 for calculational procedure



$E$	$K_{P_{A,s}}$	$\phi_{MIT}$	$(P_{A,o}/P_{A,s})$	$\eta$	$\Phi_L$		
10.0	10.0	0.40	0.9237	1.039	0.1511		
		0.60	0.8150	1.101	0.3604		
		0.80	0.6146	1.244	0.7240		
		0.90	0.4071	1.458	1.074		
		0.91	0.3665	1.511	1.138		
		0.92	0.3016	1.603	1.234		
		**0.92298	0.1395	1.889	1.463		
		**0.92416	0.2172	1.745	1.355		
		0.93	0.07772	1.987	1.563		
		0.95	0.04649	1.996	1.637		
		1.0	0.02174	1.925	1.750		
		1.0	1.0	0.50	0.6713	0.9613	0.6609
				0.75	0.3706	0.8635	1.336
				1.0	0.1665	0.7146	1.965
-0.40	-0.40	0.070	0.9717	0.9554	0.05722		
		0.10	0.9453	0.9156	0.1119		
		0.15	0.8901	0.8378	0.2304		
		0.20	0.8279	0.7584	0.3708		
		0.30	0.7024	0.6194	0.6814		
		0.40	0.5887	0.5134	1.004		
		0.60	0.4078	0.3732	1.642		
		1.0	0.1908	0.2342	2.862		
-0.70	-0.70	0.015	0.9908	0.9655	0.01859		
		0.020	0.9842	0.9416	0.03223		
		0.035	0.9572	0.8530	0.08940		
		0.050	0.9242	0.7607	0.1627		
		0.075	0.8663	0.6290	0.3027		
		0.10	0.8099	0.5293	0.4528		
		0.15	0.7078	0.3963	0.7628		
		0.20	0.6202	0.3143	1.075		
		0.30	0.4792	0.2203	1.697		
		0.40	0.3721	0.1687	2.310		
-0.90	-0.90	0.0020	0.9981	0.9760	0.003865		
		0.0030	0.9958	0.9491	0.008456		
		0.0050	0.9896	0.8792	0.02176		
		0.0080	0.9773	0.7668	0.04858		
		0.010	0.9685	0.6039	0.06919		
		0.015	0.9462	0.5639	0.1256		
		0.020	0.9242	0.4688	0.1856		
		0.030	0.8839	0.3483	0.3103		
		0.040	0.8476	0.2763	0.4376		
		0.050	0.8144	0.2287	0.5661		

<u>E</u>	<u>K<sub>pA,s</sub></u>	<u>φ<sub>MII</sub></u>	<u>(p<sub>A,o</sub>/p<sub>A,s</sub>)</u>	<u>η</u>	<u>Φ<sub>L</sub></u>
		0.070	0.7554	0.1700	0.8245
		0.10	0.6801	0.1225	1.213
10.0	-0.90	0.15	0.5780	0.08351	1.860
		0.20	0.4955	0.06328	2.506
		0.30	0.3690	0.04256	3.792

\*\*Boundary of multiple-valued region; see Section IV-B-2 for calculational procedure.

## 3. Experimental Data

## a. Raw Data

Run Number	Reactor Temperature (°C)	Total Pressure (mm.Hg.)	Feed Rates x 10 <sup>4</sup> (gr.moles/min.)			Scaled Chromatogram Areas (sq. in.)		
			C <sub>4</sub> H <sub>4</sub> S	H <sub>2</sub>	H <sub>2</sub> S	H <sub>2</sub> S	C <sub>4</sub> H <sub>10</sub> +1-C <sub>4</sub> H <sub>8</sub>	2-C <sub>4</sub> H <sub>8</sub>
5	235.6	815	0.6532	7.143	0.0000	34.130	27.810	20.070
6	236.0	807	0.6532	6.964	0.0000	31.400	27.850	19.210
19	236.0	824	0.6532	6.942	0.0000	36.040	34.950	19.080
20	235.0	805	0.6532	16.23	0.0000	17.450	15.800	13.580
32	235.8	783	0.1092	4.576	0.0000	24.330	35.750	4.458
33	235.6	788	0.1092	10.67	0.0000	9.270	13.750	2.119
35	236.1	832	0.6532	7.277	0.0000	38.100	38.550	21.950
42	236.4	811	0.6532	13.53	0.5893	61.950	9.680	7.970
44	234.8	821	0.6532	7.277	0.0000	30.980	27.840	18.850
25	250.9	832	0.6532	4.933	0.0000	86.370	103.130	27.460
26	251.1	811	0.6532	10.98	0.0000	41.800	49.140	18.260
27	251.3	811	0.6532	18.39	0.0000	26.790	30.160	13.230
28	249.9	796	0.1092	10.45	0.0000	11.740	18.060	1.638
31	250.4	783	0.1092	4.554	0.0000	25.350	41.090	3.223
36	251.2	821	0.6532	7.143	0.0000	66.420	77.560	27.030
37	250.8	811	0.6532	15.36	0.0000	33.890	36.300	17.040
38	251.4	811	0.6532	11.79	0.3839	66.200	31.460	16.030
39	250.9	842	0.6532	5.893	0.3304	120.680	60.210	20.670
22	265.0	805	0.6532	17.81	0.0000	31.790	39.560	10.560
23	265.5	805	0.6532	10.58	0.0000	60.160	75.610	16.620
24	264.3	811	0.6532	4.755	0.0000	119.450	155.870	24.040
29	266.1	796	0.1092	10.58	0.0000	8.561	13.900	1.040
30	266.2	791	0.1092	4.688	0.0000	21.170	32.750	1.223
40	265.4	831	0.6532	6.741	0.3571	138.630	89.140	21.020
43	265.0	780	0.6532	14.06	0.6250	84.170	36.720	14.370



b. Processed Data

Run Number	Average Partial Pressures (mm.Hg.)					Reaction Rates (gr.moles/min.)x10 <sup>6</sup>		Reaction Products Closure	Sulfur Balance Closure
	C <sub>4</sub> H <sub>4</sub> S	H <sub>2</sub>	H <sub>2</sub> S	C <sub>4</sub> H <sub>8</sub>	C <sub>4</sub> H <sub>10</sub>	C <sub>4</sub> H <sub>4</sub> S Disappearance	C <sub>4</sub> H <sub>10</sub> Formation		
5	50.1	719.5	22.7	11.1	11.6	20.4	10.4	5.2%	4.1%
6	52.2	711.7	21.6	10.3	11.3	19.1	9.98	1.9	1.4
19	51.9	723.7	24.2	9.98	14.2	20.8	12.2	1.9	1.6
20	19.9	760.2	12.4	6.71	5.72	25.1	11.5	-3.9	-3.7
32	2.77	747.2	16.6	2.15	14.5	9.36	8.15	-3.0	-7.3
33	1.70	773.3	6.47	1.01	5.46	8.64	7.30	-4.7	-10.7
35	47.2	730.6	27.1	11.5	15.6	23.8	13.7	-1.0	-0.9
42	29.2	733.8	40.6	3.94	3.53	13.3	6.29	0.6	0.2
44	50.8	727.8	21.2	9.80	11.4	19.2	10.3	0.7	0.5
25	56.5	656.0	59.8	14.8	45.0	33.6	25.3	1.5	2.1
26	20.8	731.8	29.2	9.33	19.9	38.2	26.0	-1.7	-2.7
27	10.8	762.7	18.7	6.74	12.0	41.4	26.5	-1.9	-3.3
28	0.26	779.3	8.23	0.81	7.43	10.6	9.55	-3.7	-10.5
31	1.74	745.5	17.9	1.53	16.4	9.95	9.10	-5.8	-15.3
36	33.0	695.3	46.3	14.1	32.2	38.2	26.5	-0.5	-0.9
37	12.2	752.0	23.4	8.80	14.6	42.8	26.7	-0.5	-0.9
38	24.1	721.1	45.8	7.93	12.0	29.5	17.8	-4.0	-3.0
39	51.0	669.0	83.6	11.6	26.8	28.1	19.6	4.4	3.4
22	9.01	752.8	21.6	5.41	16.2	46.1	34.5	-0.6	-1.2
23	13.1	711.6	40.2	8.61	31.6	49.2	38.7	0.8	1.7
24	44.6	605.4	80.5	12.8	67.7	42.0	35.4	1.7	3.1
29	2.20	781.5	6.13	0.51	5.62	8.04	7.37	-5.7	-12.2
30	4.58	757.6	14.4	0.62	13.8	8.28	7.93	-1.5	-3.4
40	30.9	654.2	95.3	11.5	39.2	40.6	31.4	2.7	3.0
43	14.5	689.1	55.3	7.09	14.1	38.8	25.8	-1.2	-1.0

## D. Illustrative Calculations for Langmuir-Hinshelwood Rate Equations, Using Experimental Data

### 1. Calculation of the Effectiveness Factor

An example of a system in which the rate of reaction is retarded by a product is the reaction of carbon dioxide with solid carbon, which is retarded by carbon monoxide. The effect is particularly marked at relatively lower temperatures. Use of the method developed in this thesis for calculating the effectiveness factor may be illustrated by taking a set of data for one run from Austin, Rusinko and Walker (77). They studied the reaction of  $\text{CO}_2$  with spectroscopic carbon, a finely porous material, at temperatures ranging from 950 to 1305°C, and at various  $\text{CO}_2$  partial pressures. The mathematical relationships for this reaction are the same as those for decomposition or isomerization of a single reactant on a porous catalyst, i.e., a Type I rate equation, except that the porosity and hence the effective diffusivity will increase as reaction proceeds. The reaction data of Walker, et al, however, are for only the first 11% of reaction so the change in diffusivity during a run is relatively insignificant.

The carbon was cylindrical in shape, 2 inches in height and 1/2 inch in diameter. A 1/8" hole was cut in the center, and a mullite rod was inserted in this hole. The top and bottom faces of the cylinder were sealed off with mullite plates so that access to the interior of the carbon was available only through the lateral exterior surface, and diffusion was truly radial. The initial weight of the carbon annulus was about 8.8 gr.

Figure 22, p. 197 of their publication, shows that at a  $\text{CO}_2$  partial pressure of 0.75 atm and a temperature of 1000°C, the rate



of reaction was 0.125 grams of carbon/hr. Presumably, the partial pressure of carbon monoxide at the exterior of the carbon was zero during the run, and it will be assumed that nitrogen, which was present in the feed stream, does not enter into the rate equation. Rates were measured over about the first 11% of burn-off, so that at the mid-point of this interval

$$\text{rate/gram} = 0.125 / 8.8 \times 0.945 = 0.015 \text{ gr.C./gr.C., hr.}$$

Figure 13 of this article shows that the average porosity (cc/cc) of this sample during the period of the burn-off is about 0.36. Taking 2.27 as the true density ( $\rho_t$ ) of carbon, the apparent density of the particle is then

$$\rho = (1 - \theta)\rho_t = (0.64)(2.27) = 1.45 \text{ gr./cc.}$$

The observed reaction rate/gross volume of carbon

$$= \frac{(0.015)}{12} \frac{(1.45)}{3600} = 5.04 \times 10^{-7} \text{ moles/cc, sec.}$$

From their Figure 16 the effective diffusivity  $D = 0.013 \text{ cm}^2/\text{sec.}$  at NTP. Diffusion apparently occurs in the transition region between Knudsen and bulk diffusion, and the authors suggest that  $D$  is proportional to about  $T^{1.30}$ , but in a more recent study on a similar graphite electrode, for  $\text{CO}_2$  counterdiffusing through helium between  $30^\circ\text{C}$  and  $400^\circ\text{C}$ , at a total pressure of 1 atmosphere, Nichols (41) reported the temperature exponent to be about 0.98. Using this value,

$$D (1000^\circ\text{C}) = 0.013 \times \left( \frac{2291}{530} \right)^{0.98} = 0.0545 \text{ cm}^2/\text{sec.}$$



The external concentration of carbon dioxide is

$$C_{A,s} = 0.75 / 82.06 \times 1273 = 7.16 \times 10^{-6} \text{ moles/cm}^3$$

The dimension  $L'$ , given by the ratio of volume to surface, can be approximated by

$$L' = \frac{V_c}{A} = \frac{1}{2} \left[ \frac{16}{64} - \frac{1}{64} \right] \times 2.54 \text{ cm} = 0.298 \text{ cm}$$

The value of  $\bar{\Phi}_L$  can now be calculated

$$\bar{\Phi}_L = \frac{L'^2}{D C_{A,s}} \text{ (observed rate/gross catalyst volume) =}$$

$$\bar{\Phi}_L = \frac{(0.298)^2 (5.04 \times 10^{-7})}{(7.16 \times 10^{-6})(0.0545)} = 0.114$$

The authors did not determine a rate equation for the reaction, but several other investigators have reported that on each of various types of carbon it is of the form:

$$r_{\text{CO}_2} = k_I p_{\text{CO}_2} / (1 + K_{\text{CO}} p_{\text{CO}} + K_{\text{CO}_2} p_{\text{CO}_2})$$

The form of carbon most similar to that studied by Walker, et al., on which kinetic information is available, is probably electrode carbon. Wu (84) reported values of the kinetic constants for electrode carbon over the temperature and pressure range of interest. Using Figure 35 of Wu's thesis, the values at 1000°C can be estimated as:

$$K_{\text{CO}_2} = 2.4 \text{ atm}^{-1}$$

$$K_{\text{CO}} = 63 \text{ atm}^{-1}$$

It will be assumed that these can be applied to the work of Austin, et al. A value of  $Kp_{A,s}$  can now be calculated. Equation (IV-23) reduces to

$$K = \left[ K_{\text{CO}_2} - \left( \frac{D_{\text{CO}_2}}{D_{\text{CO}}} \right) K_{\text{CO}} \nu_{\text{CO}} \right] / \omega$$

Assuming that the diffusivity is approximately proportional to the reciprocal of the square root of molecular weight,

$$(D_{\text{CO}_2} / D_{\text{CO}}) = \sqrt{28/44} \approx 0.80$$

$$K = (2.4 - 0.80 \times 63 \times 2) / \omega = (2.4 - 101) / \omega = -99 / \omega$$

From Equation (IV-21)

$$\omega = 1 + \sum_i \left[ K_i p_{i,s} + (p_{A,s} D_A K_i \nu_i / D_i) \right] =$$

$$1 + \left( \frac{D_{\text{CO}_2}}{D_{\text{CO}}} \right) p_{\text{CO}_2,s} K_{\text{CO}} \nu_{\text{CO}}$$

$$\omega = 1 + 0.80 \times 0.75 \times 63 \times 2 = 77$$

$$Kp_{A,s} = -(99/77) \times 0.75 = -0.965$$

Interpolating between the curves for  $Kp_{A,s} = -0.95$  and  $-0.98$  on Figure IV-4, the effectiveness factor,  $\eta$ , for this run is about 0.35. Internal diffusion effects are therefore significant. This conclusion has been confirmed in a subsequent paper by Austin and Walker. (4)

Note that if the reaction were assumed to be of simple first-order, the effectiveness factor would erroneously be calculated to be nearly unity, i. e., diffusional effects would be thought to be insignificant. Even if a simple second-order reaction were assumed, the effectiveness factor would be taken to be about 0.92.

Another study in which intrinsic reaction rate data are available on electrode carbon is that of Reif. (54) Using his values for the kinetic constants, the value of  $Kp_{A,s}$  is equal to  $-0.970$ , which is very close to the value calculated from Wu's data. Actually, Wu's correlation for coal coke gives at this temperature a value of  $Kp_{A,s}$  equal to  $-0.965$ , identical to the value for electrode carbon. The effectiveness factors for these two types of carbon would therefore be very close to the one calculated above.

An interesting perspective on the effect of complex rate equations on the effectiveness factor can be gained by calculating the value of  $D_A$  that would be necessary to produce an effectiveness factor of 0.35, assuming the reaction to be second-order. Reading from Figure IV-4,  $\Phi_L \cong 1.53$  when  $\eta = 0.35$  for a second-order reaction. Therefore,

$$D_A = \frac{0.114}{7.53} \times 0.0545 = 0.00406 \text{ cm.}^2/\text{sec.}$$

This calculation shows that an accurate knowledge of the reaction kinetics is critical if effective diffusivities are to be calculated



from kinetic data in the internal-diffusion regime. The calculation also emphasizes the importance of a knowledge of the exact rate equation, when the effectiveness factor is to be predicted. The ability to predict or measure the effective diffusivity to a high degree of accuracy is of little value if the exact kinetic equation is not known.

## 2. Examples of the Calculation of $Kp_{A,s}$

### a. Dehydration of Alcohol - Type I

Miller and Kirk (38) studied the dehydration of various alcohols over a silica-alumina catalyst, and found that their data was fitted by the equation

$$r_A = k_I \left( p_A - \frac{p_o p_w}{K_p} \right) / (1 + K_A p_A + K_w p_w + K_o p_o)$$

In the above equation, A refers to alcohol, w to water and o to olefin. For n-propanol at 450°F,  $K_p = 1200 \text{ atm.}$ ,  $K_A = 1.19 \text{ atm.}^{-1}$ ,  $K_w = 12.6 \text{ atm.}^{-1}$ ,  $K_o = 0$ .

Consider a run where  $p_{A,s} = 1.80 \text{ atm.}$ ,  $p_{w,s} = p_{o,s} = 0.20 \text{ atm.}$  These conditions are within the range investigated by Miller and Kirk. Under these conditions, the second term in the numerator of the rate equation may be neglected, and the rate equation reduces to the standard Type I Langmuir-Hinshelwood form, Equation (III-6).

Miller and Kirk did not make any diffusivity measurements, so it will be assumed that the diffusivity is proportional to the inverse of the square root of the molecular weight. Then

$$D_A / D_w = \sqrt{18/60} = 0.548$$

K is calculated from Equation (IV-23)

$$K = \left[ K_A - D_A \sum_i (K_i \nu_i / D_i) \right] / \omega = (1.19 - 0.548 \times 1 \times 12.6) / \omega$$

$$K = -5.71 / \omega$$

$\omega$  is calculated from Equation (IV-21)

$$\omega = 1 + \sum_i K_i \left[ p_{i,s} + (p_{A,s} \nu_i D_A / D_i) \right]$$

$$\omega = 1 + 12.6 (0.20 + 1.80 \times 1 \times 0.548) = 1 + 12.6 \times 1.186 = 15.9$$

$$K = -(5.71 / 15.9) = -0.359$$

$$K p_{A,s} = -0.359 \times 1.80 = -0.646$$

#### b. The Oxidation of Carbon Monoxide - Type I

Gilliland (18) reported that the kinetics of carbon monoxide oxidation over a zinc oxide catalyst could be described by the rate equation

$$r_{CO} = k_I p_{CO} / (1 + K_{CO_2} p_{CO_2})$$

at 1 atmosphere total pressure in the temperature region 210 - 240°C. For Catalyst No. 11, Series A, Gilliland found that the value of  $K_{CO_2}$  was about 0.380 (cm. Hg.)<sup>-1</sup> at 220°C.

Consider Run No. 15, which was made with an initial carbon monoxide partial pressure,  $p_{CO,s} = 40.5$  cm. Hg., an initial oxygen partial pressure,  $p_{O_2,s} = 35.6$  cm. Hg. and an initial carbon dioxide partial pressure,  $p_{CO_2,s} = 0$ . Because only the partial pressure of

carbon monoxide appears in the numerator of the rate equation, CO must be chosen to be component A.

Assuming that the effective diffusivity is inversely proportional to the molecular weight

$$\frac{D_{\text{CO}}}{D_{\text{CO}_2}} = \sqrt{\frac{44}{28}} = 1.25$$

$\omega$  is calculated from Equation (IV-21)

$$\omega = 1 + \sum_i K_i \left[ p_{i,s} + (p_{A,s} \nu_i D_A / D_i) \right]$$

$$\omega = 1 + 0.380 (0 + 1.25 \times 40.5) = 20.2$$

and K is calculated from Equation (IV-23)

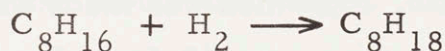
$$K = \left[ K_A - D_A \sum_i (K_i \nu_i / D_i) \right] / \omega = (0 - 1.25 \times 0.380) / 20.2$$

$$K = -0.0235 \text{ (cm.Hg.)}^{-1}$$

$$K p_{A,s} = -0.0235 \times 40.5 = -0.95$$

### c. The Hydrogenation of Codimer - Type II

Hougen and Watson (26) reported that the kinetics of the reaction



over supported nickel were best described by the rate equation



$$r_U = k_{II} p_H p_U / (1 + K_H p_H + K_U p_U + K_S p_S)^2$$

which is the standard Type II rate equation, Equation (III-9). In this expression, H refers to hydrogen, U to codimer (mixed isomers of octene) and S to octane.

They reported that, at 200°C,  $K_H = 0.383 \text{ atm.}^{-1}$ ,  $K_S = 0.489 \text{ atm.}^{-1}$ ,  $K_U = 0.580 \text{ atm.}^{-1}$ . Consider Run No. 3d, made at 200°C. For this run,  $p_{H,s} = 2.450 \text{ atm.}$ ,  $p_{U,s} = 0.530 \text{ atm.}$  and  $p_{S,s} = 0.515 \text{ atm.}$  In accordance with the rule of choosing component A to be the reactant with the smallest value of  $(Dp_s / \nu)$ , let U(codimer) be A.

Assuming that the effective diffusivity is inversely proportional to the square root of the molecular weight,

$$D_U/D_H = \sqrt{2/112} = 0.134; \quad D_U/D_S = \sqrt{114/112} = 1.01$$

$$\omega = 1 + \sum_i K_i \left[ p_{i,s} + \left( \nu_i D_A p_{A,s} / D_i \right) \right] = 1 + 0.383 (2.450 - 0.134 \times 0.530) + 0.489 (0.515 + 1.01 \times 0.530)$$

$$\omega = 2.424$$

$$K = \left[ K_A - D_A \sum_i (\nu_i K_i / D_i) \right] / \omega = (0.580 + 0.383 \times 0.134 - 0.489 \times 1.01) / \omega$$

$$K = 0.137 / 2.424 = 0.0565$$

$$Kp_{A,s} = 0.0565 \times 0.530 = 0.0300$$

E can be calculated from Equation (IV-51).

$$E = \left[ (D_B p_{B,s} / b D_A) - p_{A,s} \right] / p_{A,s} = (2.450 / 0.134) - 0.530 / 0.530$$

$$E = 33.5$$

d. The Formation of Phosgene - Type II

Potter and Baron (51) reported that the kinetics of the reaction



over activated carbon were described by the Type II rate equation

$$r_{\text{Cl}_2} = k_{\text{II}} p_{\text{CO}} p_{\text{Cl}_2} / (1 + K_{\text{Cl}_2} p_{\text{Cl}_2} + K_{\text{P}} p_{\text{P}})^2$$

where P refers to phosgene.

Consider a run at 30.6°C, with nitrogen present. Under these conditions,  $K_{\text{Cl}_2} = 4.20$  and  $K_{\text{P}} = 5.10$ . Let  $p_{\text{CO},s} = p_{\text{Cl}_2,s} = 0.200$ ,  $p_{\text{P},s} = 0.100$  and  $p_{\text{N}_2,s} = 0.500$ . These partial pressures are typical of those used in the study. Let  $\text{Cl}_2$  be component A.

Making the usual assumption about the effective diffusivities

$$D_{\text{Cl}_2} / D_{\text{P}} = \sqrt{99/71} = 1.18; \quad D_{\text{CO}} / D_{\text{Cl}_2} = \sqrt{71/28} = 1.60$$

$$\omega = 1 + \sum_i K_i \left[ p_{i,s} + \left( \nu_i D_A p_{A,s} / D_i \right) \right] = 1 + 5.10 \left[ 0.100 + 1.18 \times 0.200 \right]$$

$$\omega = 2.71$$

$$K = \left[ K_A - D_A \sum_i (\nu_i K_i / D_i) \right] / \omega =$$

$$K = (4.20 - 5.10 \times 1.18) / 2.71 = -0.668$$

$$K p_{A,s} = -0.668 \times 0.200 = -0.134$$

$$E = \left[ (D_B p_{B,s} / b D_A) - p_{A,s} \right] / p_{A,s}$$

$$E = (1.60 \times 0.200 - 0.200) / 0.200 = 0.60$$

### 3. Thiophene Hydrogenolysis

#### a. Calculation of $Kp_{A,s}$ and E

This calculation is based on the results of the present experimental study. The rate equation is given by Equation (III-19).

$$r_T = k p_T p_H / (1 + K_T p_T + K_{H_2S} p_{H_2S})^2 \quad \text{(III-19)}$$

Table III-4 contains the values of the kinetic parameters; at 235°C,  $K_T = 0.0592$  mm.Hg. and  $K_{H_2S} = 0.0420$  mm.Hg. Consider Run 44; Appendix C-3-b contains the following values:  $p_{T,s} = 50.8$  mm.Hg.,  $p_{H_2S,s} = 21.2$  mm.Hg.,  $p_{H,s} = 728$  mm.Hg.

Let thiophene be component A. Making the usual assumption regarding the effective diffusivities

$$D_T / D_{H_2S} = \sqrt{\frac{34}{84}} = 0.635$$

$$D_{H_2} / D_T = \sqrt{\frac{84}{2}} = 6.49$$

$$\omega = 1 + \sum_i K_i \left[ p_{i,s} + \left( \nu_i D_A p_{A,s} / D_i \right) \right] = 1 + 0.0420 \left[ 21.2 + (50.8 \times 0.635) \right]$$

$$\omega = 3.24$$

$$K = \left[ K_A - D_A \sum_i (\nu_i K_i / D_i) \right] / \omega =$$

$$K = (0.0592 - 0.635 \times 0.0420) / 3.24 = 0.0100$$

$$Kp_{A,s} = 0.508$$



$$E = \left[ (D_B p_{B,s} / b D_A) - p_{A,s} \right] / p_{A,s} =$$

$$E = \left[ \left( \frac{6.49 \times 728}{3} \right) - 50.8 \right] / 50.8 = 30.0$$

b. Discussion of Experimental Kinetic Study

Since  $K_T$  is larger than  $K_{H_2S}$  at all three temperatures, and since  $(D_T / D_{H_2S}) < 1$ , the parameters  $K$  and  $Kp_{A,s}$  are always positive. The value of  $E$  is equal to or greater than 30 for all the experimental runs. Under these conditions, the  $\eta - \bar{\Phi}_L$  curve lies either coincident with, or slightly above, the  $\eta - \bar{\Phi}_L$  curve for a first-order reaction. As shown in Table IV-1 of Section IV-D-1-c, the value of  $\bar{\Phi}_L$  for which the effectiveness factor,  $\eta$ , is equal to 0.95 is about 0.13. (The value of  $\bar{\Phi}_L$  for a cylinder should lie between the  $\bar{\Phi}_L$  values for a slab and a sphere.) Therefore, all runs except Run 28 probably reflect intrinsic kinetic behavior.

Appendix E

1. Calculation of the Maximum Temperature and Concentration Differences between the Catalyst Pellet and the Bulk Stream

The maximum observed rate of thiophene disappearance in any kinetic experiment was about  $50 \times 10^{-6}$  gr. moles/min. This rate was assumed in the calculations below and will produce liberal estimates of  $\Delta T$  and  $\Delta C$ .

Since the charts for the calculation of heat and mass transfer coefficients in packed beds are based on spherical particles, an equivalent spherical radius was calculated for the catalyst pellets used in this study. The equivalent radius was taken to be the radius of a sphere having the same geometrical surface area as the 1/8 inch diameter, 1/2 inch long cylinders. Thus

$$A = \left( \pi \times \frac{1}{8} \times \frac{1}{2} + \frac{2\pi}{4 \times 64} \right) = 0.00154 \text{ ft.}^2$$

$$R_s = (0.00154 / 4\pi)^{1/2} = 0.0111 \text{ ft.} = 0.338 \text{ cm.}$$

The use of such an equivalent sphere will produce liberal estimates of  $\Delta T$  and  $\Delta C$ , if the reaction rate per pellet is taken to be the product of the reaction rate per gram and the weight of the equivalent sphere.

$$\text{Reaction rate per gram of catalyst} = 50 \times 10^{-6} / 8.16$$

$$= 6.13 \times 10^{-6} \text{ moles/gr. - min.}$$

$$\text{Weight of equivalent pellet} = 1.17 \times 4 \times \pi \times (0.338)^3 / 3$$

$$= 0.189 \text{ gr.}$$

$$\text{Rate/pellet} = 6.13 \times 10^{-6} \times 0.189$$

$$= 1.16 \times 10^{-6} \text{ gr. moles/min.}$$

In order to calculate  $j_H$  and  $j_D$ , the Reynolds number, based on particle diameter must be calculated

$$N_{Re} = \frac{2R_s G}{\mu} \quad (\text{VI-10})$$

In order to calculate  $N_{Re}$ , the values of  $\mu$  and  $\rho_g$  must be known. In the calculations below, it was assumed that the gas stream is 10% thiophene and 90% hydrogen. Thus, the average molecular weight,  $\bar{M}$ , of the gas stream is

$$\bar{M} = 0.90 \times 2 + 0.10 \times 84 = 10.2$$

and therefore

$$\rho_g = \frac{P\bar{M}}{RT} = \frac{10.2}{0.730 \times 941} = 0.0149 \text{ lb. / ft.}^3$$

The viscosity of thiophene vapor at  $250^\circ\text{C}$  was calculated using the method of Licht and Stechert, which is detailed on p. 189 of Reid and Sherwood (53). The result was

$$\mu_T = 0.0130 \text{ cp.}$$

The viscosity of hydrogen at  $250^\circ\text{C}$  was estimated, from the monograph on p. 917 of McCabe and Smith (35), to be

$$\mu_H = 0.0134 \text{ cp.}$$

The viscosity of the hydrogen-thiophene mixture was calculated to be

$$\mu = 0.0178 \text{ cp.}$$

using Wilke's method, which is described on p. 199 of Reference (53).



The gas flow through the reactor was about  $0.20 \text{ ft}^3 / \text{min}$ . at  $25^\circ\text{C}$ , and the superficial cross-sectional area of the reactor was  $0.00211 \text{ ft}^2$ , so that

$$G \cong 0.20 \left( \frac{523}{298} \right) \times \frac{0.0149}{0.00211 \times 60} = 0.0413 \text{ lb/ft}^2\text{-sec.}$$

$$N_{\text{Re}} = \frac{2 \times 0.0111 \times 0.0413 \times 10^4}{0.0178 \times 6.72} = 76.5$$

The values of  $j_{\text{D}}$  and  $j_{\text{H}}$  were read from Figure (II-1) of Reference (60).

$$j_{\text{D}} = 0.152$$

$$j_{\text{H}} = 0.242$$

#### Calculation of Temperature Difference

It will be assumed that all thiophene goes completely to butane.  $\Delta H_{\text{R}}^{\circ} = -78.35 \text{ Kcal/gr.mole}$ ; use of this value tends to make the estimate of  $\Delta T$  large.

The rate of heat release per catalyst particle was

$$Q = 78,350 \times 1.16 \times 10^{-6} = 0.0909 \text{ cal/min} = 0.0216 \text{ BTU/hr.}$$

The temperature difference between the pellet surface and the bulk stream is given by

$$\Delta T = Q/HA \quad (\text{VI-11})$$

The value of  $H$  can be calculated from the known value of  $j_{\text{H}}$ .

$$j_H \equiv \frac{H}{c_p G} N_{Pr}^{2/3} \quad \text{(VI-12)}$$

$$N_{Pr} = \frac{c_p \mu}{\lambda} \quad \text{(VI-13)}$$

The value of  $c_p$  for thiophene at  $500^\circ\text{K}$  is given as 27.1 cal/ gr. mole  $^\circ\text{K}$  on p. 157 of Reference (53), and the value of  $c_p$  for  $\text{H}_2$  is about 7.0 at this temperature. The value of  $c_p$  for the hydrogen-thiophene mixture is therefore

$$\begin{aligned} c_p &= 0.90 \times 7.0 + 0.10 \times 27.1 = 9.01 \text{ cal/ gr. mole } - ^\circ\text{K} \\ &= 0.883 \text{ BTU/lb. } - ^\circ\text{F} \end{aligned}$$

The value of  $\lambda$  was estimated using the method of Brokaw, as detailed on p. 241 of Reference (53). In applying this method,  $\lambda$  of  $\text{H}_2$  was taken to be 0.20 BTU/ hr-ft- $^\circ\text{F}$ , and  $\lambda$  of thiophene was taken as 0.020 in the same units. The resulting value of  $\lambda$  for the mixture was

$$\lambda = 0.143 \text{ BTU/ hr. -ft. } - ^\circ\text{F}$$

$$N_{Pr} = \frac{0.883 \times 0.0178 \times 2.42}{0.143} = 2.66$$

$$\begin{aligned} H &= \frac{0.242 \times 0.883 \times 0.0413 \times 3600}{(2.66)^{2/3}} = \\ &16.6 \text{ BTU/ hr-ft}^2\text{-}^\circ\text{F} \end{aligned}$$

$$\Delta T = \frac{0.0216}{16.6 \times 0.00154} = 0.85^\circ\text{F}$$

Calculation of the Concentration Difference

The rate of thiophene transfer to a single catalyst particle was

$$\begin{aligned} \text{Rate} &= 1.16 \times 10^{-6} \text{ gr. moles/min.} = 1.16 \times 10^{-6} \times 60/454 \\ &= 1.53 \times 10^{-7} \text{ lb. moles/hr.} \end{aligned}$$

The concentration difference between the bulk stream and the pellet surface was

$$\Delta C_T = \frac{\text{Rate}}{A k_c} \quad (\text{VI-14})$$

The value of  $k_c$  can be calculated from the known value of  $j_D$ .

$$j_D \equiv \left( \frac{k_c \rho_g}{G} \right) N_{Sc}^{2/3} \quad (\text{VI-15})$$

$$N_{Sc} \equiv \frac{\mu}{\rho_g D_{12}} \quad (\text{VI-16})$$

It is shown in Appendix E-3 that  $D_{12}$  for the thiophene-hydrogen system is about  $1.01 \text{ cm.}^2/\text{sec.}$  The Schmidt number is

$$N_{Sc} = \frac{0.000178 \times 62.4}{1.01 \times 0.0149} = 0.738$$

$$\begin{aligned} k_c &= \frac{0.152 \times 0.0413}{(0.738)^{2/3} \times 0.0149} = 0.515 \text{ ft./sec.} = \\ &1850 \text{ ft./hr.} \end{aligned}$$

Therefore

$$\begin{aligned} \Delta C &= 1.53 \times 10^{-7} / 1850 \times 0.00154 \\ &= 0.536 \times 10^{-7} \text{ lb. moles/ft.}^3 \end{aligned}$$



This corresponds to a partial pressure drop of

$$\Delta p_T = RT \Delta C_T = 0.730 \times 941 \times 0.536 \times 10^{-7} =$$

$$\Delta p_T = 3.68 \times 10^{-5} \text{ atm.} = 0.0280 \text{ mm.Hg.}$$

Both the concentration drop and the temperature drop are negligible; there was essentially no resistance to either mass or heat transfer at the surface of the pellet.

## 2. Calculation of the Maximum Temperature Gradient within the Catalyst Pellet

It can be shown that the maximum difference between the temperature at the surface of the pellet and that at the center of the pellet is given by

$$\Delta T = \frac{(-\Delta H_R^0)(D_T)}{\lambda} C_{T,s} \quad (\text{VI-17})$$

In Appendix E-3, it is shown that  $D_T = 1.8 \times 10^{-2} \text{ cm.}^2/\text{sec.}$ , and in Section III-A-1, it was stated that  $\Delta H_R^0 \approx -78.35 \text{ Kcal/mole}$ , if thiophene goes completely to butane. This is the maximum heat effect that can occur and its use will produce a liberal estimate of  $\Delta T$ . The maximum value of  $p_T$  that occurred in any experiment was 56.5 mm.Hg. and therefore, the maximum value of  $C_{T,s}$  was about  $1.73 \times 10^{-6} \text{ moles/cm}^3$ . The value of  $\lambda$  was taken to be  $5.0 \times 10^{-4} \text{ cal/sec.-cm.}^{-\circ\text{K}}$ . This estimate is based on Table 3-2 of Reference (60).

The maximum value of  $\Delta T$  is about

$$\Delta T = \frac{78,350 \times 1.8 \times 10^{-2} \times 1.7 \times 10^{-6}}{5.0 \times 10^{-4}} = 4.8^{\circ}\text{C}$$

It is improbable that a temperature difference of this magnitude ever occurred during the experiments. Equation (VI-17) is based on the assumption that  $C_{T,0} = 0$ , a condition that almost certainly did not exist in practice.

The assumption of isothermal operation of a catalyst pellet can be assessed by examining the quantities  $\beta$  and  $\gamma$  which are defined below.

$$\beta = \frac{\Delta T}{T_s} \quad (\text{VI-18})$$

$$\gamma = \frac{E_a}{RT_s} \quad (\text{VI-19})$$

In the present case

$$\beta \approx 4.8 / 523 = 0.0092$$

$$\gamma \approx 13,000 / 1.99 \times 523 = 12.5$$

The calculation of  $\gamma$  is based on an activation energy of 13 Kcal. / mole, which value is close to that found in the present study.

Examination of Figures (3-4) and (3-5) in Reference (60) reveals that the  $\eta - \Phi$  curve for the above values of  $\beta$  and  $\gamma$  is indistinguishable from the curve for an isothermal pellet. Therefore, the assumption of an isothermal catalyst particle is justified.

### 3. Calculation of the Effective Diffusivity of Thiophene

The "parallel path" model of a porous catalyst pellet was used for this calculation. In order to apply this model, a cumulative curve

of the pore volume (cc/ gr.) versus the pore diameter must be available. This curve was supplied, for the catalyst used in this thesis, by the manufacturer. The curve was broken into segments, and the average pore diameter for each segment,  $d_j$ , was determined, along with the incremental volume,  $\Delta V_j$  (cc./ gr.), and the effective diffusion coefficient of thiophene,  $D_j$ , associated with each average pore diameter. The overall effective diffusivity of thiophene,  $D_T$ , was then given by

$$D_T = \rho \sum_j \Delta V_j D_j \quad (\text{VI-20})$$

In order to calculate the values of  $D_j$ , the diffusion regime, which is dependent on the average pore diameter, must be known. For all but the smallest pore sizes in the present catalyst, diffusion was in the transition region. This fact, together with the occurrence of multi-component diffusion, means that  $D_j$  will be concentration dependent, and makes the calculation of  $D_j$  prohibitively difficult. However, in all the kinetic experiments, hydrogen was present in great excess; in no case was the hydrogen mole fraction less than about 0.75. It was therefore assumed that binary diffusion of thiophene in hydrogen was taking place.

The equation for binary diffusion in the transition region was presented by Scott and Dullien (65) among others. Their formula, when applied to a hydrogen-thiophene system with hydrogen in great excess, reduces to

$$\frac{1}{D_j} = \frac{1}{D_{12, \text{eff.}}} + \frac{1}{D_{K, \text{eff.}}} = \frac{\tau}{D'_{12}} + \frac{\tau}{D'_K} \quad (\text{VI-21})$$



The tortuosity,  $\mathcal{T}$ , was discussed in Section IV-A-1. For this calculation,  $\mathcal{T}$  was taken to be 6.0. This value is at the upper end of those determined experimentally, and consequently the estimate of  $D_j$ , and therefore  $D_T$ , was conservative.

The values of  $D'_K$  were computed from Equation (1-27) of Reference (60), using a temperature of 523°K. The result was

$$D'_K = 12,100 d_j \text{ (cm.}^2\text{/sec.)} \quad \text{(VI-22)}$$

The value of  $D'_{12}$  was computed from Equations (1-16), (1-17), (1-18), (1-19) and (1-20) and Tables (1-2), (1-3), and (1-4) of Reference (60). A temperature of 523°C and a pressure of 1 atmosphere were used. The result was

$$D'_{12} = 1.01 \text{ cm}^2\text{/sec.} \quad \text{(VI-23)}$$

Thus, from Equations (VI-21), (VI-22) and (VI-23)

$$D_j = \frac{2,033 d_j}{1.01 + 12,100 d_j} \quad \text{(VI-24)}$$

Table VI-4 below summarizes the pore size distribution curve for the present catalyst and illustrates several of the steps in the calculation of  $D_T$ .

Table VI-4

Pore Size Distribution and Calculation of  $D_T$

<u><math>d_j</math> (cm) x <math>10^8</math></u>	<u><math>\Delta V_j</math> (cc/gr.)</u>	<u><math>D_j</math> (cm<sup>2</sup>/sec)</u>	<u><math>D_j \Delta V_j</math></u>
20,000	0.030	0.119	0.00357
12,000	0.030	0.0992	0.00298
8,000	0.030	0.0824	0.00247
6,000	0.030	0.0704	0.00211
4,500	0.030	0.0588	0.00176
2,800	0.030	0.0421	0.00126
1,500	0.030	0.0255	0.000765
650	0.030	0.0121	0.000363
50	<u>0.230</u>	0.00100	<u>0.000230</u>
	0.470		0.015508

$$D_T = 1.17 \times 0.0155 = 0.0181 \text{ cm}^2/\text{sec.}$$

## F. Nomenclature

Any consistent set of units may be used. Those specified below are used in Reference (60).

### English Letters

- A = geometrical surface area of catalyst particle, (cm.)<sup>2</sup>
- a = constant, see Eqns. (III-21), (IV-4), (VI-4), and (VI-5)
- b = stoichiometric coefficient of component B,  $b = -\nu_B$
- C = concentration, gr. moles/(cm.)<sup>3</sup>
- $c_p$  = heat capacity, cal./gr. - °C
- D = effective diffusivity, based on total cross-section of catalyst, (cm.)<sup>2</sup>/sec.
- $D_{12}$  = molecular diffusion coefficient (not effective), cm.<sup>2</sup>/sec.
- $D_K$  = Knudsen diffusion coefficient (not effective), cm.<sup>2</sup>/sec.
- $D'$  = diffusion coefficient in a straight, round pore, (cm.)<sup>2</sup>/sec.
- d = diameter of pore, cm.
- $d_c$  = diameter of capillary tubing, cm.
- E = parameter defined by Eqn. (IV-51)
- $E_a$  = activation energy, Kcal./mole
- $E_i$  = heat of chemisorption of species i, Kcal./mole
- F = volumetric flow, (cm.)<sup>3</sup>/sec.
- $F'$  = elliptic integral of the first kind
- f = fraction of butene molecules reacting before desorption



- G = mass velocity of gas, gr./sec.-cm.<sup>2</sup> (superficial area)
- $g_c$  = Newton's Law conversion factor, cm./sec.<sup>2</sup>
- H = individual heat transfer coefficient, cal/sec.-cm.<sup>2</sup>-°C
- h = grid size, cm./cm.
- $j_H, j_D$  = j-factors for heat and mass transfer, respectively, see Eqns. (VI-12) and (VI-15)
- K = parameter defined by Eqn. (IV-23)
- $K_A, K_i$  = adsorption constants in the Langmuir-Hinshelwood rate expressions, (atm.)<sup>-1</sup> (except for  $K_p$  and  $K_f$ )
- $K_f$  = equilibrium constant, based on fugacity, atm.
- $K_p$  = equilibrium constant, based on pressure, atm.
- $K_i^*$  = pre-exponential factor for the adsorption constant  $K_i$ , (atm.)<sup>-1</sup>
- k = reaction-rate constant, see Eqn. (III-11), g.moles/(gr.)(min.)(atm.)<sup>( $n_T + n_D$ )</sup>
- $k_c$  = mass transfer coefficient, cm./sec.
- $k_n$  = rate constant for n-th order reaction, g.moles/(sec.)(cm.)<sup>3</sup>(g.moles/cm.<sup>3</sup>)<sup>n</sup>
- $k'$  = rate constant, see Eqn. (III-10), g.moles/(atm.)(cm.<sup>3</sup>)(sec.)
- $k''$  = rate constant, g.moles/(cm.)<sup>3</sup>(sec.)
- $k^*$  = pre-exponential factor for k, g.moles/(gr.)(min.)(atm.)<sup>( $n_T + n_D$ )</sup>
- $k_I$  = rate constant in Type I L-H equation, see Eqns. (III-6) and (III-8), g.moles/(atm.)(cm.<sup>3</sup>)(sec.)
- $k_{II}$  = rate constant in Type II L-H rate equation, see Eqn. (III-9), g.moles/(atm.<sup>2</sup>)(cm.<sup>3</sup>)(sec.)
- $k_I^1$  = modified rate constant, see Eqn. (IV-22), g.moles/(atm.)(cm.<sup>3</sup>)(sec.)

- $k'_{II}$  = modified rate constant, see Eqn. (IV-39), g. moles / (atm.<sup>2</sup>)(cm.<sup>3</sup>), sec.  
 $L$  = thickness of catalyst slab, cm.  
 $L'$  = characteristic dimension, see Eqn. (IV-8)  
 $l$  = length, cm.  
 $M$  = parameter defined by Eqn. (III-12)  
 $\bar{M}$  = average molecular weight  
 $m$  = manometer reading, cm.  
 $N$  = number of moles, g. moles  
 $N_{Re}$  = Reynolds number, see Eqn. (VI-10)  
 $N_{Pr}$  = Prandtl number, see Eqn. (VI-13)  
 $N_{Sc}$  = Schmidt number, see Eqn. (VI-16)  
 $n$  = reaction order  
 $n_i$  = reaction order with respect to species  $i$  in numerator of L-H rate equation  
 $n_D$  = power of denominator in L-H rate equation  
 $P$  = total pressure, atm.  
 $\bar{P}$  = average total pressure in capillary, atm.  
 $p$  = partial pressure, atm.  
 $Q$  = rate of heat release per catalyst particle, cal. / sec.  
 $R$  = gas constant, (atm.)(cm.)<sup>3</sup> / (g. moles)(°K)  
 $R_s$  = radius of sphere, cm.  
 $r_A$  = rate of disappearance of component A, gr. moles / (cm.)<sup>3</sup>(sec.)  
 $r_c$  = rate of formation of butane, gr. moles / gr. cat., min.

- $r_T$  = rate of disappearance of thiophene, gr. moles/  
gr. cat., min.
- $s$  = constant, see Eqn. (III-21)
- $T$  = absolute temperature,  $^{\circ}\text{K}$
- $t$  = time, sec.
- $V_c$  = volume of catalyst,  $(\text{cm.})^3$
- $\bar{v}$  = average velocity, cm./sec.
- $x$  = Cartesian dimension, cm.
- $y$  = mole fraction
- $z$  = parameter defined by Eqn. (IV-52)

#### Greek Letters

- $\alpha$  = parameter defined by Eqn. (IV-44)
- $\alpha'$  = parameter in elliptic integral, see Eqns. (IV-57),  
(IV-58) and (IV-59)
- $\beta$  = parameter defined by Eqn. (VI-18)
- $\gamma$  = parameter defined by Eqn. (VI-19)
- $\Delta$  = difference operator
- $\Delta H_R^{\circ}$  = enthalpy of reaction, Kcal./gr. mole
- $\Delta V$  = increment in pore volume of catalyst,  $\text{cm.}^3/\text{gr.}$
- $\eta$  = effectiveness factor, see Eqns. (II-1), (IV-30), (IV-45)
- $\tilde{\eta}$  = approximate effectiveness factor, see Eqns. (IV-33) and  
(IV-48)
- $\theta$  = void fraction of catalyst particle,  $(\text{cm.})^3/(\text{cm.})^3$



$\lambda$	= thermal conductivity, cal. / sec. - cm. - °K
$\mu$	= viscosity, gm. / sec. - cm.
$\nu$	= stoichiometric coefficient, taken to be negative for reactants
$\rho$	= apparent density of catalyst particle, gr. / (cm.) <sup>3</sup>
$\rho_g$	= density of gas, gr. / (cm.) <sup>3</sup>
$\rho_M$	= density of manometer fluid, gr. / (cm.) <sup>3</sup>
$\rho_t$	= density of solid material in catalyst, gr. / (cm.) <sup>3</sup>
$\sigma$	= fractional surface coverage
$\tau$	= tortuosity, see Eqn. (IV-1)
$\Phi_L$	= modulus defined by Eqn. (IV-12)
$\Phi_s$	= modulus defined by Eqn. (IV-10)
$\phi_L$	= Thiele modulus for slab, defined by Eqn. (IV-6)
$\phi_s$	= Thiele modulus for sphere, defined by Eqn. (IV-5)
$\phi_{MI}$	= modified Thiele modulus, defined by Eqn. (IV-28)
$\phi_{MII}$	= modified Thiele modulus, defined by Eqn. (IV-43)
$\phi'$	= parameter in elliptic integral, see Eqns. (IV-57), (IV-58) and (IV-59)
$\chi$	= parameter defined by Eqn. (IV-38)
$\omega$	= parameter defined by Eqn. (IV-21)

Superscripts

$\wedge$	= refers to rate equation for butane formation
----------	--

### Subscripts

Only frequently-used subscripts are listed below. For subscripts not listed, look for the primary symbol above.

A	=	index denoting species A (A is always a reactant with a stoichiometric coefficient of unity)
B	=	butene (in Section I-B, II and III), chemical species B (in Sections I-C and IV)
eff.	=	effective
F	=	forward
f	=	feed
i	=	index denoting any species other than A
j	=	index applying to segments of cumulative pore volume curve
H	=	hydrogen
o	=	sealed surface, $x = L$
r	=	reverse
STP	=	standard temperature and pressure
s	=	exposed surface, $x = 0$ (unless used on $\phi$ , $\Phi$ or $R$ , then see above)
T	=	thiophene

### Other Symbols

$\nabla$	=	del operator
----------	---	--------------

G. Literature Citations

1. Akehata, T., S. Namkoong, H. Kubota and M. Shindo, Can. Jnl. Chem. Eng., 39, 127 (1961)
2. Aris, R., Chem. Eng. Sci., 6, 262 (1957)
3. Atroshchenko, V.I., B.A. Zhidkov and A.P. Zasorin, Kinetics and Catalysis (USSR), 605 (1962), p. 529 of Consultant's Bureau English Translation
4. Austin, L.G. and P.L. Walker, Jr., A.I.Ch.E. Jnl., 9, 303 (1963)
5. Badger, E.H.M., R.H. Griffith and W.B.S. Newling, Proc. Royal Soc. (London), A197, 184 (1949)
6. Bischoff, K.B., A.I.Ch.E. Jnl., 11, 351 (1965)
7. Boreskov, G.K., V.A. Dzisko and M.S. Borisova, Zhur. Fiz. Khim., 28, 1055 (1954)
8. Boudart, M., A.I.Ch.E. Jnl., 2, 62 (1956)
9. Butt, J.B., A.I.Ch.E. Jnl., 9, 707 (1963)
10. Carberry, J.J., A.I.Ch.E. Jnl., 8, 557 (1962)
11. Carberry, J.J., A.I.Ch.E. Jnl., 7, 350 (1961)
12. Carberry, J.J., Chem. Eng. Sci., 17, 675 (1962)
13. Cawley, C.M. and C.C. Hall, J. Soc. Chem. Ind. (London), 62, 116 (1943)
14. Chu, C. and O.A. Hougen, Chem. Eng. Sci., 17, 167 (1962)
15. Condon, F.E., "Catalytic Isomerization of Hydrocarbons", in "Catalysis, Volume 6", P.H. Emmett, ed., 43, Reinhold Publishing Corp., New York (1958)
16. Cunningham, R.E. and J.M. Smith, A.I.Ch.E. Jnl., 9, 419 (1963)



17. Franklin, P., "Elliptic Integrals", in "Methods of Advanced Calculus", 273, McGraw-Hill, New York (1944)
18. Gilliland, H.E., "The Effect of Electron Irradiation on the Catalytic and Electrical Properties of N-Type Semiconductor Zinc Oxide", Sc.D. thesis, Massachusetts Institute of Technology, Cambridge, Mass. (1965)
19. Girdler Catalysts, Chemical Products Division - Chemetron Corporation "Physical and Thermodynamic Properties of Elements and Compounds", Louisville, Ky. (1958)
20. Griffith, R.H., J.D.F. Marsh and W.B.S. Newling, Proc. Royal Soc. (London), A197, 194 (1949)
21. Hammar, C.G.B., Proc. 3rd World Petroleum Congr., Sect. IV., 295, The Hague (1951)
22. Hendricks, G.W., H.C. Huffman, R.L. Parker, Jr., and R.I. Stirton, "Catalytic Desulfurization of Petroleum Distillates", Petroleum Division Preprints, A.C.S. Meeting (1946)
23. Hinshelwood, C.N., "The Kinetics of Heterogeneous Reactions", in "The Kinetics of Chemical Change", 178, Clarendon Press, Oxford, Great Britain (1940)
24. Hoel, P.G., "Introduction to Mathematical Statistics", Second Edition, 129, John Wiley and Sons, New York (1954)
25. Hougen, O.A. and K.M. Watson, "Catalytic Reactions", in Chemical Process Principles, Part III, Kinetics and Catalysis", 902, John Wiley and Sons, New York (1947)
26. Ibid., p. 943
27. Kirsch, F.W. and S.E. Shull, Ind. Eng. Chem., Product Research and Development, 2, 48 (1963)
28. Kittrell, J.R., C.C. Watson and W.G. Hunter, "Nonlinear Least Squares Analysis of Catalytic Rate Models", A.I.Ch.E. Preprint No. 18d, (December, 1963)
29. Komarewsky, V.I. and E.A. Knaggs, Ind. Eng. Chem., 43, 144 (1951)

30. Kunze, K.S., "Numerical Analysis", 200, McGraw-Hill, New York (1957)
31. Langmuir, I., J. Am. Chem. Soc., 38, 2221 (1916)
32. Lapidus, L. and T.I. Peterson, "Heterogeneous Reaction Analysis by Nonlinear Estimation", A.I.Ch.E. Preprint No. 18c, (December, 1963)
33. Loftus, J., "Partial Oxidation of o-Xylene in Vanadium Pent-oxide Melts", Sc.D. thesis, Massachusetts Institute of Technology, Cambridge, Massachusetts (1963)
34. Masamune, S. and J.M. Smith, A.I.Ch.E. Jnl., 8, 217 (1962)
35. McCabe, W.L. and J.C. Smith, "Unit Operations of Chemical Engineering", McGraw-Hill, New York (1956)
36. McKinley, J.B., "The Hydrodesulfurization of Liquid Petroleum Fractions", in "Catalysis, Volume 5", P.H. Emmett, ed., 405, Reinhold Publishing Corp., New York (1957)
37. Mickley, H.S., T.K. Sherwood and C.E. Reed, "Applied Mathematics in Chemical Engineering", Second Edition, 96, McGraw-Hill, New York (1957)
38. Miller, D.N. and R.S. Kirk, A.I.Ch.E. Jnl., 8, 183 (1962)
39. Moldavski, B.L. and N.J. Prokoptschuk, Chem. Zentr., I, 3835 (1933), J. Applied Chem(USSR), 5, 619 (1932)
40. Moldavski, B.L. and Z.I. Kumari, Chem. Zentr., II, 515 (1935), J. Gen. Chem. (USSR), 4, 298 (1934)
41. Nichols, J.R., Ph.D. thesis, Pennsylvania State University, State College, Pa. (1961)
42. Nicholson, D.E., Analytical Chemistry, 34, 370 (1962)
43. Østergaard, K., "The Influence of Intraparticle Heat and Mass Diffusion on the Selectivity of Parallel Heterogeneous Catalytic Reactions", Preprint, Third Int. Congr. on Catalysis, Amsterdam (1964)



44. Otani, S., N. Wakao and J.M. Smith, A.I.Ch.E. Jnl., 10, 130 (1964)
45. Owens, P.J. and C.H. Amberg, "Thiophene Desulfurization by a Microreactor Technique", in "Advances in Chemistry Series, No. 33", 182 (1961)
46. Owens, P.J. and C.H. Amberg, Can. Jnl. Chem., 40, 941 (1962)
47. Ibid., p. 947
48. Pawlowski, J., Chemie Ing. Techn., 33, 492 (1961)
49. Pease, R.N. and W.B. Keighton, Jr., Ind. Eng. Chem., 25, 1012 (1933)
50. Perry, J.H., ed., "Chemical Engineer's Handbook", Third Edition, 237, McGraw-Hill, New York (1950)
51. Potter, C. and S. Baron, Chem. Eng. Progr., 47, 473 (1951)
52. Prater, C.D. and R.M. Lago, "The Kinetics of the Cracking of Cumene by Silica-Alumina Catalysts", in "Advances in Catalysis, VIII", 293, Academic Press, New York (1956)
53. Reid, R.C. and T.K. Sherwood, "The Properties of Gases and Liquids", McGraw-Hill, New York (1958)
54. Reif, A.E., J. Phys. Chem., 56, 778 (1952)
55. Richardson, J.T., Ind. Eng. Chem. Fundamentals, 3, 154 (1964)
56. Roberts, G.W. and C.N. Satterfield, to be published in Ind. Eng. Chem. Fundamentals, (August, 1965)
57. Rothfeld, L.B., A.I.Ch.E. Jnl., 9, 19 (1963)
58. Rozovskii, A. Ya. and V.V. Shchekin, Kinetics and Catalysis (USSR), 313 (1960), p. 286 of Consultant's Bureau English Translation
59. Rozovskii, A. Ya., Kinetics and Catalysis (USSR), 572 (1962), p. 500 of Consultant's Bureau English Translation



60. Satterfield, C.N. and T.K. Sherwood, "The Role of Diffusion in Catalysis", Addison-Wesley, Reading, Mass. (1963)
61. Saraf, S.K., "Gas Diffusivities in Alumina-Based Catalyst Pellets", Sc.D. thesis, Massachusetts Institute of Technology, Cambridge, Mass. (1964)
62. Schilson, R.E. and N.R. Amundsen, Chem. Eng. Sci., 13, 226 (1961)
63. Ibid., p. 237
64. Scott, D.J., Can. Jnl. Chem. Eng., 40, 173 (1962)
65. Scott, D.J. and F.A.L. Dullien, A.I.Ch.E. Jnl., 8, 113 (1962)
66. Silveston, P.L., A.I.Ch.E. Jnl., 10, 132 (1964)
67. Smith, N.L. and N.R. Amundsen, Ind. Eng. Chem., 43, 2156 (1951)
68. Taylor, T.I., "Hydrogen Isotopes in the Study of Hydrogenation and Exchange", in "Catalysis, Volume 5", P.H. Emmett, ed., 257, Reinhold Publishing Corp., New York (1957)
69. Thiele, E.W., Ind. Eng. Chem., 31, 916 (1939)
70. Thiele, E.W., Personal Communication, Notre Dame University, South Bend, Indiana (April 28, 1964)
71. Tinkler, J.D. and A.B. Metzner, Ind. Eng. Chem., 53, 663 (1961)
72. van Looy, H. and G. Limido, Compt. rend. congr. intern. chim. ind., 31<sup>e</sup>, Leige (1958), Ind. chim. belge, Suppl., 1, 645 (1959)
73. Vernon, L.W., Personal Communication, Humble Oil and Refining Company, Baytown, Texas (August 21, 1964)
74. Wakao, N. and J.M. Smith, Chem. Eng. Sci., 17, 825 (1962)
75. Wakao, N. and J.M. Smith, Ind. Eng. Chem. Fundamentals, 3, 123 (1964)

76. Walas, S.M., "Fluid-Phase Reactions Catalyzed by Solids", in "Reaction Kinetics for Chemical Engineers", 149, McGraw-Hill, New York (1959)
77. Walker, P.L., Jr., F. Rusinko, Jr. and L.G. Austin, "Gas Reactions of Carbon", in "Advances in Catalysis, XI", 133 (1959)
78. Wei, J., Jnl. Catalysis, 1, 526 (1962)
79. Weisz, P.B. and J.S. Hicks, Chem. Eng. Sci., 17, 265 (1962)
80. Weisz, P.B. and C.D. Prater, "Interpretation of Measurements in Experimental Catalysis", in "Advances in Catalysis, VI", 143, Academic Press, New York (1954)
81. Weisz, P.B. and E.W. Swegler, J. Phys. Chem., 59, 823 (1955)
82. Weller, S., A.I.Ch.E. Jnl., 2, 59 (1956)
83. Wheeler, A., "Reaction Rates and Selectivity in Catalyst Pores", in "Advances in Catalysis, III", 250, Academic Press, New York (1951)
84. Wu, P.C., "The Kinetics of the Reaction of Carbon with Carbon Dioxide", Sc.D. thesis, Massachusetts Institute of Technology, Cambridge, Mass. (1949)
85. Zeldowitsch, J.B., Acta Physicochimica U.R.S.S., 10, 583 (1939)

H. Biographical Note

The author was born on August 9, 1938 in Bridgeport, Connecticut and attended elementary and high school in Newark, N.J. He graduated from West Side High School in January, 1956 and worked for the New York Stock Exchange before entering Cornell University in September, 1956. With financial support from the National Newark and Essex Bank and from Cornell, he completed his B.Ch.E. degree at Cornell in June, 1961.

The author entered the Graduate School of Massachusetts Institute of Technology in September, 1961, and was awarded a National Science Foundation Fellowship in September, 1962. This fellowship has provided his financial support since that time. He was the winner of the Eastman Kodak Award in June, 1964.

On August 24, 1963, the author married the former Mary Gould Perdriau. At the conclusion of the present work, he will be employed as a development engineer by the Rohm and Haas Company in Philadelphia, Pa.